City Research Online

City St George's, University of London

Citation: Soomro, A.H. (2021). Induction machine based flywheel energy storage system for isolated microgrid applications. (Unpublished Doctoral thesis, City, University of London)

This is the accepted version of the paper.

This version of the publication may differ from the final published version. To cite this item please consult the publisher's version.

Permanent repository link: https://openaccess.city.ac.uk/id/eprint/28629/

Copyright and Reuse: Copyright and Moral Rights remain with the author(s) and/or copyright holders. Copies of full items can be used for personal research or study, educational, or not-for-profit purposes without prior permission or charge, unless otherwise indicated, provided that the authors, title and full bibliographic details are credited, a hyperlink and/or URL is given for the original metadata page and the content is not changed in any way. For full details of reuse please refer to City Research Online policy.

City Research Online: http://openaccess.city.ac.uk/ publications@citystgeorges.ac.uk

Induction Machine Based Flywheel Energy Storage System for Isolated Microgrid Applications

A thesis submitted for the fulfilment of the requirements for the degree

of

Doctor of Philosophy

Department of Mechanical Engineering and Aeronautics

School of Mathematics, Computer Science and Engineering

at

City, University of London

Author: Abid Hussain Soomro

London, December 2021

Abstract

Cleaner production of energy is urgently needed in today's world due to concerns about global warming and growing population. This need has promoted widespread renewable energy sources and distributed generation, integrated into electricity networks. If renewable sources of energy are added into microgrids powered previously only by fossil-fired engines, their intermittency combined with fluctuation in demand leads to further stability challenges. Energy storage systems offer a solution, which can mitigate the effects of RES intermittency by not only providing a balance between electricity supply and demand but also improving the stability of microgrids. ESS can also reduce the power rating of the generating engine to meet peak demand and enables power production to meet average demand and reducing generation cost. Batteries are nearly always used as the ESS for this application but the subject of this thesis explores an alternative ESS, the flywheel energy storage system (FESS). FESS is one of the earliest forms of energy storage technologies having several benefits of long service time, high power density, low maintenance and insensitivity to environmental conditions. FESS has been an important area of research in recent years. This thesis describes the modelling and analysis of a small-scale energy storage system incorporating FESS with a solar PV system and a diesel engine for use in an islanded system which is supposed to be highly intermittent or non-existent grid infrastructure. In this application, the performance of FESS in the islanded system is assessed and found to be beneficial in comparison to a system either without storage or with alternative ESS technology such as Li-ion batteries. The thesis consists of a description of FESS configured for electrical storage which explains its components and structure; bearing system, flywheel rotor, casings, electrical machine and associated electronic parts. The FESS and its associated control are described in the thesis along with the equations and modelling, carried out in MATLAB/Simulink environment. The simulation of FESS operation is performed over 24hrs which is rarely found in the literature. The operation of FESS for 24hrs provides better

assessment of flywheel operation and fuel consumption of DGen. The FESS model is integrated with PV hybrid microgrid system (PVHMS) incorporating dynamic residential load models, diesel generator and PV system. The presented system will be highly useful for the islanded systems or for the areas where there are weak grids or extension of transmission lines is not a feasible option.

Acknowledgements

I would like to express my sincere gratitude to my energetic supervisor Professor Keith R. Pullen for his patience and tolerance, motivation, immense knowledge and continuous support in guiding me with his valuable feedback throughout this Ph.D. His guidance helped me in all the time of research and writing of this thesis. I could not have imagined having a better supervisor and mentor for my Ph.D studies.

A special mention goes to my second supervisor, Dr. Daniel Nankoo for his insight comments and encouragement. Dr. Nankoo has been my truly dedicated mentor. Apart from academic support, I thank him for providing me teaching opportunities throughout my Ph.D journey.

I thank my colleague and fellow lab mate, Amiryar E. Mustafa for being an excellent teaching partner with motivating discussions and a great support in MATLAB/Simulink. Amiryar E. Mustafa has been my great inspiration and his motivational discussions helped me to face great challenges throughout my Ph.D.

I am grateful to my father Mr. Arbab Ali Soomro and my mother Zeenat Khatoon who have been a great inspiration for me to do the Ph.D in the first place. I am also thankful to my brothers and sisters for supporting me spiritually throughout this Ph.D and my life in general.

Last but not least, I would like to thank my lovely wife Dr. Shafaq Saeed, for her love support and being my side while completing the Ph.D, living every single minute of it and to my dear daughter Khadija for her tolerance and understanding, who both have made it possible for me to complete what I started.

Declarations

I grant powers of discretion to the University Librarian to allow this dissertation to be copied in whole or in part without further reference to me. This permission covers only single copies made for study purposes, subject to normal conditions of acknowledgment.

List of Figures

Figure 1-1 emission and expected warmings by 2100 [11]. 2
Figure 1-2 Energy consumption in world regions [12] 4
Figure 1-3 Energy production by source [12] 5
Figure 1-4 Contribution of countries indifferent renewable energy sources until 2021[19] 6
Figure 1-5 Charge and discharge times of energy storage technologies. 9
Figure 1-6 Power density and energy density regions 11
Figure 2-1 Hourly generated power of wind turbine [4]. 21
Figure 2-2 Hourly generated power of PV system [48]. 22
Figure 2-3 Detailed classification of energy storage technologies 24
Figure 2-4 Schematic diagram of SMES system[71]. 26
Figure 2-5 CAES system with heat storage with turbine [73]. 27
Figure 2-6 Schematic of working principle of PHSS [36]. 29
Figure 2-7 Schematic Diagram of Flywheel energy flow 30
Figure 2-8 Lifetime Vs temperature characteristics for a lead-acid battery 32
Figure 2-9 Li-ion battery structure and components [97] 33
Figure 2-10 Capacity lost curve of Li-ion [98]. 34
Figure 2-11 Efficiency and charge-discharge cycles of different Energy storage technologies [19]. 37
Figure 2-12 The two main microgrid topologies (a) aggregated (b) distributed 40
Figure 2-13 Corliss Centennial Engine using large flywheels [77] 49
Figure 2-14 Flywheel electric generators were used from 1902 until the 1950s [46]. 49
Figure 2-15 Structure of FESS assembly. 51
Figure 2-16 Hollow cylinder type rotor 54
Figure 2-17 Shape factor for different rotor geometries [162] 55
Figure 2-18 Structure and components of SRM [181] 57
Figure 2-19 Cross-sectional view of BLDC machine [124]. 58
Figure 2-20 A cross-sectional view of PMSM [185]. 59
Figure 2-21 Structure of Variable Switched Reluctance Machine [188]. 60
Figure 2-22 Structure of HSM[193]. 60
Figure 2-23 a) Smooth solid rotor; b) Slotted solid rotor; c) Coated solid rotor; d) Caged solid rotor [185]. 61
Figure 2-24 Cross-sectional view of BHM [202]. 63
Figure 2-25 Working diagram of Active magnetic bearing [208]. 64

Figure 2-26 Passive magnetic bearing system[209]. 65
Figure 2-27 a) SMB installed in FESS assembly; b) SMB bearing rotor [212] [211]. 66
Figure 2-28 Schematic of SGB installed in FESS assembly[215]. 67
Figure 3-1 Structure and configuration of FESS 84
Figure 3-2 Cutaway view of squirrel cage induction machine [285]. 86
Figure 3-3 Schematic of SCIM windings 87
Figure 3-4 Vector representation of reference frames 90
Figure 3-5 Vector control block diagram 93
Figure 3-6 Control system of the GSC 95
Figure 3-7 Control structure of MSC 97
Figure 3-8 Cascaded control structure [292] [291]. 99
Figure 3-9 The PI flux controller 100
Figure 3-10 Current control loop of the voltage controller 102
Figure 3-11 Schematic diagram of DC link voltage controller 103
Figure 3-12 a) %SoC of the flywheel; b) Energy stored by the flywheel 104
Figure 3-13 a) Torque of the flywheel; b) Zoomed in view of the torque curve 105
Figure 3-14 a) DC link voltage; b) Magnified view of DC voltage 106
Figure 3-15 a) Flywheel Speed; b) % SoC of flywheel; c) Electrical energy of flywheel; d) Electromagnetic torque of flywheel 107
Figure 3-16 a) Stator phase currents of flywheel; b) Magnified image of the currents 107
Figure 3-17 Specific core losses of SCIM-FESS: (a) Stator core losses; (b) Rotor core losses. 111
Figure 3-18 Stray load loss at different speeds 112
Figure 3-19 Windage loss vs speed at 0.01Pa and 0.1Pa 115
Figure 3-20 Windage loss vs speed at 1Pa and 10Pa 116
Figure 3-21 Bearing losses of FESS at different speeds 118
Figure 4-1 PVHMS system with FESS 121
Figure 4-2 Schematic diagram of a PV cell 122
Figure 4-3 Schematic diagram of synchronous generator. 123
Figure 4-4 Energy consumption profile of UK residents for the month of April over 24 hours (100 dwellings) 125
Figure 4-5 Energy consumption profile of UK residents on weekend for the month of August over 24 hours (100 dwellings) 126
Figure 4-6 Energy consumption profile of Indian residents on weekend for the month of August over 24 hours (100 dwellings) 127

Figure 4-7 Energy consumption profile of Indian residents on weekend for the month of April over 24 hours (100 dwellings) 127

Figure 4-8 Schematic design of proposed PVHMS 128

Figure 4-9 Model of PV array in MATLAB/Simulink environment 129

Figure 4-10 Characteristics of PV array for specified irradiances at 25℃ 130

Figure 4-11 V-P and V-I plots of 285 PV arrays at 1000W/m2 at different temperatures 131

Figure 4-12 Simulink model of diesel generator 131

Figure 4-13 List of outputs at terminals of synchronous machine diesel generator 132

Figure 4-14 Control system of speed controller 132

Figure 4-15 MATLAB/Simulink model of PVHMS 135

Figure 4-16 Load demand profile n weekend in New Delhi for the month of July 137

Figure 4-17 Solar irradiance in Delhi of a typical cloudy weekday for the month of July 138

Figure 4-18 Load demand profile on weekday in Mumbai for the month of June 139

Figure 4-19 Solar irradiance in Mumbai of a typical cloudy weekday for the month of June 139

Figure 4-20 Load demand profile n weekend in Kolkata for the month of June 140

Figure 4-21 Solar irradiance in Kolkata of a typical cloudy day for the month of June on weekend 141

Figure 4-22 a) PV power; b) DGen power; c)Load demand; d) Combined power curves of load, DGen and PV system 142

Figure 4-23 a) DC link voltage; b) Magnified view of DC link voltage; c) PV output voltage; d) Magnified view of PV voltage 143

Figure 4-24 a) DGen stator currents; b) Magnified view of DGen three phase currents 143

Figure 5-1 Logical power flow chart of PVHMS 148

Figure 5-2 Power curves a) PV output power; b) DGen power; c) Load demand model 1; d) Combined power curves 150

Figure 5-3 a) Phase current of DGen; b) Zoomed in view of current; c) DC link voltage; d) Zoomed in view of voltage 150

Figure 5-4 Power curves a) DGen power; b) PV output power; c) Load demand model 1; d) Combined power curves 152

Figure 5-5 a) DGen phase current; b) zoomed in view of currents; c) DC link voltage; d) zoomed in view of DC link voltage 152

Figure 5-6 Power curves a) DGen power; b) PV output power; c) Load demand model 1; d) Combined power curves 153

Figure 5-7 a) Phase currents of DGen; b) zoomed in view of currents; c) DC link voltage; d) Zoom in view of DC link voltage. 154

Figure 5-8 a) Load Demand; b) PV output power; c) Flywheel Power; d) DGen Power 156

Figure 5-9 a) %SoC of flywheel; b)Flywheel energy 157

Figure 5-10. Magnified view of power curves between 10am to 4pm. a) Load Demand; b) PV output power; c) Flywheel Power; d) DGen Power 158

Figure 5-11 Magnified view of charge-discharge cycles between 10am to 4pm 158

Figure 5-12 Magnified view of power curves between 7am to 9am. a) Load Demand; b) PV output power; c) Flywheel Power; d) DGen Power 159

Figure 5-13. Magnified view of %SoC of the flywheel and energy between 6hrs to 8hrs 159

Figure 5-14 a) DC link voltage; b) zoomed in view of DC link voltage 160

Figure 5-15 a) DGen phase current; b) Zoomed in view of currents 160

Figure 5-16 Power curves at 75% of DGen operation: a) Load Demand; b) PV output power; c) Flywheel Power; d) DGen Power 161

Figure 5-17 a) Flywheel power curves at 100% loading; b) Flywheel operation at 75% DGen loading 162

Figure 5-18 a) Load Demand; b) PV output power; c) Flywheel Power; d) DGen Power 163

Figure 5-19 a)%SoC of flywheel; b)Flywheel energy 163

Figure 5-20 Magnified view of power curves between 10am to 2pm. a) Load Demand; b) PV output power; c) Flywheel Power; d) DGen Power 164

Figure 5-21 Magnified view of power curves between 10am to 4pm. a) Load Demand; b) PV output power; c) Flywheel Power; d) DGen Power 164

Figure 5-22 Power curves of the flywheel system during charging and discharging states 165

Figure 5-23 a) DGen phase current; b) Zoomed in view of currents 165

Figure 5-24 a) DC link voltage; b) zoomed in view of DC link voltage 166

Figure 5-25 Power curves at 75% of DGen operation: a) Load Demand; b) PV output power; c) Flywheel Power; d) DGen Power 167

Figure 5-26 %SoC of the flywheel at 75% and 100% loading capacity of DGen 167

Figure 5-27 DGen operation at 100% and 75% Loading capacity 167

Figure 5-28 a) Load Demand; b) PV output power; c) Flywheel Power; d) DGen Power 168

Figure 5-29 a)%SoC of flywheel; b)Flywheel energy 169

Figure 5-30 Magnified view of power curves between 11am to 13pm. a) Load Demand; b) PV output power; c) Flywheel Power; d) DGen Power 170

Figure 5-31 Magnified view of %SoC of the flywheel and energy between 11am to 1pm 170

Figure 5-32 a) DGen phase current; b) Zoomed in view of currents 171

Figure 5-33 a) DC link voltage; b) zoomed in view of DC link voltage 171

Figure 5-34 a)%SoC of flywheel; b)Flywheel energy 172

Figure 5-35 a) Load Demand; b) PV output power; c) Flywheel Power; d) DGen Power 172

Figure 5-36 Fuel Consumption Curve for the Diesel Generator 174

Figure 5-37 Diesel Fuel Consumption Comparison with and without Flywheel Operation 176

List of Tables

Table 2-1 Technical Characteristics of Energy Storage Technologies [14] [73] [60] [56] [57] [93].....36

Table 2-2 Chosen examples of existing microgrid projects around the world [109] [118, 119, 120]. 43

Table 2-3 Advantages and drawbacks of commonly used electrical machines in FESS [171, 176, 195, 196, 139] 61

Table 2-4 Characteristics of flywheel from different manufacturers [133] [231] - [237].....71

Table 3-1 Manufacturer's loss data for M470-50HP electrical steel. 110

Table 3-2 Values of stray load losses for different power outputs [77] 112

Table 3-3 Values of z and y. Adapted with permission from [302]. 117

Table 4-1 General ratings of the diesel generator 134

Table 4-2 Parameters of all sources used in microgrid. 135

Table 5-1 DGen fuel consumption calculations for all three presented load models.....174

Table 5-2 Fuel cost comparison of DGen with and without flywheel 177

Table 5-3 CO_2 emission of DGen with and without FESS 178

Table of Contents

Chapter 1 1
Introduction 1
1.2. Problem Statement and Research Questions: 14
1.3 Research Questions 16
1.4 Methodology 16
1.5 Structure of the thesis 19
Chapter 2 21
Literature Review 21
2.1 Overview of Energy Storage 21
2.2 Description of Energy Storage Technologies 24
2.2.2 Mechanical Energy Storage 26
2.2.3 Electrochemical Storage 31
2.3 Comparison of Energy Storage Technologies 35
2.4 Overview of Microgrids 39
2.4.1 Components within microgrids 45
2.5 Background of Flywheel Technology 47
2.6 Technical Characteristics and Structure of FESS 51
2.8 Chapter Summary 82
Chapter 3 84
Modelling and Control of the Flywheel Energy Storage System 84
3.1 Mathematical Modelling of Squirrel Cage Induction Machine 86
3.2 Modelling of the Control System of FESS 91
3.3. Proportional-Integral-PI Controller Design 99
3.4 Validation of FESS and its Control System in MATLAB/Simulink 103
3.5 Modelling of System Losses 107
3.5.1 Electrical Losses 108
3.5.2 Mechanical Losses 112
Chapter 4 119
Modelling of PV Hybrid Microgrid System 119
4.1 Modelling of Solar PV System 121
4.2 Modelling of Diesel Generator 122
4.3 Modelling of Loads in the Microgrid 124

4.4 Simulink Model of Solar PV System 128
4.5 Simulink model of Diesel Generator 131
4.6 Modelling of photovoltaic hybrid mini-grid system (PVHMS) 134
4.7 Modelling of Residential Loads 135
4.8 Validation of Solar PV and Diesel Generator Model 141
Chapter 5 144
Results and Analysis 144
5.1 Operation Scenario 1 145
5.3 Results and Analysis 148
5.3.2 Operation Scenario 2 154
5.4 Analysis of generator fuel consumption 173
5.5 Chapter Summary 180
Chapter 6 183
Conclusions 183
6.1 Contributions of the research 189
6.2 Future Research 190
Appendix A 193
Reference Frame Transformation 193
A.1 Clark's Transformation 193
A.2 Park's Transformation 194
Appendix B 195
Manufacturer specifications of Generac diesel genset 195
Appendix C 199
Load profiles for Delhi city over the period of 12 months 199
Appendix D 202
Space Vector Pulse Width Modulation - SVPWM 202
Appendix E 207
Works Cited 220

Abbreviations

AMB	:	Active magnetic bearing
BESS	:	Battery energy storage systems
BHM	:	Bearingless homopolar machine
CREST	:	Centre for Renewable Energy Systems Technology
CAES	:	Compressed air energy storage
DGen	:	Diesel Generator
dq	:	Direct-quadrature
DG	:	Distributed generation
DoD	:	Depth of discharge
DTC	:	Direct torque control
DVR	:	Dynamic voltage restorer
DFIM	:	Doubly fed induction machine
ESS	:	Energy storage system
EMF	:	Electromagnetic force
FESS	:	Flywheel energy storage system
FOC	:	Field oriented control
GA	:	Genetic Algorithm
GSC	:	Grid side converter
GHG	:	Greenhouse gas
HRES	:	Hybrid renewable energy system
HSM	:	Homopolar synchronous machine
IM	:	Induction machine
IGBT	:	Insulated gate bipolar transistor
MSC	:	Machine side converter
MM-EMS		Mixed mode management strategy
OECD	:	Organisation for Economic Co-operation and Development
PHS	:	Pumped hydro storage
PVHMS	:	PV hybrid microgrid system
PWM	:	Pulse width modulation
PMB	:	Passive magnetic bearing
PMSM	:	Permanent magnet synchronous machine
PCC	:	Point of common connection
RES	:	Renewable energy source
SDG	:	Sustainable development goals
SMES	:	Super magnetic energy storage system
SCES	:	Supercapacitor energy storage
SoC	:	State of Charge
SoS	:	System of system
SRM	:	Switched reluctance machine
SCIM	:	Squirrel cage induction machine

SVPWM	:	Space vector pulse width modulation
SGB	:	Spiral groove bearing
THD	:	Total harmonic distortion
UN	:	United Nations
UPS	:	Uninterruptible power supply
VRM	:	Variable reluctance machine
V-P	:	Voltage and power
V-I	:	Voltage and current

Nomenclature

a	:	Length of the flywheel rotor
B	:	Frictional co-efficient
B_m	:	Peak magnetic flux density
C_0, C_1	:	Empirical constants
C_s	:	Static load rating
C_m	:	Torque coefficient
$E(t)$	:	Time dependent DC-link voltage
e_v	:	Energy density per volume
e_m	:	Energy density per mass
D_p	:	Pitch circle diameter of bearing
F_s	:	Static equivalent load
F_b	:	Load on a bearing
f_e	:	Electrical angular frequency
f_0	:	Lubrication factor
f_{sl}	:	Slip frequency
G	:	Irradiation in W/m2
I_0	:	Saturation current
$I_{q,g}$	:	Q-axis grid current
i_{ar}, i_{br}, i_{cr}	:	Rotor phase currents
i_{dqs}	:	Stator currents
i_{as}, i_{bs}, i_{cs}	:	Stator phase currents
i_{dqr}	:	Rotor currents
i_{qs}^*	:	Reference q-axis current
i_{ds}^*	:	Reference d-axis current
J	:	Inertia
K_{pt}	:	Proportional gain of torque controller
K_{P-flux}	:	Proportional gain of flux controller
K_{I-flux}	:	Integral gain of flux controller
K_{hys}	:	Steinmetz co-efficient
K	:	Shape factor
K_{it}	:	Integral gain of torque controller
K_{pt}	:	Proportional gain of torque controller
L_m	:	Mutual inductance
L_g	:	Grid side inductance
L_r	:	Rotor Inductance
P_{core}	:	Core power loss
P_{DC}	:	DC Link power
P_g	:	Generated power
P_{grid}	:	Grid power
P_{stator}	:	Stator power loss
P_{stray}	:	Stray power loss

P_r	:	Rated power
P_{rcl}	:	Rotor copper loss
Q	:	Electric charge
R_g	:	Grid side resistance
R_{r}	:	Rotor resistance
R_e	:	Reynolds number
R_{sh}	:	Shunt resistance
R_{sr}	:	Series resistance
R_s	:	Stator resistance
r_1	:	Inner radius of the flywheel rotor
r_2	:	Outer radius of the flywheel rotor
s	:	Slip of induction machine
T	:	Temperature in Kelvin
T_{em}	:	Electromagnetic torque
T_L	:	Load torque
T_r	:	Rotor time constant
t_v	:	Torque due to viscous friction
t_l	:	Torque due to applied load
t_f	:	End flange friction torque
$V_{ar}\ V_{br}\ V_{cr}$	:	Rotor phase currents
$V_{\mathrm{abc},s}$	:	Stator three phase voltages
V_{DC}	:	DC link voltage
$V_{g,q}$	:	Q-axis grid voltage
n	:	Bearing speed
k	:	Boltzmann's constant
$\lambda_{ar},\lambda_{br},\lambda_{cr}$	:	Rotor flux linkages
$\lambda_{as},\lambda_{bs},\lambda_{cs}$	:	Stator flux linkages
λ_{dqr}	:	Rotor flux linages
λ_m	:	Mutual flux
λ_{dqs}	:	Stator flux linkages
λ_{dr}^{est}	:	Estimated flux
μ	:	Dynamic viscosity of air
ρ	:	Mass density
σ_{max}	:	Maximum tensile strength
τ	:	Time constant
v_0	:	Kinematic oil viscosity
v_s	:	Grid side voltage
v_{dqs}	:	Stator voltages in *d-q* reference frame
ω_{sl}	:	Slip frequency
ω_{cb}	:	Control bandwidth
ω_g	:	Grid frequency
ω_e	:	Rotor electrical speed

Chapter 1

Introduction

Access to energy is a basic need for economic sustainability and growth in modern society. The growth in energy consumption of any country is linked to its modernization, rapid development in technologies and industrialization. However, global energy demand is escalating rapidly with population size which in turn is negatively affecting society due to damage to the environment. Global energy demand has increased greatly (400 exajoule annually) of which, much of the energy produced is still based on fossil fuels and this has adversely affected our environment [1]. Environmental experts and organizations have increased awareness about global warming over the past few decades, however, climate change is still a persistent global threat to the environment [2]. To lessen greenhouse gases (GHG), global regulations and policies to limit the use of fossil fuels have been enforced by the United Nations (UN) which include formulation of the Kyoto Protocol, which was made in 1997 to set emissions targets mainly for developed countries who had high levels of GHG emissions. In 2015, one hundred and ninety-three countries agreed to the sustainable development goals (SDGs) named as the 2030 Agenda for the global development of SDGs which focuses on objectives of mitigation of air pollution and a significant reduction in health effects due to hazardous elements [3]. Also, the broad international agreement made at the Paris UN Climate Conference in 2015 to limit the global temperature rise to 2 °C was one of the steps taken by the UN to combat global warming. Developed countries around the world are taking steps in the right direction to reach net-zero emission targets of CO_2 emissions.. UK is the first of the G7 major countries to make commitments to net-zero greenhouse gas emissions by 2050. The, UK has been closely followed by France in the same commitment. Sweden and Norway were the first countries to legally commit to net-zero targets, similarly South

Korea and Japan have committed to reach net-zero target by 2050. R recently in 2020 China has committed to reach carbon neutrality by 2060, whereas Fiji and Chile are amongst the countries who have yet to approve their net zero targets. Figure 1.1 presents the projections of expected warming of the earth by end of the century against current policies and pledges by the countries.

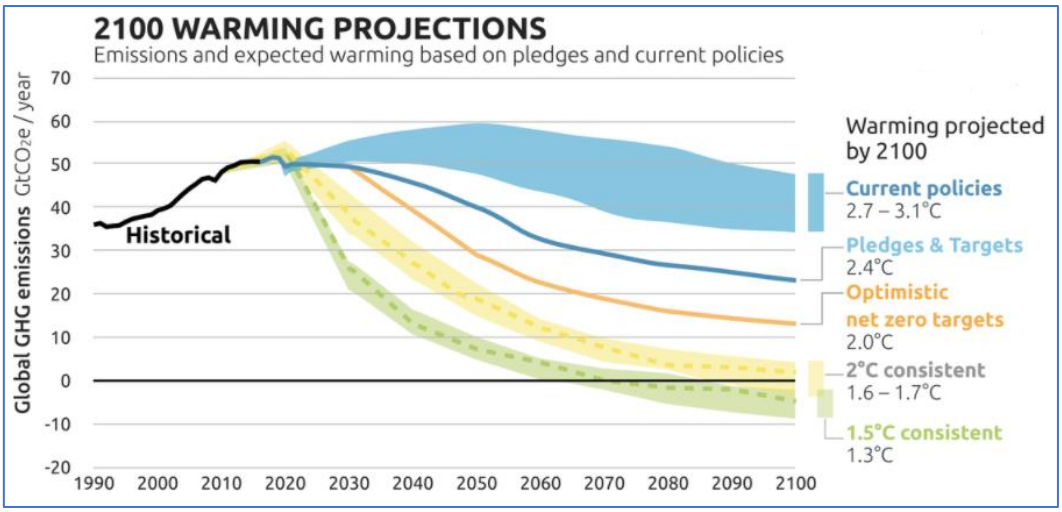

Figure 1-1 emission and expected warmings by 2100 [11].

The recent data presented in [4] shows the positive outcomes of the efforts made by countries to combat global warming. In 2020 there was an overall drop of 4.4% in coal fired generation, the largest decline ever in the past 50 years. Majorly the European union was responsible in contributing 23% of this decline and United States accounted almost half of the global net decline with the decrease in coal usage due to growth of renewable energy sources. Also, projection of current policies suggests that the increase in warming will result in about 2.9°C global temperature rise. The targets and pledges and net-zero targets made by the countries would limit the warming to 2.4°C. To limit warming to 1.5°C, greenhouse gas emissions need to be reduced rapidly with effective polices and more concrete steps in place by the countries which should bring emissions to zero around mid-century [5]. Global energy consumption is predicted to increase 40% by 2050 compared to the consumption in 2010, which is a 10 to 25 trillion kWh increase which consequently will have a serious impact on climate change [6] unless a major shift away from fossil fuels takes place. Also, the CO_2 emissions are

likely to increase to 43.08 billion metric tons in 2050 compared to the emissions in the year 2018 which was 35.3 billion metric tonnes [7] unless serious action is taken. This will lead to environmental issues such as the melting of polar ice caps, extreme weather patterns, more acidic oceans, and an increase in sea level. Despite formal commitments, for a country to reach net-zero targets, there is need of urgent and effective policies to reduce emissions. The contribution of coal fired plants in the UK to electricity generation mix was 40% in 2012 and this has fallen to 5% in 2018 which is a significant step to reduce greenhouse gases [8].

In the countries outside the Organisation for Economic Co-operation and Development (Non-OECD), the increase in energy consumption is mainly due to rapid population growth, strong economic growth, and increased access to the energy market. By 2040, Non-OECD countries are expected to account for 64% of the 780 quintillion joules of total world energy consumption [3]. According to International Energy Outlook 2019, energy consumption by transportation is expected to rise 40% by 2050 compared to the consumption which will be largely driven by the Non-OECD countries which accounts for 80% of the increased consumption [9]. In the OECD countries, the growth in energy consumption is slower due to slower economic and population growth, more efficient energy systems, and less growth in energy intensive industries [10]. Amongst all regions of the world, Asia is the biggest consumer of energy due to it being the largest region by population and having a majority of non-OECD countries (Singapore, Thailand, Indonesia, Philippines, etc) and the largest energy consumers such as India and China. Figure 1.2 shows the global trend of energy consumption in regions of the world for more than 53 years.

Additionally, over the last decade, 70% of the total electricity generated is reported to have been still sourced from fossil fuels [11]. Depletion of fossil fuels and unexpectedly changing of oil prices motivated the world to prioritise the effective use of renewable energy sources and fossil fuels and to make a dramatic shift from fossil fuels to clean and reliable fuels. To meet carbon reduction targets and considering the

serious changes in climate globally and never-ending energy demand, the future energy generation should progress with less dependence on fossil fuels with the growing use of renewable energy sources.

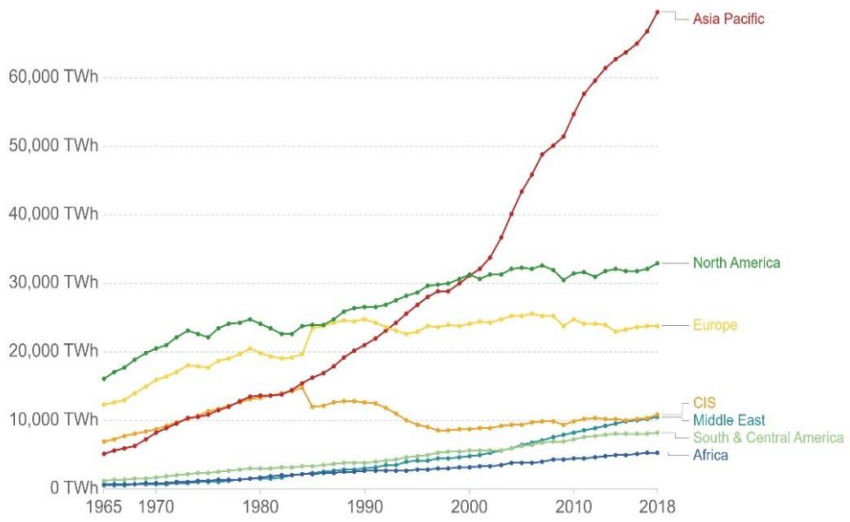

Figure 1-2 Energy consumption in world regions [12]

For clean energy, renewable sources are the promising options but their technical and economic challenges are of serious concern when implemented them on large scale [13, 14]. However, the share of environmentally benign renewable energy sources, for example wind and solar, is still not significant growing from a very small base. Figure 1.3 shows the share of energy sources in energy production up to 2018. Therefore, it is a matter of serious concern to fulfil the increasing global energy demands with alternative arrangements for power generation. According to the recent report of the International Energy Agency (IEA) in 2018, 10159 trillion kWh energy was produced from coal and 783 trillion kWh from oil which is the biggest share compared to the generation from other resources such as solar PV, hydro, biofuels, and others [15].

To achieve sustainable energy generation, renewable energy technologies are expected to take the leading role in future energy generation. Renewable energy (RE) is obtained from natural sources having huge potential for clean power generation employing technologies such as solar, hydro, biomass, wind, and tidal energy. Due to their dependency on seasonal variations, and intermittent power output, RE affects

the operational characteristics of the microgrid. However, the use of RE is expected to grow rapidly from 2018 to 2050 and will rise by an average of 3.6% per year. It is reported in [10], that the countries including the USA, OECD Europe, India, and China will have 75% of the world's RE generation by 2050. Moreover, the global installed capacity of wind energy has increased 59% in 2020 compared to 2019 bringing total wind power capacity up to 743 GW. This includes 93 GW of new installations and the global cumulative installations are expected to reach 1 TW before 2025. It is also reported that offshore wind technology can provide 10% of the required carbon reduction by 2050 for the 1.5^{0}C pathway [16].

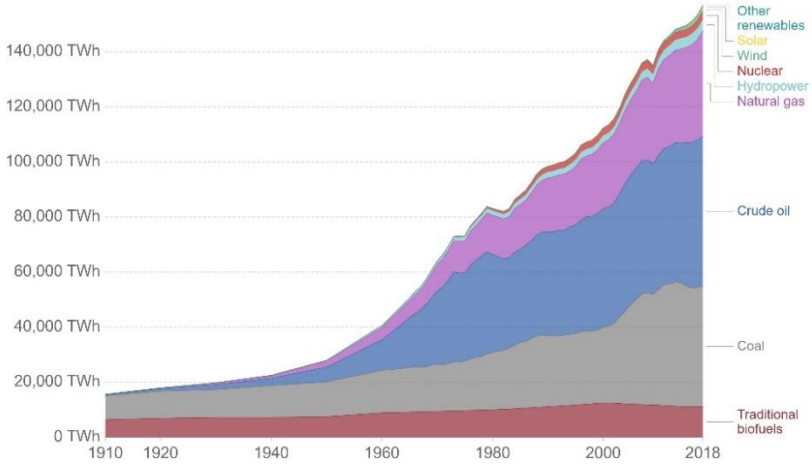

Figure 1-3 Energy production by source [12]

On the other hand, solar energy is expected to accelerate during 2023-25. Solar PV and wind energy are on course to surpass natural gas generation by 2023 and coal generation in 2024. Solar PV alone is expected to account for 60% of all renewable capacity additions by 2025 [17]. It is reported in [18], that the total installed capacity of solar PV was 627 GW with new annual additions expected to reach 149 GW by 2022. By 2025 renewables will be the largest source of electricity generation globally and will overtake coal, they are expected to supply one-third of the world's electricity demand [17]. Followed by US and EU, China alone accounts for half of the global increase in renewable electricity generation in 2021, The RE is also set to reach 8,300TWh by the end of 2021. Figure 1.4 shows the contribution of countries in

renewable energy by technology around the world , the solar PV and wind energy contribute two-third of the total growth [19].

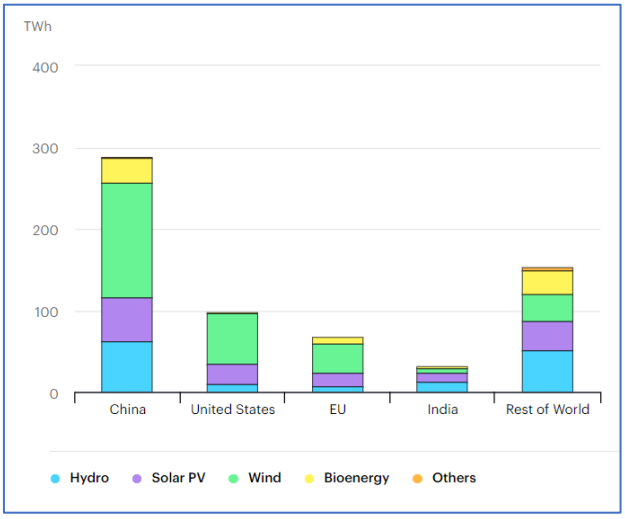

Figure 1-4 Contribution of countries indifferent renewable energy sources until 2021 [19]

The curtailment of high emissions of CO_2 has driven the transition from centralised large power generation to decentralised (distributed) small scale generation of power. Distributed generation ideally occurs from renewable sources and is typically located in low voltage networks in distribution systems close to the consumers [20]. This concept increases the penetration of renewable energy (wind and PV) leading to cleaner energy generation and reduction of greenhouse gases and leads to emergence of microgrids. Implementation of microgrids is growing fast as blackouts and power interruptions become frequent due to extreme weather conditions and aging power system infrastructure. The use of distributed generation systems is rapidly penetrating commercial, residential and industrial sectors in form of small wind turbines, solar photovoltaics, fuel cells, backup diesel generators and combined heat and power system. The global market of distribution generation is expected to hit USD183.2 billion by 2050 with growing focus on reducing carbon emissions in power generation and transmission systems [21] with added advantage of reduction in losses of transmission and distribution systems [22]. Integration of renewable energy sources (RES) in microgrids, powered previously only by fossil-fired engines, the intermittency combined with fluctuation in demand leads to further stability

challenges which make use of RES more challenging. Also, the power generated by RES cannot be entirely injected into the microgrid at the point of common coupling (PCC), this would restrict the renewable energy production during low demand periods. There are also other several challenges in microgrid energy management due to RES technologies such as: i) RES cannot be dispatched, therefore, it must be utilised as soon it is generated ii) RES cannot respond to volatility of the electricity price iii) availability of solar and wind energy varies according to the weather conditions. To solve these problems and avoid energy wastage during low demand periods, integration of an energy storage system (ESS) with RES technologies is the most attractive option [23, 24].

ESS offers a solution, which can mitigate the effects of RES intermittency by providing a balance between electricity supply and demand [25, 26]. With large-scale ESS, energy can be stored for use in the microgrid during off-peak times and can be delivered back to the microgrid during peak times. This allows power plant generators to operate at high efficiency throughout the year and run power networks with energy security and flexibility [24]. Integration of ESS in power systems offers economic benefits when ESS shaves peak demands and avoids overload conditions. This enables power networks (transmission and distribution) to operate with increased efficiency and at rated capacity which reduces the need for further investments for structural reinforcements such as installation of more feeders and system upgrades. Also, due to the variable load and output of RES, the need for frequency regulation can be avoided with the application of ESS [27].

ESS provide a means of making the electricity supply clean and more economical. ESS provides load-shifting which not only reduces the carbon emissions but also increases the efficiency of power plants which as a result generates the maximum amount of power. ESS can also reduce the power rating of the generating engine to meet peak demand and enables power production to meet average demand and reducing generation cost [28] hence making the power microgrid cleaner, efficient and more

resilient. Also, there are various solutions proposed to ensure network stability and reliability with RES including demand management, interconnection with external grids, and ESS [29]. The issue of frequency instability has so far been dealt with the combination of ESS and demand-side management (DSM). To avoid blackouts in AC power systems, the frequency should remain within ±1% of its mean value. When connecting RES into microgrids, the lack of inertia in microgrids results in system instability, blackouts or loss of generating units. Therefore, microgrids need a special control mechanism to emulate inertia and rapidly inject or absorb power in the system [30] [31]. In remote areas which are located outside of the national grid network there microgrids rely heavily on diesel generators. However, a fast response ESS can eliminate the need for running diesel generator for 24hrs resulting in cost savings and improved system reliability.

Given future large installations of renewable power plants in major electricity consuming countries such as the United States, China, Europe, and India, it will be necessary to install an additional 310 GW of grid-connected storage to meet seasonal, daily, and hourly electricity demand. Global growth in the ESS market is exponential, annual installation of energy storage in 2017 was 6 GW from base of 0.3 GW and it is expected to have installations of 20 GW by 2022 [37]. With rapid technological development in different emerging ESS technologies and estimated per unit cost reductions, energy storage systems are proving to be a practical and useful, if not essential technology for power systems. Governments of the European Union (EU), United States (US), Japan and Australia have granted their national programs on ESS recently and storage is estimated to increase by 10-15% of countries like US, EU countries and Japan [32].

There are a range of systems available to provide energy storage, which can convert, store and deliver energy on demand. The performance of these systems depends on the amount of energy they can store, the storage time, and the delivery of energy with minimum losses [33]. Therefore, high power capability, high efficiency, low capital

cost, and environmentally friendly attributes improve the value of ESS [34]. The techno-economical evaluation of energy storage requirements has been based on the implementation of renowned technologies such as compressed air energy storage (CAES), pumped hydroelectricity storage (PHS), battery energy storage system (BESS), and Flywheels [35]. Figure 1.5 shows the duration of storage of different energy storage technologies with their respective area of applications.

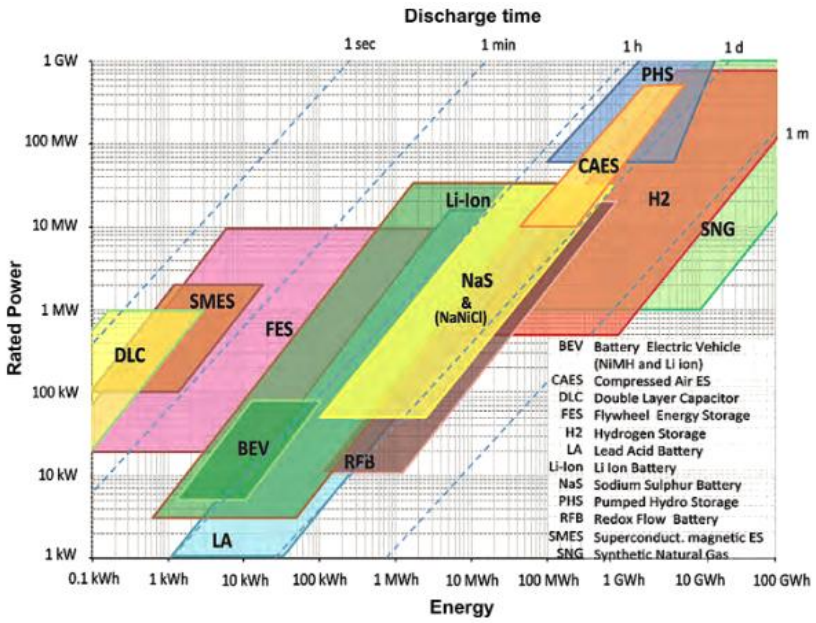

Figure 1-5 Charge and discharge times of energy storage technologies[36].

Battery energy storage systems (BESS) are one of the oldest forms of storage technology, BESS are suited for electrical energy storage applications [32]. Battery energy storage is mature storage technology with high voltage and high energy density, they are categorised based on the electrolyte material, the various types include Sodium-sulphur (NaS), lead-acid (Pb-acid), lead-carbon, nickel-cadmium (NiCd), flow batteries, zebra batteries (Na-NiCl2) and lithium-ion (Li-ion) batteries [37]. NiCd and Pb-acid batteries are used to provide pulse power however, they are large and heavy compared to Li-ion batteries, apart from this, they contain toxic metals which are not environmentally friendly. However, Pb-acid batteries can be almost fully recycled very effectively. The NaS battery is smaller in size and lighter compared to NiCd and Ni-MH batteries but has to operate at high temperatures such

as 300°C and constant heat input is required to maintain a molten state of electrolytes, also Zebra batteries have a similar problem [38]. Li-ion batteries are commonly used for storage solutions, they have the highest energy density and charge and discharge efficiency at 95% [39]. Li-ion batteries with appropriate electronics control can provide energy storage for the duration of one to two hours allowing additional revenue streams such as arbitrage, load shifting, and other electrical grid ancillary services. The requirement for long periods of storage duration have made it difficult for flywheels and supercapacitors to compete with Li-ion batteries. Whether or not technologies other than large-scale Li-ion might be able to meet the growing future storage needs is a question? The answer to this question is not so simple since there are technological advancements that affect future developments with great interdependency. Moreover, recycling Li-ion batteries and their manufacturing from questionable sources is already a matter of serious concern [40].

It is still a matter of debate that lowering the C rating (kW/kWh) would enable Li-ion to meet 8 hours storage need with the fast response but this would increase the cost of the system. Moreover, reduced capital cost of ESS, lower CO_2 emissions in manufacture, ease of recyclability and lifetime over 20 years are desirable attributes of ESS. Currently, Li-ion is not able to meet these characteristics. Storage technologies having the above-mentioned attributes include pumped hydro, flow batteries, engines or fuel cells running on renewable fuels, and compressed/liquid air. However, none of these technologies have fast response capability in terms of sub-second ramp up from start up. To make most of the storage system and minimize its capacity and cost it should be used many times a day, to allow power to feed into the microgrid during high demand and allow time-shifting of the demand [41]. The ability of the ESS to provide multiple cycles a day and have fast response has become more important in weak power grids and remote areas of developing countries which have no transmission infrastructure and power grid but rely on diesel engines and renewable energy augmentation as means of power sources. Given the requirement from the

energy storage technology may be as low as minutes of storage, flywheel technology could offer an alternative to battery systems. Part of the reason for this is that the diesel engine is generally already available so can be used to provide power during periods of no or low renewable generation. More will be explained about this hypothesis after introducing flywheel technology.

A flywheel is a simple device with a rotating mass that can maintain its inertia to store energy in the form of kinetic storage. The flywheel stores and gives back electrical power during charge-discharge cycles, the transfer of energy to or from the flywheel taking place through an electrical machine (motor/generator). High energy efficiency, high energy, and power density are the main attributes of the flywheel technology which enable it to compete with other storage technologies in power, space satellite, and transportation applications. The most common applications of flywheel technology are power quality improvement and uninterruptible power supply (UPS), in these applications electrochemical batteries and Superconducting magnetic energy storage (SMES) are major competitors of flywheel energy storage systems (FESS) [42]. SMES technology offer high efficiency but less energy density they are not economically viable [43]. Figure 1.6 compares the power density vs energy density region for flywheels with other fast response energy storage technologies.

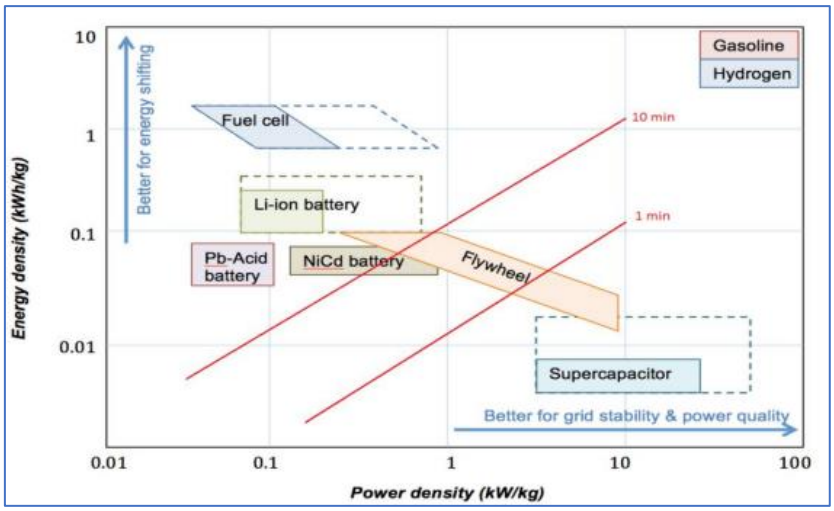

Figure 1-6 Power density and energy density regions [44]

In FESS, the size of the electrical machine determines the maximum power level. Very high-power levels can be achieved even with a small flywheel if the storage time is short (10s sec to minutes). To reduce windage and aerodynamic losses, the rotating assembly of the FESS is placed in a containment held at vacuum pressure. The majority of the frictional losses created by the bearings can be minimised by using suitable bearing technology such as permanent magnet passive bearings to take the majority of the load with lightly loaded bearings providing rotor stabilisation. The energy stored by a flywheel depends on the speed and inertia of the flywheel. The performance of FESS is not affected by high temperatures, they can typically operate at any ambient temperature with a simple water-cooling system for the electrical machine and power electronics. Moreover, losses developed in an electrical machine can be minimised by design choices and the type of the machine.

The flywheels can be good candidates for the improvement of power quality and to facilitate distributed generation (DG). As power line disturbances last less than 10s and the 5-second time interval is sufficient for the plant to switch smoothly from one power source to another, for bridging this gap FESS technology can supply short-term reliable storage (seconds to minutes) to facilitate switching of a power plant from one power source to another.

For several other reasons, flywheel technology may be a better storage technology than battery systems. The life of the flywheel is 3-5 times more than the battery system. The FESS can deliver a large amount of short-term stored energy. Unlike FESS, the performance of BESS is affected by many factors and importantly the temperature [45]. Hence, the BESS is less favourable in countries where temperatures are high throughout the year and it cannot withstand high charge-discharge rates [46]. The probability of a battery storage failure is seven times more likely than that of flywheel storage which makes BESS less reliable than FESS [47]. Power flow in the FESS is generally limited by power electronics, the performance of the flywheel is independent of the depth of discharge (DoD), it can withstand frequent load

variations by shallow or deep discharge cycles. In contrast, frequent load variations are challenging for electrochemical batteries as power is limited by their electrochemistry therefore combination of high and low power loads makes optimisations of the design difficult. Also, determination of the state of charge (SoC) of the battery is more difficult than of the flywheel.

The cost of the ESS is however, generally the deciding factor in selecting the storage technology. The commercial viability of flywheel technology depends on the possibilities of cost reduction compared to other storage technologies. A flywheel can be a viable solution for energy storage when two conditions are met; i) Deployment of flywheel technology provides an economic return which consequently gives rise to its market. ii) It provides a cost-effective solution when compared to other storage technology i.e. batteries. Costs of batteries have reduced significantly in recent years and have the added advantage of durations of around one to two hours so they may provide power for longer periods. The considerable cost reductions in materials that are used to produce flywheel rotors are more likely with advancement in materials. The important factor affecting uptake of the flywheels is their cost reduction challenge which can be overcome by large scale manufacture and low-cost design. The cost of electric machines and their associated power electronic interfaces have a major impact on overall cost of the flywheel, therefore, developing high voltage transistor (MOSFETs) can lead to reduced cost and losses [48]. Also, improved size and specific energy of the rotor materials can further reduce the cost of bearings and housings which can bring down overall cost of the flywheel.

The applications where flywheels are effective technically and cost-effective are microgrid power management, commercial power management, uninterruptible power supply (UPS), mobile applications, and commercial power management. Furthermore, the increased use of ESS and electric machines in transportation (Electric vehicles) has considerably impacted the supply chain of power electronic drives which are used in machine drives and magnetic bearing of FESS. Over the last decade,

the cost of the power electronics machine drive has dropped and is near to $5/kW [49], this can lead to further cost reductions of the flywheel technology and making it more competitive to the battery system.

1.2. Problem Statement and Research Questions:

The objective of this research is to determine whether flywheel energy storage offers a solution to enable the decarbonisation of microgrids in countries with weak or partially existent grids. It is proposed that a microgrid, currently serviced by diesel generator power, is transformed to one in which energy is provided predominantly by intermittent renewables, with such a system enabled by employing flywheel energy storage and diesel engine back up. The storage technology of choice for the energy storage system would be a Li-ion battery or possibly Lead Acid but this research anticipates the potential of significant cost reduction for flywheel systems and the need for more robust forms of energy storage as needed in less developed countries.

Li-ion batteries are the common choice for energy management applications due to having longer storage duration. As the performance of chemical batteries is temperature sensitive and they need to be thermally maintained, in the countries where the temperature remains high, control of the batteries to avoid overheating is difficult. Also, the recycling of batteries in developing countries is lacking or being done without following necessary protocols which are very unsafe. The following cases have been identified where flywheel technology could be the better choice compared to chemical batteries.

1.2.1 Energy management in islanded networks

In a standalone PV system, the intermittent output of the PV dictates that imbalance between supply and demand will occur regularly. If the PV output exceeds demand, excess power can be dissipated so there is no issue. However, if PV power is not sufficient, another source of power is required and a diesel generator (DGen), typically already existing can be used as a backup power source, potentially operating on

renewable fuel. However, without any storage system, such a system will be unstable and will not be able to provide an uninterrupted supply. By adding a flywheel, power is not interrupted and, if the PV system is still no longer providing sufficient supply, the DGen can be started. For short imbalances, either excess peak loads or PV drop out with cloud passing, the flywheel can bridge the gap and the DGen does not need to be started. The flywheel can limit the operation time of the generator considerably by charging from excessive PV output power and then discharging when the demand is higher than PV power.

1.2.2 High lifetime and operation cycles

If the chemical battery is used as the ESS for the energy management application which requires a large number of cycles and high DoD, it would degrade very quickly. Therefore, FESS with a high life cycle can be the sustainable choice over the battery as an ESS.

1.2.3 In weak grids

Remote areas of developing countries with highly intermittent power demand having no grids or weak grids, there the electricity is supplied inefficiently by a DGen. The flywheel working as ESS in the system can increase the efficiency of the DGen by making it operate near its maximum output power during charging.

This thesis presents the research work on flywheel energy storage for energy management applications. In this research, a model of the flywheel is integrated into an islanded system consisted of a standalone solar photovoltaic (PV) system, diesel generator set (DGen), and the flywheel providing backup storage for the variable residential load. Modelling and simulation of flywheel storage systems integrated with a standalone PV system and the diesel generator are focused specifically in this research. The key purpose of the flywheel in the islanded network is to increase the reliability of the system and reduce the operation timing of the diesel generator (for reduced fuel consumption) to meet the residential load demand.

The type of machine used in the electrical drive plays an important role in the characteristics governing electrical losses as well as standby losses. Permanent magnet synchronous machines (PMSM) and induction machines (IM) are the two most common types of electric machines used in FESS applications where the latter has negligible standby losses due to its lower rotor magnetic field until energised by the stator. For this reason, the type of electrical machine employed in the FESS used in this research was the IM. More will be explained about this choice later in the thesis.

The following questions are to be addressed to achieve the objectives of the research.

1.3 Research Questions

The direction of the research is set by the formulation of the following questions. The research questions are addressed by a methodology which is defined in the section.

- What are the technical benefits of flywheel technology compared to other energy storage systems in microgrid applications?
- What are the suitable strategies to integrate flywheels in islanded standalone PV systems?
- What are the design methods of hybridization of the flywheel with a PV system?
- Where does flywheel stand in competition with other slow responding ESS for long-term storage applications in the energy storage market?
- What are methods of control of the flywheel with other power sources in the islanded network?
- How can induction machines can play their part in reducing the total losses of the flywheel system by minimising standby losses?

1.4 Methodology

The above research questions were addressed by following the research methodology now described in this section. To analyse the application of flywheel technology in an islanded network together with other power sources (PV and DGen), different

operation scenarios were created to perform charge-discharge operations of the flywheel and the following steps were followed to reach to achieve the final results.

- A thorough literature review was conducted into the history and emergence of the flywheel technology leading to a clearer understanding of the main features and applications of the flywheel. The other storage technologies which are competitive to the flywheel were identified and compared.
- A comprehensive study was carried out to get a proper understanding of electrical machines used in FESS and their controlling techniques. This led to identifying the research gap in choose the suitable electrical machine and its associated control methods.
- For analysing the performance of the flywheel (charge-discharge cycles), modelling of the entire assembly of FESS was carried out through mathematical modelling techniques. This includes modelling of electrical machines, controlling techniques of the machine and power electronics converters, loss calculations and analysis of bearings systems and the machine, and the mathematics of rotor and requirements of the flywheel housing. The FESS was simulated in MATLAB/Simulink environment to perform operations based on real-life scenarios to test the fitness of the model in energy management in microgrid applications.
- For an islanded network, models of the PV system and diesel generator were developed. The analysis of their performance and control techniques have been discussed. Before incorporating the model of the flywheel system into an islanded system, the performance of the model of each power source was evaluated separately to evaluate the competence of an islanded system.
- To ensure maximum accuracy in the results the source of the parameters of each model was chosen very carefully. The parameters of the solar PV system were taken from National Renewable Energy Laboratory (NREL) System Advisor Model (open source). The parameters of the diesel generator were used from the

manufacturer's datasheet. Based on the available parameters, fuels consumption and efficiency of the diesel engine can be easily calculated.

- The data for the residential load was sourced from the high-resolution CREST model produced by Loughborough University. The model contains integrated thermal-electrical demand (diversity) with the timing of output variables appropriately correlated by occupancy, irradiance, and external temperature sub-models. The data for the load profile is generated by defining the type of day of the week, the month of the year, and the number of dwellings. Switching events of lighting, appliances, and water-fixture (hot and cold water) are calculated on basis of stochastic sequences of occupancy for each dwelling which determines electricity demands of dwellings. The CREST demand model uses a bottom-up methodology for simulation of switching of individual appliances to create spikiness. Based on the residential load demand data obtained from the CREST model, different load profiles were created for various months of the year and days of the week to analyse the dynamic performance of the standalone PV system. The data of the load demand was considered to be of a small town in a remote area consisted of 100 dwellings, representing a village. The model generates the load demand data based on occupancy and activities of the consumers in homes. The model considers all types of consumers in a developing country, in this case India.
- To optimize the performance of islanded networks the coordination between power sources should be well defined in the control system. The logical control system was designed for proper coordination between the flywheel, PV system, and diesel generator. It was done by creating different operation strategies and logical conditions.
- After the formation of the islanded model, selection of input data, and development of a logical control system, simulation of the islanded model was performed in MATLAB/Simulink environment. The performance of the solar PV system, the flywheel storage, and the diesel generator and their control systems were analysed.

1.5 Structure of the thesis

The structure of the thesis is set as follows:

Chapter 1 Introduction: This chapter contains the background of world energy consumption, climate change crisis, the importance of renewable energy sources and energy storage systems in microgrids and effect of reduction in their inertia with penetration of renewables.

Chapter 2 Literature Review: This chapter contains the literature research of current storage technologies, their comparisons, current development, and research being done for flywheel energy storage, research gap, and contribution of our research to address those gaps. A brief review of microgrids, its components and applications has also been added. Also, this chapter describes flywheel technology, components, and its attributes supported with data and figures. The detailed review on applications of flywheel technology has also been presented in this chapter.

Chapter 3 Modelling of Flywheel Energy Storage System and its Validation: This includes an introduction to control systems, types of control systems, mathematical modelling of the induction machine, mathematical modelling of a control system of induction machine, PI controller, voltage controllers, speed controllers, torque controllers, and their schematics. The implementation of mathematical model of FESS is then implemented in MATLAB/Simulink software together with validation of the model supported with result and analysis.

Chapter 4 Modelling of PV Hybrid Microgrid: This chapter includes introduction on modelling of microgrids, methods of modelling, Mathematical and Simulink modelling of components used in microgrids (Loads, diesel generator and PV) and their validation in MATLAB/Simulink supported with results.

Chapter 5 Results and Analysis: Presentation of results, analysis of results and discussion, and then conclusion together with detailed results and figures.

Chapter 6 Conclusion: This chapter provides a conclusion of each chapter, summary of work done, achievements in the research and recommendations of work to be done in future research.

Chapter 2

Literature Review

This chapter provides a comprehensive literature review of energy storage technologies and their comparison, an overview of microgrids, the brief history of flywheel technology, its technical characteristics and applications. The chapter concludes with a chapter summary.

2.1 Overview of Energy Storage

The growth in energy generation from renewable sources has been remarkable worldwide but these cannot easily follow and be adjusted to match load demand. However, decentralised power generation from renewable sources makes the supply of the power to the consumer more secure according to Ibrahim *et. al* [50]. Solar and wind energy are the most abundantly used renewable sources for electrical power generation but still the power generated by solar and wind is uneven due to their variability and dependence on nature (wind speed and interruption of solar irradiance by clouds and nightfall). They cannot produce power evenly as their power production varies with minutes, hours, months, days and seasons. Figures 2.1 present typical example of variations in power generated by a wind turbine, making it less reliable to be qualified for stable and primary sources and power generation.

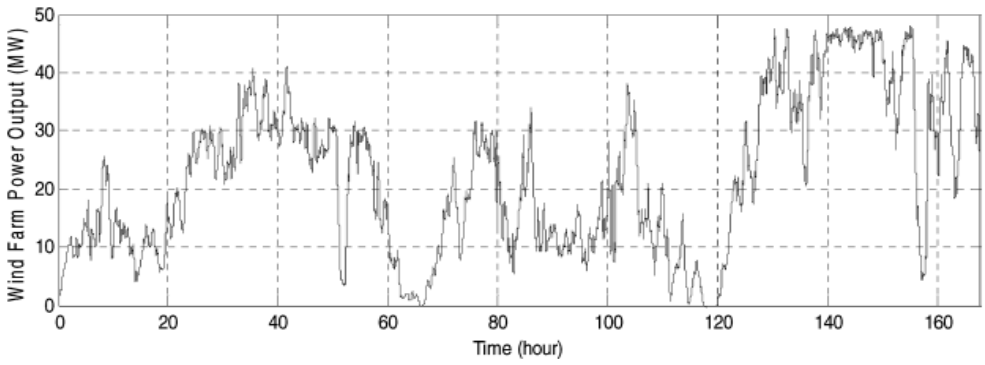

Figure 2-1 Hourly generated power of wind turbine [4].

Figure 2.2 presents the power output of solar PV on a typical cloudy day. It can be seen that the availability of solar power cannot be guaranteed over 24 hours of time.

Considering the rapid growth of renewables globally, clear policies and research and development are required to ensure the secure and cost-effective integration of renewables into the power system.

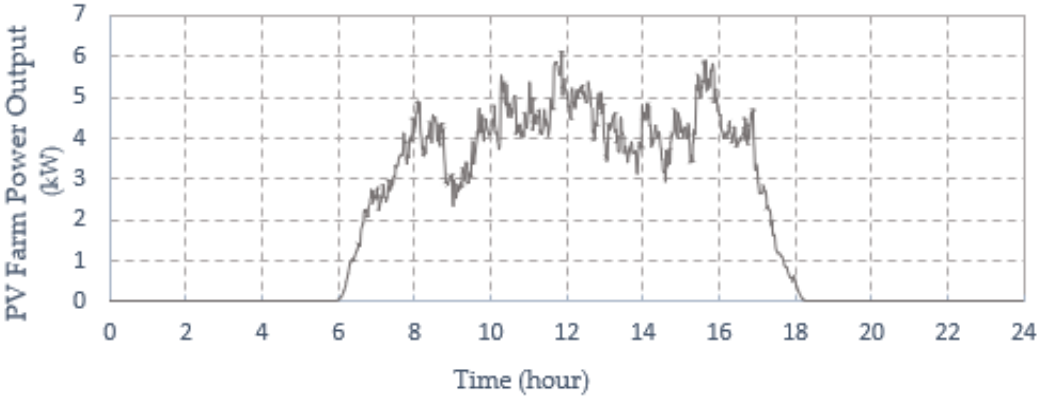

Figure 2-2 Hourly generated power of PV system [51].

The commercial market of RES shows that the specific investment cost is declining. Atanasoae *el al.* report in [52] that the installation cost of utility scale PV projects decreased by 68% from 2010 to 2017. Apart from the cost the demand of renewable energy increasing too, according to a report of IEA [53], there was 1% increase in renewable energy demand globally in 2020, while the global energy demand is set to decrease 5% due to lower economic activities in 2020. Increasing the penetration of renewable energy sources in any power system will lead to need for regulation of the power supply.

Also, the intermittent nature of RES creates challenges to the stability of the power system when integrated. To deal with the alternating nature of RES at a large scale, several solutions are proposed. In [54], Muljadi *et al*. propose the integration of wind power plants to weak power grids via bulk transmission lines without reducing stability, this allows higher penetration of renewables. However, the proposed method is expensive due to the higher level of energy in magnitude involved to make it profitable. Anderson *et al.* in [55] purpose a fast forward algorithm to improve forecasting which reduces the dispatch errors; however, this does provide full economic opportunity to the power generator. Hydropower can mitigate the

variability of RES by quickly responding to some of the fluctuations in wind power outputs [56]. In [57], Ding *el al.* have proposed a new coordination operation mode of the wind farm and hydropower based on day-ahead wind power output forecast to alleviate the negative effects of wind power fluctuations on the microgrid. However, the hydro resources are limited and their location of installation is a great challenge. An increase in dispatchable backup power might increase the ability of the system to cope with dispatch error, however, it increases greenhouse gas emissions, since these units require fossil fuels for power [58]. The solution presented above provides some relief against the intermittent nature of RES, however, they do not mitigate all challenges presented by them. Amongst all the solutions, electrical energy storage (EES) has been recognised as one of the most promising and viable solutions which can mitigate the intermittency of RES and can provide stability to the electrical power system. EES denotes a process of converting one form of energy to a storable form and storing it in some mediums and when needed the stored energy can be converted back into electrical energy [59, 60]. With the integration of energy storage devices in the microgrids, short-term random fluctuations can be avoided and electricity can be stored and utilised to meet the varying demand and accommodate the peak demand. ESS can provide multiple other benefits such as reduced consumption of primary fuel, improved efficiency of the system, reliable energy supply and reduced damage to the environment. While choosing storage technology for any application several factors are considered and analysed, those factors include life cycle, self-discharge rates, environmental impacts, lifetime, power, energy, efficiency, storage duration, technical maturity and capital cost [61, 59].

There are several well-established energy storage technologies and many developing technologies having huge energy storage potential for electricity production. There are four main classes of energy storage technologies, namely electrical, mechanical, chemical and thermal storage technology, each offering different advantages and

disadvantages. Figure 2.3 shows the detailed classification of energy storage technologies.

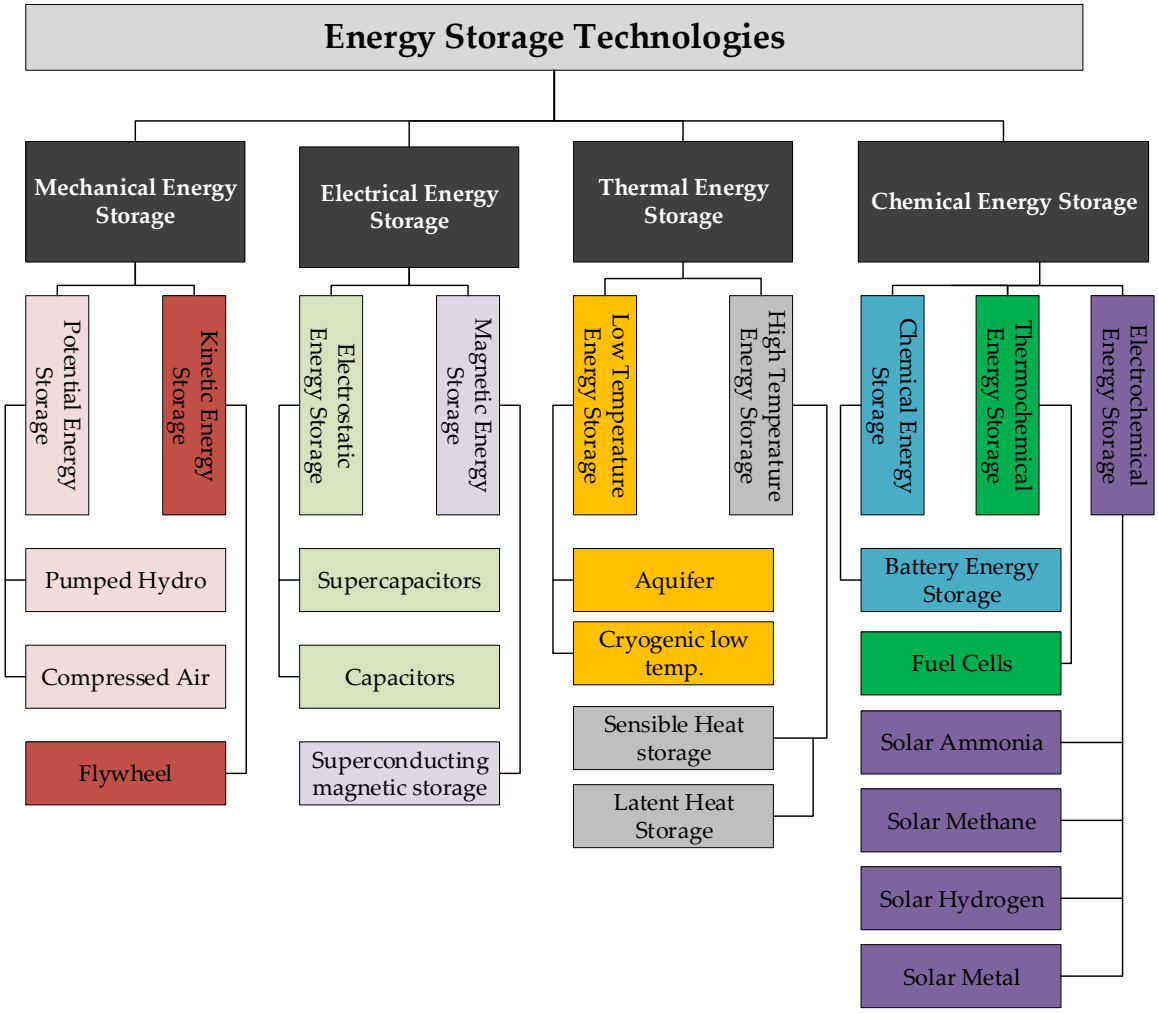

Figure 2-3 Detailed classification of energy storage technologies

2.2 Description of Energy Storage Technologies

2.2.1 Electrical Energy Storage

Electrical energy storage (EES) systems store energy to produce electricity and release it when it is needed. ESS can be further classed as electrostatic including capacitors and supercapacitors, magnetic storage which includes superconducting magnetic energy storage. Each of these is described briefly below in sections.

Capacitor and Supercapacitors

Capacitors store energy in an electrostatic field in a dielectric material, energy stored in capacitors depend on the breakdown characteristics of dielectric material [59] [32].

Capacitors have high power density, short charging time, low energy density and high self-discharge losses. Due to low energy density, capacitors can only deliver high currents for short periods [62]. Capacitors can be used for power quality problems and energy recovery systems in mass transit systems [59]. For large energy storage capacity, a very large area of dielectric would be required which makes use of capacitors uneconomical [32].

Supercapacitors have a working principle similar to the ordinary capacitor except the dielectric material is replaced by an electrolyte ionic conductor which helps to produce ionic movement along conducting electrodes with large specific surfaces providing higher energy density [63]. In supercapacitors, energy is stored in the form of polarised liquid which is formed when voltage is applied to the terminals of the capacitor [64]. Supercapacitors can be connected to form storage modules that can be added together for energy storage units. The performance and life of the supercapacitor are temperature-dependent. In reference [65], authors have demonstrated that how the super capacitance is affected by temperature variations and it has been concluded that energy storage in a supercapacitor is reduced for lower temperatures. In comparison with battery technology, supercapacitors can provide energy for few seconds to minutes and the life cycle of a supercapacitor is up to 10 years, with high efficiency. They have a high estimated cost and self-discharge rate plus low voltage ratings (2.5Vdc) [66]. Supercapacitors also can provide high peak power output and high charge-discharge cycles without damage [67]. Supercapacitor energy storage can be used for power quality applications because of its ability to provide energy for a short duration, supercapacitor technology with high energy densities over 20kWh/m^3 is yet under development [68]. With the advancement in research and materials supercapacitors can be promoted in grid-scale applications, the main drawback of supercapacitors is high self-discharge loss, short storage duration and load energy density [32] [69]. However, researchers at the Massachusetts Institute of Technology have developed a new class of ionic liquids (electrolyte) that may

improve the efficiency and stability of supercapacitors while reducing their flammability along with improved energy density [70].

Superconducting magnetic energy storage (SMES)

SMES is based on the use of superconductors, offering the lowest resistance to electronic flow which reduces the losses nearly to zero, energy storage taking place in the magnetic field of a DC current flowing in a superconducting [71]. SMES technology has high efficiency up to 95% and it offers a very rapid response and high power during the charge and discharge process. Due to the power requirements for refrigeration and cooling, the high costs SMES means it can only be used for short duration energy storage [72]. SMES can provide the power of 1-10MW in time of seconds, however, larger-scale storage systems of 10-100MW for time for minutes are under research and development [32]. SMES can be used for frequency stabilization, power factor improvement, UPS implementation, voltage control, improvement of transient stability [72] [73]. Figure 2.4 shows the schematic diagram of a SMES.

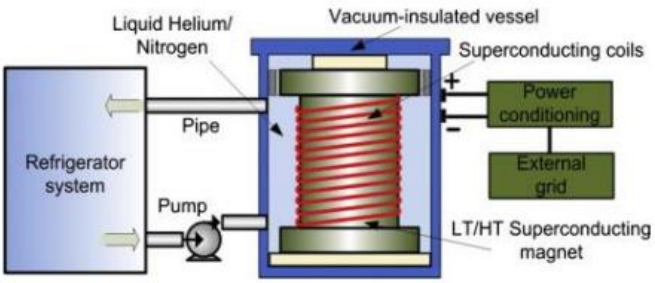

Figure 2-4 Schematic diagram of SMES system [74].

SMES can provide power from 100kW to 10 MW within 5 microseconds, they can be integrated and used with other energy storage systems which can improve their performance and peak power availability [75].

2.2.2 Mechanical Energy Storage

Mechanical energy storage systems store energy in the form of kinetic and potential energy. Kinetic energy is stored by flywheel device and potential energy is stored by

compressed air storage device and pumped hydro energy storage systems. The description of each mechanical energy storage system is given in following sections.

Compressed Air Energy Storage System (CAES)

In a CAES system, the compressor is the key component which compresses air during an off-peak time when the cost of electricity is low, compressed air is then stored in an air reservoir which is called the charging state. During discharging state plant uses the compressed air to operate its turbine. The turbine provides mechanical energy to the generator to operate which produces electricity. During the discharge state, natural gas is also burnt similarly as it is burnt during the gas generation in a conventional combustion turbine plant [63]. Figure 2.5 represents the working principle and component involved in CAES.

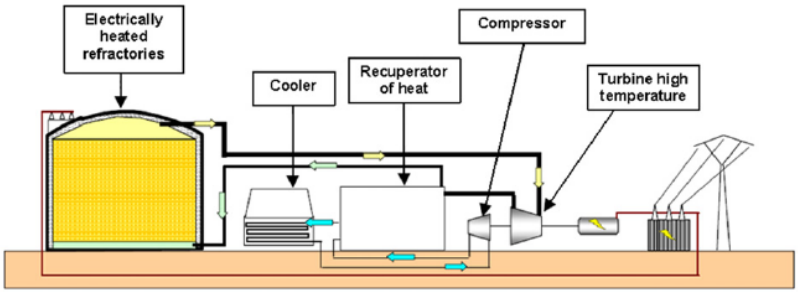

Figure 2-5 CAES system with heat storage with turbine [76].

Despite the maturity of CAES technology, it is not widely implemented in the world. Only two generation plants are in operation worldwide, 290 MW plant is constructed in Germany and another in the USA having capacity of 110MW [76]. The first utility-scale CAES 290 MW plant was installed in Germany; it operates with 8 hours of compressed air charging and 2 hours of discharge operation [59]. A Highview Power 5MW CAES system is under development in Vermont, the plant will be able to store 4000 MWhs for 4 hours. This energy storage services will be used to facilitate the integration of RES and to add stability to the microgrid by providing grid-synchronous inertia [77].

CAES is the most workable competitor for large scale energy storage after pumped-hydro storage with an estimated efficiency of 70% and a lifetime of 40 years [78]. CAES

technology offers energy storage in MWhs at low cost, according to ref. [79], an annual life cycle cost for conventional CAES plant is $215-255/kW-year and levelized cost of conventional is $96-121/MWh. CAES plants are capable of black start and have fast start-up time and CAES plants can be operated as a condenser for injecting and withdrawing the VARs from the grid. [80] A major drawback of CAES is low efficiency and access to suitable geological sites [81]. CAES operates with the advantages of a longer lifetime, high reliability, low maintenance and operation cost and low self-discharge rates. The economic feasibility and profitability of CAES depend on natural gas and electricity market prices. CAES installations with smaller ratings (<100 kW) use pressurized tanks to store energy in form of heat, whereas the large scale CAES utilize underground caverns for storage therefore, for large scale CAES geological suitability remains a significant challenge affecting the capital cost [82] [83]. Also, expansion and compression cycles of CAES is problematic as it requires extra equipment (pump cooler) which leads to energy wastage [83].

Pumped Hydro Storage System (PHSS)

A pumped hydro storage system consists of two water reservoirs at different heights. Water is pumped from lower reservoir to higher reservoir during off-peak hours when electricity is cheap. Water stored in a higher reservoir is made to flow through turbines to produce electricity during a period of high demand [84]. PHSS is a mature technology with 300 systems operating globally. The lifetime of PHSS is 30-50 years with an efficiency of 65-75% and capital costs of 500-1500 Euros/kW [63]. By 2018, the total installed capacity of PHS reached to 161 GW and it is predicted to be double by 2050 [85]. PHS contributes to more than 3% of global generation capacity [86]. The major disadvantage of PHS is the availability of a suitable location for the construction of two large reservoirs or dams [32]. However, there are advancements in technology allowing a 300 MW seawater based PHS in Hawaii to be built. PHS plants in Okinawa Yanbaru in Japan and the Mount Hope project in New Jersey are using flooded mine

shafts, underground caves and oceans as reservoirs [59] [86]. The working principle of PHS is illustrated in Figure 2.6.

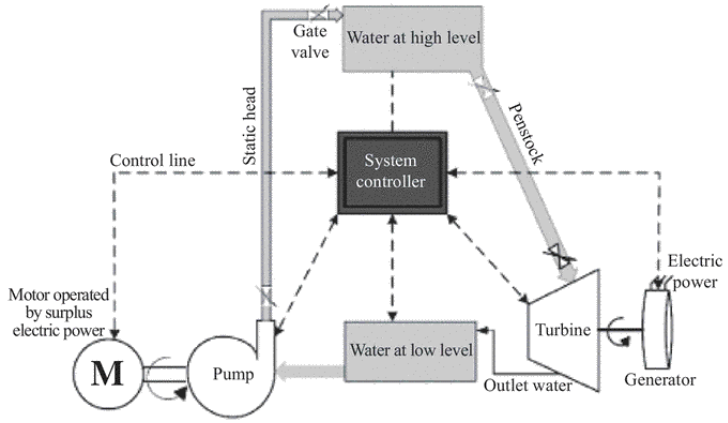

Figure 2-6 Schematic of working principle of PHSS [36].

PHS is an economical energy storage system that can be used for power and frequency regulations, they have long life, low self-discharge rates and low operation and maintenance cost with high round trip efficiency [87] [88]. PHS with its fast ramping can mitigate the challenge of intermittent power produced by RE systems. Dinorwig hydropower station in Wales can reach to its maximum generation of 1.8 GW in less than 16 seconds [89]. The Kops II PHS plant in Austria can produce 180 MW in 20 seconds [90]. The facility of quick start has made PHSS particularly useful for application in wind energy. However, high capital cost and long pack back time and uncertain profitability are the drawbacks of PHSS [82]. Also, when compared to flywheels, batteries and supercapacitors the response time of PHS is slower which makes it less suitable for behind-the-meter applications [91].

Flywheel Energy Storage

Flywheel energy storage systems (FESS) are one of the earliest forms of energy storage technologies with several benefits of long service time, high power density, low maintenance, and insensitivity to environmental conditions being important areas of research in recent years. A flywheel stores rotational energy that can be withdrawn instantaneously. A flywheel contains a spinning mass in its centre called the rotor and, to rotate flywheel at very high speed, an electric machine is required which acts as a

motor to convert electrical energy into rotational energy. This is called the charging mode of a flywheel. When stored energy is to be converted to electrical energy, an electric machine is used as a generator, it is called discharging mode of the flywheel.

The useful life of FESS technology is more than 20 years [63]. FESS has high efficiency and power density but low energy density which make it suitable for high power applications but can also be viable for energy applications [92]. In the electricity market, it is at the level of project demonstrations and is developing slowly because of its weakness such as storage for a very short duration of time [45]. Figure 2.7 shows the concept principle of the energy flow in a flywheel system although typically the motor and the generator are the same physical machine, a motor-generator or simply an electric machine.

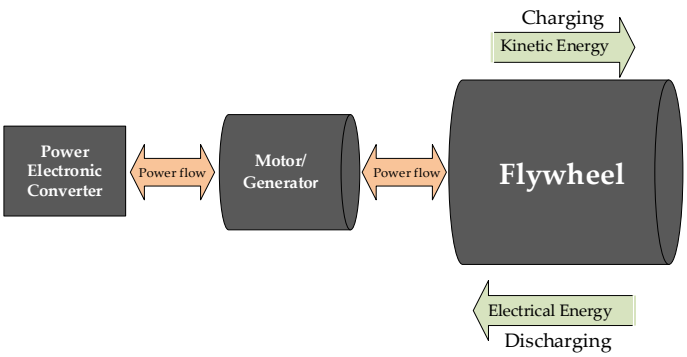

Figure 2-7 Schematic Diagram of Flywheel energy flow

Presently, flywheel materials, high-speed electrical machines, the capability of bearings and array technology for flywheels are the main areas of research focus which would make can make it the most suitable option for energy storage when compared to BESS and other ESS [59]. The main advantage of FESS technology is that it provides high charge-discharge cycles in the range of 10^5 up to 10^7 in the entire lifetime [84]. A detailed description of FESS technology is provided later in this chapter.

2.2.3 Electrochemical Storage

Electrochemical energy storage includes conventional batteries such as nickel-metal hydride, lithium-ion (Li-ion), flow batteries, and lead-acid. The following section provides a brief most widespread chemical storage option.

Battery Energy Storage System (BESS)

Battery Energy Storage System is based on power electronics that can minimize the power fluctuations in the system and increase the integration of RESs through a suitable cooperative control [93]. In BESS, energy is stored is converted from electrical to chemical energy which is stored in a battery that is made of stacked cells. The chemical energy of the battery is then converted back to electrical energy with the help of suitable power electronics control system. Batteries are rated in terms of their power and energy capacities [94]. The type of batteries most commonly used in power systems applications are Lead Acid, Sodium Sulphur, Lithium-ion, Metal Air and Flow Batteries. Within these main battery types are also many sub-types with difference chemistries and constructions.

Lead Acid batteries

Lead-Acid battery is the oldest and most mature technology [86] [95], there are currently large Lead-Acid battery installations deployed as a standard technology for grid stabilization but they are suitable for many applications [96]. The theoretical specific energy of a Lead-Acid battery is 171 Wh/kg but, in practice, it may vary from 30-50 Wh/kg due to the need for water and other components [86]. The Lead-Acid battery has the lowest cost amongst all the battery technologies. However, given limited capability, proper recycling is not a feasible option in developing countries where safe recycling is not available and it is done is a way dangerous to human health and environment. This has given Lead-Acid batteries a bad name environmentally whereas recycling is can be done very effectively to a high percentage in factories in developed countries. Additionally, Lead-Acid battery technology is disadvantaged due to the need for internal connectors and to structural grids to support the heavy

lead materials [18]. However, Lead-Acid batteries can provide reliable service for many years, the capacity of a battery improves when it reaches a peak and declines until the battery reaches its end of life. After 80% capacity reduction, accelerated deterioration of the battery occurs plus it is then more prone to high discharge rates and sudden failures. According to a general rule of thumb, above 25 ^{0}C the life of the battery is reduced by 50% for every +9.5 ^{0}C, therefore under ideal conditions if a battery aimed to run for 5 years at 25 ^{0}C will only operate for 2.5 years at 35 ^{0}C [97]. Figure 2.8 shows the lifetime curve of a battery against temperature.

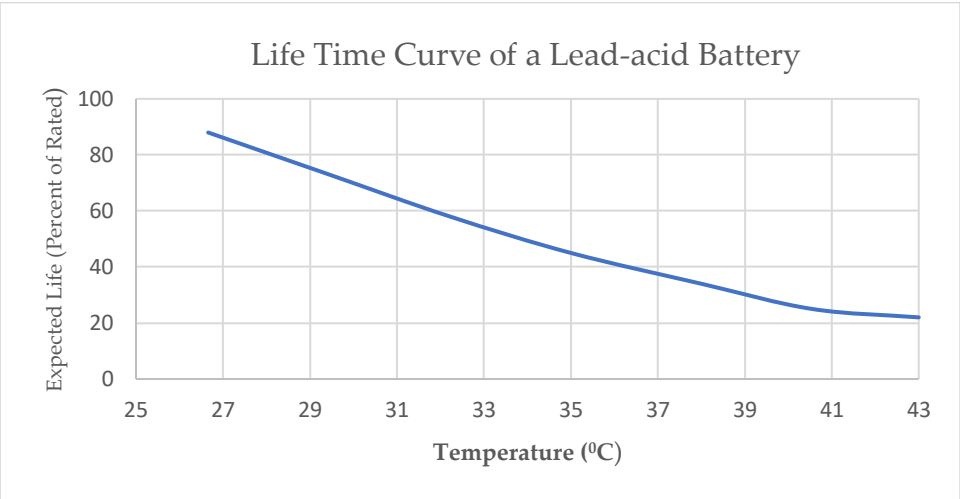

Figure 2-8 Lifetime Vs temperature characteristics for a lead-acid battery

Sodium Sulphur Batteries

Sodium-Sulphur battery technology was developed as an alternative to Lead-Acid batteries, offering high power and energy density. Sodium sulphur battery technology has a fast response (millisecond) for charging and discharging operations. Which makes it a suitable technology to be used in microgrids for power regulations. The energy density of sodium sulphur batteries is 151 kWh/m^3 and has an efficiency of 85% [63]. However, Sodium Sulphur batteries have a high-temperature requirement for operation at around 300-350 ^{0}C and high capital cost of $2000/kW according to [16]. A 350 MWe Sodium sulphur BESS has been installed by Amplex group in UAE for ancillary services [92].

Flow Batteries

Flow batteries are types of rechargeable batteries which contain dissolved electroactive species which act as an electrolyte, flowing through an electrochemical cell, converting chemical energy into electricity [92]. Flow batteries are also called redox flow batteries, they have high power and energy ratings, long duration and rapid response time (1ms charge and discharge cycle). They have lower efficiency and high losses due to the energy needed to make electrolyte flow and other chemical losses [94].

Lithium-Ion Batteries

Amongst all types of batteries, Li-ion battery technology has high efficiency (close to 100%) and the highest energy density [95]. The key parameters of Li-ion batteries are cycle life, power density, energy density and cost per kilowatt hours [98]. The use of Li-ion batteries is predominant in portable electronic devices and other energy storage applications. Li-ion batteries are the most common battery storage option globally and it dominates 90% of the global battery storage market, with ongoing advancement in materials such as replacing graphite with silicon will make batteries competitive for long-term energy storage [99]. The Li-ion battery is good for applications where response time is in milliseconds is required such as voltage and frequency regulations [100]. Figure 2.9 shows the image and components of a Li-ion battery.

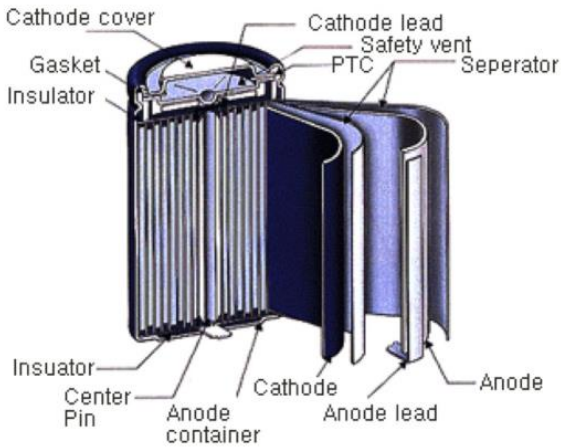

Figure 2-9 Li-ion battery structure and components [100]

The main drawback of Li-ion batteries is that their depth of discharge (DoD) cycles affect their lifetime and their overall cost, also, their lifetime is temperature-dependent and they can degrade much faster at high temperatures [59]. The performance of Li-ion batteries degrades at high temperatures and their storage capacity is decreased when overcharged, the capacity loss occurs even the batteries are unused, the ideal environment for Li-ion batteries to work efficiently is below ambient temperature, also, Li-ion batteries should not be stored when they are fully charged. At 100% charge a Li-ion battery will lose its capacity per year with increase in the temperature, Figure 2.10 shows the % loss of Li-ion battery capacity per year with increase in temperature [101].

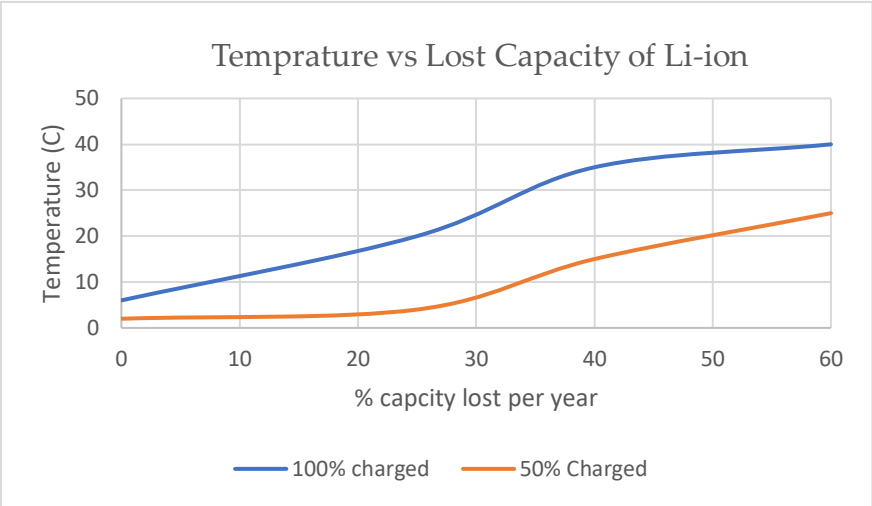

Figure 2-10 Capacity lost curve of Li-ion [101].

Also, for microgrid applications (back-up source) large scale batteries are required and there are some challenges for making large scale batteries, large-scale batteries require special protection circuits and packaging which makes the cost of the Li-ion batteries as high as more than $600/kWh [63] providing 1500 cycles, whereas, in references [14] and [32], it is reported as high as $1200/kWh for providing 3000 cycles at 80% DoD. Zubi et al. in [102] provides detailed levelized cost calculations of a 2.5kWh Li-ion battery for solar home systems, the author has reported the specific energy cost of Li-ion would drop to 1230$/kWh in 2030 compared to 1710$/kWh in 2020. However, according to world energy outlook the cost of Li-ion battery packs has fallen 90% since

2010 to $150/kWh in 2019. Also, the massive installation of batteries in EVs would reduce a 50% cost of Li-ion battery by 2040.

2.3 Comparison of Energy Storage Technologies

As mentioned in chapter 1, an ideal energy storage system should have a long lifetime, high density, high efficiency, low cost, be environmentally friendly and be mature. These all requirements are not met by any single energy storage system [16]. For any ESS with higher power and energy densities, the volume of the required ESS will be smaller for rated energy given the amount of energy [59]. Table 2.1. presents the comparison of technical characteristics of energy storage technologies.

Supercapacitors, flywheels and SMES have the highest capital cost expressed in $/kWh due to short operating times, however, they show the highest maximum efficiency. PHS shows the least energy density compared to all technologies, however, PHS systems have the highest capacity by a large margin. PHS being mature technology and has been widely implemented worldwide yet it has a low power density which limits its use to large scale ESS [15]. Also, PHS is not environmentally friendly as the construction of reservoirs affects the local ecological system and destruction of green landscape. From Table 2.1 It can also be seen that flywheels, batteries and fuel cells have relatively moderate power densities and energy. CAES and have lower densities and are mainly used in stationary applications. Capacitors and have very high-power densities but low energy densities. CAES can provide high MWhs of energy at low cost but it has low efficiency and it is suitable to accessible geological sites requiring long transmission lines distance [60].

Table 2-1 Technical Characteristics of Energy Storage Technologies [14] [76] [63] [59] [60] [96]

Technology Type	Energy Density (Wh/L)	Power Density (W/L)	Specific Energy (Wh/kg)	Power ratings (MW)	Rated energy capacity (MWh)	Efficiency (%)	Run Time (h)	Charge time	Lifetime Cycles
Mechanical Storage									
PHS	0.5-1.5	1	0.5-1.5	100-5000	500-8000	75-85	Jan-24	Hours	>13,000
CAES (Large scale)	3-6	0.5-2	30-60	300	<1000	70-89	2-4	Hours	>13,000
Flywheel	20-80	1000-2000	10-30	0.1-20	up to 5	93-95	ms-15m	Minutes	>100,000
Chemical Storage									
Li-ion battery	200-500	1500-10,000	75-200	1-100	0.04-100	85-90	m-h	Hours	4500
Lead-acid battery	50-80	10-400	25-50	0-40	0.001-40	70-90	s-h	Hours	2000
Na-S battery	150-250	140-180	150-240	<34	0.4-244.8	80-90	s-h	Hours	4500
Ni-Cd battery	60-150	80-60	50-75	0-40	6.75	60-65	s-h	Hours	3000
Electrical Storage									
SMES	0.2-2.5	1000-4000	10-75	0.1-10	0.0008	95-98	ms-8s	Minutes	>100,000
Capacitor	2-10	10,000+	0.05	0-0.05	--	60-65	ms-60m	Seconds	>50,000
Supercapacitor	10-30	100,000+	0.05-15	0.3	0.0005	90-90	ms-60m	Seconds	>100,000

Figure 2.11 shows the comparison of charge-discharge cycles and efficiency of different energy storage technologies, it can be seen that Li-ion batteries have high efficiency and charge-discharge cycles compared to other types of batteries, however, flywheels, SMES and supercapacitor technologies are better in terms of lifetime and charge-discharge cycles when they are compared to Li-ion batteries. Although, according to [19] supercapacitors have higher efficiency and a greater lifetime than flywheels, they are not suitable for microgrid applications given their very short energy storage duration and the life of supercapacitors degrades with rise in temperature [103]. The cycle lifetime of flywheels and certainly calendar life are greater for flywheels than supercapacitors according to many other reports. Also, the energy density of supercapacitors is not high, due to low energy density supercapacitors are not compact. The energy density of supercapacitors can be increased by increasing the surface area of electrode material in a double layer capacitor, which requires more research to develop materials with high surface area [103].

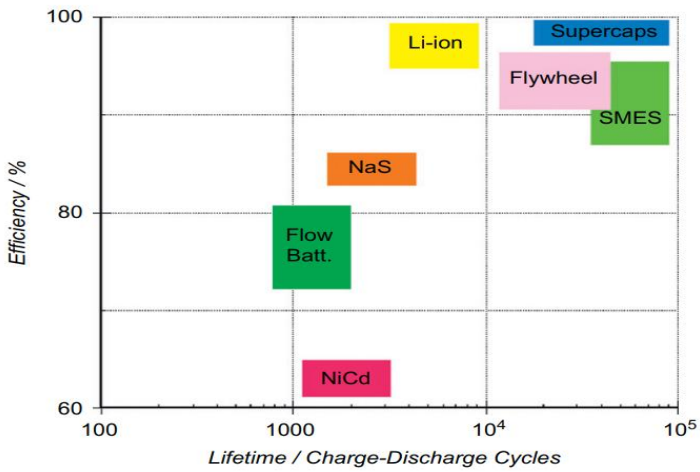

Figure 2-11 Efficiency and charge-discharge cycles of different Energy storage technologies [19].

Moreover, research in material sciences is required to come up with new electrodes and electrolytes through batteries that have considerable potential but efforts are required to make BESS more feasible at high-duty applications and reduction in the cost of ancillary products such as overcharge protection circuitry and maintenance costs [71]. Li-ion batteries having high power and energy density are suitable for

widespread use in portable devices and transportation applications. FESS is a mature technology from an electrical aspect [104], the FESS is termed as clean ESS technology, it has high efficiency and energy density compared to BESS, CAES and other ESS technologies. FESS is also environmentally friendly, unlike other ESS such as CAES, PHS, BESS, SMES and SCES [32], Flywheel consists of discs made up from metals or carbon fibres that are non-hazardous, the life cycle of FESS has an operational lifetime of several million full depths of discharge cycles according to [105].

The Li-ion battery is the most advanced technology (in BESS family) having a power density of 500-2000W/kg but it involves high cost, the lifetime of the battery is temperature-dependent therefore, it is not suitable for backup applications [84]. Li-ion batteries can be the best option for low power applications due to their lowest possible self-discharge, for systems of few kWh (in renewable systems) as shown in Figure 2.11. Li-ion can provide the best performance but it has the drawback of being expensive. For systems up to 100 kWh, along with lead-acid battery systems, CAES, fuel cells and flow batteries are preferred options but they are either expensive, have high maintenance costs or are less efficient. For high energy storage (MWh) CAES and flow batteries can be viable choices but they are not in the field yet. For the applications of power quality, load levelling an ideal device is supposed to have good cycling and energy release capacity which can be provided by flywheels and Supercapacitors [76]. Li-ion batteries are widely used in electric vehicles (EVs) due to having high energy density, however, initial cost and limited driving range are still hurdles to the adoption of battery technology. Also, Li-ion batteries pose many technical challenges which need a lot of research on battery management, battery materials (electrodes), cost reduction, safety, increasing driving range to meet people's demand and improving the overall efficiency of EVs, and it also brings increased safety problems to EVs [106].

FESS is a promising technology over BESS and SCES in many applications such as UPS, power quality, ride-through capability, load levelling, emergency back power,

energy management, voltage regulation and control, spinning reserves, motor starting, low voltage ride through, grid network fluctuation suppression and telecommunication back-up [59]. FESS can play a complementary role when used in combination with other ESS. When used in combination with BESS, FESS can increase the lifetime of a battery as it is more effective at delivering a large amount of power for a short period [45] [107]. For high power applications, in the transportation and power industry capacitors and batteries are strong competitors to flywheels for applications of high power and short duration [45]. However, capacitors can only provide power for shorter periods than flywheels. Flywheel technologies by Piller, Calnetix, Active Power and others can provide more power storage than capacitors for the same duration of time. On the other hand, batteries have a longer duration of discharge compared to flywheels but can provide less power. The flywheel technology of Beacon Power (20MW plant in New York) can provide more power storage for the nearly same duration of time as a battery [108]. With more research and development, flywheel technology has the potential to grow faster and can be a suitable alternative for ESS over batteries. Much more research on bearing technology and electric machines is required to reduce idling losses, by bringing improvement in bearing technology of flywheels which can improve discharge duration. Flywheels, when on standby can suffer self-discharge losses up to 20% of total stored energy and material advancement may help in the design of build flywheel rotors to improve efficiency and energy density. More research is required to bring improvements in the Motor/Generator along with power electronics interface to improve FESS performance in terms of response time [59] [63].

2.4 Overview of Microgrids

The expansion of high voltage conventional electrical networks to remote areas can be lengthy and expensive due to administrative approval processes and financial constraints, whereas the integration of renewable energy sources in low-voltage power systems avoids these issues. However, integration of renewables causes

transients, voltage dips and voltage swells. To solve these issues and ensure secure operation of renewable sources, the concept of microgrids with storage system is a promising approach to increase penetration of RES at distribution level. Also, the development of microgrids is quicker than the expansion of a conventional electric network since it takes less time and expense [109]. A microgrid is a small electric power system, it contains a load, distributed generators and an energy storage devices or devices. A microgrid is an approach that can smooth energy generated from intermittent sources with the appropriate control system. Figure 2.12 shows two typical topologies, aggregated and distributed for microgrids based on the integration of distributed generation (DG) sources and energy storage systems [110].

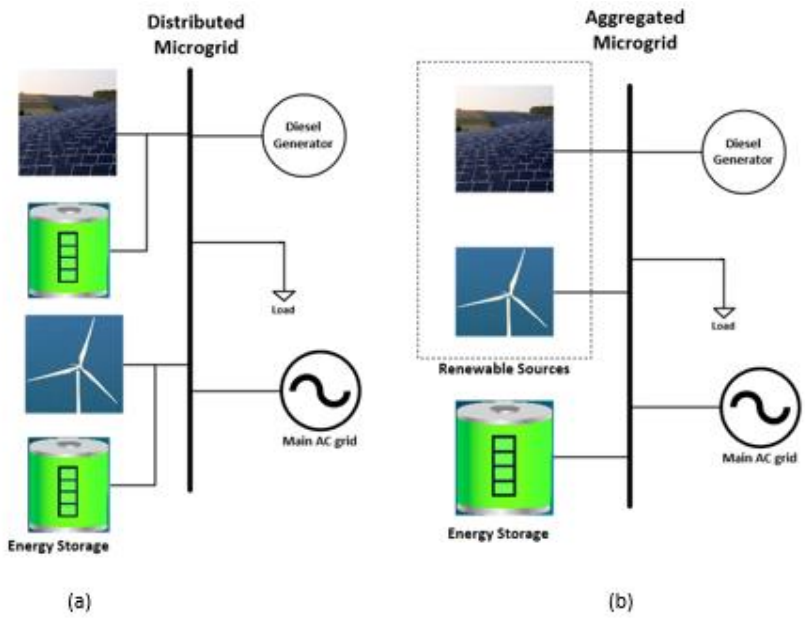

Figure 2-12 The two main microgrid topologies (a) aggregated (b) distributed

In the aggregated topology, energy storage systems are grouped and connected to an AC bus as combined sources of energy whereas, in the distributed topology, energy storage systems are separately connected to each DG source with different interfaces depending on the type of energy source. For example, an AC/DC/AC interface is required for connection with wind turbine generators. The value of microgrids is their ability to work even when the main electric grid is not available to supply the power, in that case, distributed energy sources and storage devices provide power to the load.

Energy storage devices are charged using excess power produced by renewable energy sources, this regime of power flow makes the main electric grid decentralised in terms of power production and its control system. Microgrids can operate in islanded or grid connected mode. In isolated mode the microgrid is not connected to the main electric grid. The balance of reactive power in an islanded microgrid is challenging due to absence of an infinite bus (connection to the main grid), this makes stability of voltage and frequency in islanded mode more difficult. In the grid connected mode of operation, the microgrid is connected to the main utility grid at point of common connection through a static switch, and in grid connected mode the exchange of power is bidirectional. However, the control of the power in grid connected mode is more complex [111]. The microgrid has the potential to deliver an economical, innovative and environmentally friendly solution that leads to reliable and clean electrical energy. The advantage of a microgrid is that it can supply power to loads with lower losses than a centralised system due to not having long network lines, reducing fuel consumption and investment cost of the distribution network. Also, the goal of microgrids is to give energy stability, smart control and communication systems for generation and load management, improve operational efficiency, increase integration of energy storage in power systems and reduced greenhouse gases (GHG) [112]. The benefits of microgrids encourage the widespread use of microgrids in developing countries where rural electrification is a major issue. Apart from this, the development of microgrids helps developing countries comply with global sustainable agreements such as the Paris Climate Accords [113] and to promote green energy policies. It has been reported in [114] that by 2040 about 80 million people will be getting access to electricity through microgrids. There are many other initiatives that are taking place around the world to provide clean energy for people in remote areas where the provision of electricity through a centralised power system is not possible. TP Renewable Microgrid Limited in partnership with the Rockefeller Foundation has proposed provision of clean energy through microgrids to 10,000 villagers across India which will have an impact on 25 million people over

the next 10 years [115]. In the United States (US), less than 0.2% of electricity is currently provided through microgrids but their capacity is expected to double over the next three years. In the US, development of microgrids is rising because they are capable of sustaining service during natural disasters [116]. The company Tesla has developed 120 microgrids to date with the integration of battery storage systems [117]. A project, 'More Microgrids' has been launched by 11 countries including 22 partner companies to increase penetration of renewable energy sources in electrical power systems and to investigate alternative control strategies, network designs and multigrid management operation [118]. Details of more examples of microgrid setups around the world are presented in Table 2.2.

The introduction of microgrids in existing power system networks can cause issues in electrical networks in terms of power quality, energy management and control systems. Also, integration of new technologies requires investigation of their effects on distribution systems along with load and demand management in distribution systems. Load and demand management can be more critical with the penetration of intermittent renewable energy sources and advanced infrastructure. Making a microgrid a smart grid is also an issue for electrical networks, with smart grids being defined as those including cyber and physical systems for information and communication technologies. Protection from cyber-attacks and other technical issues needs to be investigated as well according to [119].

The connection of a microgrid to the main grid is highly important due to the low capacity of generation and high penetration of DG sources including renewables and loads. In case of a disconnection from the main grid, energy management of a microgrid in what is described as an islanded mode is highly important. A microgrid in an islanded mode operates with no support from the main grid. This makes the control of a microgrid more complex and microgrids more prone to load variations and power fluctuations due to its attribute of the low system inertia. Therefore, a reliable energy storage system is required in an islanded mode of operation [120].

Table 2-2 Chosen examples of existing microgrid projects around the world [112] [121, 122, 123].

Country	Storage	DG source	Load	Application
Canada	N/A	Hydro, Diesel	Residential	Energy security and sustainability
China	Battery	Wind, PV	Static	Energy security and sustainability
Denmark	N/A	Diesel, Steam, Wind, Biogas	Static	penetration of renewables, reduction of GHG and load management
Germany	Battery	PV, Wind	Residential and commercial	Reduction of GHG, penetration of renewables and load management, integration of energy storage
Greece	Battery	PV, Diesel	Residential	Load management, penetration of renewables and reducing GHG emissions.
India	N/A	Fuel cell, Diesel	Static	N/A
Italy	Flywheel Battery	PV, Wind, Diesel and CHP	Static	Reduction of GHG and infrastructure cost, penetration of renewables and load management, integration of energy storage
Japan	Battery	PV, Wind, Biogas	Commercial	N/A
Netherland	Battery	PV	Residential and commercial	Reduction of GHG, penetration of renewables and load management
Portugal	N/A	CHP, Diesel	Commercial	Load Management
Spain	Flywheel, Battery, SC	PV, Wind, Diesel	Commercial	Load management, storage integration, GHG emissions, penetration of renewables
UK	Flywheel	Diesel	Static	Integration of energy storage
UK	Battery	Hydro, PV, Wind, biomass	Static	Penetration of renewables, storage integration and reduction of GHG
US	Battery	Natural Gas	Static	load management and energy storage integration

N/A = not available , CHP = combined heat and power

Microgrids must also have a separate control system which ensures effective coordination and operation of connected energy sources: the control system of the microgrid controls the power flow and interconnection to the main grid at the point of connection (PC). Control of a microgrid is often based on a hierarchical scheme: Load control, microgrid central control or distribution management-side control. Load control is an independent control system within a microgrid for increasing the reliability of the system and power flow. Microgrid central control system is used for monitoring and supervision of the system and communication with distributed generators and their regulation. Distribution management-side control provides an interface used to exchange information with the main grid network [124, 120, 125].

Operational strategies and control of microgrids are highly important to nullify the impacts of stability issues such as grid voltage fluctuations or blackouts caused by dependence on large scale penetration of DGs [126]. Therefore, effective strategies for integration and planning including control functions, boundaries and limits are important requirements for the modelling of microgrids. Reference [127] proposes a mixed mode energy management strategy (MM-EMS) for effective energy management in microgrids. The MM-EMS is based on different strategies to reduce operating timings of fuel cells and to increase usage of battery storage based on their charging state. An optimized model for short-term joint operation of a microgrid is presented in [128], the model includes the joint operation of PV, wind and energy systems which can smooth the power fluctuations and improve the controllability of power renewable sources. Reference [119] presents different aspects of microgrid management with the latest developments and studies about microgrids. Optimization of microgrids and their modelling along with control methods is presented in [109]. Furthermore, different control strategies for better energy management in microgrids have been reported in [120] [129] [130] [131] [132] [133]. To achieve the optimized performance of microgrids, the design of the components in

the microgrids should meet critical properties. The following section briefly describes the major components of a microgrid.

2.4.1 Components within microgrids

Distributed generators (DGs)

There are a range of DGs which are commonly integrated into microgrids which include solar PV systems, wind turbines (WTs), induction generators, synchronous generators, hydropower systems, ocean energy systems, geothermal and biogas [112]. The DGs most commonly used are solar PV, diesel generators and WTs. Each DG requires a controlling mechanism along with a power electronic interface for their integration in a microgrid. DC-DC converters are required for a PV system and AC-DC converters are required for the integration of WTs for energy conversion. Power electronic converters can be bidirectional which facilitates the flow of electrical energy to and from the energy storage devices. The threshold (TH) rating of DGs is always lower than centralised generation units and they are in a range of 10-15MW [134], however, commonly low rated DGs are around 100 kW [135].

Energy Storage

Due to the low capacity of DGs in microgrids, they have low inertia, therefore they are not capable of responding to sudden changes in energy demands. Integration of an energy storage system is therefore crucial for maintaining the balance between demand and supply of power in microgrids. Also, the long response time constrains some DGs (diesel generators and fuel cells) so incorporation of these in the microgrid demands a fast-acting storage device that can provide power in case of load changes or disturbances [135]. Energy storage systems provide ride through services and facilitate switching of microgrids from grid-connected to islanded modes. There are different types of energy storage which are applicable for integration in microgrids such as flywheels as reported in [136] [137] [138] [139] [140] [141] [142], batteries [95] [143] [144] [145] [146] [147], fuels cells [148] [150] [151] [152] [149] and supercapacitors in [153] [145]. From these references it can be concluded that application of energy

storage devices depends on the type of application, their response time, self-discharge, cost, energy and power density.

Loads

Loads in microgrids are connected and disconnected based on their nature (critical or non-critical) and available power at terminals of DGs and energy storage systems. Commercial and industrial loads are classified as critical loads and they require high power quality whereas residential loads are termed as non-critical load and they require load service quality, they can be disconnected and managed if the power in the system is available to supply critical load only [134]. A detailed classification of loads has been presented in [119]. The classification of loads in a microgrid is to facilitate net import/export of power in grid-connected mode, to stabilize voltage and frequency, improve reliability and power quality and reduce peak loads [154]. Furthermore, electric vehicles (EVs) have been widely acting as controllable loads in low voltage distribution systems. Integration of EVs in microgrids has resulted in these being both a potential supplier and a consumer of energy. The charging pattern of EVs (as a consumer) may not match with the power generation pattern of a microgrid however. A customer may like to charge their vehicle anytime during the day when needed which can cause disturbance in the grid. However, there is a wide body of literature available suggesting possible control schemes for EV charging demand [155] [156] [157] [158] [159].

There are numerous studies presented in literature on the application of isolated microgrid systems used either for rural electrification or for giving support to the main grid. A hybrid PV diesel battery system for remote loads in India is presented in [161], where the authors have shown the cost saving and reduction of GHG by using battery energy storage. However, analysis of the effect of high environmental temperatures impacting the life of the battery has been ignored and modelling of the system is not clear. A similar study has been presented in [162] , the study uses a techno-economic based analysis approach for energy management of stand-alone microgrid using

battery storage but technical analysis of the components of the microgrid is ignored. A hybrid system having a diesel generator, PV system and micro hydro plant is studied in [163], the authors have proposed an approach to optimize operation and control a multisource hybrid system for meeting energy demand with increased reliability. The calculation of fuel consumption of a diesel generator and impact of GHG are completely neglected. A flywheel-based PV standalone system has been presented in [136], where the authors have made a comprehensive analysis of diesel fuel consumption and cost savings by using flywheel technology. However, the calculation and analysis of carbon emissions is missing and the size of the system is much smaller (10kW) than the system considered in this research which is serving large residential loads. Another example of a microgrid with flywheel energy storage has been presented in [164], the system is proposed for frequency regulation in wind-diesel powered microgrid by using flywheel and fuel cells. During high speed winds, the surplus energy is used to charge the flywheel and it is discharged during low speeds and low demand. The system is used to support the wind-diesel hybrid system. However, the analysis of the impact of the flywheel on the diesel generator and environment along with cost analysis has been neglected. Studies of microgrids vary based on the location and type of the load and environmental conditions of the site, potential for renewable whether solar or wind and weather conditions. Studies on isolated grids with energy storage systems for different countries can be found in [165] - [166].

2.5 Background of Flywheel Technology

Flywheel energy storage systems (FESS) are one of the earliest forms of energy storage technologies with several benefits including long service time, high power density, low maintenance, and insensitivity to environmental conditions. A FESS is a device with a rotating mass that can store energy by virtue of its rotational inertia in the form of kinetic storage. Flywheels have been used as a component in machinery to smooth the flow of energy since the invention of the potter's wheel, the first use of a flywheel

has been reported in the literature as early as 6000BC [49]. During the 15th century (BC), flywheels were used in shipbuilding applications to make ropes by twisting leather strips [167]. As early as 1200 AD, flywheels were used to maintain the spin of cylinders in the process of thread manufacturing. Flywheels were first used extensively in boats, steam engines and trains during the industrial revolution in the 18th century [168].Until the introduction of steam engines in the 1780s, flywheels remained human-powered and were small in size [49]. Flywheels have been used in many configurations ranging from 'wagon wheel' shape in stationary steam engines to the multi-purpose disks used in automotive engines [49]. Flywheels allowed the development of larger and more complex machines such as internal combustion engines and steam engines by facilitating the delivery of constant and continuous torque from pulsating power sources [80]. Development of the first turbo generators operating at higher speeds ranging from 1800rpm-2000rpm, took place in 1884 and 1897 which led to a significant step in the development of kinetic energy storage systems. Since the development of steam engines, the use of flywheels has appeared in many applications throughout history such as in mines, inertial starter machines, transport energy storage systems and weapons [167]. The first use of flywheel specifically for energy storage application was made in 1883 by John A. Howell, the steel rotor flywheel of 21,000 rpm, with a mass of 160kg and 450mm diameter was used for military applications. In the late 1800s, machines using flywheels grew in size and power, the largest engine stood 12.1 meters tall and employed flywheels of 9.1 meters in diameter, and the machine produced a power of 1.04MW (Figure 2.13) [108].

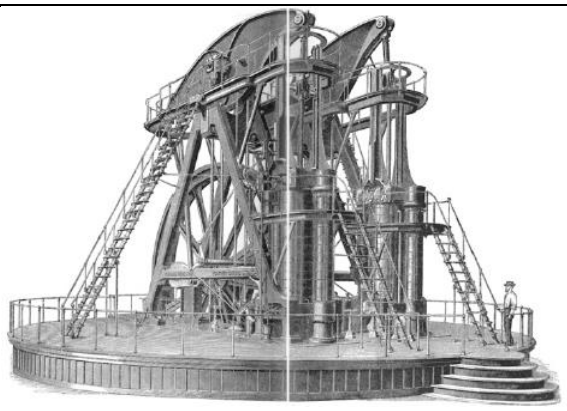

Figure 2-13 Corliss Centennial Engine using large flywheels [80]

During the 19th century further developments like cast steel and cast iron brought forward very large flywheels with curved spokes [167]. In large-scale power systems, one of the first applications of flywheels was for smoothing the output of low-speed steam piston engines driving generators. Figure 2.14 shows flywheel electric generators used from 1902 to the 1950s [80].

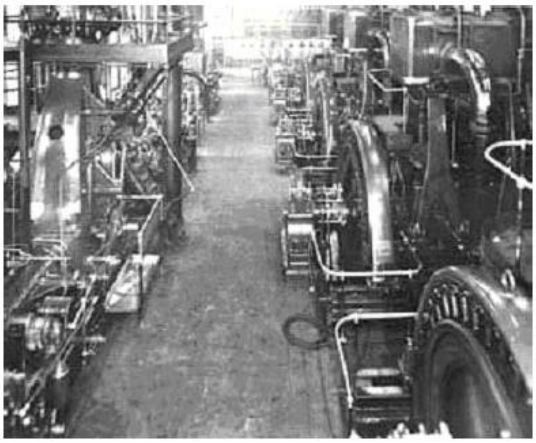

Figure 2-14 Flywheel electric generators were used from 1902 until the 1950s [49].

During the 1950s flywheels were used to power Gyro buses incorporating 1500 kg mass steel rotors produced by Swiss company Oerlikon [169]. During the 1960s and 1970s, the flywheel was starting to be recognised as an independent means of energy storage. Due to the introduction of efficient power electronics inverters and converters, it became possible to control the input and output frequency independently of motor-generator speed. This allowed the flywheel's momentum to be more fully utilised, storing more energy hence adding operating time, in ride-

through applications [80]. In the 1970s and 1980s, after the development of magnetic bearings and fibre composite rotors, flywheels emerged as a primary and potential energy storage device for stationary power backups as well as for vehicles [170]. Progress in the flywheel technology continued, with the investment in research and development of flywheels furthered in NASA sponsored space programs. With the development of strong lightweight materials, fibre composite rotors were built and tested by US Flywheel Systems in a laboratory [171]. Modern flywheels came into existence with advancements in materials and power electronics which enabled flywheels with higher storage capacity to be built. Also, environmental issues and targets for reduction in CO_2 emissions resulted in the importance of energy storage devices being highlighting as devices to decrease pollution and reduce energy costs [172].

A modern steel rotor flywheel with a weight of 1t can run at a peripheral speed of up to 500 m/s compared to the flywheels used in stationary steam engines during the industrial age, which could barely exceed the peripheral speed of 20 m/s. Modern flywheels with rotors of weight 1 tonne can store up to 25 kWh of useable energy when compared to the industrial age flywheels that weighed 50 tonnes and could store only 5 kWh of energy [49]. Modern flywheels can achieve high round trip efficiency of more than 90% with frictional losses of less than 1-3% of the energy stored per hour and a lifetime of over 20 years with high power and energy density. If a low-pressure vacuum is maintained, carbon fibre flywheels can reach up to rotational speeds of 100,000 RPM [80, 142]. However, the development of flywheel technology has declined with advancements in electric grid systems and substantial cost reductions of Lithium Ion batteries. Despite this, FESS has appeared as a strong option for energy storage applications due to recent advancements in power electronics, high-speed electric machines, rotor materials and magnetic bearings [173].

2.6 Technical Characteristics and Structure of FESS

A FESS is an assembly of a rotating mass, electrical machine, power electronics converter, bearing system and containment. A flywheel storage system works in three modes of operation, acceleration, standby and deceleration. During acceleration mode, the flywheel charges and stores kinetic energy and the power flows from the microgrid to FESS. In deceleration mode, the flywheel discharges and delivers electrical energy so the power flows from the flywheel to the microgrid or the load. In standby mode, the flywheel spins idle and no flow of energy takes place to or from the FESS assembly unless the controller is configured such that the rotor speed is kept constant by feeding in a small amount of power equivalent to the standby power loss.

The structure of a FESS consisting of the assembly of components listed earlier is shown in Figure 2.15.

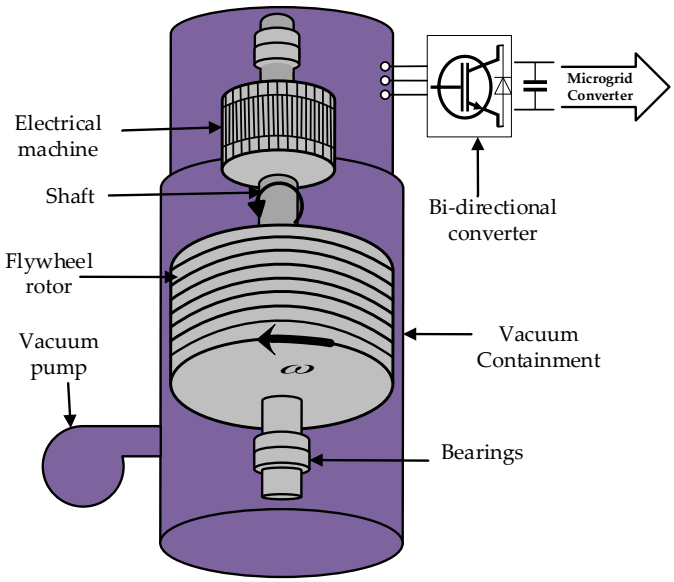

Figure 2-15 Structure of FESS assembly.

All these components together determine the overall efficiency of the FESS and are briefly described in the following sections.

2.6.1 Flywheel Rotor

The design of the rotor used in FESS depends on the materials from which they are made. There are two basic types of flywheel rotors. 1) Flywheel rotors are made up of

non-isotropic materials like carbon fibre. These rotors have high specific energy. 2) The second type of rotors are traditional flywheels and are built from steel, they can be used for both high and low speed applications. For weight sensitive applications such as motor sports and space applications, carbon fibre rotors being light in weight offer great benefits, however carbon fibre rotors have higher material cost than steel rotors. The effective shape of flywheel rotor is disc or cylinder with no hole which is mainly used by steel rotors, whereas the carbon fibre rotors made of non-isotropic materials develop strength in one direction and they use hollow cylindrical shape which reduces the shape factor. The rotor of the flywheel having a rotating mass m (kg) with inertia J (kg·m^2) that spins at an angular velocity of ω (rad/s), operation of the flywheel can be represented by Equation 2.1.

$$J\frac{d\omega}{dt} = T_{em} - k\omega \tag{2.1}$$

where:

T_{em} : electromechanical torque

k : frictional co-efficient.

The kinetic energy E(joules) stored by the flywheel is proportional to the mass and square of its velocity as given by Equation 2.2.

$$E = \frac{1}{2}J\omega^2 \tag{2.2}$$

The useable stored kinetic energy of a flywheel spinning between a minimum velocity (ω_{min}) and maximum velocity (ω_{max}) is given by Equation 2.3.

$$E = \frac{1}{2}J(\omega_{max}^2 - \omega_{min}^2) \tag{2.3}$$

where the moment of inertia J is a function of flywheel geometry and mass.

In the case of a disc type rotor with mass m (kg), density ρ (kg/m^3) and length l (m), the angular velocity can be expressed by Equation 2.4.

$$\omega = \frac{2}{r}\sqrt{\frac{E}{\rho\pi l}} \tag{2.4}$$

Therefore, the stored energy is expressed by Equation 2.5

$$E = \frac{1}{2}J(\omega_{max}^2 - \omega_{min}^2) \tag{2.5}$$

In the case of a hollow cylindrical type flywheel rotor with an inner radius r_1 and outer radius r_2, the stored kinetic energy is given by Equation 2.6.

It can be interpreted from Equation 2.6 that the greater radius of the disk or high-density material, the greater will be the energy stored by the flywheel.

$$E = \frac{1}{4}m(\omega_{max}^2 - \omega_{min}^2)(r_2^2 - r_1^2) \tag{2.6}$$

For disk or cylinder rotor type, a moment of inertia is given by;

$$I = \tfrac{1}{2}mr^2 \tag{2.7}$$

When the mass of the flywheel is expressed as $m = \pi\rho a r^2$ then a moment of inertia is a function of rotor density and physical dimensions.

$$I = \tfrac{1}{2}a\rho\pi r^4 \tag{2.8}$$

a : length of the rotor

ρ : mass density

r : disk radius

Therefore, for a hollow cylindrical type rotor as shown in Figure 2.16 having r_2 as inner and r_1 as outer radius, a moment of inertia is expressed by Equation 2.9.

$$I = \tfrac{1}{2}m(r_1^2 + r_2^2) = \tfrac{1}{4}a\rho\pi(r_1^4 - r_2^4) \tag{2.9}$$

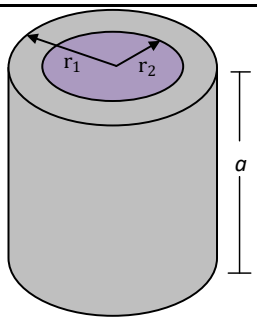

Figure 2-16 Hollow cylinder type rotor

Therefore, energy stored in the hollow cylinder rotor is expressed in terms of speed, mass and geometry of the rotor

$$E = \frac{1}{4} a\rho\pi\omega^2 (r_2^4 - r_1^4) \tag{2.10}$$

The maximum energy that may be stored for a given mass is achieved by a flywheel made from the material which combines high tensile strength with low density which justifies the use of composite materials looking to be a better option than metals. Maximum energy stored by the flywheel rotor in terms of tensile strength is expressed as:

$$E_{max} = \frac{1}{2} m \frac{\sigma_{max}}{\rho} \tag{2.11}$$

*w*here σ_{max} maximum is the tensile strength of the material, it defines the capacity of the material to withstand centrifugal forces affecting the flywheel and upper limit of the angular velocity [142]. Further, the maximum tensile strength of a thin rotating ring is expressed by Equation 2.12.

$$\sigma_{max} = \rho\omega^2 r^2 \tag{2.12}$$

As expressed by Equation 2.12, the maximum tensile strength is proportional to the density of the material and square of the angular velocity if the radius is kept constant. The shape factor K can be introduced to accommodate rotor geometries and simplify the more complex equations. The maximum energy density concerning mass (J/kg) and volume (J/m^3) is given by Equations 2.13 and 2.14 respectively.

$$e_m = K\frac{\sigma}{\rho} \tag{2.13}$$

$$e_v = K\sigma \tag{2.14}$$

In stress limited cases, K is the measure of shape efficiency of the rotor [108]. The shape factor is an important factor for determining the speed limit of the rotor, its value depends on rotor geometry [172]. It is different for different rotor designs, it is 0.5 and 0.25 for thin-walled cylindrical and disk type rotors respectively. Shape factors for different rotor geometries are given in Figure 2.17 [174].

Shape	*Geometry*	K_G	K_σ	$K_s = 0.5{K_G}^2/K_\sigma$
Thin ring	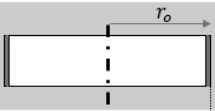	0.500	1.000	1.000
Thin disc	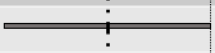	0.606	0.413	0.707
Thin disc (tiny hole)		0.303	0.826	0.707
Thin disc (large hole)	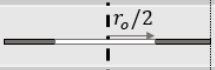	0.379	0.869	0.791
Practical Laval disc		0.887	0.146	0.510
Rimmed Laval disc		0.720*	0.360*	0.720*
Thick solid cylinder	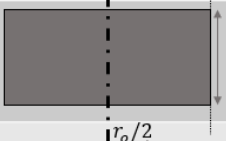	0.553	0.452	0.707
Thick hollow cylinder	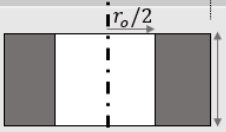	0.347	0.902	0.791

Figure 2-17 Shape factor for different rotor geometries [162]

2.6.2 Electric Machines

The electrical machine is a key part of a FESS that performs the charge-discharge cycles and is responsible for the majority of losses in the process in combination with converter power electronics. The electrical machine is coupled with the flywheel and acts as a motor to accelerate and charge the flywheel transforming electrical energy into kinetic energy when positive torque is applied on the mechanical shaft. The same machine can function as a generator to decelerate and discharge the flywheel to transform kinetic energy into electrical energy with a negative torque. Desirable

features for an electrical machine to be used in FESS are high efficiency, low standby losses and low cost. The machine has to operate from as low as one-third of the maximum speed to full speed at constant power and maximum torque will therefore occur at the lowest speed but maximum centrifugal stress at the highest speed. Typically, an electric machine should be placed inside the flywheel in case of carbon composite flywheel rotor due to obvious hollow space inside it. In the case of the steel rotor, the machine has to go to the side of the flywheel but any standard design can be used [174]. The choice of the electrical machine must be carefully made according to the application requirements and thermal management of the flywheel rotor. Therefore, the objective of the machine design for the flywheel is to minimize the heat dissipation in the rotor. However, thermal management is not an issue in the case of steel rotors when used for UPS applications as the electric machine is operated occasionally and little energy is deposited in the rotor. For composite rotors, thermal management is crucial and permanent magnets machines are usually needed with composite rotors but suffer standby drag as a result [108]. Machines commonly used in FESS are induction machines (IM), permanent magnet (PM) machines, switched reluctance machines (SRM) and homopolar synchronous machines (HSM).

Switched Reluctance Machine (SRM)

SRM is a robust design type and can be constructed from high-strength, low-cost materials. SRM has the fault-tolerant capability and the ability to operate in high-temperature environments; however, it is less commonly used because of its complex torque current and high current ripples [175]. Due to the avoidance of permanent magnets, there is no concern of demagnetization and hence they are more reliable than permanent magnet machines [176]. No excitation at zero torque would lead to no idling losses (no-load condition) [177]. Figure 2.18 shows the structure and components of SRM.

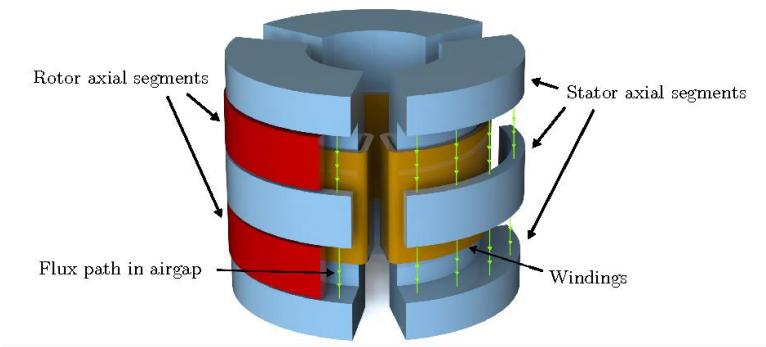

Figure 2-18 Structure and components of SRM [178]

In the generator mode, SRM requires excitation to produce power [25] using an electronic converter [179], but it will result in extra losses. The highly nonlinear behaviour of SRM makes the selection of suitable control gains difficult and this makes the design of the control system challenging and problematic [180].

Synchronous Reluctance Machine (SyncRM)

The design of SyncRM does not contain permanent manets, therefore there is no risk of demagnetisation and idling loss when flywheel is on standby mode in vacuum [181] SyncRM have very simple and robust mechanical structure, the machine has capability of fault tolerance and high torque density, the machine normally produces sinusoidally smooth torque [182]. The rotor of SyncRM consists bonded sections of nonmagnetic and ferromagnetic steels, since the rotor is not radially therefore extreme care is taken to ensure low rotor losses [183]. SyncRM are inherently more reliable than permanent magnet machines, they can be constructed entirely from high-strength and low-cost materials [183].

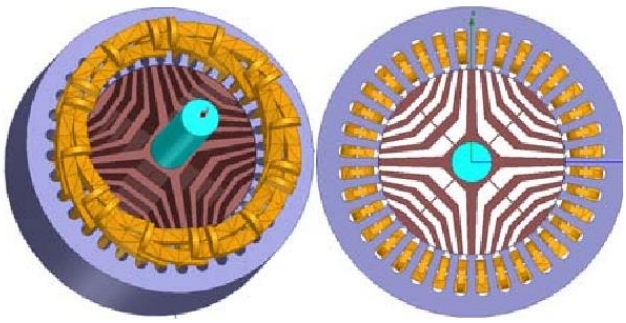

Figure 2-19 Rotor structure of Synchronous Reluctance Machine [184].

Permanent Magnet Machine (PM)

The types of permanent magnet machines used in flywheel technologies are mainly brushless dc (BLDC) machines, PM synchronous machine (PMSM) and Halbach array machines (HAM). BLDC has trapezoidal flux distribution created using permanent magnets and its three-phase stator windings are fed from a DC source through an inverter. In contrast, in a PMSM, the coils on the stator are wound in a sinusoidal manner, the waveform of the back *emf* is also of sinusoidal nature. BLDC machines have a very high mechanical power density and provide constant mechanical torque [185]. The advantages of BLDC machines are high efficiency, no electromagnetic interference, mechanical stability, compact design and low maintenance cost [175]. The cross-sectional view of a BLDC machine is shown in Figure 2.19.

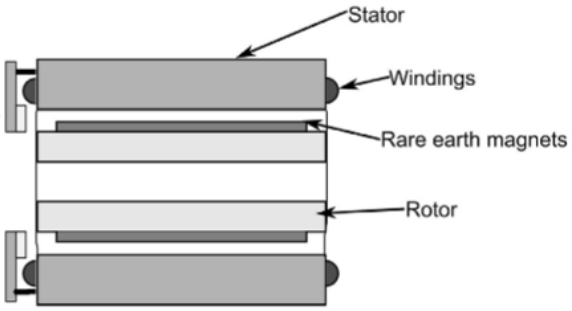

Figure 2-20 Cross-sectional view of BLDC machine [124].

PMSM are the most commonly used machines in FESS due to their high efficiency. PMSM has low rotor losses due to permanent magnets generating the magnetic flux, it has robust rotor structure and high energy density [104, 137]. PMSM is used in high-speed applications due to its very high efficiency. The design considerations of PMSM for high-speed flywheel applications have been discussed in [186] and [187]. A cross-sectional view of a typical PMSM is shown in Figure 2.20.

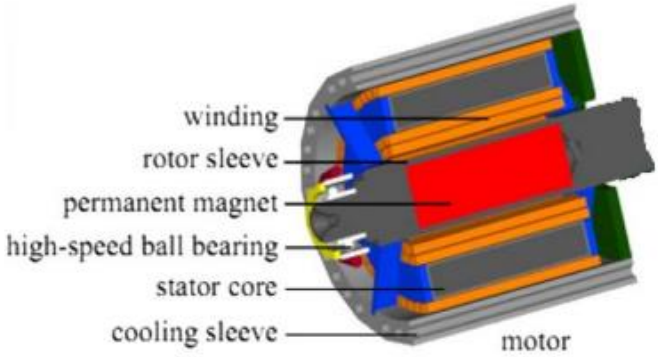

Figure 2-21 A cross-sectional view of PMSM [188].

PMSM has the disadvantage of accidental demagnetization with the increase in temperatures, plus the magnets have high cost and low tensile strength. In BLDC the stator field position is changed over discrete positions to generate torque, the output current waveforms of BLDC take square waveform shape. The BLDC machines are used for highspeed applications which require continuous operation such as ventilation systems, pump and compressors. In PMSM (also called brushless AC machine-BLAC), the placement of stator magnet is modified in a result the waveform of back-EMF in the machine takes shape of sinusoidal waveform with the current waveform following back-emf waveform as well. PMSM machines are complex in structure compared to BLDC machines which increases their cost. PMSMs are used in high-end industrial speed control applications as they require accurate position feedback control system for torque generation [189].

Variable Reluctance Machine (VRM)

A new machine type, variable reluctance machine (VRM) has been proposed for FESS which has no risk of demagnetization as torque in VRM is produced due to variation in reluctance. VRM have high tensile strength, low losses and reduced cost compared to PMSM [190]. In VRM the reluctance varies with rotor position in order to align itself with magnetic flux line. The VRMs are recently developed magnet less machine, they have double salient structures similar to SRM [191]. VRM have advantages of less acoustic noise and reduced vibration. Figure 2.21 shows a typical structure of VRM.

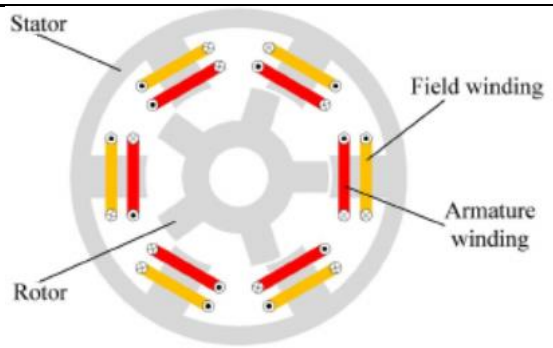

Figure 2-22 Structure of Variable Switched Reluctance Machine [191].

Homopolar synchronous machines (HSM)

Homopolar synchronous machines (HSM) are used for long-term energy storage in high speed and high-efficiency applications. HSM have a robust rotor design and due to their lower standby losses compared to PMSM, they can be used as an alternative to PMSM in high-speed applications [175, 192, 193]. Figure 2.22 shows the structure and components of HSM.

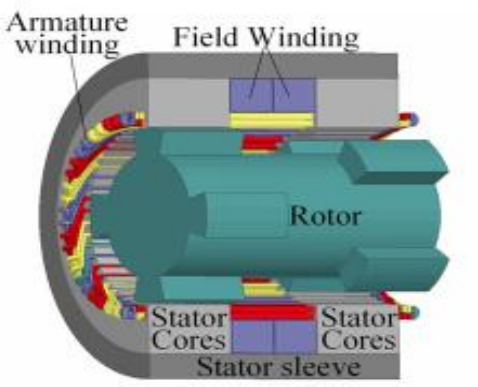

Figure 2-23 Structure of HSM [194].

HSM have been shown to operate in a speed range of 30krpm – 60krpm with an average efficiency of 83% [195]. However, the main disadvantage is the difficult design of HSM due to its complex magnetic flux paths and geometry [196].

Squirrel Cage Induction Machine (SCIM)

An IM can be used for high-power applications due to its rugged construction low, high torque and high reliability. Squirrel cage induction machine (SCIM) and doubly-fed induction machine (DFIM) are two types of IM. The DFIM has been recently used in FESS applications, due to its robust construction it allows mitigation of power

electronics sizing [175]. The SCIM machine can be established with high strength material with low cost [15] and have no electromagnetic spinning losses due to zero torque in the absence of an excitation field [16]. Hence SCIMs can be an attractive option for low loss FESS with long term energy storage capabilities. A challenge for SCIM is the mechanical design in the high-speed application, which can be overcome by using appropriate solid-rotor topologies such as slotted solid rotor, coated solid rotor, caged solid rotor and smooth solid rotor (Figure 2.23).

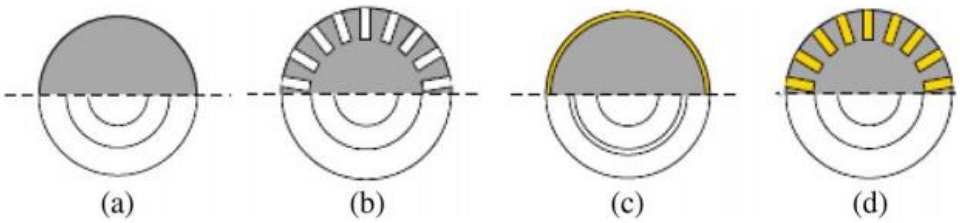

Figure 2-24 a) Smooth solid rotor; b) Slotted solid rotor; c) Coated solid rotor; d) Caged solid rotor [188].

As a disadvantage, induction machines inherently have significant rotor heating which would be a major problem for composite flywheels, however, this is much less of an issue in steel flywheel rotors. SCIM and its associated inverters have been modelled previously for different industrial applications. However, its application in flywheels is different and introduces new challenges to its operation such as progressive torque requirement due to slow dynamic response of the SCIM in high inertial flywheels applications [197].

The advantages and drawbacks of commonly used electrical machines in FESS are presented in Table 2.3.

Table 2-3 Advantages and drawbacks of commonly used electrical machines in FESS [170, 175, 198, 199, 142]

	SCIM	PMSM	SRM
Advantages	Rugged construction	Simple rotor design	Robust simple structure
	No risk of demagnetization	High power, high load and high torque density	High power density
	Low cost	Easy to install and maintain due to smaller size	Low cost
	High efficiency (93.4%)	Very high efficiency (95.5%)	High efficiency (93%)

	No idling losses due to its lower rotor magnetic field at zero torque value, consequently this reduces a total electrical loss of IM	No field winding losses due to the use of permanent magnets	No idling losses
	High torque and high power capability	Suitable to operate in a low-pressure vacuum with negligible rotor losses	Wide speed range
Drawbacks	Difficult mechanical design for high-speed applications	Risk of sudden demagnetization	Significant rotor eddy current losses due to the time-varying magnetic field
	Difficult to operate in absolute vacuum due to complex heat transfer system	Due to the use of permanent magnets, PMSM have the low tensile strength	High torque and current ripples
	Limited speed and larger volume	High cost	Difficult to regulate the speed
	Copper losses in electromagnets during field excitation due to high inrush currents	Idling losses at zero torque due to presence of magnetic field	High losses due to need for excitation

Bearingless Homopolar Machine (BHM)

Some special machines have been recently proposed in the literature for flywheel applications. A bearingless homopolar machine (BHM) is one amongst them and it is reported in [200], BHM incorporates together the function of magnetic suspension and torque generation in a single machine, they have a simple structure, small in size and are less expensive [175]. The BHM can be used in high-speed flywheel applications [201]. Authors in [202] have presented high-speed superconducting bearingless machines for flywheel energy storage, it has been demonstrated that due to bearingless design, the mechanical friction is reduced with improved self-discharging rate. The variation in excitation of BHM can increase the efficiency of the flywheel system for low excitation during idling operation and high-speed operation [196]. However, unstable magnetic suspension of the machine rotor could occur at some field excitation levels at some speed [203]. More topologies of the bearingless machine are presented in [201] and [204]. The cross-sectional view of a BHM is shown in Figure 2.24.

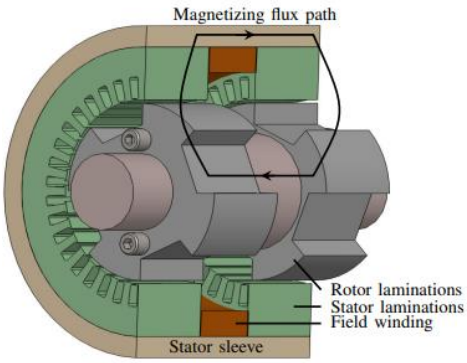

Figure 2-25 Cross-sectional view of BHM [205].

2.6.3 Bearing Systems

The bearing system supports the rotor and allows the flywheel to spin freely. The bearings help to reduce the friction and keep the flywheel rotor in place. In high-speed flywheels, low loss bearing systems are desirable to reduce dissipation of flywheel stored energy. The selection of a bearing system depends on many factors but the most important ones are lifetime, cost, weight and level of acceptable losses [171]. Any lubricants used in the bearings should be capable of working in a vacuum environment. Fluid film bearings using a liquid lubricant are a feasible option. However, the losses are typically too high given which is important given a flywheel is likely to have to operate much of the time in standby mode. Gas cannot be used as a lubricant in bearings due to vacuum requirements. Given these types are eliminated, there two types of bearings commonly used in FESS are: 1) mechanical bearings and 2) magnetic bearings. Mechanical, or rolling element bearings are simple in structure but have friction losses and given deterioration of lubricants, they require periodic maintenance such as lubrication replacement. Attempting to carry all the load with rolling element bearings will usually result in unacceptably high losses.

Magnetic bearing systems work using magnetic attraction and do not have any contact with the mechanical shaft of the flywheel. They are stable and low loss bearing systems due to negligible friction and are suitable for high-speed applications in FESS [206]. Magnetic bearings can be used for high-speed applications above 40krpm, below this, mechanical bearings (ball bearings) are a better choice due to their weight

advantage and relatively low drag losses [207]. Magnetic bearings that use permanent magnets for levitation are called passive magnetic bearings (PMB) whereas active magnetic bearings (AMB) are the type that makes use of a feedback system with electrical coils [208]. AMB require continuous power for energisation of the magnetic levitation system [170]. AMB use attractive forces of electromagnets this makes them unstable as their displacement increases with an increase in attractive forces. AMB, at high speeds, requires electronics equipment (microprocessors) to operate and electromagnets require considerable power to operate (for levitation) which consequently increases the size of the system [209]. The high cost, complexity and low force density of AMB makes them less favourable for mobile applications. However, due to low drag torque, damping characteristics and high maximum speeds they can be used where there is no need for lubrication such as in space where lubricants are unwanted [210]. A schematic diagram of an AMB is shown in Figure 2.25.

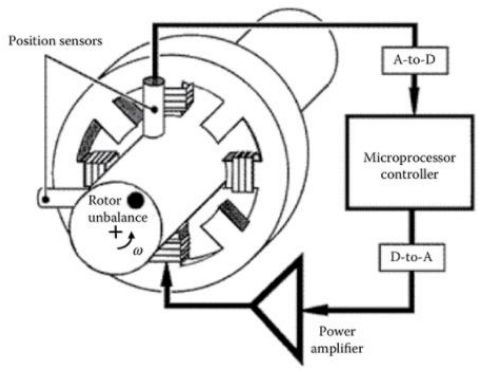

Figure 2-26 Working diagram of Active magnetic bearing [211].

The PMB work by use of repellent forces of permanent magnet poles, PMB is used in conjunction with conventional bearings due to their inability to withstand high forces, as they can touch down under relatively light loads which can result in a disastrous touchdown, however, PMB can be promising technology when used with high-temperature superconducting (HTS) bearing system [209]. PMB offer low losses due to the absence of electromagnetic drag and they have a low initial cost. They are also used as auxiliary bearing if required [212].

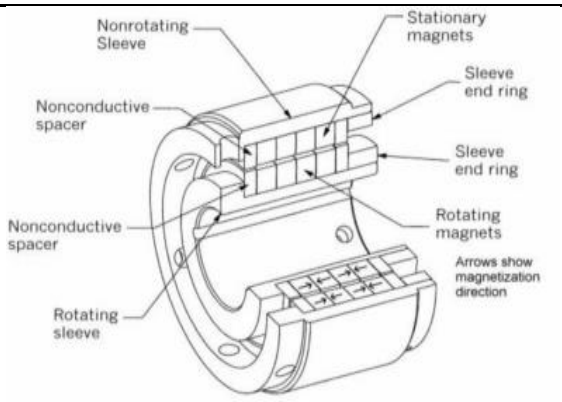

Figure 2-27 Passive magnetic bearing system [212].

Compared to magnetic and mechanical bearings, HTS bearings incur half of the rotational loss of conventional mechanical bearings. Parasitic losses in mechanical bearings are more compared to magnetic bearings and they depend on the total energy storage of the flywheel [172]. Authors in [172] claim that the parasitic losses of mechanical bearings are about 5% of the total stored energy of the flywheel, this can further be reduced to 0.1% by using HTS bearings but in ref [213], authors have reported that rotational losses can be reduced to less than 2% of total stored energy by using a developed technique by Argonne National Laboratory to produce HTS bearing system. Furthermore, the losses and complexity of the control system can be reduced by using hybrid bearings (mechanical and magnetic bearings), the losses of hybrid bearing systems are in order of 0.1-0.3W/kg but may vary according to the design particulars [174].

Superconducting magnetic bearings (SMB)

Superconducting magnetic bearings (SMB) have a longer life span, less frictional loss and stable operation but the operation of SMB is temperature-sensitive, they require a cryogenic cooling system to work at low temperatures to avoid bearing failure [80]. This requirement leads to the added cost to the system hence making use of SMB very expensive. SMB require broader air gaps and have lower force density, SMB has limitations concerning the load weight (i.e. flywheel rotor), SMB has low energy consumption and high reliability compared to AMB [214]. The SMB is best for high-speed application and it can stabilize the flywheel system without electricity or

positioning system [173]. Figure 2.27 shows the SMB bearing rotor with superconducting magnets.

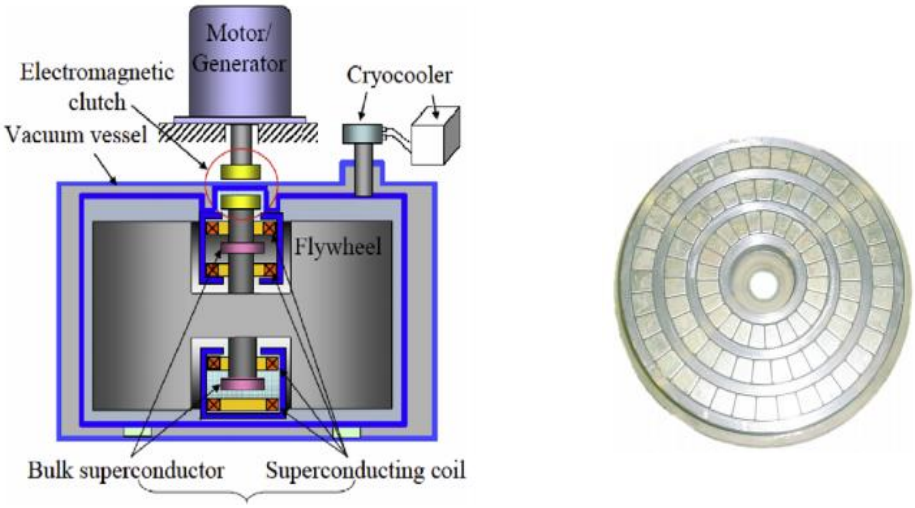

(a) (b)

Figure 2-28 a) SMB installed in FESS assembly; b) SMB bearing rotor [215] [214].

The combined use of magnetic and mechanical bearing in FESS can make the system more stable, cost-effective and less complex; an example of such a system is discussed in [216]. In a combined magnetic and mechanical bearing system, the levitation in vertical orientation is maintained by magnetic bearings while the rotational and torsional levitation is maintained by mechanical bearings [173]. Another type of bearing called spiral groove bearing (SGB) is a low loss bearing system, used for low-speed applications of less than 10 m/s. A SGB can be used in combination with magnetic bearing for flywheels with larger storage capacity and fewer frequency vibrations of the rotor [217]. A SGB has a conical form, with the increase in the rotor speed, the required pressure is produced by hydrodynamic SGB to keep surfaces lubricated and separated due to the pumping effect of the groves [218]. A schematic of spiral groove bearings is presented in Figure 2.28.

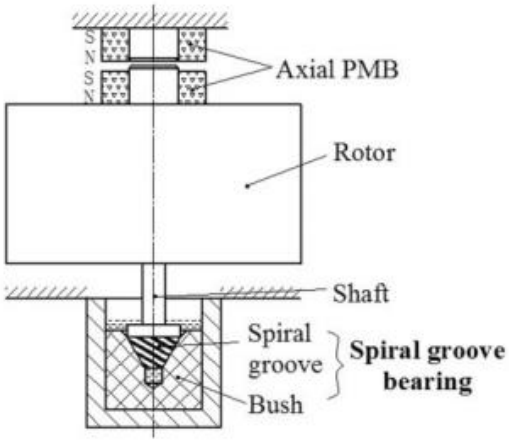

Figure 2-29 Schematic of SGB installed in FESS assembly [218].

2.6.4 Power Electronics Interface

The electrical machine is connected to a power electronics converter interface to make power flow from the microgrid to the FESS and back to the microgrid during the acceleration and deceleration of the flywheel. Bi-directional converters help exchange power between the microgrid and FESS by controlling the operation of the electrical machine. The power electronics interface consists of a bidirectional converter/inverter and a drive system. Power electronics converters are based on electronic switches such as IGBT and MOSFETs. The selection of electronic switches depends on the current-carrying capability, switching frequency and blocking voltages. The higher the switching frequency, the lower the torque ripples and the machine current, but this increases the switching losses [142].

In recent years, the IGBT has been commonly used in power converters due to its higher switching frequencies and high-power capability, IGBT can be used for voltages up to 6.7kV and currents up to 1.2kA [170]. The power electronics inverter, which is near to the electrical machine, controls rotor magnetic flux and speed of the electrical machine with a suitable modulation technique, it makes the electrical machine behave like a motor and generator according to the energy needs. Different topologies can be used for FESS applications such as AC-DC-AC, AC-AC, DC-AC. An AC-AC converter can be used in medium voltage applications. This converter has the disadvantage of high total harmonics distortion (THD), complex control and complex

design [219]. An AC-AC converter leads to an increase in reliability of system and power density [220, 221]. The AC-DC-AC is the most commonly used configuration in FESS, it is also known as Back-to-Back (BTB) converter, it is the most widely used topology in FESS applications [199]. In this configuration AC voltage is converted to DC by converter and DC voltage is converted into AC voltage and frequency by machine side converter. This is commonly connected with DC-link using DC-AC converter [219] the converter which is near to the machine is used to control active power and flux of the machine in FESS [137].

Different topologies of power electronics converters used in FESS are discussed in detail in [175]. To keep the flywheel system stable, it is vital to keep the DC link voltage constant, this is achieved by controlling the torque of the electrical machine. The constant DC link voltage behaves as an ideal DC voltage source like a battery. An AC-DC converter (grid side converter) with a suitable modulation technique is used to maintain a constant DC-link voltage by following grid side reference currents to control the flow of active and reactive power [222].

The design of the converter and its switching technique are responsible for the power quality of the system considering that nearly sinusoidal stator currents, low total harmonic distortion THD (less than 5%) and stable DC-link voltage are the factors affecting the power quality in FESS [223]. Oliveira in [224] has discussed implementation and control of AC-DC-AC conversion in FESS. A new DC-DC boost inverter topology used for low-speed flywheels is proposed in [225], with proposed topology the voltage boost capability is facilitated in a single stage with undersized passive elements. For efficient operation of FESS, a high-efficiency electrical interface is vital, in [226] zero-voltage transition (ZVT) and zero current transition (ZCT) has been proposed which improves energy savings from 2.5% to 3.5%. In [227], the power converter is presented which is used to control power flow in a hybrid microgrid, the system ensures zero current switching power loss for both buck and boost with improved efficiency. Experimental results show power savings of 2.5-3.5%. In

reference [228], the author has presented the operation of a converter with unity power factor under variable frequency and has implemented droop characteristics to control bidirectional power flow between AC and DC sources.

2.6.5 Containment

The flywheel rotor must be enclosed in a containment casing for safety and for reducing aerodynamic losses. The containment should prevent collateral damage which can happen due to the bearing failure releasing the rotor or rotor failure itself, for example, growth of a crack in case of a solid steel rotor flywheel. A fatigue crack may grow to cause the rotor to break in large fragments and can cause huge damage to surroundings if not contained [49]. In the case of carbon composite flywheel rotors, failure occurs due to circumferential fractures of a rotor in a layer or propagation of cracks in the rotor. This can cause the rotor to disintegrate into rings or may result in fragments and powder of carbon fibre that is highly flammable [229]. The rapid disintegration of a composite rotor can also lead to a very high-pressure build-up only contained by thick casing or bunkering. To increase the safety of solid steel and carbon composite flywheels, they are usually installed in underground bunkers [4]. This can be eliminated by the use of laminated steel designs which greatly limits any rotor failure to small energy release since only a small fraction of the rotor is ejected. Horizontal axle FESS has more possibility of mass centre displacement than vertical axle FESS that causes instability of the rotor [170]. The aerodynamic losses are reduced by creating a low-pressure environment for the rotor in the containment. Depending on the peripheral speed of the flywheel, containment casings can be made of high strength steel or composite materials [199]. For higher speed flywheels, the containment is filled with helium or evacuated to reduce windage losses, considering that the windage losses are negligible for less than 0.01 mbar pressure [230].

2.7 Applications of Flywheel Energy Storage System

2.7.1 Frequency Regulation

Due to daily and seasonal load variations, power consumption from the grid is concentrated during different time zones of a day which causes power quality issues such as lack of active or reactive power, voltage sag and instantaneous interruptions. This increases the response time of the generator besides increased fuel cost and CO_2 emissions. Therefore, the frequency regulation is a key parameter of the electric power system, it needs to be maintained within an acceptable limit of fundamental frequency for the power system to remain stable and reliable.

Flywheel technology has been used by electric utilities in hybrid distributed resources, transmission and distribution (T&D) grid stability and load levelling. Many manufacturers have been actively producing flywheel systems for utility applications. Different manufacturers and flywheel systems produced by them are listed in Table 2.4. The application of any ESS for frequency regulation will require extremely fast response and numerous charge and discharge cycles. Li-ion batteries which are inexpensive to install are commonly used for frequency regulation applications. However, their storage capacity is prone to degradation due to their fast-cycling requirement [142]. Flywheels and batteries being fast-acting storage systems are preferred by grid operators. However, flywheels are likely to dominate over the batteries in frequency regulation applications due to their frequent charge-discharge and fast-acting capabilities. For each megawatt of power produced, the flywheel can deliver twice as much frequency regulation whilst cutting CO_2 emissions in half according to [231]. A flywheel system of a small capacity can be used with BESS to suppress the frequency variations, this can reduce the size of the BESS, improve battery life and cycling capability [232]. A hybrid energy storage system consisting of Li-ion batteries of 8.8MW and six flywheels of 3MW of capacity is reported in [233].

Table 2-4 Characteristics of flywheel from different manufacturers [136] [234] - [235]

Manufacturer	Vacuum type	Bearing	Rating	Standby loss	Rotor Type	Speed (rpm)	Application
Piller	Helium	Magnetic & mechanical	1100 kW	4.5%	Steel	3,600	UPS, Railways
Active Power	Rough vacuum	Magnetic & mechanical	250 kW	0.76%	Steel	7,700	UPS
Urenco Power	Vacuum	Magnetic	250 kW	0.28%	Graphite Composite	36,000	Frequency regulations and maintenance
Beacon power	Vacuum	Active Magnetic	2 kW	3.5%	Graphite Composite	22,500	Recuperation
Pentadyne	Vacuum	Magnetic	120 kW	0.10%	Graphite Composite	60,000	Microgrid stabilisation, Cranes
BluePrint Energy	N/A	Magnetic	120 kW	*N/A*	Graphite Composite	28,000	Satellites, hybrid vehicles
Power Thru	Rough vacuum	Active Magnetic	190 kW	*N/A*	Fibre composite	52,000	UPS, electric vehicles
Flybrid	Vacuum	*N/A*	*N/A*	*N/A*	Carbon Fibre	60,000	Hybrid vehicles
Kinetic Traction systems	Vacuum	Magnetic and Hydrodynamic	333kW	*N/A*	Fibre Composite	36,000	Power quality, UPS, Railway
Vycon Energy Systems	Air	Active Magnetic	500 kW	<2%	Steel	36,750	UPS, cranes, train stations
ABB	Helium	Magnetic	1650 kW	0.72%	N/A	3,600	Microgrid stabilisation
GE	Air	Magnetic	300 kW	<2%	Steel	36750	UPS

The system provides stabilising primary frequency control in the transmission grid. The hybrid system is reported to have protected batteries from degradation and ensured their longer life cycle. The world's largest flywheel energy storage system is installed in Stephentown, a 20MW storage plant based on 200 magnetically levitated flywheel units is used for regulating the New York city frequency within the permissible level (60 Hertz) with the response time of less than 4ms, each flywheel weighs 1150kg and spins up to 16,103 rpm, the flywheel units are manufactured by Beacon power and they can perform 3000 to 5000 full depth of discharge cycles a year [170] [236]. Another 20MW FESS facility for frequency regulation is also reported in [237]. The plant in Hazle Township, Pennsylvania is installed by Beacon power, it provides frequency regulation services to a transmission organisation called the PJM Interconnection. The facility has a 20-years of lifespan and is comprised of 200 flywheels connected in parallel, each having a capacity of 100kW/25kWh. It is capable of performing 100,000 full depth of discharge cycles and can provide frequency support in less than 2ms.

2.7.2 Power Quality Enhancement

The power quality of the system is also linked with the quality of the bus voltage at the PCC. Ideally, the bus voltage is maintained sinusoidally at rated voltage and frequency. Some other common power quality issues are voltage sag, harmonic distortion and voltage unbalance. A power quality issue can lead to severe problems that can affect the security of microgrids. Microgrids having low inertia are usually prone to power quality issues, therefore, it is required for microgrids to have a fast-acting spinning reserve. Further power quality issues in are discussed in detail a [238]. FESS is a potential storage technology to compensate power fluctuations by supplying active and reactive power with fast response. FESS can best be used in wind energy management when power fluctuations affect the power quality due to variations in wind speed and lack of its controllability, an example of such study is presented in [140]. Control techniques for power, voltage and frequency have been proposed in

[239] to resolve power quality issues with the integration of FESS in wind energy systems.

Globally, FESS is used as the backup electrical power source to support critical loads. FESS can power critical loads until a backup diesel generator is brought into the system and synchronized [49]. The presence of flywheels in UPS supplies has been seen in the 21st century: it has been used for critical industries where continuous power is required. A flywheel UPS system is often used for power quality control and load levelling in place of batteries due to a lower maintenance requirement and smaller size [33]. If an AC disturbance in the power system lasts less than 3s, the standby generator can support the critical loads within 10s or less [240] with the flywheel being a fast-acting and mature technology that can replace the generator and electrochemical batteries for UPS applications. The operation of FESS can last up to 10 minutes for reactive power support and voltage regulation to improve power quality in computer servers and communication facilities [32]. However, if losses are kept minimal the operation period can be extended to hours without losing a considerable amount of energy [41]. For UPS applications, flywheels can provide power at a maximum rate of 15 seconds or more depending on the design whereas batteries provide the power at their maximum rating for over 15 minutes. Since standby generators can reach up to their maximum capacity within 10 seconds, therefore using a flywheel for UPS application instead of batteries is cost-effective. Moreover, regardless of the use of a standby generator, if a flywheel is used together with a battery-backed UPS system, this extends the battery life significantly by providing the power for short durations and saving the battery storage for longer duration disturbances [107].

A 20 MW flywheel technology designed by Piller Power Systems can ride through at 1.65 MW load for 10s, it operates at 1500 to 3600 rpm [13]. Ref. [241] presents the 18MW ABB flywheel installed in Coral Bay Australia. The flywheel plant provides power support to hybrid diesel and wind turbine systems for grid stabilization. The

plant uses bi-directional high-speed inverters which determine the power support needed by the system and significantly improves the power quality. A FESS plant based on 25 industrial flywheel units connected in parallel, having a power and capacity of 50 MW/650 MJ respectively was investigated in 2001. The plant can supply 50MW peak power for 13 s with an efficiency of 91-95%. The plant is used to supply energy for a large UPS system, plasma experiments and acceleration of heavy masses [170]. Ref. [242] presents the case study of 1.6 MVA FESS connected to a 20 kV distribution network. A feasibility study of the system was carried for application as a UPS system. The objective of the system is to improve voltage dips and power cuts caused by disturbances in the network. The system is operated along with a diesel generator system which supplies the power during long-duration power cuts.

In [243], a low-speed FESS has been used as a hybrid UPS comprising an engine generator and a flywheel to improve voltage fluctuations to less than 2%. To support emergency loads when the main grid supply is disconnected, successful utilisation of a FESS used as a UPS instead of BESS is reported in [244].

A 5 MW FESS developed by STANTEC is used to provide power support to the 13.8 kV distribution system at Guelph hydropower station Ontario, Canada. The system is comprised of 10 parallel flywheels each having capacity of 500 kW operating at 480 V [245]. There are numerous commercially available flywheels with power ratings of between 2 kW to 2 MW and energy capacity between 1 to 100 kWh. The flywheel can be connected in parallel to get larger power ratings [33]. The high-speed steel rotor flywheels systems manufactured by Vycon energy can be used for UPS applications as an alternative to the batteries, the Vycon flywheel can provide power at a rated capacity of 14 seconds, it can spin within the speed of 14500-36750 rpm [246]. The Piller company provides flywheels for UPS applications, the steel rotor flywheel spinning within range of 1500-3600 rpm provides a maximum rated power of 1.65 MW for around 10s [247]. Another manufacturer which produces flywheels for UPS applications is Active Power. Active Power manufactures a low-speed flywheel (2500-

7700 rpm) rated at 250 kW and operates in a vacuum. This FESS provides power support for 14s and has a standby efficiency of 99.8% [248].

The other major power quality issue for which FESS is successfully used is voltage sag. Voltage sag is caused by remote system faults, large motor start-ups or poor system maintenance. Without protection against this, it leads to tripping of equipment, decreasing lifetime and efficiency [238]. Voltage sag affects sensitive loads in industries hence hinders their production manufacturing ability. In three-phase networks, voltage sag increases the line losses, additional losses in electric drives and conductor overloads. Amongst power quality issues, about 92% of problems are related to voltage sag and 80% of voltage sag issues last only for 5-20 ms [41].

To mitigate voltage sag, series voltage compensation can be added to the power line using an energy storage system. FESS is a viable solution for voltage sag correction having numerous advantages such as fast response, the greater number of charge-discharge cycles and high-power density [249]. A 10 kW FESS used in a distribution network for power support is presented in [250]. The system can maintain the distribution voltage within a range of 98-102% with the capability of providing 10 MJ of energy for 15 minutes. In [251], Zhou et al. have presented a flywheel system for voltage sag correction in a distribution power network to protect critical loads by using a dynamic voltage restorer (DVR). The DVR mitigates voltage sags by injecting amplitude and phase-controlled voltage to restore the load voltage. Power systems onboard ships are isolated and vulnerable to voltage sag which occurs due to pulsed loads and faults causing power interruption to critical loads on board. FESS can be used in warships to mitigate voltage sag and maximise survivability in battle conditions. In [249], such an example of the study is present, the FESS is proposed for the shipboard power system to reduce voltage sags.

2.7.3 Transportation systems

FESS in transport systems reduces fuel consumption, maintenance requirements, noise and air pollution and provides short bursts of power for acceleration and

climbing hills [171]. In the 1940s the first flywheel bus (gyro-bus) was developed by Oerlikon, the flywheel could store 6.6kWh at speed of 3000rpm. In 1950 in Switzerland two flywheel buses were publicly operating for 10 years, however, due to high energy consumption, maintenance requirements and weight, these buses were taken off the road [167]. For an ordinary bus operating in urban areas, there are a huge number of starts and stops which makes the flywheel an excellent fit for traction power handling [234], this attribute of the flywheel has been reported to recover 30% of braking energy and can reduce the voltage drop at substation from 180V to 100V [252]. About 500 London buses were planned to be equipped with 0.4kWh flywheels from Williams Hybrid Power which was enough to accelerate the bus up to 50 kph. The system could save about 20 to 25 per cent of energy and provided savings of 5300 litres of diesel per bus annually. The system was about to be installed in existing buses which could lead to easy and inexpensive hybridization of buses, however, the project was later cancelled [234]. At the University of Texas, Austin a hybrid electric bus was being tested to replace the battery system with the flywheel. The FESS can store 7.2MJ of energy to accelerate the fully loaded bus to 100 km/h and has a 150kW power capacity. The flywheel used in the bus is expected to have 3-5 times more life span than the battery system and it is smaller in size and lighter in weight than the battery pack [252] [253]. The flywheel has been used in Formula 1 racing cars in the 2009 season by Flybrid systems. The Flybrid System develops flywheel systems for motorsport and road vehicles. The FESS developed by the Flybrid can store 400kJ of energy at a 60kW power ratings, the system can run at a speed of 64500 rpm with an efficiency of more than 70%. The system can be used in road cars, trucks, buses and trains as well. Simulations of the Flybrid system predicted 45% fuel cost savings on a 17t London bus, 35% on a 2.6t SUV and 18% on a 1.7t saloon car [254]. In 2011, the FESS was trialled in a hybrid car Jaguar XF, the system providing 12Wh of energy for 7s at the rated speed of 60,000rpm and a maximum power of 60kW with 20% savings on fuels cost, [255]. Some more applications of flywheel systems in the cars are reported in [256] [257] and [258].

Flywheel systems have also been deployed in rail applications. The ratings of the flywheel system (power and energy) for rail applications are determined by the speed and maximum weight of the train. For a high-speed train having nine cars, a flywheel system would need to store 470MJ of energy and provide 2MW of peak power [252]. Flywheel systems in rail provide several benefits such as improved fuel efficiency, better acceleration and reduced round trip time. Also, with the principle of regenerative braking, when the train decelerates its kinetic energy can be converted into electricity which can then be stored or provided to the electric grid for a short duration of time [175]. Flywheels have been used in DC metro lines in the US and UK. A 300kW FESS was tested on the Piccadilly Line train for providing energy savings and improved system's receptivity. The data showed that the system can switch between motoring and generation modes within 5 ms with minimum maintenance requirements. Following the trails on the Piccadilly Line, the flywheel system by Urenco Power was commercially used in the Far Rockway line in New York. Along with the energy, the system provided voltage support to the infrastructure [259]. Vycon installed a flywheel energy storage system in 2014 at Red Line Westlake Par subway station [260]. The purpose of the project was to recover energy from trains by regenerative braking, the results showed annual energy savings are estimated to be 541MWh which is sufficient to power 100 homes in California. Recent research on FESS in light rail systems is published in [261], the results show that the flywheel in the rail system saves 21.6% of energy and improves voltage drops by 29.8% and reduces the power loading by 30.1% on the substation. Moreover, energy storage systems can potentially reduce the power consumption of metro rail by 10% globally with cost savings of $90,000 per station [49].

Flywheels have also found an application in roller coasters, when a roller coaster slides down the hill, the flywheel is charged and then the stored energy is used to accelerate the train. The Incredible Hulk roller coaster at one of the theme parks in Orlando, Florida uses a friction wheel to accelerate the train at the speed of 18m/s,

with several flywheels (each 4500kg) charge continuously at 200kW and discharge at 8MW (for 2 seconds) to launch the roller coaster [49]. Also, the flywheel has been used in cranes operating for material handling. Diesel generators are usually used to provide power to the cranes to lift the heavy load/containers, when lowering the container, the energy can be stored in the flywheel and can be used when required [234]. Two units of the flywheels 60kW each was installed and tested in a crane by Vycon together with the University of Texas Austin at the ports of Long Beach and Los Angeles. The system stored 0.3kWh of energy (each flywheel) It was seen that fuel consumption was reduced by 21% and it was estimated that annually 100MWh of energy saving could be theoretically possible [234].

2.7.4 Spacecraft

In space, solar energy is generally converted into electrical energy which is used to energise electronic devices. However, during the eclipse period, having an energy storage system is vital to provide backup power due to the lack of solar energy [262]. Flywheels have attractive attributes for space applications, they can occupy the same space and weigh the same as the chemical battery. Flywheel units in space can power the load twice as long as chemical batteries without recharging. The flywheel developed by NASA has an efficiency of 93.7% can store 15MJ of energy and can deliver maximum power of 4.1MW. The space station can carry 48 flywheels equivalent to required battery boxes producing 150 kW altogether and it is estimated that savings of about $200 million can be achieved [252]. A flywheel demonstration project was started at Glenn Research Centre to replace the battery system on International Space Station, a comparison between the NiH_2 battery system and the flywheel showed that the flywheel system would be 6.7% smaller in volume and 35% lighter in mass [262]. In [263] a flywheel was tested on the International Space Station for flight experiments to replace the old batteries and upgrade the energy storage capability. Flywheel energy storage has been used in many space applications such as

altitude control for satellites, energy management, backup source and momentum control, few applications are discussed in [264] - [265].

2.7.5 Renewable Energy Systems

Increasing use of renewable energy in microgrids has affected the performance and reliability of microgrids significantly due to the intermittent supply from renewable energy sources. Also, the intermittent nature of renewable energy sources limits their application in stand-alone systems as a primary source of energy [137]. The output power of solar varies gradually during the day during non-cloudy days whereas the power output of the wind system varies frequently. However, during cloudy days, solar system output can vary considerably, particularly under broken cloud days as opposed to overcast clouds. Flywheels can smooth out both frequent and gradual power variations in electricity produced by solar and wind renewable sources [49]. Large wind turbine plants integrated into microgrids may cause frequency deviations, instability and voltage flicker [266]. With the use of appropriate energy storage technologies equipped with advanced control, the stability of the microgrids can be improved by compensating the variable power output of renewable energy resources [50]. The fast response of the flywheels makes them highly suitable for response to frequency imbalance caused by the irregular output power of renewable energy sources. FESS can improve the frequency of the system by responding to wind oscillations. In a PV based system, FESS can be integrated with battery systems to stabilize the system power output and improve the life cycle of the battery [170]. Wind and solar PV systems can run in parallel to a diesel generator to reduce its fuel consumption by allowing it to turn off when excess power is available from renewables. For a few occasions, the diesel generator is kept running at the no-load condition when power from renewables drops for a few seconds or minutes. This operation of a diesel generator is inefficient but can be minimised in a system with storage. The integration of the flywheel can further reduce fuel consumption by storing energy from giving back to the system when required and leaving the

generator turned off [235]. The application of FESS in hybrid renewable (solar and wind) with diesel generator are discussed in [136] [139] [266] - [267].

A 50kW, 0.6kWh flywheel system for active and reactive power support is discussed in [268]. The flywheel is integrated with a wind-diesel generation system is designed to power for 1.8m at a rated voltage of 750V to compensate for voltage and frequency. In 2005, Azores Electricity Company together with Power Corps integrated a 350kW/5kWh FESS in the hybrid power plant consisting of 2 wind turbines, 4 diesel generators and 4 hydro generators at Flores Island, Portugal for network stability and increased penetration of wind energy [269]. The results obtained from the project encouraged a follow on the installation of a flywheel system in Graciosa Island. A large-scale FESS was installed by ABB in Nullagine and Marble Bar in Western Australia for UPS applications leading to increased penetration of solar PV system. ABB's PowerStore flywheel can respond in 1ms, the integration of flywheels in the power network has enabled the PV system to supply 60% of energy needs for residential loads. Also, the incorporation of flywheels in the system has led to savings of 400,000 litres of diesel fuel and 1100 metric tons of emissions annually [270] [271]. Another project by the ABB company was installed in northern Kenya at Marsabit wind farm to serve a remote community of 5000. The 500kW flywheel system was integrated to maximise the penetration of 275kW capacity wind turbines in the network and boost the renewable energy integration [272]. The renowned flywheel manufacturers, Vycon Technology, Beacon Power, Urenco Power and ABB have developed a wide range of systems for penetration of renewable energy systems [266] [141].

2.7.6 Other Applications

Flywheel technology has been implemented in various other applications such as military, mining, flexible AC transmission (FACT) devices and research facilities. Extensive research on flywheels is being carried on by the US Department of Energy. The US Department of Energy (DOE) is considering flywheel technology for hybrid

electric vehicle (HEV) applications. The ability of flywheels to produce high-power pulses in HEVs is being explored [273]. Flywheels have found their place in mining applications for excavation purposes. The cyclic nature of an electrically powered dragline can enable a flywheel to store energy when lowering the loads. In Alaska, a 6MW electric dragline operates in the Usibelli coal mine and this is connected to Golden Valley Electric Association (GVEA) grid. This coal mine employs a 40-tonne flywheel to smooth the load fluctuations caused by the dragline. Before this installation, the dragline caused a flickering problem for the consumers connected to the grid which was then mitigated by the flywheel [49] by providing stored power during load variations. Moreover, the FESS system provides fuel savings of 32% - 38% when used with a generator set of 410kW [235] [274]. At the University of Texas, an experiment was performed using two 60kW flywheels spinning between 10,000 to 20,000 rpm installed in a container crane that could store 0.13kWh of energy. Theoretically, the data suggested that the system can achieve the energy savings of 100MWh/year if the flywheel is operated for 365 days in a year and a daily duration of 10 hours [234].

For pulsed power applications, a flywheel has been used in an electromagnetic aircraft launch system (EMALS). For aircraft launch assist, a flywheel has been used to energize the EMALS to replace the large and heavy catapults [275]. The power from the electrical system of the ship is used to charge the flywheel and the energy is released to produce pulse power during the launch of an aircraft, the pulse power lasts for 2 to 3 seconds. The array of flywheels used in EMALS can store 121MJ of energy, each running at 6400rpm [49]. Ref. [276] proposes a flywheel system for fusion experiments to extend plasma discharge times, the flywheel is used to energise a fusion device using toroidal field coils. The flywheel provides the peak power of 57kW for 1.3 sec at 1500rpm.

2.8 Chapter Summary

This chapter provided a detailed literature review on energy storage technologies and their applications with more focus on FESS. A brief history and emergence of the flywheel technology was presented together with its technical characteristics, structure of the flywheel and recent developments and contemporary work on the FESS.

The concept of kinetic energy storage dates back to ancient times with flywheel development progressing with the industrial revolution during the 18th century. During the 19th century with the emergence of modern machinery, the flywheel was used to smooth fluctuations in steam and combustion engines. With the advancement in high strength materials, bearings systems and power electronics, the flywheel has emerged as potential storage technology and the flywheel system has become commercially viable and it is frequently found in transport, space satellites and other high-speed power applications.

To make flywheel technology more efficient, the use of bearing systems is employed to minimize the energy loss due to friction. Three two types of bearings are mechanical and magnetic. Mechanical bearings have higher frictional loss compared to magnetic bearings and although lower cost, need maintenance for lubrication deterioration as a disadvantage. Magnetic bearings have high load capacity, fast response, long lifetime and low losses. There are three types of magnetic bearings AMB, PMB and SMB each has its operational characteristics and limitations. The hybrid bearing system which is the combination of mechanical and magnetic bearing is commonly preferred due to the increased reliability of the system.

The electric machine is the key part of the FESS which performs charge and discharge cycles based on the energy demand. The common type of machines used in FESS are IM, PMSM and SRM. PMSM is a widely used machine in FESS due to its high-power density and high efficiency. An IM is used for high-power applications due to its rugged construction low, high torque and high reliability. SRM has a robust design

and can be constructed from high-strength, low-cost materials. SRM can operate in high-temperature environments. It is less commonly used because of its complex torque current and high current ripples. A detailed comparison of the machines was provided in the chapter.

The power electronics converter is the main component in FESS assembly which makes power flow possible from and to the flywheel system. There are many topologies of the converters which are explained in the chapter. The most commonly used topology is AC-DC-AC which is called a back to back converter. The converters make use of transistor switches such as MOSFETS and IGBTs. For the safe and efficient operation of the flywheel, it is enclosed in solid containment. The containment is built from high strength materials. To reduce windage losses the sealed environment of the enclosure is kept at low pressure forming a vacuum environment. The peripheral velocity, material and design construction of the rotor determine the thickness of the casing for safe containment in the event of rotor structural failure.

Chapter 3

Modelling and Control of the Flywheel Energy Storage System

The energy conversion system for all energy storage systems consists of common components including a grid side converter (GSC), a machine side converter (MSC), an inductive filter, switchgear and a coupling transformer. The GSC interfaces the microgrid with the DC link and it regulates the DC link voltage and the reactive currents exchanged with the microgrid. The three-phase currents and the power flow from the microgrid are controlled by the GSC making use of IGBT power switches. Additionally, the GSC ensures that the control system of the MSC works properly. The MSC controls the exchange of power between the microgrid and storage device. Based on the power electronics interface, the topology of the MSC for flywheel energy storage (FESS) is different from the topology needed for other storage devices such as batteries, flow batteries, super capacitors and super magnetic energy storage (SMES) systems [277]. For the FESS, the structure of the MSC resembles the structure of the GSC, in that both converters are used to form an AC-DC-AC bi-directional cascaded configuration for power conversion with the help of an associated control system. The structure and configuration of the energy conversion system for FESS as connected to a microgrid is shown in Figure 3.1.

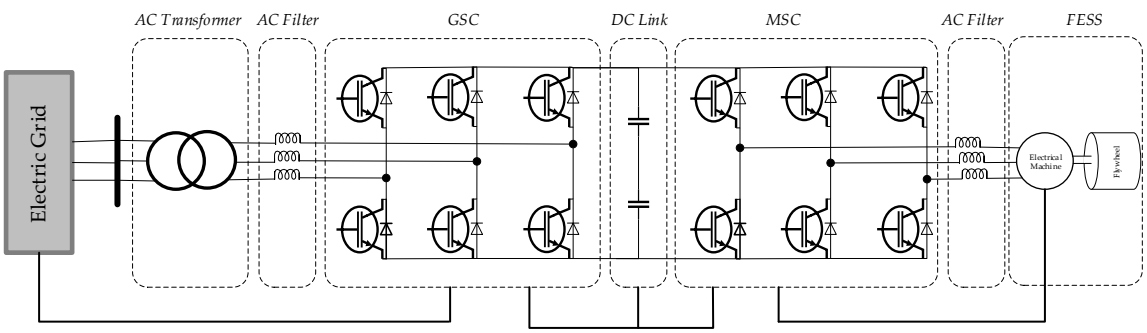

Figure 3-1 Structure and configuration of FESS

The electrical machine acting as a motor-generator (MG) is mounted on the same shaft as the flywheel rotor. Therefore, operation of the FESS is controlled by the MG set which performs energy conversion operations [278]. The type of electrical machine used in FESS is responsible for most of the system losses and is a key component affecting both performance and efficiency for the FESS. The operation of the flywheel is based on three modes i.e. acceleration, standby and deceleration. During acceleration mode the electrical machine acts as a motor to provide kinetic energy to the rotor of the flywheel, the MSC acts as an inverter and draws the power from microgrid and the GSC acts as rectifier maintaining a stable DC link voltage. While in deceleration mode the GSC acts as an inverter and the MSC acts as a rectifier delivering power from the electric machine (generator in this case) to DC link. In the case of standby mode, the flywheel runs at constant speed with trickle energy flow to make up for losses. Whilst in standby mode, ideally the flywheel is held at 50% state of charge which allows an equal amount of energy to be released or stored.

The charge and discharge operations of the flywheel depend on the %SoC of the flywheel and polarity of the torque signal produced by the MSC. Negative torque discharges the flywheel and positive torque charges the flywheel whereas when the flywheel goes into standby mode, there is a very small positive torque. The energy rating of the FESS is determined by the maximum and minimum speed of the flywheel whereas the power rating is limited by torque produced at shaft of the electrical machine which is related to electric current [277]. Since it is preferable to specify the maximum power of the flywheel to be independent of speed, maximum torque occurs at the lowest operating speed and the torque reduces inversely with speed as speed increases.

In this chapter, section 3.1 presents the mathematical modelling of SCIM, modelling and control of FESS is presented in section 3.2, modelling of PI controllers is described in section 3.3 and validation of FESS is presented in section 3.4.

3.1 Mathematical Modelling of Squirrel Cage Induction Machine

As stated earlier, performance of the FESS is highly dependent on the type of MG set which is the key component generating or absorbing power from microgrid. In this research, a squirrel cage induction machine (SCIM) was chosen to perform the energy conversion operation (kinetic energy (K.E) to electrical and vice versa). SCIM is best used for high power applications as they have high torque, reliability and robustness [170] [137]. The machine can be established with high strength material with low cost [137] and have no electromagnetic spinning losses due to zero torque in the absence of excitation field [279]. SCIMs are therefore an attractive option for low loss FESS with long term energy storage capabilities. Figure 3.2 presents the cutaway view of an industrial standard SCIM but the higher speed version required for the FESS would have a similar rotor and stator topology.

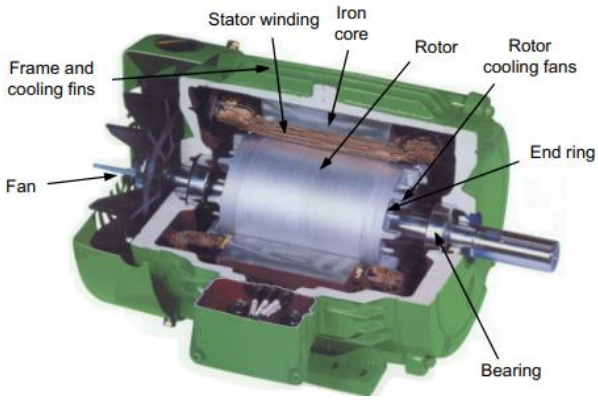

Figure 3-2 Cutaway view of squirrel cage induction machine [279].

Torque in induction machines is produced from the interaction of axial currents in the rotor bars and the radial flux. Torque acts in the direction of rotating field and the rotor is moved along the field. For an SCIM to operate, there must always be a difference between velocities of the rotating magnetic field of the stator and rotor which is described as slip. In motoring mode, positive rotor torque is only possible when rotor speed is less than speed of the stator magnetic field and, in generating mode, the speed of stator field is less than the speed of the rotor [280]. In a SCIM, the ends of rotor bars are electrically joined by end-rings, the types of material (aluminium or copper) being used for rotor bars depending on the size and application of the

machine. The construction of the rotor of the SCIM is done in such a way that no direct electrical connection can be made with rotor windings, therefore, the rotor currents are induced through air-gap fields. The stator winding of the SCIM is directly connected to the MSC. The rotor is not externally accessible which makes control of the SCIM more difficult, however it provides with more robustness [281]. The schematic diagram of stator and rotor windings of the SCIM is shown in Figure 3.3.

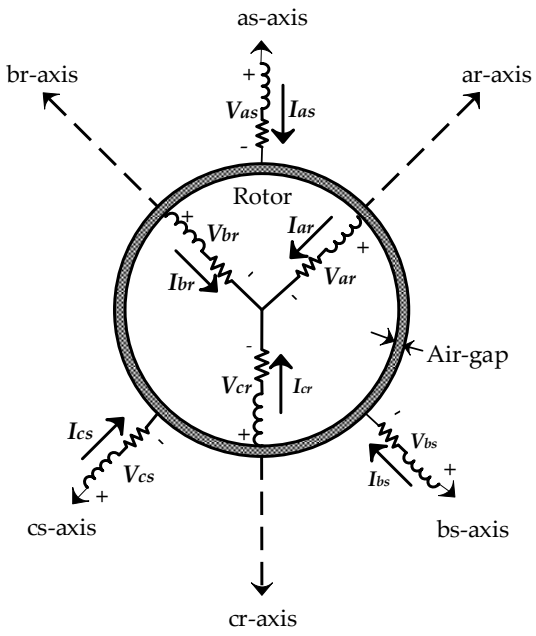

Figure 3-3 Schematic of SCIM windings

The SCIM can be modelled by applying electromagnetic laws (Faraday's and Lenz's law) and equations of motion to a moving rotor carrying a load. When the AC supply is connected to stator of induction motor, a rotating magnetic field is generated, according to the Faraday's and Lenz's laws, currents start flowing in the rotor windings leading to generation of rotating magnetic field. For efficient operation of induction machine, the slip speed must be kept as small as possible [281]. By applying the electromagnetic laws to rotor and stator circuits of SCIM, the voltage and flux equations are given by equations 3.1 and 3.2 respectively.

$$\begin{bmatrix} V_{as} \\ V_{bs} \\ V_{cs} \end{bmatrix} = R_s \begin{bmatrix} i_{as} \\ i_{bs} \\ i_{cs} \end{bmatrix} + \frac{d}{dt} \begin{bmatrix} \lambda_{as} \\ \lambda_{bs} \\ \lambda_{cs} \end{bmatrix} \tag{3.1}$$

$$\begin{bmatrix} V_{ar} \\ V_{br} \\ V_{cr} \end{bmatrix} = R_r \begin{bmatrix} i_{ar} \\ i_{br} \\ i_{cr} \end{bmatrix} + \frac{d}{dt} \begin{bmatrix} \lambda_{ar} \\ \lambda_{br} \\ \lambda_{cr} \end{bmatrix} \tag{3.2}$$

where :

V_{as}, V_{bs}, V_{cs} : stator phase voltages

i_{as}, i_{bs}, i_{cs} : stator phase currents

$V_{ar}\ V_{br}\ V_{cr}$: rotor phase voltages

i_{ar}, i_{br}, i_{cr} : rotor phase currents

$\lambda_{as}, \lambda_{bs}, \lambda_{cs}$: stator flux linkages

$\lambda_{ar}, \lambda_{br}, \lambda_{cr}$: rotor flux linkages.

The flux produced by a winding (stator or rotor) will not only be linked with the current within itself but also it will be linked to the currents flowing in other windings in the circuits. The stator and rotor flux linkage relations are given in equations 3.3 and 3.4.

$$\begin{bmatrix} \lambda_{as} \\ \lambda_{bs} \\ \lambda_{cs} \end{bmatrix} = L_s \begin{bmatrix} i_{as} \\ i_{bs} \\ i_{cs} \end{bmatrix} + L_m \begin{bmatrix} i_{ar} \\ i_{br} \\ i_{cr} \end{bmatrix} \tag{3.3}$$

$$\begin{bmatrix} \lambda_{ar} \\ \lambda_{br} \\ \lambda_{cr} \end{bmatrix} = L_r \begin{bmatrix} i_{ar} \\ i_{br} \\ i_{cr} \end{bmatrix} + L_m \begin{bmatrix} i_{as} \\ i_{bs} \\ i_{cs} \end{bmatrix} \tag{3.4}$$

where:

L_s : stator winding inductance.

L_r : rotor winding inductance.

L_m : mutual inductance between stator and rotor windings.

The flywheel rotor coupled with the SCIM is modelled as an inertia added to the shaft of the SCIM. The dynamics of SCIM-flywheel can be analysed and represented by Equation 3.5.

$$J_0 \frac{d\omega}{dt} = T_e - T_L - B\omega \tag{3.5}$$

where:

T_e : electromechanical torque

T_L	: load torque
ω	: angular velocity of the flywheel
J_0	: combined inertia ($J_0 = J_{SCIM} + J_{flywheel}$) of the IM and flywheel rotor (kg.m^2)
B	: damping coefficient.

Except in the standstill condition, the angular position (θ_e) of the rotor varies with time, hence the flux linkages and mutual inductance are the time varying quantities. Therefore, the voltage equations of stator and rotor are presented by time varying differential equations together with time dependent coefficients. The solution and analysis of time varying differential equations is complex hence making the modelling of the machine difficult. The modelling of a SCIM can be made simpler by use of two quadrature axes current instead of three phase currents.

There are two types of reference frames, the stationary reference frame (Clarke's transformation) and the rotating reference frame (Park's transformation). In the stationary reference frame, the three phase quantities (currents and voltages) are transformed into orthogonal quantities α and β. The coordinates do not rotate but remain stationary and these quantities are obtained by using Clarke's transformation technique. In rotating reference frame, the three phase quantities are transformed into *d-q* axes, the coordinates of *d-q* axes rotate at arbitrary speed ω. The *d-q* coordinates in the rotating refence frame are obtained by using Park's transformation technique [279, 282]. Figure 3.4 shows the vector stationary and rotating frame of references used in Clarke's and Park's transformation respectively.

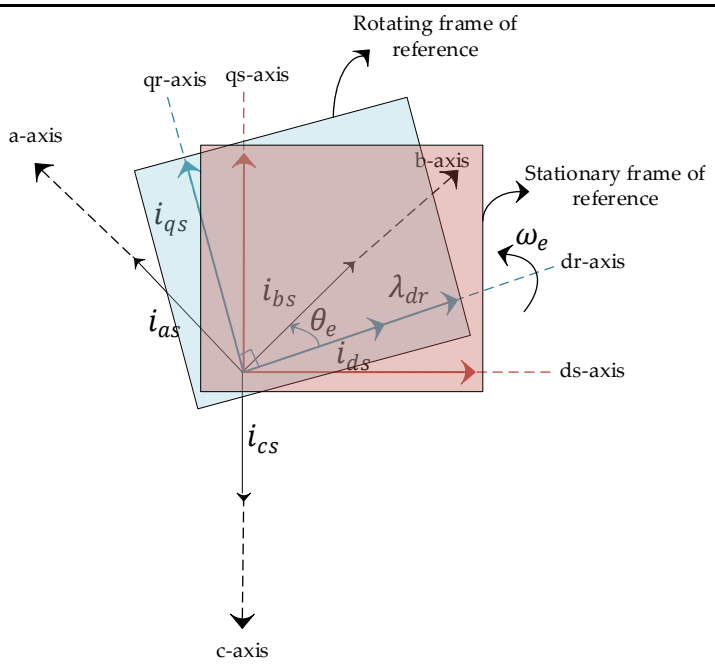

Figure 3-4 Vector representation of reference frames

The purpose of the rotating reference frame is to transform time varying sinusoidal quantities into a constant value in one reference frame having the same frequency, this makes the quantities easier to be controlled. Hence, for the ease of analysis and modelling of the control schemes, constant quantities are used instead of time varying sinusoidal quantities. Therefore, the time varying equations are transformed into *d-q* rotating frame by Park's transformation method which will reduce the complexity of equations. Application of Park's transformation will eliminate the time varying inductances in the voltage equations and the three phase quantities are converted into the *d-q* coordinate system.

The dynamic equations of the stator and rotor voltages of the SCIM shown in Figure 3.5 are presented in Equations 3.6 and 3.7, respectively.

$$\begin{cases} v_{ds} = R_s i_{ds} - \omega_e \lambda_{qs} + \frac{d}{dt}\lambda_{ds} \\ v_{qs} = R_s i_{qs} + \omega_e \lambda_{ds} + \frac{d}{dt}\lambda_{ds} \end{cases} \tag{3.6}$$

$$\begin{cases} 0 = R_r i_{dr} - (\omega_e - \omega_r)\lambda_{qr} + \frac{d}{dt}\lambda_{dr} \\ 0 = R_r i_{qr} + (\omega_e - \omega_r)\lambda_{dr} + \frac{d}{dt}\lambda_{qr} \end{cases} \tag{3.7}$$

Also, the dynamic equations of stator and rotor flux linkages are present in equations 3.8 and 3.9 respectively.

$$\begin{cases}\lambda_{dr} = L_s i_{dr} + L_m i_{ds} \\ \lambda_{qr} = L_s i_{qr} + L_m i_{qs}\end{cases} \tag{3.8}$$

$$\begin{cases}\lambda_{ds} = L_s i_{ds} + L_m i_{dr} \\ \lambda_{qs} = L_s i_{qs} + L_m i_{qr}\end{cases} \tag{3.9}$$

where:

v_{dqs} : stator voltages in *d-q* reference frame

λ_{dqs} : stator flux linkages

λ_{dqr} : rotor flux linages

i_{dqr} : rotor currents

i_{dqs} : stator currents

ω_e : rotor electrical speed

The electromagnetic torque (T_e) of the SCIM having *P* number of poles in *d-q* frame is expressed in terms of *d-q* currents which is given by Equation 3.10

$$T_e = \frac{3PL_m}{4}(i_{ds}i_{qs} - i_{ds}i_{qr}) \tag{3.10}$$

3.2 Modelling of the Control System of FESS

The torque of the electrical machine is the key parameter for its control system as the speed of the loads or their position can be controlled by the output torque of the driving machine. The two main torque controlling techniques are average torque control and instantaneous torque control. Average torque control is used in applications where accurate torque or speed control is less important such as fans, pump drives and blowers. The average torque control technique is based on scalar control method such as voltage frequency (V/*f*) control. The V/*f* method can be used to control torque only in steady state conditions however, it cannot be used to control the dynamic performance of a motor [279]. For high performance operation of motors, the instantaneous torque control method must be used where high precision speed or

torque control of motors is required such as is also used for applications such as CNC machines, motor drive lines, elevators and robots.

The control of an SCIM is not as easy as for separately excited DC machines because of the nonlinear and complex model needed for an SCIM. Instantaneous torque control for AC machines is complicated when compared to DC machines. For control of an SCIM, the linearity between input and output has to be maintained by means of a decoupled relationship between torque and the rotor flux for dynamic performance. In order to obtain linearity, space vector representation of the SCIM is used to overcome the problem. This space vector representation helps to transform the otherwise complicated model of an SCIM into a simple model as used for a DC machine and it helps to achieve decoupled control of torque and the flux.

Field-oriented control (FOC) and direct torque control (DTC) are commonly used techniques for instantaneous torque control, however, FOC is widely used despite being complex in design. The design of the control system for a FESS requires variable speed and instantaneous torque control for smooth operation of the system within entire range of speed [279]. A similar technique is used in this research for control of the speed of SCIM and power exchange between DC link and the flywheel.

3.2.1 Vector Control of SCIM

The vector control technique can be used to control an SCIM over a wide speed range. In vector control, three phase quantities are converted into *d-q* quadrature components, these are then responsible for flux level and generation of torque in the machine. Modelling of an AC motor is done in such a way so that it resembles the DC motor vector for simplicity and provides the decoupled control of rotor flux and motor torque. The synchronous reference frame is selected and linked to the flux linkage space vector because the synchronous reference frame moves in synchronism with space vector. The vector control can be modelled simply by using constant currents called direct current (I_d) responsible for flux generation quadrature current (I_q)

responsible for torque generation in the SCIM. The block diagram presenting the concise concept of the vector control system for the SCIM is shown in Figure 3.5.

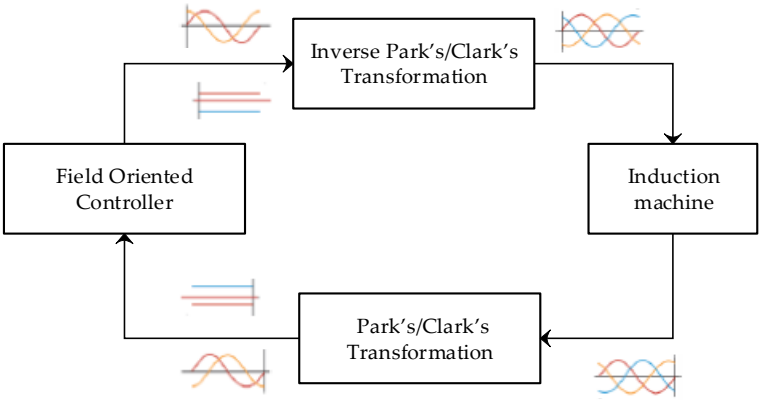

Figure 3-5 Vector control block diagram

The necessary requirement of a vector control system for an SCIM is knowledge of the instantaneous angle of rotor flux vector aligned with the rotating reference frame. Vector control of an SCIM can be classified based on the method used for determination of flux angle. One way to obtain the information of flux angle is from flux itself by measurements or estimation methods, this control is called direct vector control (DVC). The other method is to obtain flux angle indirectly from slip angular velocity which is used to separate three phase stator currents into torque and flux producing currents, this method is called indirect vector control (IVC). In DVC, direct measurements of flux require the use of Hall sensors or flux sensing coils in motor air gaps to measure air-gap flux. However, the implementation of sensors is an inconvenient option as this detracts from the ruggedness of SCIM. In addition to this, using the sensor adds more cost to the system. Therefore, estimation methods are used to calculate the flux value from other measured variables such as stator currents and voltages.

3.2.2 Vector control of Grid Side Converter

The grid side converter (GSC) controls the reactive power exchange with the microgrid. The topology of the GSC involves the inductive filter, AC power source and an inverter. The sinusoidal three phase microgrid currents and voltages are

transformed into direct and quadrature axis components which are 90^0 apart. The control system for the GSC consists of inner and outer current control loops. The inner current loop ensures that the *d*-*q*-axes currents follow the specified setpoints produced by the outer control loop. The voltage and current equations in rotating reference frame are presented by Equation 3.18

$$\left.\begin{aligned} L_g \frac{di_{ds}}{dt} &= -R_g i_{ds} + \omega_g \lambda_{qs} + v_s - v_{ds}^* \\ L_g \frac{di_{qs}}{dt} &= -R_d i_{qs} - \omega_g \lambda_{ds} - v_{qs}^* \end{aligned}\right\} \tag{3.18}$$

where:

L_g : grid side inductance

R_g : grid side resistance

v_s : grid side voltage

ω_g : grid frequency

For the GSC, the direct vector control scheme is used to control i_d and i_q in order to regulate the DC-link voltage during the charge, discharge and standby modes of the flywheel. Input variables to the controller are three phase currents (i_{abc}), three-phase voltages (v_{abc}), grid frequency (ω) at the point of grid connection and DC-link voltage (V_{dc}). The reference input variables to the controller are the reference DC-link voltage (V_{dc}^*) and *d*-axis reference current (i_{ds}^*), which is produced by a DC voltage regulator. In this control strategy, a unity power factor is assumed, therefore, $i_q = 0$ and $i_{d,ref}$ are generated by a PI controller by comparing the reference (V_{dc}^*) and measured DC voltage (V_{dc}).

The compensator term ($\omega\lambda_{dqs} = \omega L_g i_{dqs}$) eliminates coupling between *d*-*q* axes components and also reduces the error in the reference voltage (v_{ds}^*) produced by P-I regulator in order to accurately produce command voltage for modulation and generation of gating signals for switching devices. Using reference voltages, (v_{ds}^* *and* v_{ds}^*) the controller produces the set point values of voltages in the stationary reference frame ($v_{\alpha\beta}^*$) at the terminals of the IGBT voltage source converter to produce PWM

switching pulses at the desired frequency. For simplification of the control system, the d-axis component of the two-phase system is oriented to the direction of the microgrid voltage vector, therefore the grid side voltage (v_s) is equal to d-axis voltage (v_d) of the two phase coordinate frame ($v_s = v_d$) and the q-axis component is gained as $v_q = 0$ [283]. The angle for transforming three-phase currents (i_{abc}) into d-q reference frame is provided by a phase locked loop (PLL) at grid frequency. The control strategy of the GSC is shown in Figure 3.6.

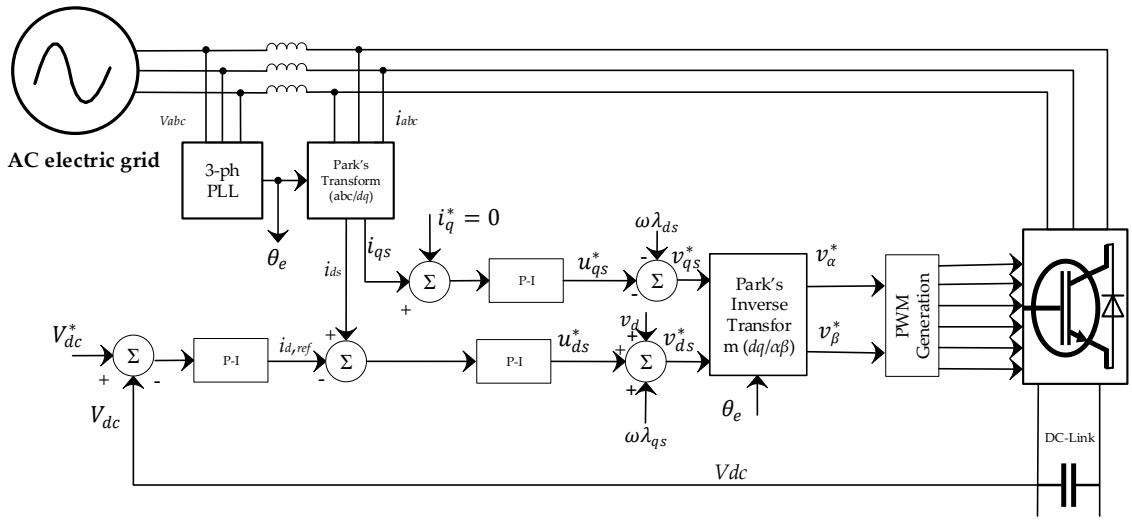

Figure 3-6 Control system of the GSC

During the charge and discharge cycles of the energy storage system, a flywheel in this case, the exchange of power takes place between the MSC and GSC via the DC link. The power calculated at the DC link is the difference between the power entering the DC link (P_{grid}) and the power leaving ($P_{storage}$) the DC link (from either side i.e. MSC or GSC), it is expressed by Equation 3.19

$$P_{DC} = P_{grid} - P_{storage} \tag{3.19}$$

The power consumption in the DC link capacitor is given Equation 3.20

$$P_{DC} = \frac{1}{2} C \frac{d}{dt} E(t)^2 \tag{3.20}$$

where:

C : Capacitance

$E(t)$: time dependent DC-link voltage.

Also, the AC power from the microgrid in the *d-q* reference frame during charging mode is given by Equation 3.21

$$P_{grid} = \frac{3}{2}(i_{d,G}v_{d,G} + i_{q,G}v_{q,G}) \tag{3.21}$$

where :

$i_{dq,G}$: *dq*-axes grid currents

$v_{dq,G}$: *dq*-axes grid voltages

P_{grid} : grid active power

3.2.3 Vector control of the Machine Side Converter

For stable operation of the FESS in any state of operation (Charge-discharge) , the speed of the flywheel rotor is fed back to the MSC through the speed feedback loop to control of torque and flux of the machine. The MSC manages the speed of the flywheel and energy power absorbed or injected from the microgrid. The DC-link voltage is fed back via voltage loop to MSC and GSC in order to maintain the voltage stable. The Proportional Integral (PI) controller are used to control the torque and speed of the flywheel. The PI control design are presented in section 3.3. The FOC controls the torque producing current (i_q) and magnetic flux producing current (i_d) separately leading to a simple control structure as of a DC machine with less uncertainty of parameter variations [284]. The vector control structure of the MSC is shown in Figure 3.7. The feedback loop in the MSC is formed by measuring three-phase stator currents, which are then transformed into the synchronous *d-q* reference frame by Park's transformation. DC stator currents i_{ds} and i_{qs} are compared with reference currents ${i_{ds}}^*$ and ${i_{qs}}^*$ using PI current controllers which will produce reference voltage signals ${v_{ds}}^*$ and ${v_{qs}}^*$ for generating gate pulses for MSC by SVPWM modulator. SVPWM is a modulation technique widely used in three phase inverters, it gives less harmonic distortion, lower torque ripples and switching losses in AC machines. More detail about SVPWM is provided in Appendix D.

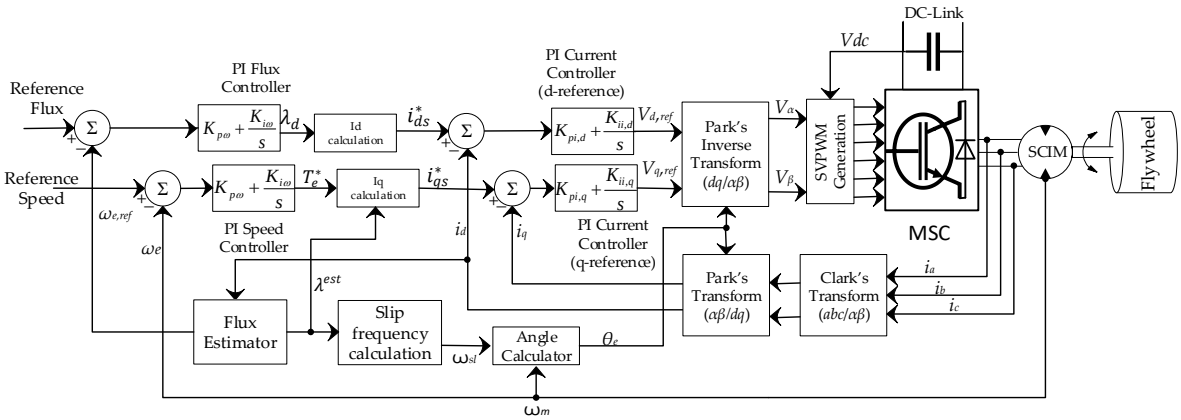

Figure 3-7 Control structure of MSC

As the working principle of the MSC controller is based on calculation of rotor flux, the position of the flux is assigned to the *d*-axis. Therefore, the rotor flux vector is synchronised with the *d*-axis in the *d-q* reference frame. Hence the rotor flux has no *q*-axis component but it is only associated with the *d*-axis component [279].

Therefore, $\lambda_{qr} = 0$ and the rotor flux linkage is represented by Equation 3.22

$$\lambda_{dr} = \lambda_r = \lambda_{dr}^{*} - \lambda_{dr}^{est} \tag{3.22}$$

where :

λ_{dr}^{*} : reference flux

λ_{dr} : *d*-axis rotor flux

λ_{dr}^{est} : estimated flux, calculated by using Equation 3.23

$$\lambda_{dr}^{est} = \frac{L_m i_{ds}}{1+sT_r} \tag{3.23}$$

A flux estimator calculates the actual magnitude of rotor magnetic flux using Equation 3.22 and 3.23 which is then compared with the reference flux. Reference *d-q* axis currents i_{ds}^{*} and i_{qs}^{*} are calculated using currents (i_d *and* i_q) calculator blocks.

The stator three phase currents are transformed into the *d-q* coordinate reference frame which is locked to the rotor flux vector rotating at the stator electrical frequency (ω_e). Due to decoupling of variables, torque and flux is controlled by i_d and i_q respectively.

Hence, i_d and i_q can be controlled separately and are represented by Equation 3.24 and 3.25 respectively

$$i_{qs}^* = \frac{2}{3} \cdot \frac{2}{P} \cdot \frac{L_r}{L_m} \cdot \frac{T_e^*}{\lambda_{dr}} \tag{3.24}$$

$$i_{ds}^* = \frac{\lambda_{dr}}{L_m} \tag{3.25}$$

where:

T_e^* : reference torque

P : number of poles

The reference values of stator currents in the synchronous *d-q* reference frame are compared with actual stator currents to produce reference voltages (V_{dref} and V_{qref}). Depending on the PWM technique, reference currents i_{ds}^* and i_{qs}^* are utilised accordingly. If current regulators are used to produce PWM pulses for the machine side inverter then i_{ds}^* and i_{qs}^* are converted to the reference three phase currents, i_a^*, i_b^*, i_c^* which are then compared to the actual three phase stator currents i_a, i_b, i_c to generate PWM. In the adopted technique i_{ds}^* and i_{qs}^* are fed to the PI current controllers to create reference voltages v_{ds}^* *and* v_{qs}^*. These are then used for SVPWM to create pulses for the machine side three phase inverter (Figure 3.7).

The calculation of rotor flux position is a key part of the control system and it is required for coordinate transformation as well. For rotor flux position, knowledge of stator slip frequency is essential, which is calculated from the *d-q* axes current commands for the required torque and flux production. The slip angular frequency required for calculation of rotor angle is given by Equation 3.26.

$$\omega_{sl} = \frac{1}{T_r} \cdot \frac{i_{qs}^*}{i_{ds}^*} \tag{3.26}$$

where:

T_r : rotor time constant and is given by $T_r = \frac{L_r}{R_r}$.

i_{qs}^* : reference *q*-axis current

i_{ds}^* : reference *d*-axis current

The electrical rotor flux angle can be obtained from knowledge of rotor speed (ω_m) and slip frequency (ω_{sl}). The relation between rotor speed and rotor slip frequency is given by Equation 3.27.

$$\omega_e = \omega_m + \omega_{sl} \tag{3.27}$$

By manipulation of Equation 3.27, the rotor position can be obtained by Equation 3.28.

$$\theta_e = \int(\omega_m + \omega_{sl})dt \tag{3.28}$$

3.3. Proportional-Integral-PI Controller Design

The design and structure of the controller depends on the order of the transfer function. For the first order transfer function, a PI controller is used and for the second order transfer function, a PID controller is used [285]. For the electrical drive and power electronics converter, a cascaded topology of the controller is used because of its flexibility. The cascaded control system is composed of speed, current and position control loops. The speed of the response increases towards the inner most loop when torque loop is required to be fastest and position loop to be slowest [286]. In a cascaded control system, the outer loop controls the speed or position of the machine or voltage of power converter. The inner current controller loop controls the current flow. The cascaded structure of the PI control is shown in Figure 3.8.

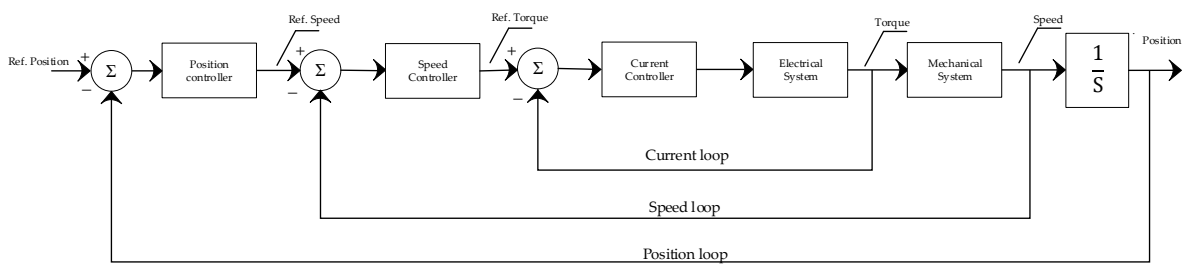

Figure 3-8 Cascaded control structure [286] [285].

The speed, position and torque of the flywheel rotor are controller by using a PI controller. By comparing the reference set values, the PI controller follows the changes in torque, speed and position of the rotor. In order to achieve linearity of the current systems, feedback control with high gain is used for the inner current control loop.

The PI controller is widely used in AC drive systems for position and speed control of the machines.

3.3.1 Flux Controller

Flux control of the SCIM increases the stability of the system when the machine operates at constant flux level. The magnitude of the SCIM machine flux is controlled by the d-axis current (i_{ds}), based on the gains of the PI controller, therefore output of PI controller has to be d-axis current. A block diagram of the PI flux controller is shown in Figure 3.9

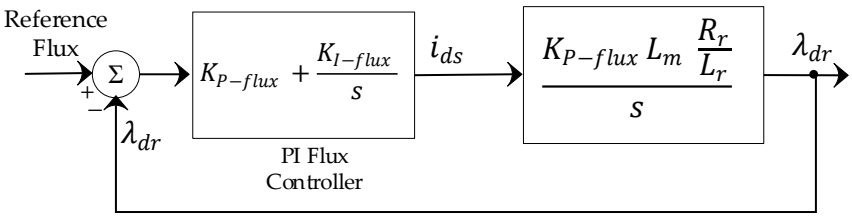

Figure 3-9 The PI flux controller

For better control design, the dynamics of the d-axis current should be aligned to the rate of change of rotor flux. The transfer function used in the flux controller is given by the Equation 3.29.

$$T(s) = \frac{K_{P-flux} L_m \frac{R_r}{L_r}}{s} \tag{3.29}$$

The gains (K_{I-flux} and K_{P-flux}) of the PI flux controller are a function of control bandwidth (ω_{cb}). The proportional and integral gains of the controller are represented by Equation 3.30 and 3.31

$$K_{P-flux} = \frac{L_r}{R_r L_m} \omega_{cb} \tag{3.30}$$

$$K_{I-flux} = \frac{\omega_{cb}}{L_m} \tag{3.31}$$

3.3.2 Speed Controller

Torque in the SCIM is produced as a result of interaction between the current and flux linkages. The speed of the SCIM is determined by the electromagnetic torque (T_e), the load torque (T_L) , inertia of the load (J) and the friction. The output of the speed

controller is always the reference electromagnetic torque. Therefore, in order to control the speed of the SCIM, the torque should be controlled. By controlling i_{qs}, the torque of the SCIM can be controlled instantaneously. Assuming a constant d-axis current, the relationship between i_{qs} and the reference torque is given by Equation 3.32.

$$T_e = \frac{2}{3} \cdot \frac{\mathrm{P}}{2} \cdot \frac{L_m^2}{L_r} i_{ds} i_{qs} \tag{3.32}$$

The control of output torque of the SCIM requires the following conditions to be met

- The i_{qs} and i_{ds} are in quadrature (at 90 degrees)
- The i_{qs} can be controlled instantaneously
- The i_{qs} and i_{ds} can controlled separately

The PI controller sets the speed of the rotor closer to the reference speed and calculates the reference value of torque (T_e^*). The gains of the PI controller reduce the error between measured speed (ω_m) and reference speed and help the PI controller to follow reference and track the reference speed value. The reference value of the torque will set the reference value for machine to generate required electromagnetic torque (T_e) to overcome the load torque (T_L) in order to follow the reference speed value.

The proportional (K_{pt}) and integral (K_{it}) gains of the torque controller are given by Equations 3.33 and 3.34 respectively. The gains of the controller are the function of bandwidth and machine parameters such as inductance and resistance.

$$K_{pt} = L_s \omega_{cb} \tag{3.33}$$

$$K_{it} = R_s \omega_{cb} \tag{3.34}$$

3.3.3 Voltage Controller

The DC link voltage varies during exchange of power between the FESS and microgrid during charge and discharge operations of the FESS. Therefore, the voltage controller is implemented to stabilise and maintain the DC link voltage close as possible to the reference value. The DC link voltage is regulated to adjust the active power at the DC

link from AC source. The three phase currents from the microgrid are transformed into the *d*-*q* rotating reference frame using the transformation technique. The *q*-axis current is called active power current and *d*-axis current is termed as reactive power current and is related to reactive power of the system. Assuming a unity power factor and minimum loss, the *d*-axis current will be zero. The DC current (from GSC) as a function of *q*-axis current is represented by Equation 3.35. The liner relationship between active power current ($I_{q,g}$) and DC link current ($I_{DC,g}$) constitutes the transfer function and PI gains for voltage controller.

$$I_{DC,g} = \frac{3}{2}\left(\frac{V_{g,q}I_{q,g}}{V_{DC}}\right) \tag{3.35}$$

The voltage controller contains two cascaded current loops, the reference quadrature current (I_q^*) is generated by the outer current loop for the inner control loop. The *q*-axis current control loop in shown in Figure 3.10.

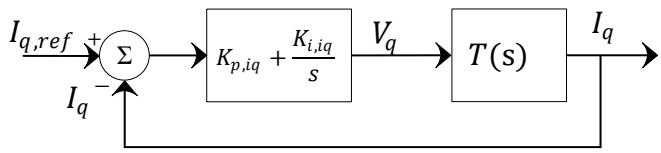

Figure 3-10 Current control loop of the voltage controller

The transfer function of the current control loop is given by Equation 3.36

$$M(s) = \left(\frac{K_{p,iq}S+K_{i,iq}}{s}\right)T(s) \tag{3.36}$$

where $T(s)$ represents the first order function and it represented by Equation 3.37.

$$T(s) = \frac{Cs+R}{LCs^2+RLs+L} \tag{3.37}$$

For the full bridge voltage source converter having capacitance *C*, resistance *R* and inductance *L*, the schematic diagram of voltage controller is represented in Figure 3.11. The closed loop transfer function between reference DC link voltage and measured DC voltage can be written as follows:

$$G(s) = \left(\frac{K_pS+K_i}{s}\right)\left(\frac{3}{2}\frac{V_{g,q}I_{g,q}}{V_{DC}}\right)\left(\frac{1}{Cs+R}\right) \tag{3.38}$$

The gains of the PI controller K_p and K_i are time dependent and they are functions of inductance and resistance and they can be obtained by using Equation 3.39

$$\begin{cases} K_p = \frac{L}{\tau} \\ K_i = \frac{R}{\tau} \end{cases} \tag{3.39}$$

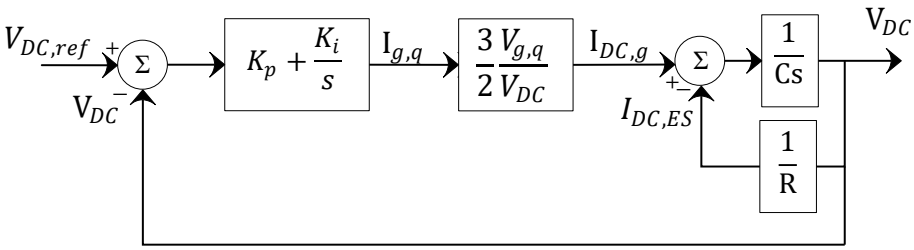

Figure 3-11 Schematic diagram of DC link voltage controller

During the charging and discharging states of the FESS, the gains of the PI-controller can be determined by using the equations presented in the chapter. The gains are a function of parameters of the SCIM and the power electronics converters. The PI controllers are further tuned in the MATLAB environment for compensation of any possible error and to achieve the better accuracy.

3.4 Validation of FESS and its Control System in MATLAB/Simulink

In reference to the dynamic equations and control structure presented in the above sections, the model of SCIM-FESS was developed in MATLAB/Simulink environment. The SCIM-FESS was set to run for 24min as sufficient length of time for testing the simulation and also because this was the maximum run time which could be afforded until a solution was found for later simulation runs. The dynamics of the FESS during acceleration and deceleration states were tested within the design operating speed range of 10–20 krpm. In these initial simulations, the FESS is directly connected to the electric grid and exchange of power takes place between the grid and the FESS. During the acceleration state, the flywheel receives electric power from the grid and based on the magnitude of the power, a positive torque is generated to charge the FESS. During the deceleration mode, when demand of power from electric grid arises, power is delivered to the grid from the FESS, based on power demand, a negative torque is

produced by the controller to convert stored kinetic energy into electricity and the FESS delivers energy to the electric grid. The SCIM-FESS is designed to deliver 5kWh of useable energy during which the DC-link voltage is set to 600V and maintained by the GSC and MSC during different states of operation. The results are presented in next sections to show different modes of operation of the flywheel.

Acceleration-Standby Mode

The performance of the FESS under the condition of acceleration to maximum speed followed by standby is presented in Figure 3.12. During this acceleration mode, a power of 50kW (half of maximum) is injected into the flywheel from the electric grid and a positive torque is generated which charges the flywheel. It takes 6 mins for the FESS to reach 100% of charge (20krpm speed). At t = 6 min the FESS goes into standby mode of a type which allows rundown as opposed to sustaining a constant speed by means of a small power injection. In this way, the small fall in speed could be detected to ensure windage and bearing losses were being captured correctly.

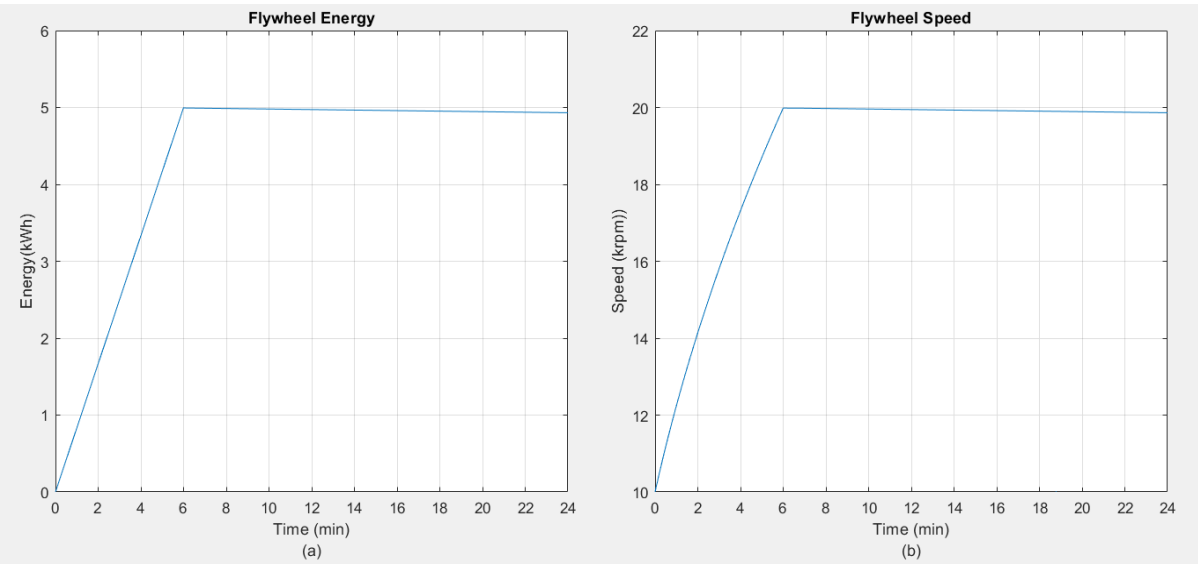

Figure 3-12 a) Energy stored by the flywheel; b) Flywheel speed

During this form of standby mode, the flywheel speed and SoC decrease gradually due to the system losses including the aerodynamic and bearing friction losses. The copper losses are zero because currents stop flowing in the stator of the SCIM during the standby mode due to the rotor being de-energised. During standby mode, the

flywheel state of charge drops to 95.8% due to self-discharge giving about 258Wh of energy loss in 18 minutes which is 5.16% of maximum stored energy. The total power loss (p.u.) in standby mode is calculated from the ratio of the change in kinetic energy of the flywheel ($\Delta KE_{flywheel}$) in Joules over the period of (Δt) in second, with respect to the rated kinetic energy of the flywheel ($KE_{rated\ FESS}$) in Joules, as expressed by Equation (3.40) [287]. Calculation of power loss gives 9.5% of total power loss over the period of 24m. A detailed description on electrical and mechanical losses of the flywheel is given in section 3.5.

$$\%P_{loss} = \frac{(\Delta KE_{FESS})}{\Delta t \times KE_{rated\ FESS}} \times 100 \tag{3.40}$$

Figure 3.13 shows the torque curve of the flywheel, it can be seen that the torque of the flywheel decreases as flywheel approaches its nominal speed (20krpm) because the torque applied to the shaft of the flywheel is function of its speed and power. The DC link voltage presented in Figure 3.14 shows stability during entire operation of 24 mins and at remains at nominal value of 600V.

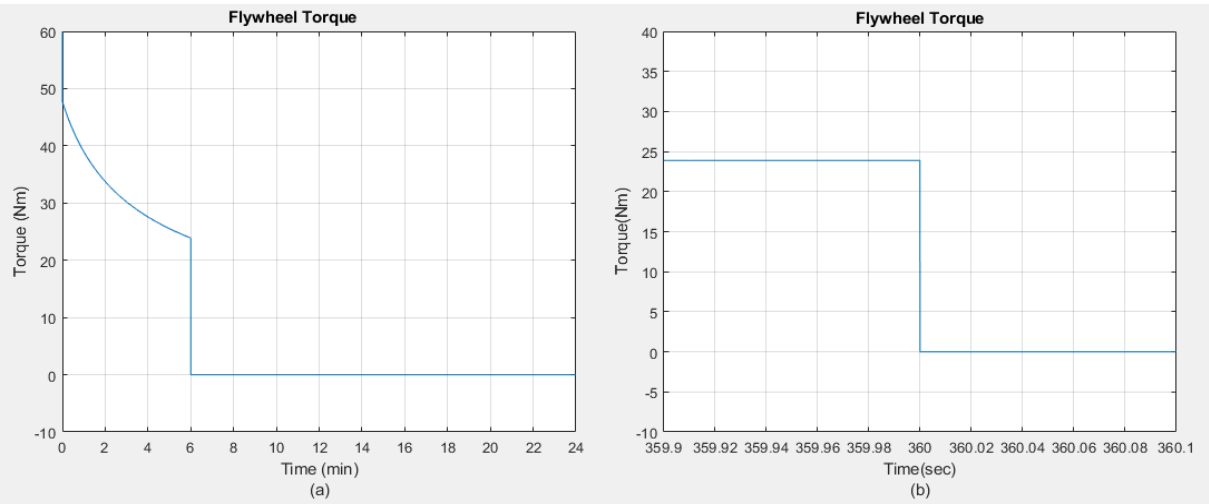

Figure 3-13 a) Torque of the flywheel; b) Zoomed in view of the torque curve

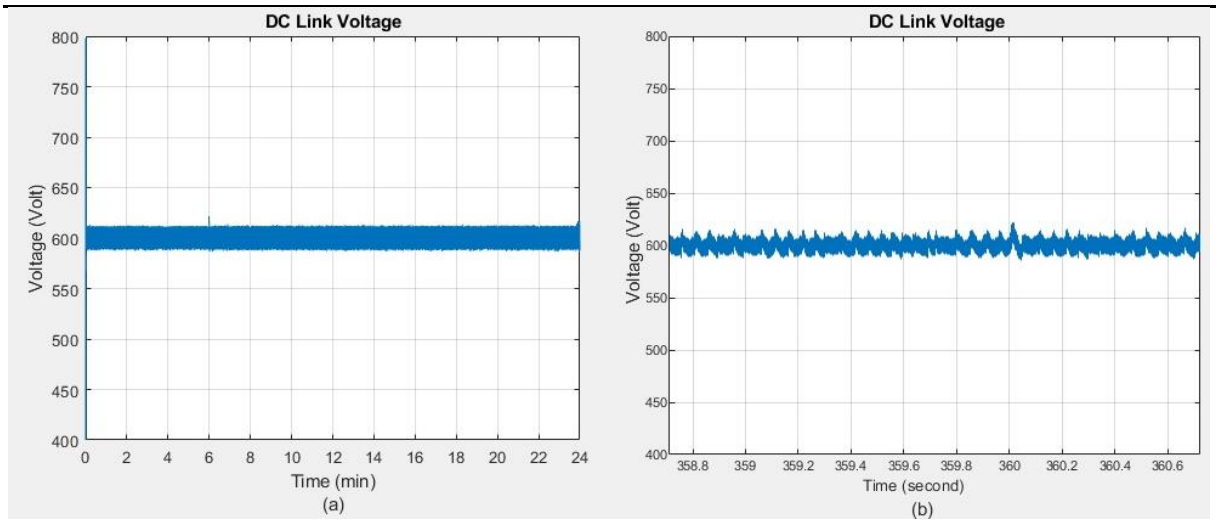

Figure 3-14 a) DC link voltage; b) Magnified view of DC voltage

Deceleration-Acceleration Mode

To analyse the flywheel performance during acceleration and deceleration states, different charge-discharge operations were performed during a period of 24 min to show the system responsiveness due to torque variations corresponding to load variations in real life situations. The flywheel is initially charged for 6 min, then switched to standby mode for approximately 5 min before its discharge operation.

At t = 11 min the flywheel is discharged and the stored kinetic energy is converted into electrical energy which is supplied to the electric grid. At t=1.44 min, the flywheel starts charging for 1.5 min and the flywheel again reaches to 100% SoC. At t = 16 min the flywheel is discharged at higher rate compared to its first charging cycle this is due to high power demand and higher torque experienced by the FESS. The flywheel is completely discharged and reaches to 0% SoC t =18.4 min and goes into standby mode. During standby mode at 0% SoC the flywheel is spinning at 10krpm and no usable kinetic energy is available since this is the minimum operating speed. Speed and torque curves for the flywheel are shown in Figure 3.15 for the different charging and discharging states of the flywheel. Magnified images of phase stator currents and torque are shown in Figure 3.16 where it can be seen that the SCIM smoothly switches from generating to motoring mode without any major spikes or transients in the

current waveforms showing the compliance and better performance of the machine side control system (MSC).

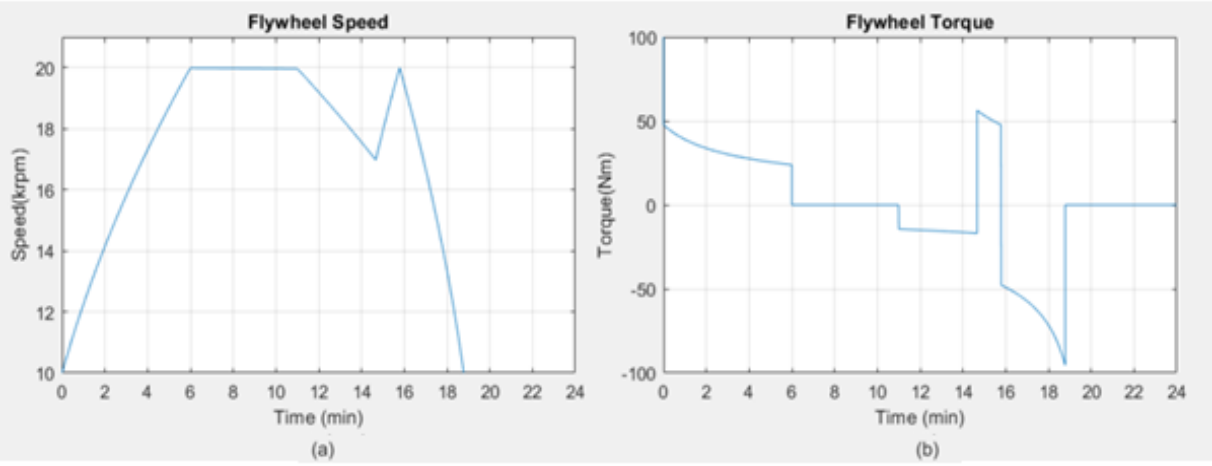

Figure 3-15 a) Flywheel Speed; b) Electromagnetic torque of flywheel

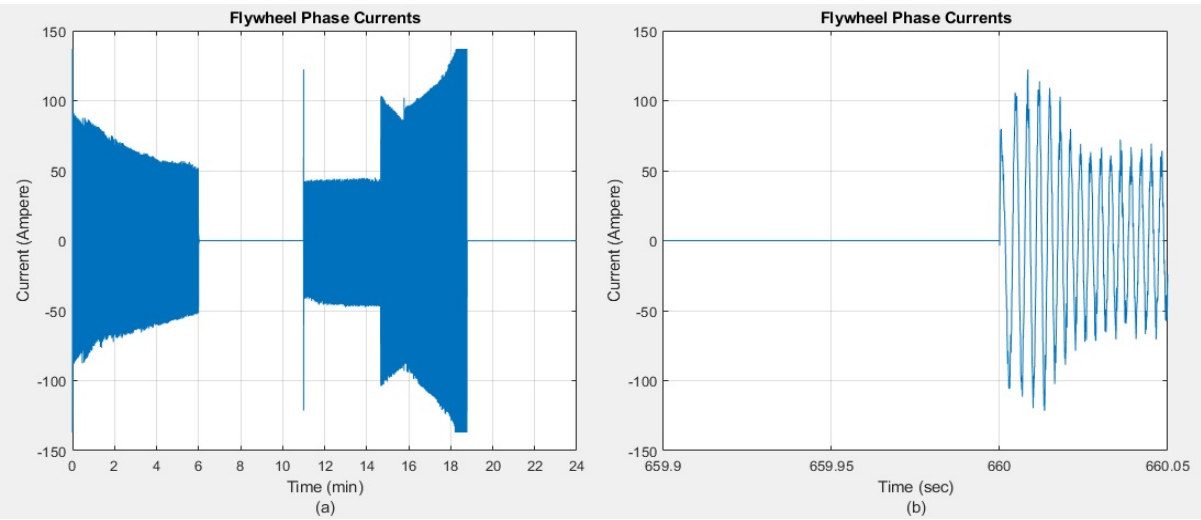

Figure 3-16 a) Stator phase currents of flywheel; b) Magnified image of the currents

3.5 Modelling of System Losses

The aerodynamic drag and bearing friction are main sources of loss in the FESS. Although they are small compared to losses in the electrical machine, when operated, they are present all the time so the energy losses can mount up. To reduce the drag loss, the flywheel rotor is contained in a vacuum containment. Despite the setup of a vacuum environment in the containment, the drag loss still accounts for major portion of total power losses of flywheel system but this could be reviewed and losses reduced by reducing the pressure further. The pressure was chosen to be 0.01mbar, a pressure

not too low since higher vacuum would require a more sophisticated vacuum pump. As mentioned, in this research, the considered flywheel system is a cylindrical rotor type made of steel laminates and operated in low to medium pressure vacuum running between a speed range of 10–20 krpm. The type of bearings used are single row radial ball bearings with micro drip type of lubrication. The detailed calculation and analysis of the switching and conduction losses in power electronics converters were not carried out here but assumed with a fixed value not to exceed more than 2% of the total energy produced in one cycle. This is added to the electrical and mechanical losses when the total system losses are calculated.

3.5.1 Electrical Losses

The electrical losses in FESS are mainly due to the stator and rotor losses in the motor/generator set whilst energy is being withdrawn or supplied. The stator electrical losses are the combination of copper losses (P_{scl}) in the stator winding and core losses (P_{core}) in the stator core. The stator copper losses are proportional to the square of the RMS magnitude of stator currents I_s and are dependent on the value of the stator resistance R_s. Core losses (eddy current and hysteresis losses) are a function of electrical angular frequency f_e and maximum magnetic flux density B_m. Equation 3.40 presents the general relation of core losses in the electrical machine while the total electrical losses in the stator of IM are given by Equation 3.41.

$$P_{core} = (K_{hys} f_e + K_e f_e^2) B_m^2 \tag{3.40}$$

$$P_{stator} = 3 I_s^2 R_s + (K_{hys} f_e + K_e f_e^2) B_m^2 \tag{3.41}$$

where K_{hys} is the Steinmetz co-efficient, B_m is peak magnetic flux density and K_e is a constant factor as given by Equation 3.42 [288]

$$K_e = \frac{\pi^2 t^2 \sigma}{6\rho} \tag{3.42}$$

where t is the thickness of laminations, σ is electrical conductivity and ρ is the density of the electrical steel. The rotor copper losses (P_{rcl}) are also a combination of copper and rotor iron losses (P_{core}) and are given by Equation 3.43.

$$P_{rotor} = 3I_r^2 R_r + (K_{hys} f_{sl} + K_e f_{sl}^2) B_m^2 \tag{3.43}$$

where, $f_{sl} = s f_e$, s is the slip, R_r is rotor resistance and I_r is the RMS magnitude of rotor currents in one phase of the rotor.

For calculation of Steinmetz coefficient (K_{hys}), Equation 3.44 is divided by the term $f_e B_m^2$ to create a linear relationship.

$$\frac{P_{core}}{f_e B^2{}_m} = (x + y f_e) \tag{3.44}$$

where, $x = K_{hys}$ and $y = K_e$ which can be simply calculated by substituting the values of parameters (t, ρ and σ) into Equation 3.43 , giving $y = 3.34 \times 10^{-3}$ Hz. The value of x can be calculated by linear fitting of Equation 3.44 for the best approximation of the data. The iron loss varies in an identical pattern when temperature of the laminations is 40 ^{0}C and 100 ^{0}C, however, at iron losses vary on different pattern when flux density and frequency are same. Figure 3-17 shows the B-H curves of the stator and rotor core at different temperatures. It can be seen temperature affects iron losses significantly. Different models on iron losses are discussed and presented in [289], [290].

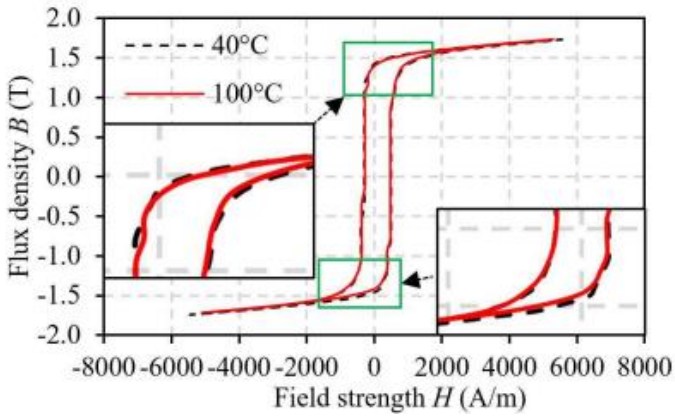

Figure 3-17. B-H loops at different temperatures [291].

The stator and rotor core of the SCIM are assumed to be made of electric steel M470-50HP. Manufacturer's core loss data for M470-50HP is shown in Table 3.1 where the core loss data for specific electrical frequencies of 50 Hz, 100 Hz, 200 Hz and 400 Hz is provided. The electrical frequency of SCIM-FESS presented in this paper at 20 krpm is 333 Hz that lies between 200 Hz and 400 Hz. Therefore, the values of Bm at 333 Hz

is approximated between 0.6–0.7 Tesla as calculated based on the methodology discussed in [292]. Electrical parameters of rotor and stator core material are provided in Appendix F. The flux density curves adopted from ref [292] are shown in Figure 3.18.

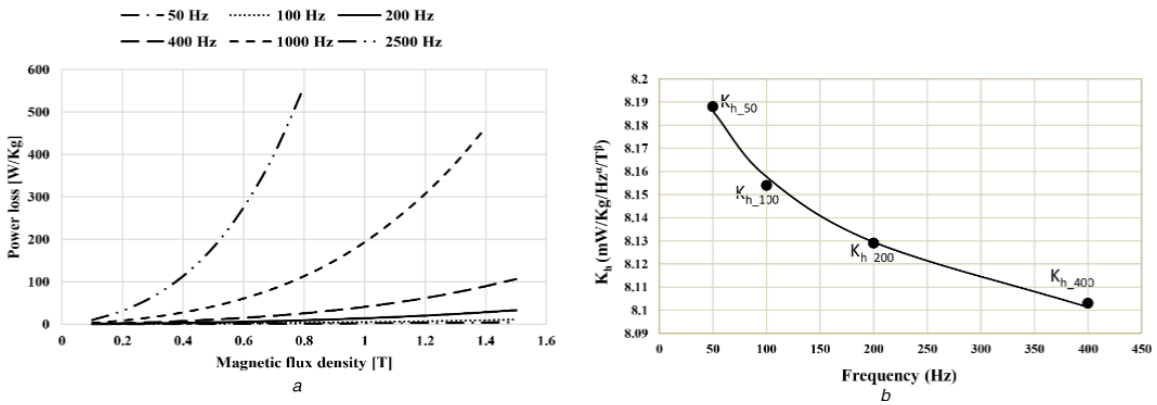

Figure 3-18. a) Magnetic flux density; b) Hysteresis coefficient curve of the material

Table 3-1 Manufacturer's loss data for M470-50HP electrical steel.
Adapted with permission from [293] Cogent Power Inc., 2019.

B_m (T)	W/kg at 50 Hz	W/kg at 100 Hz	W/kg at 200 Hz	W/kg at 400 Hz
0.1	0.03	0.07	0.23	0.58
0.2	0.13	0.29	0.84	2.14
0.3	0.26	0.61	1.71	4.37
0.4	0.43	1.00	2.78	7.17
0.5	0.63	1.46	4.03	10.6
0.6	0.85	1.98	5.48	14.7
0.7	1.09	2.55	7.12	19.6
0.8	1.34	3.19	9.02	25.4
0.9	1.62	3.91	11.2	32.4
1	1.94	4.71	13.7	40.6

Substituting the values of x and y in Equation 3.45, the relation of P_{core} can be written as:

$$P_{core} = (0.0487 f_e + 1.4 \times 10^{-3} f_e) \tag{3.45}$$

Using Equation 3.45 and substituting the values of resistances into Equations 3.41 and 3.43, the total electrical losses of the stator and rotor are given by:

$$P_{stator} = (0.099 I_s^2) + (0.048 f_e + 1.4 \times 10^{-3} f_e) \tag{3.46}$$
$$P_{rotor} = (0.027 I_r^2) + (9.6 \times 10^{-4} f_e + 2.8 \times 10^{-4} f_e) \tag{3.47}$$

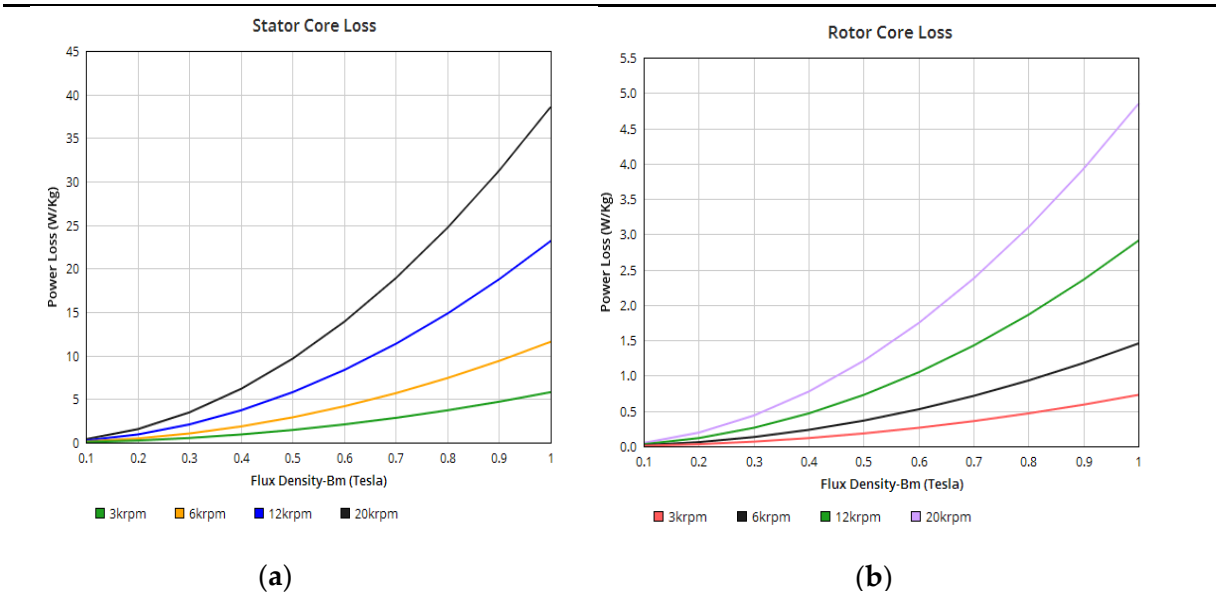

Figure 3-19 Specific core losses of SCIM-FESS: (a) Stator core losses; (b) Rotor core losses.

Stator and rotor specific core losses of the SCIM-FESS are shown in Figure 3.19. The core losses occur in largest fraction in the stator of the SCIM because at low slip, the SCIM operates at synchronous speed and the relative speed of magnetic fields over the rotor surface are slow, therefore, rotor core losses are very small compared to stator core losses [294].

As shown in Figure 3.19a, the specific core losses increase exponentially with increase in speed and magnetic flux density. The stator specific core losses are not significant for values of magnetic flux density up to 1 Tesla and 3krpm speed. However, the specific core losses in the stator of the SCIM increase significantly above 3krpm and even at 0.648 Tesla, the power losses due to hysteresis and eddy currents in stator core of SCIM operating at 20krpm are 16.48W/kg. Rotor specific core losses of the SCIM are shown in Figure 3.19b and it can be seen that rotor specific core losses increases exponentially with increase in maximum magnetic flux density.

Stray Losses

Eddy current loss, core loss and losses in other metallic parts of the machine are called stray losses. They are caused due to the flux leakages and of the machine. Stray losses in SCIM can be categorised as stator and rotor stray losses. Stray losses in rotor of a

SCIM depend on the rotor slip as they are function of frequency. According to the IEEE standard 112, stray load loss for different power outputs of typical SCIM are given in Table 3.2. An Equation 3.49 is general equation for stray loss of the machine according to the IEEE standards. Figure 3.20 shows the stray loss curve of a SCIM at different range of speed.

Table 3-2 Values of stray load losses for different power outputs [295]

Rate output power (kW)	Ps/Pout (%)
1-90	1.8
91-375	1.5
376-1850	1.2
1851 and greater	0.9

$$P_{stray} = 0.005\frac{P_g^2}{P_r} \tag{3.49}$$

Where P_g is generated power and P_r is rated power.

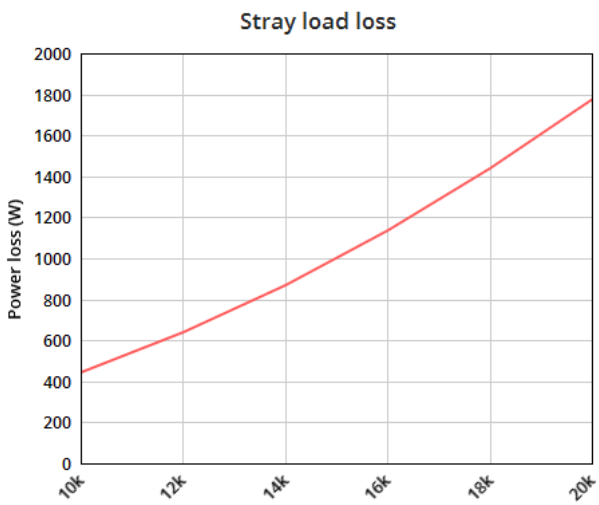

Figure 3-20 Stray load loss at different speeds

3.5.2 Mechanical Losses

Windage Loss

The windage losses in a FESS are due to the friction between the rotating surfaces and the surrounding medium, which is air in most cases. The windage loss increases with increase of the flywheel speed and is proportional to the cube of the flywheel angular velocity [296]. In order to reduce the windage loss, the pressure around the flywheel needs to be reduced. With decrease in air pressure in the containment the behaviour

of the air flow changes from turbulent to laminar and to molecular at low pressures (<0.1Pa) [297].

There are different types of air flows depending on the degree of rarefaction and can be classified based on Knudsen number (K_n), the air flows are classified as molecular flow ($K_n > 0.01$), continuum flow($K_n < 0.01$), transition flow ($K_n > 0.1$), slip flow ($K_n > 0.01$) and free molecule flow ($K_n > 10$). The Knudsen number is dimensionless parameter and it is defined as ratio between mean free path of a molecule (λ) to length of the presented object (l) [298]. The mathematical expression of Knudsen number is given by Equation 3.50.

$$K_n = \frac{\lambda}{l} = \sqrt{\frac{\pi\gamma}{2}} \cdot \frac{M_a}{R_e} \tag{3.50}$$

where:

γ : ratio of specific heats

M_a : Mach number

R_e : Reynolds number

The expressions for Mach and Reynolds numbers are given by Equation 3.51 and 3.52 respectively.

$$M_a = \frac{V}{\sqrt{\gamma RT}} \tag{3.51}$$

$$R_e = \frac{\rho dV}{\mu} \tag{3.52}$$

where:

ρ : coolant density (air)

μ : dynamic viscosity of air

R : universal gas constant

V : velocity

d : flywheel rotor air gap

T : temperature

The drag or skin friction coefficient is function of geometry of the object (rotor) and speed. The expression of drag coefficient as a function of shear stress(τ_s) cylindrical rotor is given by Equation 3.53.

$$C_d = \frac{\tau_{ab}}{\frac{1}{2}\rho U^2} \tag{3.53}$$

According to Beck calculations [299], the mathematical expression for shear stress between two plates *a* and *b* with the medium having molecular mass (*m*) and number density (*n*) is given by Equation 3.54.

$$\tau_{ab} = \frac{1}{2}\left(\frac{4K_n}{1+2K_n}\right)\left(mnV\sqrt{\frac{RT}{2\pi}}\right) \tag{3.54}$$

Substituting Equation 3.51 in 3.52 the Beck expression for drag coefficient is given by Equation 3.55.

$$C_d = \left(\frac{4K_n}{1+2K_n}\right)\left(\frac{1}{(\sqrt{2\pi\gamma})M_a}\right) \tag{3.55}$$

Using Equation 3.55 the expression of shear stress in terms of Mach and Reynolds number is expressed by the following Equation.

$$\tau_{ab} = \rho V^2\left(\frac{1}{M_a\sqrt{(2\pi\gamma)}+R_e}\right) \tag{3.56}$$

Using Equation 3.56 and 3.57 the equation of power loss due to windage is given by the following expressions.

$$P_{wd} = \left(\frac{2\pi l r^2\omega}{M_a\sqrt{(2\pi\gamma)}+R_e}\right) \tag{3.57}$$

After the manipulation, Equation 3.57 can be expressed as follows:

$$P_{wd} = \left(\frac{2\pi l\rho r^4}{M_a\sqrt{(2\pi\gamma)}+R_e}\right)\omega^3 \tag{3.58}$$

The windage losses of the FESS were estimated based on the derived equations and the methods described. The windage loss mainly depends on friction between the flywheel rotor and the gas or air in the containment. The windage loss is proportional to cubic value of speed and the surrounding pressure. The windage loss is

uncontrollable if containment pressure is not maintained. The windage loss reduces if low pressures levels are maintained in the containment. The pressure level below atmospheric pressure creates rarefied condition for surrounding gas due to sufficient space between molecules of the gas. Figure 3.21 presents the windage loss at 0.01Pa and 0.1Pa, each loss curve presents the loss for different speed levels. The loss curves show that the windage loss increases exponentially. The lowest pressure of 1Pa is assumed in the presented system, the windage loss at 1Pa for the flywheel running at 20krpm is 100W, whereas the windage power loss at 0.1Pa is 12W for same speed. It can be seen in Figure 3.22 the windage loss becomes unacceptable when pressure is increased to 10Pa, the loss increases to 0.6kW when FESS operates at 20krpm, it can increase 10 times higher when pressure is increased to 100Pa which is undesirable.

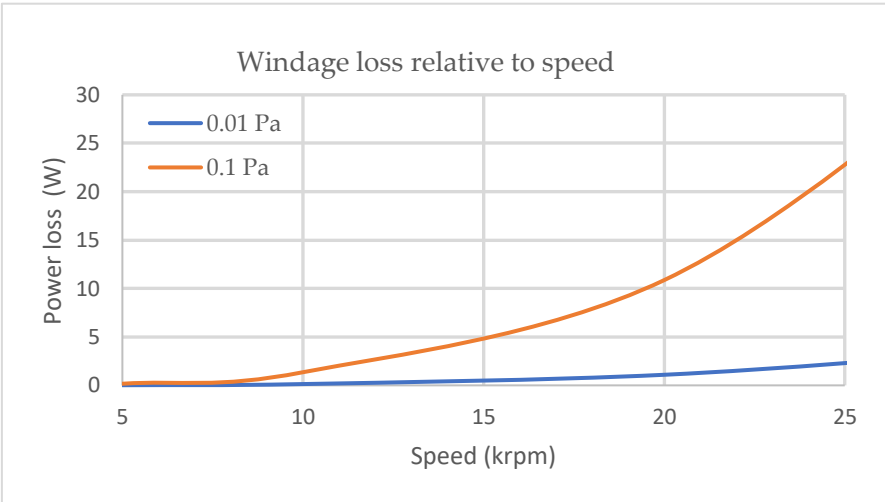

Figure 3-21 Windage loss vs speed at 0.01Pa and 0.1Pa

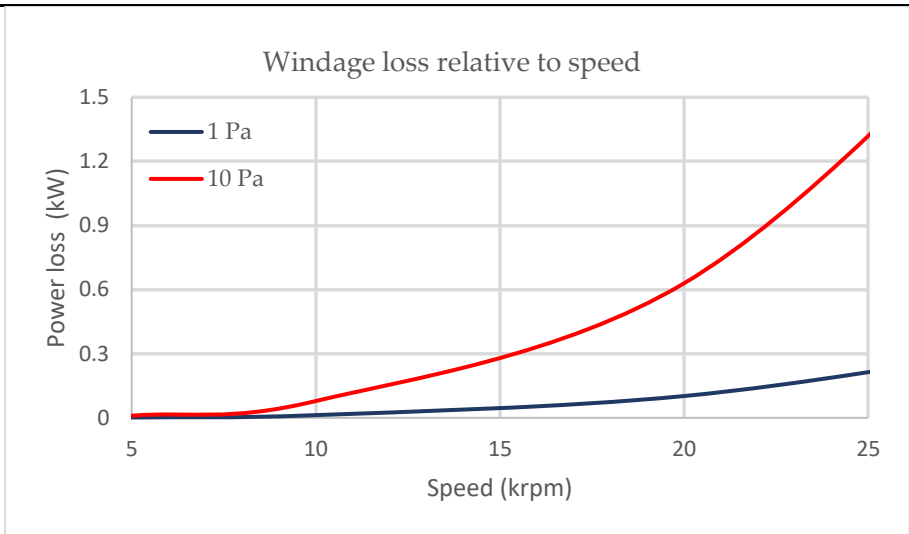

Figure 3-22 Windage loss vs speed at 1Pa and 10Pa

Bearing Losses

Bearing losses are usually calculated using the empirical methods as recommended by the bearing manufacturers. Considering the rotating contacts, the bearing losses in FESS can be defined by Equation 3.59 [300].

$$t_b = t_l + t_v + t_f \tag{3.59}$$

where, t_l is the torque due to an applied load and depends on the type of the load and design of bearing, t_f is end flange friction torque which is only applicable in roller type bearings and is negligible in ball bearings, and t_v is the torque due to viscous friction that is dependent on the speed and property of the lubricant used. The values for t_l and t_v can be calculated using Equations 3.60 and 3.61, respectively [301].

$$t_l = f_l F_b D_p \tag{3.60}$$

$$\left.\begin{aligned} t_v &= 10^{-7} f_0 (v_0 n)^{\frac{2}{3}} D_p^3 & v_0 n \geq 2000 \\ t_v &= 160 \times 10^{-7} f_0 (v_0 n)^{\frac{2}{3}} D_p^3 & v_0 n < 2000 \end{aligned}\right\} \tag{3.61}$$

where f_l is the design dependent factor and is defined by Equation 3.62.

$$f_l = z \left(\frac{F_s}{C_s}\right)^y \tag{3.62}$$

where :

C_s : static load rating defined by the manufacturer's datasheets

F_s : static equivalent load.

F_b : load on the bearing

D_p : is the pitch circle diameter (m)

n : bearing speed (rpm)

v_0 : kinematic oil viscosity (centistokes)

f_0 : lubrication factor which depends on type of bearing and lubrication.

The values of z and y depend on the type and contact angle of the bearing as given in Table 3.2.

Table 3-3 Values of z and y. Adapted with permission from [300]. Taylor and Francis Group LLC, 2019.

Bearing Type	Nominal Contact Angle (Degrees)	z	y
Radial deep-groove	0	0.0004–0.0006	0.55
Thrust	90	0.0008	0.33
Double-row self-aligning	10	0.0003	0.4
Angular-contact	30–40	0.001	0.33

The power losses of a rolling element ball bearing can be simply defined in terms of the bearing torque and speed as presented in Equation 3.63 [302].

$$P_{bearing} = (t_l + t_v)\omega \tag{3.63}$$

Substituting the values of the parameters from Table 3.2, Equation 3.64 can be simplified as:

$$P_{bearing} = 8.489\omega + 0.174\omega^{1.66} \tag{3.64}$$

The bearing loss of the flywheel system as a function of the rotational speed is shown in Figure 3.23. Since the bearing loss is a function of the speed and the load on the bearing, for the maximum rated speed of 20,000 rpm, the bearing friction loss is calculated to be 760W. However, the system losses need to be kept at a minimum and particularly the standby losses, which is directly affected by the aerodynamic and bearing losses.

Figure 3-23 Bearing losses of FESS at different speeds

Chapter 4

Modelling of PV Hybrid Microgrid System

For electrification of remote isolated grids, a diesel generator (DGen) has typically been chosen as the source of power. However, consumers cannot forecast how much power they need to generate at any given time so consumers using a DGen to meet their energy demand are unlikely to utilise full power capacity of the DGen. This leads to poor energy efficiency since the DGen is often operating at part load, increasing emissions, and this is also not good for the engine in terms of degradation. Adding a renewable energy source can contribute highly to reducing emissions. However, as explained previously, adding an energy storage device is essential to assure a secure and stable microgrid energy system. This allows the DGen to be used as little as possible and operate much of the time at higher loads when it is more efficient. Stable operation of the microgrid does, however, face some technical challenges such as bidirectional power flows, low inertia of energy sources, stability and modelling. The capability of a microgrid operating in isolated mode, including withstanding the impacts of faults, requires reliable communication and control models. Modelling of a microgrid is not a simple process since it includes the matching of unpredictable renewables with uncertain energy demand profiles. The type of model used for modelling a microgrid depends on the types of components used and their integration at point of connection. A dynamic model of a stand-alone microgrid is presented in [303], the stand-alone microgrid includes the distributed source and load. In [304], Sanchez *et al.* have presented an information model of a microgrid based on logical nodes of IEC standards. The presented model has an interoperability feature for a quick response to maintain the balance of power in the network. An optimization model based on the demand response mechanism for microgrid energy scheduling with loads and distributed generation is presented in reference [305]. The proposed model of the microgrid uses a Genetic Algorithm (GA) to formulate an optimal

scheduling strategy to reduce operational of cost of the microgrid and maximise use of clean energy. Hu *et al* in [306] have presented an autonomous microgrid with controlled loads. In this study, an optimal reduction method technique is used to achieve error minimization by using a particle swarm optimization (PSO) algorithm. A fixed-point algorithm for simplified modelling of three phase microgrids is presented in [307], where the load flow algorithm determines the equilibrium points by reducing the state variables, differential equations and computational time. Sen and Kumar [308] have categorised the modelling of microgrids into component-wise modelling leading to an aggregate, lumped or single entity model, dynamic equivalent modelling and stochastic/predictive modelling. Here, component-wise modelling of microgrids has a separate model of each energy source and loads along with network parameters to form an aggregate model of a microgrid. For the work described in this thesis, component-wise modelling is discussed and implemented, the description of rest of the modelling techniques are similar to reference [308] should the reader require more background information to supplement the model description given in this chapter.

In this research operation of the microgrid is considered in islanded mode, it is assumed that the microgrid is located in a remote area where there is either a very weak grid or no grid since an extension of transmission lines is not an economically feasible option. A PV hybrid microgrid system (PVHMS) is considered for study using a flywheel as an energy storage device. The components in operation of the PVHMS include a DGen, PV system , residential load and a FESS with their necessary control systems and power electronics interfaces. A concept diagram of the PVHMS studied in this research is shown in Figure 4.1.

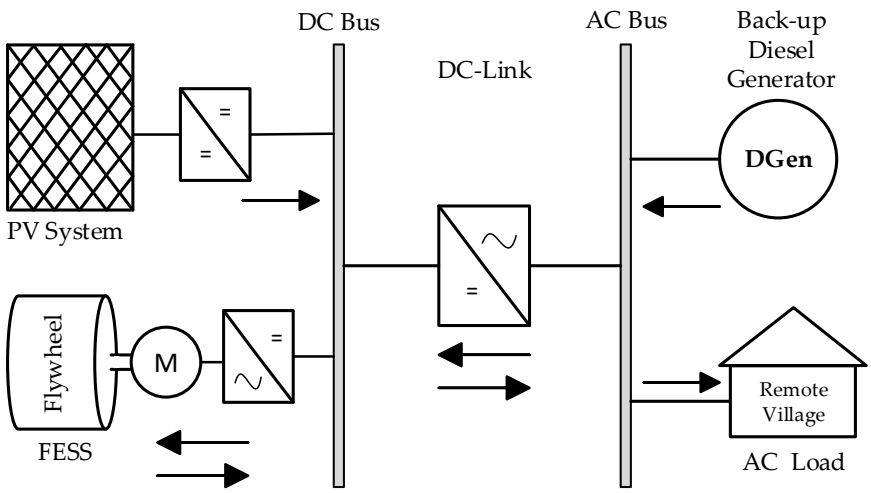

Figure 4-1 PVHMS system with FESS

In this chapter, mathematical modelling of the PV system is presented in section 4.1, section 4.2 presents the modelling of the DGen, modelling of residential loads is presented in 4.3. Simulink modelling of PV, DGen, PVHMS and load models are presented by sections 4.4, 4.5, 4.6 and 4.8 respectively. In section 4.8 validation of the MATLAB model is presented where results are discussed and analysed.

4.1 Modelling of Solar PV System

A typical configuration of the PV array, as used for power system application to feed the loads, is formed by connecting PV cells in series and parallel. Detailed modelling of PV arrays has been discussed in [309] - [310]. Parallel connection of PV cells affects the overall current for the PV module therefore the output current of a PV module ($I_{PV\ array}$) depends on number of PV panels (N_{PV}) connected in parallel. The overall current is given by Equation 4.1.

$$I_{PV\ array} = I_{PV\ panel} \times N_{PV} \tag{4.1}$$

where:

$I_{PV\ panel}$: total current of each panel connected in parallel.

The equivalent circuit diagram of the solar PV cell is shown in Figure 4.2. The model of the PV cells consists of ideal current sources which represents the optical

irradiations in parallel with a diode and a shunt resistor (R_{sh}). The combination of diode and shunt resistor is then connected with a series resistor (R_s) [311].

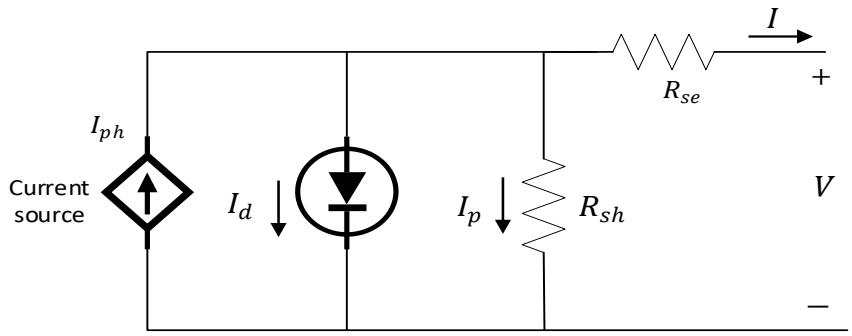

Figure 4-2 Schematic diagram of a PV cell

The parameters of R_{sh} and R_s are mainly determined by the panel power output and efficiency respectively. The voltage-current (V-I) characteristics of the PV cell can be expressed by Equations 4.2 and 4.3.

$$I = I_{ph} - I_0\left\{e^{\frac{q(V+IR_S)}{nkT}} - 1\right\} - \frac{V+IR_S}{R_{sh}} \tag{4.2}$$

$$I_{ph} = (C_0 + C_1T) \times G \tag{4.3}$$

where:

C_0 : empirical constant

C_1 : empirical constant

k : Boltzmann's constant

q : electric charge

T : temperature in Kelvin

G : irradiation in W/m2

I_0 : Saturation current

4.2 Modelling of Diesel Generator

A diesel generator (DGen) is used for back-up energy support if the load demand is not satisfied by the energy storage device and solar PV system. The DGen is able to provide a constant supply of power regardless of weather conditions and during night-time unlike the PV system. A DGen is simply a power source coupled to an

electrical machine operating as a generator. A schematic diagram of a DGen circuit model is shown in Figure 4.3. Input to the engine is given by a governor which controls speed of the engine by controlling fuel intake [312]. The energy generated by diesel generator is expressed by Equation 4.4

$$E_{DG} = P_{DG} \times \eta_{DG} \times t \tag{4.4}$$

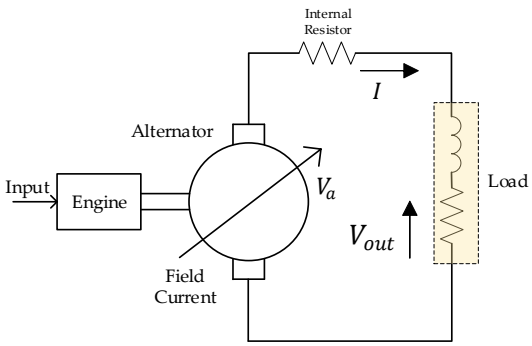

Figure 4-3 Schematic diagram of synchronous generator.

The stator voltage and currents equation of synchronous generator are expressed by Equations 4.5 and 4.6

$$V_q = R_s I_q + L_q \frac{dI_q}{dt} + \omega_e L_d I_d + \omega_e \lambda_m \tag{4.5}$$

$$V_d = R_s I_d + L_d \frac{dI_d}{dt} + \omega_e L_q I_q \tag{4.6}$$

Similarly, the electromagnetic torque developed by the synchronous machine in the dq reference frame is given by Equation 4.7

$$T_e = \frac{3P}{4}(\lambda_m I_q + (L_d - L_q) I_d I_q) \tag{4.7}$$

where :

L_d : Direct axis inductance (H)

L_q : Quadrature axis inductance (H)

I_d : Direct axis stator current (A)

I_q : Quadrature axis stator current (A)

λ_m : Rotor field flux (V/rad/s)

P : Number of poles

T_e : Electromagnetic torque (N·m)

ω_e : Rotor's electrical speed (rad/s)

4.3 Modelling of Loads in the Microgrid

There are different types of load which may be connected into microgrids including residential, commercial and industrial. Continuity of the power supply is ensured based on the sensitivity of whether loads are critical or non-critical. In this research residential load models were considered; the demand models being created by using stochastic models of energy demand over periods of 24 hours.

The Centre of Renewable Energy Systems and Technology (CREST) at University of Loughborough has developed an integrated thermal-electrical demand model based on a bottom-up methodology [313]. Their model uses stochastic techniques to represent thermal and electrical demand models. The bottom-up approach used effectively captures the spikiness which occurs when switching appliances on and off. The energy consumption trends of residents are determined as based on UK and Indian survey data. This considers the activity of residents in dwellings considering that they can be at home or away and also active or asleep. The activity-based model considers the activities performed by individuals, firms and households during the day [313].

Stochastic demand models as recommended for use by [314] are the best input models for consumption trend simulations since they are able to match the disordered consumption of electricity whilst keeping the aggregate trend intact. They produce data sets which have similar probability distributions compared to those found in real world. Therefore, in this research, a high-resolution stochastic model was created and developed using the stochastic methodology [315]. The data for the load profile is generated by defining the type of day of the week, month of the year and number of dwellings. Switching events of lighting, appliances and water-fixtures are calculated on the basis of stochastic sequences of occupancy for each dwelling which determines

electricity demands of dwellings. The CREST model also allows creation of solar PV supply for typical weather conditions as affected by cloud cover. Examples of electricity demand profiles as generated by the model for typical days in April and August on a weekday and weekend are shown in Figure 3.8. and Figure 3.9 respectively. Further research work on residential demand models has been presented and discussed in [313] - [316].

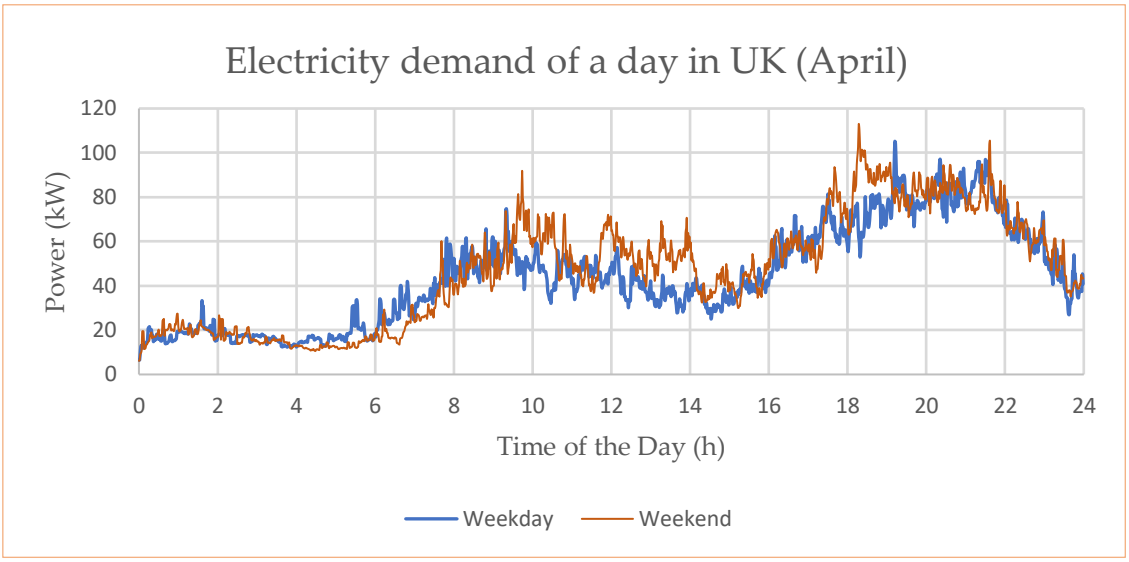

Figure 4-4 Energy consumption profile of UK residents for the month of April over 24 hours (100 dwellings)

Figure 4.4 represents the load demand of 100 UK dwellings of a weekday in the month of April (UK-April-WD). It can be seen that the electricity consumption starts increasing from 6:00 to 10:00 with peak demand of 78 kW in the morning. The demand decreases after 10:00 this can be due to the fewer activities of occupants as most of the consumers leave houses in the morning for work. This lower consumption prevails for 6 hours between 10:00 to 16:00. The demand again starts increasing after 16:00 in the evening. Between 18:00 to 20:00, the demand rises to a peak of 100 kW. The consumption trend shows that maximum electricity demand occurs between 16:00 and 21:00 and 6:00 to 10:00. Given PV output is greatest around noon, a system sized to provide a suitable average power level may not be enough to meet load demand during these times.

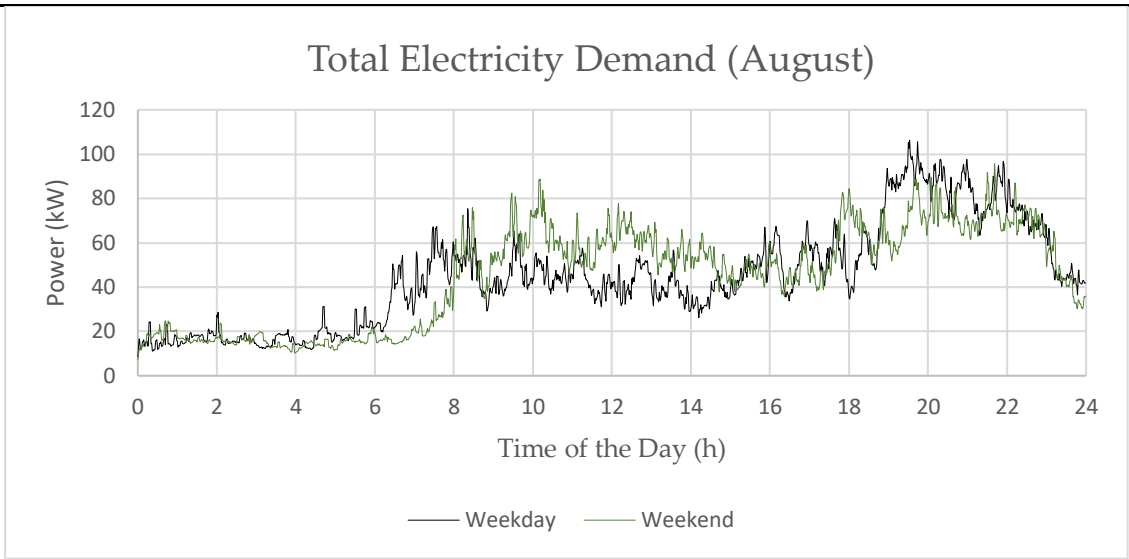

Figure 4-5 Energy consumption profile of UK residents on weekend for the month of August over 24 hours (100 dwellings)

Figure 4.5 shows the load profile of UK consumers for the month of August for weekend (UK-Aug-WND). It can be seen that electricity usage is very low from midnight until 6:00, it increases exponentially after 6:00 due to increased activity of the residents. The electricity consumption remains high throughout the day, except between 2:00 am to 6:00 pm when dip in the consumption is seen. Average electricity demand during the day on weekend is higher than on weekday because of increased activity of inhabitant in houses. It can be seen from Figure 4.4 and Figure 4.5 that the demand on weekdays follows a trend of energy consumption related to daily routine activities and occupancy in home, whereas the consumption on weekend depicts the different trend of energy consumption showing higher demand during afternoons and less peaks and spikes in the morning (between 6am to 10am). The operation of FESS in this research is tested and analysed for both weekday and weekend load demands. The load models selected for the analysis of the results are presented in next section. Figure 4.6 and 4.7 represent energy demand cure based on Indian consumption trend, the Figures show energy consumption trend for both weekdays and weekends for the month of April and August.

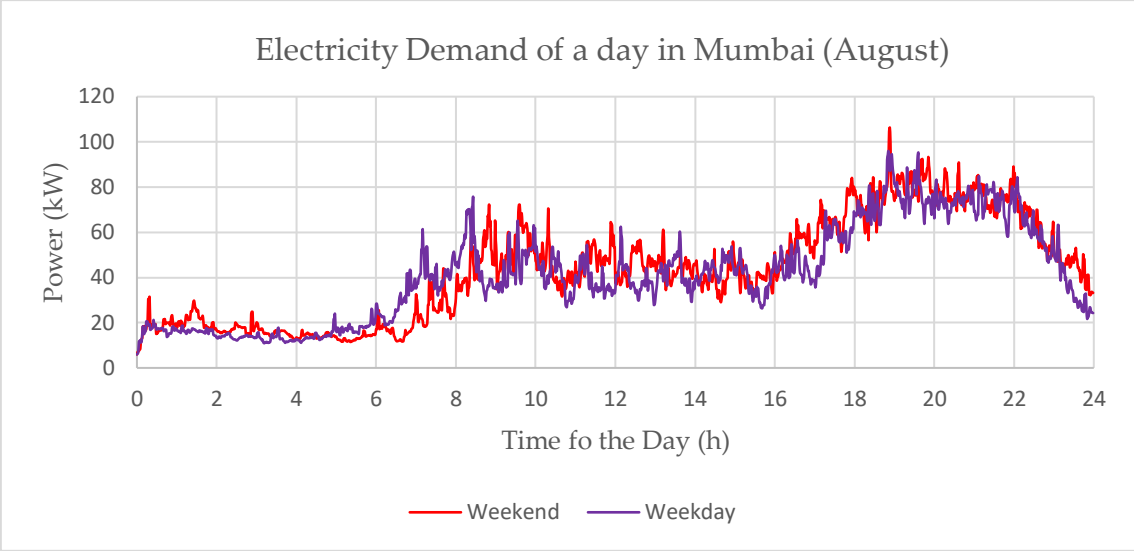

Figure 4-6 Energy consumption profile of Indian residents on weekend for the month of August over 24 hours (100 dwellings)

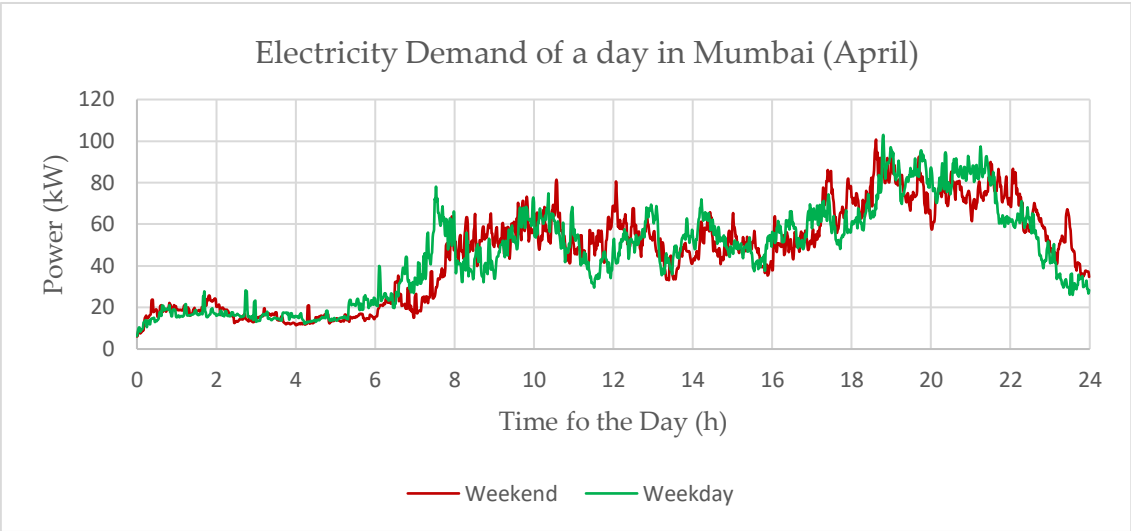

Figure 4-7 Energy consumption profile of Indian residents on weekend for the month of April over 24 hours (100 dwellings)

The energy consumption trend on a weekday is similar in the UK and India, the demand remains very low in both cases before 6am. However, on weekends the demand profile of UK consumers is peaky and higher than the Indian residents. The weekday demand profile for the month of April in Mumbai has more variations compared to the demand on weekend which is steady. The demand profile of August on weekday in Mumbai shows an obvious variation when compared to the energy consumption on weekend. For Indian data, in both cases the demand on the weekend starts increasing after 8am in the morning and remains high till 16hrs. Whereas, the

consumption on weekdays reaches to the peak before 8am representing a typical working days and regular morning activities of the residents.

As explained earlier, this system utilized a FESS as an alternative to battery technology to support the PV system and meet the peak demand of a small residential town with 100 dwellings. The diesel generator (DGen) is used in the islanded system as a spinning reserve to maintain the stability of the islanded system when the PV system and flywheel storage cannot meet the load demand. The stand-alone system consisted of PV system, diesel generator, FESS and a dynamic variable residential load has been modelled in MATLAB/Simulink environment and detailed results are presented and analysed. A schematic diagram of PVHMS studied is shown in Figure 4.8. The FESS and the PV system are connected to the same bus (DC-link) therefore the proposed network topology does not require a DC-AC grid inverter for the FESS which reduces the cost of the system and reduces the power electronics losses.

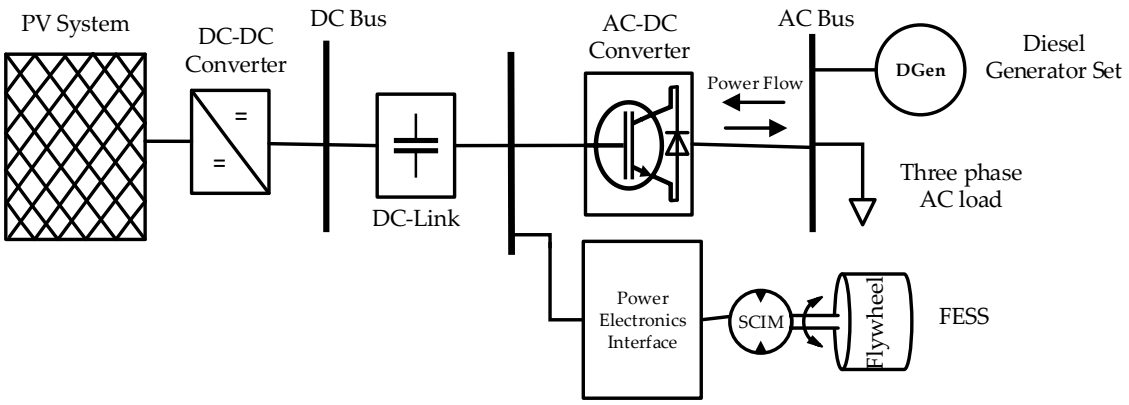

Figure 4-8 Schematic design of proposed PVHMS

The PV system, FESS and DGen are connected to the DC bus which all supply the AC dynamic load. The load demand profiles were generated by using a high-resolution CREST methodology [315]. The data for the load profile is generated by defining the type of the day of the week, month of the year and number of dwellings.

4.4 Simulink Model of Solar PV System

The built in Simulink model of the PV system requires the cell temperature in ^{0}C and solar irradiance in $Watt/m^2$ as an input parameter, the output parameters of the PV

model are PV dc voltage (*V_PV*) and dc current (*I_PV*). The PV array is connected to DC link via DC-DC boost converter which controls the power produced by PV system. The Simulink model of the PV system is shown in Figure 4.9.

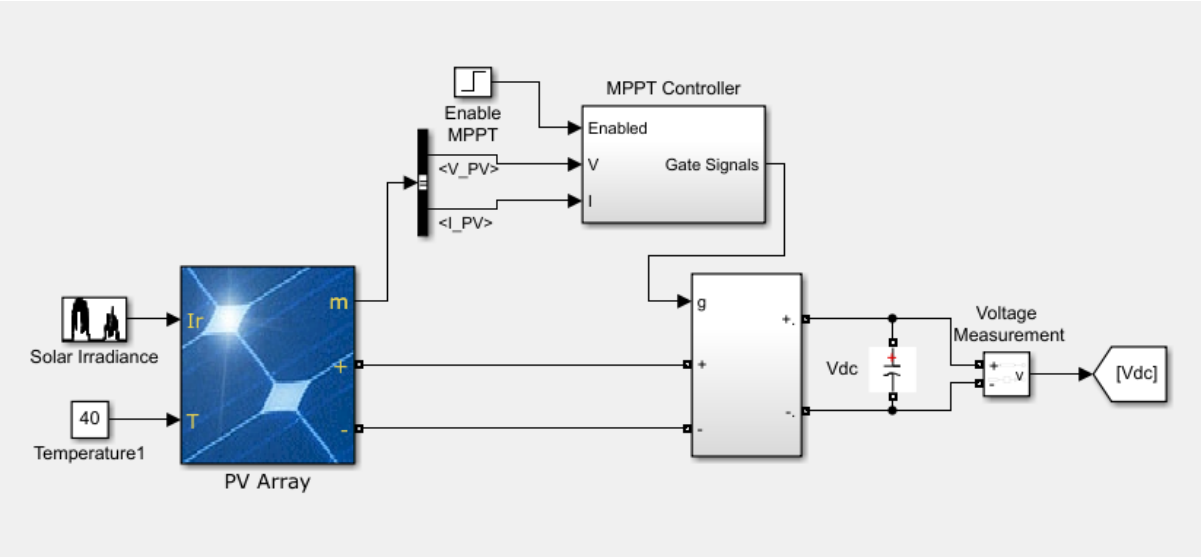

Figure 4-9 Model of PV array in MATLAB/Simulink environment

The PV system model was obtained from the library of National Renewable Energy Laboratory (NREL) System Advisor [317]. The parameters of the model are user defined and can be selected by defining number of parallel built-in strings, specified irradiances and temperature. Each string of PV array consists of series connected PV modules. The voltage- power (V-P) and voltage-current (V-I) characteristics of the PV system for 57 parallel strings each with 5 series connected modules are plotted in Simulink based on the specified temperature and irradiance level is shown in Figure 4.10.

The V-P characteristics of the selected PV array at 250, 500 and 1000 W/m were at a constant temperature of 25 ℃. The V-P and V-I characteristics plots provide the information required to configure the PV arrays so that it can operate close to maximum peak power point. The peak power is the point where PV arrays produces the maximum power when exposed to solar radiation equivalent to 1000W/m^2.

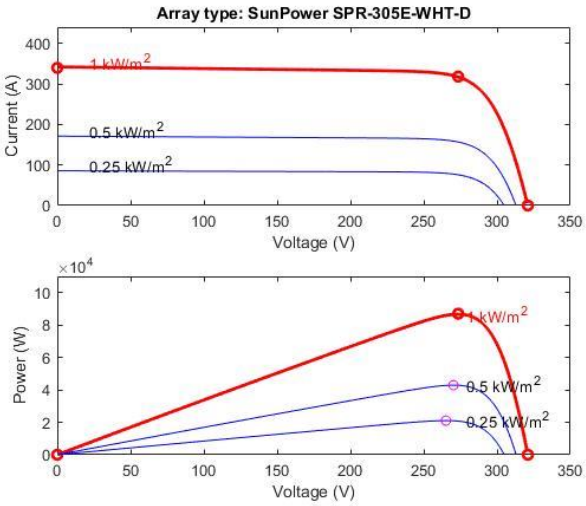

Figure 4-10 Characteristics of PV array for specified irradiances at 25℃

It can be seen in Figure 4.10 that the current of the PV module remains constant until maximum voltage is reached and maximum power is also produced. The PV array based on 250 modules (5x57) produces a maximum power of 90kW at a maximum voltage of 290V, whereas each module produces 305W. The V-P and V-I characteristics of the PV system can also be generated at constant solar irradiances and at specified temperatures. The characteristics plots based on variable temperatures of 0, 25 and 50℃ are shown in Figure 4.11. It can be seen in Figure 4.11 that power produced is the same at all different temperatures before the maximum voltage is reached (i.e. 290V) which is due to maximum power point tracking (MPPT) technique used to control the power output of the PV system.

The MPPT technique is used to regulate the voltage at DC bus and provides gating signals for DC-DC boost converter. The MPPT controller measures the current and voltage of PV module and reduces the error by using integral regulator. The output of the regulator produces the duty cycle which is then compared with its reference value. The duty cycle is inputted to PWM generator in order to produce the switching pulse for the boost converter.

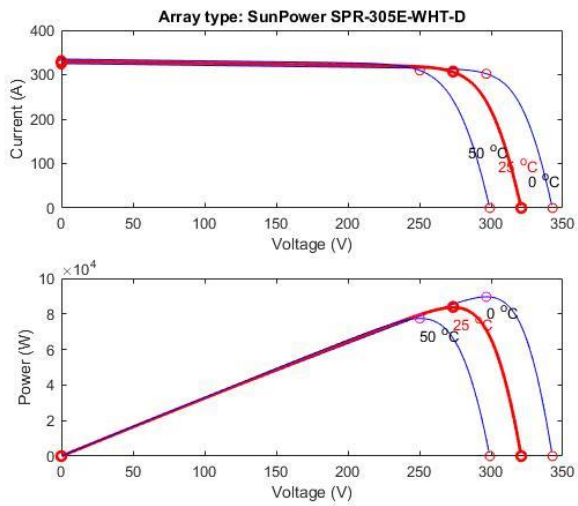

Figure 4-11 V-P and V-I plots of 285 PV arrays at 1000W/m2 at different temperatures

4.5 Simulink model of Diesel Generator

The diesel generator model was developed in Simulink by using Simulink blocks in the MATLAB environment. Figure 4.12 shows the Simulink model of diesel generator. The synchronous diesel generator is connected to AC bus in the network rather than DC bus for minimising the complexity, cost and components of the system. The diesel generator is connected to the bus via three phase circuit breakers in order to take generator on and off the network according to the need. The switching of circuit breaker is controlled by the external signal generated by the controller based on the load demand, PV output power and %SoC of the flywheel.

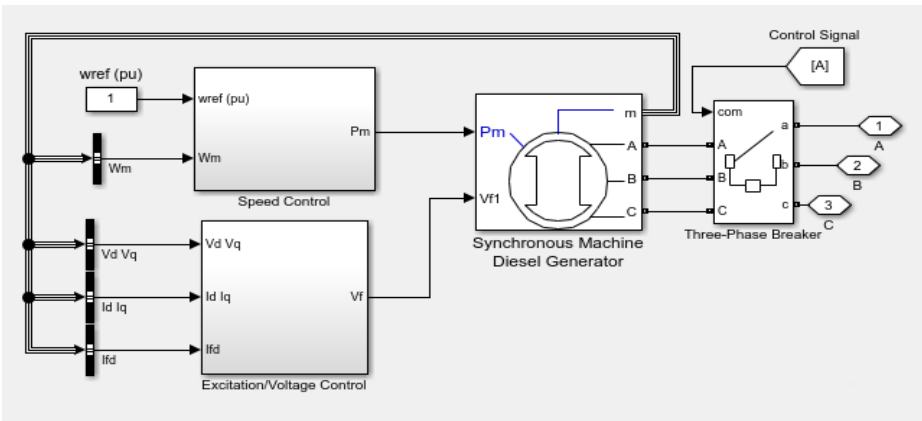

Figure 4-12 Simulink model of diesel generator

The input parameters of the synchronous machine are field voltage (V_f) and reference mechanical power (P_m). The output of the diesel generator can be chosen by using the

bus selector. Figure 4.13 shows the list of outputs available at the terminals of the machine.

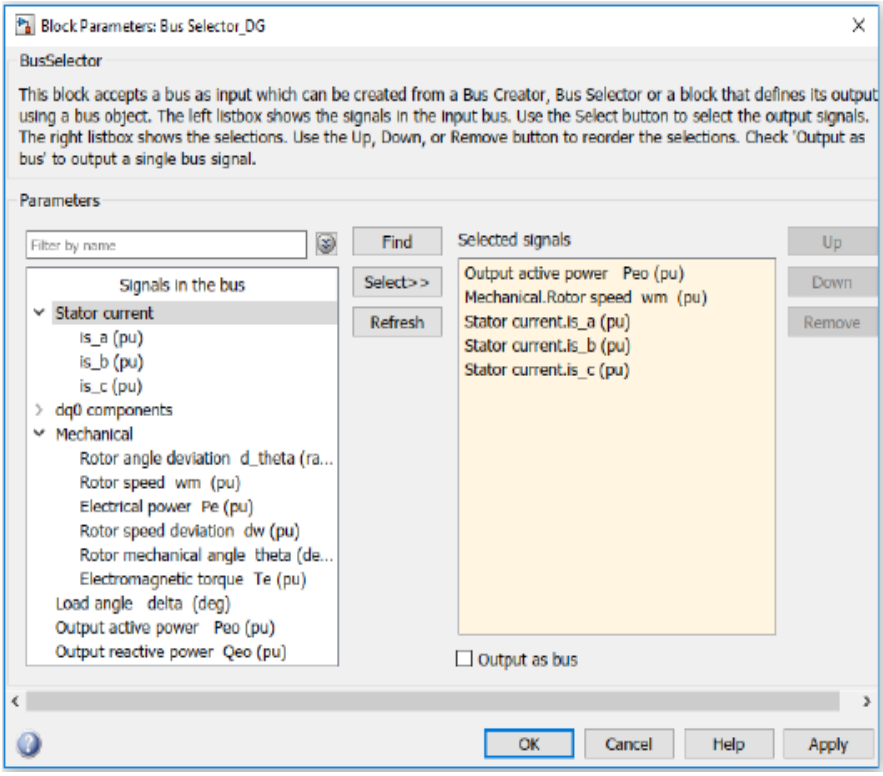

Figure 4-13 List of outputs at terminals of synchronous machine diesel generator

The engine control system of the diesel generator is composed of speed control and voltage/excitation control systems. The measured speed of the synchronous machine is fed back to speed controller via feedback loop, the controller calculates the difference between the reference and measured speed based on the calculation of mechanical power required from the diesel generator which then results in adjustment of engine fuel. The control system of the speed controller is shown in Figure 4.14.

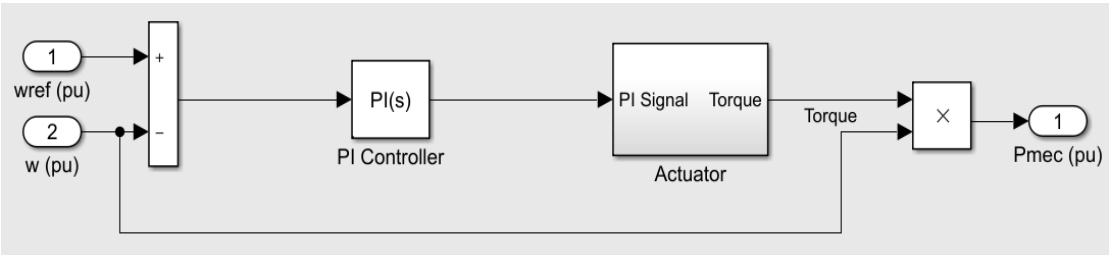

Figure 4-14 Control system of speed controller

The excitation voltage control system shown in figure 4.12 acts as an alternator which drives the diode rectifier to produce the field voltage which is required by the synchronous machine. The voltage regulator provides voltage in per unit (p.u) with lower limit imposed by the diode rectifier. Input parameters of excitation system are reference voltage, terminal voltage and stabilizer voltage. Output of the excitation system is the field voltage (Efd) and stator field current (Ifd). The detailed diagram of excitation system is shown in Figure 4.15.

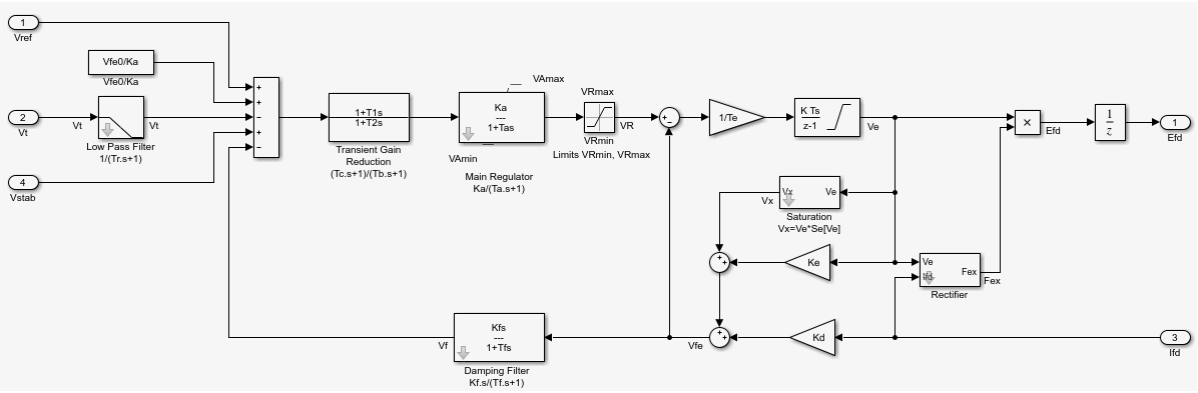

Figure 4-15. Excitation and voltage control system of DGen

The voltage of the diesel generator varies with load at the terminals of the machine, with increase in the load, the flow of current increases hence the voltage reduces. Therefore, it is vital to keep output voltage of the diesel generator stable under all load conditions. The excitation system controls the output of diesel generator and regulates the magnetic field of the machine (by varying its field current) in order to maintain required output voltage by comparing the measured output voltage with the reference voltage. The error signal produced by the controller is used to change the excitation of the generator. The ratings of the generator selected in the research are presented in Table 4.1 The specification sheet of the diesel generator is provided in Appendix B. The proposed DGen operates on high voltage ratings in order to accommodate MATLAB model configuration and discreet time settings. Therefore, the step down transformer is used to provide low voltage to control FESS and other control circuits.

Table 4-1 General ratings of the diesel generator

Parameter	Standby mode	Prime mode
Power	90 kW	100 kW
Voltage	25 kV	23 kV
Power factor	0.8	0.8

4.6 Modelling of photovoltaic hybrid mini-grid system (PVHMS)

The photo-voltaic (PV) hybrid mini grid system consists of a PV system, diesel generator (DGen), the dynamic residential load and the flywheel energy storage system (FESS). The FESS is now connected to the PV system instead of an electrical grid (see Figure 4.2) The PVHMS is developed in MATLAB/Simulink environment based on the control schemes for the PV, FESS and DGen presented in previous sections. The PCC for residential load and diesel generator is an AC bus whereas the PV system and the flywheel are connected at the DC bus. An AC-DC converter is used to facilitate power flow at the DC-link from and to the residential load. The Simulink model of PVHM is shown in Figure 4.16 and the parameters of all the power sources used in the model are presented in Table 4.2.

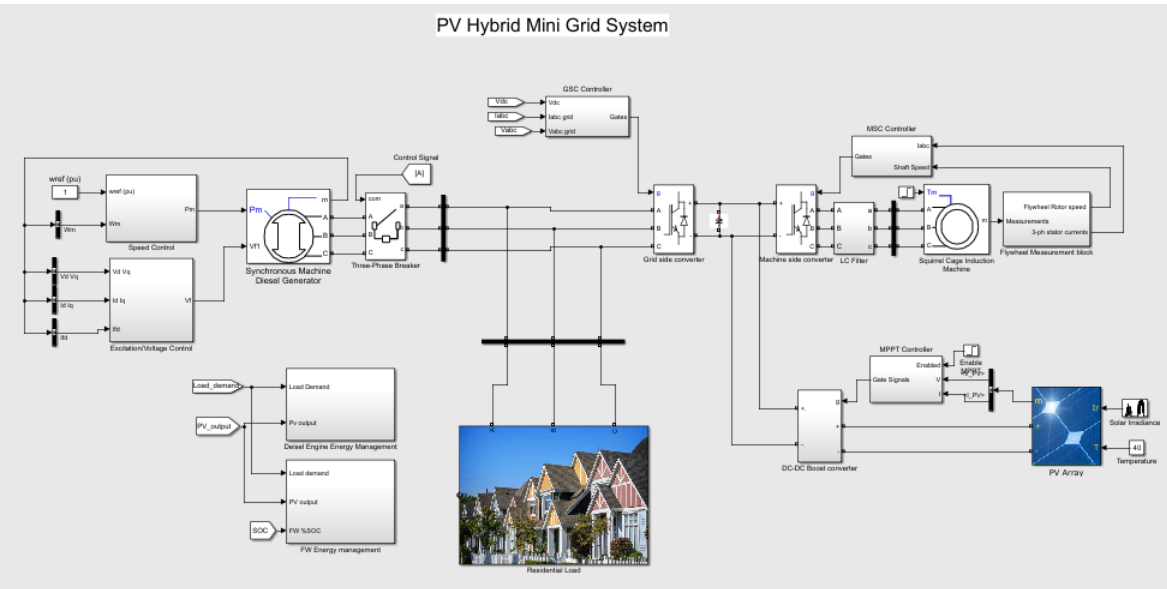

Figure 4-16 MATLAB/Simulink model of PVHMS

The load connected to the AC bus is a dynamic residential load. The varying dynamic load is updated at every second from the lookup table. A detailed description of the dynamic load is provided in the next section.

Table 4-2 Parameters of all sources used in microgrid.

Source Type	Specification	Value/Description	
Synchronous Diesel Generator	Nominal Power	100 (kW)	
	Nominal Frequency	50 (Hz)	
	Power Factor	0.8	
	Fuel Consumption	% Load	liter/hr.
		100	26.7
		75	20.2
		50	14.1
	Model	SD100	
	Engine Speed	1800 (rpm)	
	Engine Make	Generac	
Solar Photovoltaic System	Model	SunPower SPR-305E-WHT-D	
	Maximum power	305.226 (W)	
	Temperature	40 (^{0}C)	
	Maximum irradiance	1200 (W/m^2)	
	Maximum power point current	5.58 (A)	
	Maximum power point voltage	54.7 (V)	
	Parallel strings	50	
	Series connected strings	5	
SCIM-FESS	Stator Resistance (R_s)	11.85 mΩ	
	Rotor Resistance(R_r)	9.29 mΩ	
	Stator leakage inductance(L_{ls})	0.2027 mH	
	Rotor leakage inductance(L_{lr})	0.2027 mH	
	Mutual Inductance(L_m)	9.295 mH	
	Rated magnetic flux (λ_m)	0.75 Weber	
	Power rating	100 kW	
	Maximum speed	20 krpm	
	Minimum speed	10 krpm	
	Switching frequency	20 kHz	
	SCIM stator outer diameter	0.85m	
	SCIM rotor outer diameter	0.4m	
	Stack length	1m	
	DC bus voltage	600 V	
	Flywheel rotor inertia	10.95 kgm^2	
	Shaft diameter	0.025m	
	Flywheel rotor height	0.5m	
	Flywheel rotor outer diameter	0.4m	
	Rotor mass	500kg	

4.7 Modelling of Residential Loads

The Centre of Renewable Energy Systems and Technology (CREST) at the University of Loughborough [51] has developed an integrated thermal-electrical demand model

based on bottom-up methodology as explained before. The stochastic approach represents the thermal and electrical demand models. Based on UK and Indian data survey which considers the activity of the residents in dwellings such as residents can be at home or away and active or asleep. The activity-based model considers the activities performed by individuals, firms and households during the day [313].

The selection of load models was based on availability of data and locations having good solar potential. Therefore, for better analysis and demonstration, the electricity demand model present energy consumption trends of Indian cities of Mumbai, Kolkata and Mumbai. For further reference the load profiles of New Delhi city for entire year is presented in Appendix C. The operational scenarios were created based on the three location load profiles, each for day and night-time. The correct functionality of the FESS operation is demonstrated according to the activity of the residents and their inhabitancy. The load profiles are selected based on worst case scenarios considering electricity demand on weekday and weekends.

Load model of New Delhi for the month of July on Weekday (ND-July-WD)

Load Model ND-July-WD represents total electricity demand for 100 dwellings in rural areas on a weekday for the month of July. The demand model has been considered for New Delhi, a major city in India (Figure 4.17). The morning peak of 100 kW appears around 6 am and it spreads over 2 hours, there is low electricity consumption demand between 10 am and 5 pm due to reduced occupancy in homes. The demand starts to increase and reaches approximately 85 kW during late evening which is second peak in 24 hrs. The electricity consumption decreases after 10 pm in the evening due to lessened activities of residents in the dwellings.

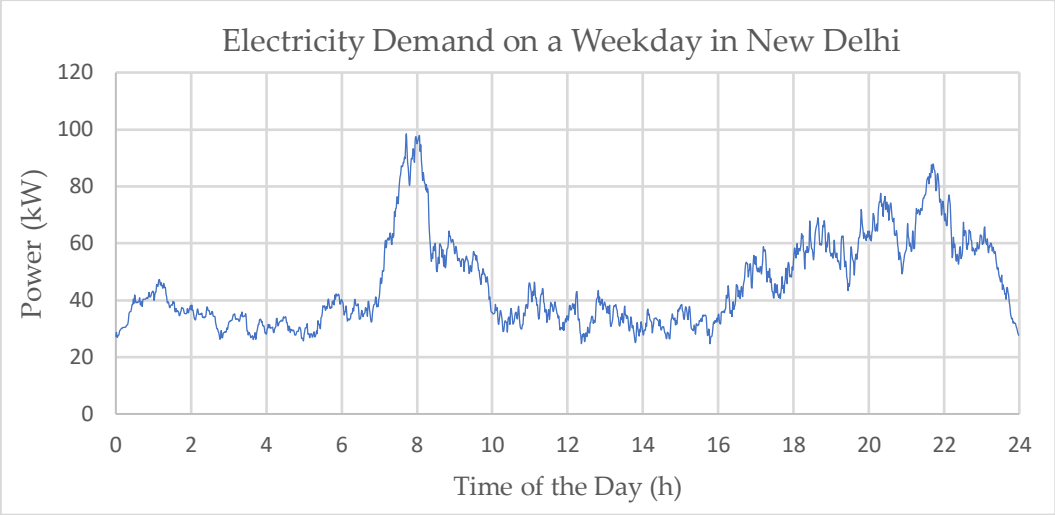

Figure 4-17 Load demand profile n weekend in New Delhi for the month of July

Figure 4.18 shows the total irradiance of a weekday for the month of July associated with the demand model shown in Figure 4.17 , it can be seen that there are fluctuations in the irradiance which represents a cloudy day. The peak PV output power is expected to be generated between 12 pm and 4 pm during which the demand is low, this creates an opportunity to store excessive power in the hybrid system and use it during the evening when demand is high (Figure 4.17). The irradiance before 5am is zero hence no power will be generated by solar PV system, therefore the power interchange is expected to only happen between the DGen, the FESS and the loads. During the night-time (before 6 am) the DGen can be turned on to meet the electricity demand of the dwellings and charge the flywheel until it is 100% charged. The DGen can be turned off and energy stored in the flywheel can be utilized to meet the electricity demand until it is fully discharged. It is particularly important to analyse the dynamic performance of the PVHMS between 10am to 12pm and 4pm to 6pm when there are significant fluctuations in PV power output.

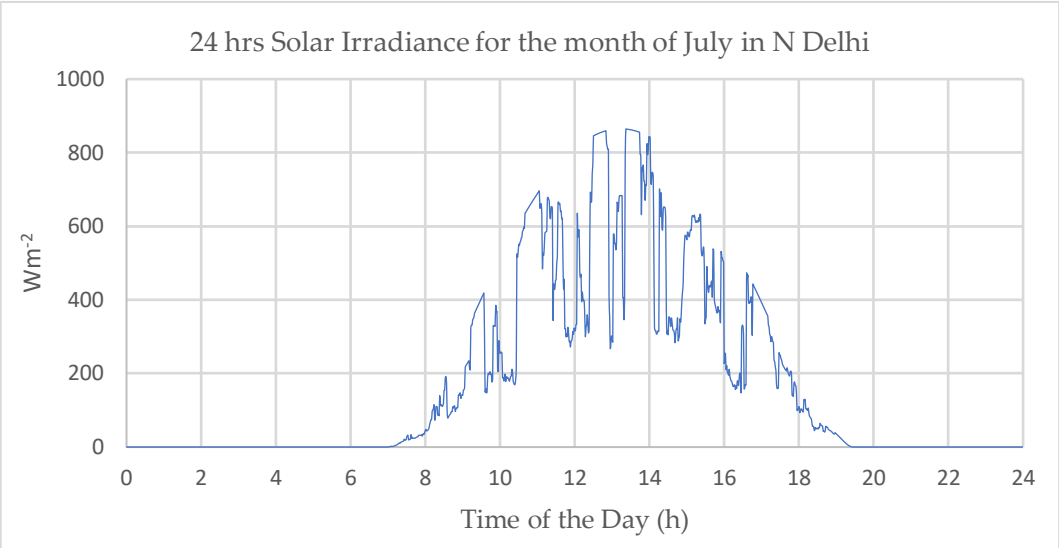

Figure 4-18 Solar irradiance in Delhi of a typical cloudy weekday for the month of July

The average demand for Load Model ND-July-WD is about 60kW but the diesel engine and the PV system should be designed for the maximum load of 100kW even though the maximum demand of 100kW lasts for only a small period of time. This is when application of the storage system becomes important and the flywheel is best suitable for such conditions providing high power for a short duration with a quick response.

Load Model for the month of July in Mumbai on Weekday (MB-July-WD)

The load Model MB-July-WD of the electricity demand represents the electricity consumption trend for 100 dwellings for the month of July in Mumbai, the city in India (Figure 4.19). In this model, the morning peak lasts for a longer compared to Load Model ND-July-WD. The morning peak appears at 6 am and last till 10am. The power demand again starts to rise from 4 pm and decreases from 10pm during this time the load profile experiences more fluctuations compared to the morning peak. During afternoon (10am – 4pm) the load demand is low except few spikes after 12am. There are more spikes and fluctuations in this model compared to Load Model ND-July-WD.

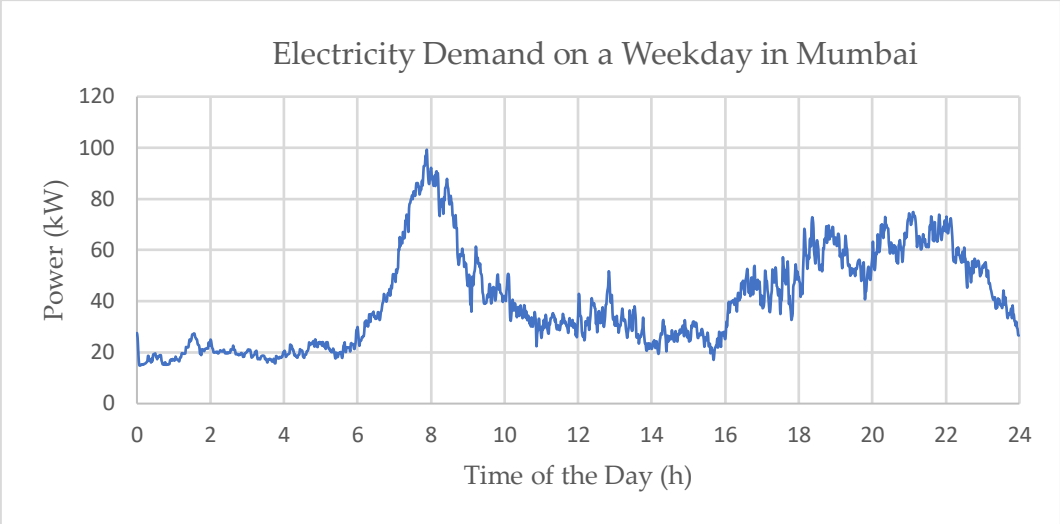

Figure 4-19 Load demand profile on weekday in Mumbai for the month of June

Figure 4.20 shows the solar irradiance of a typical cloudy day on a weekend for the month of June. The solar output power is relatively different than for ND-July-WD.

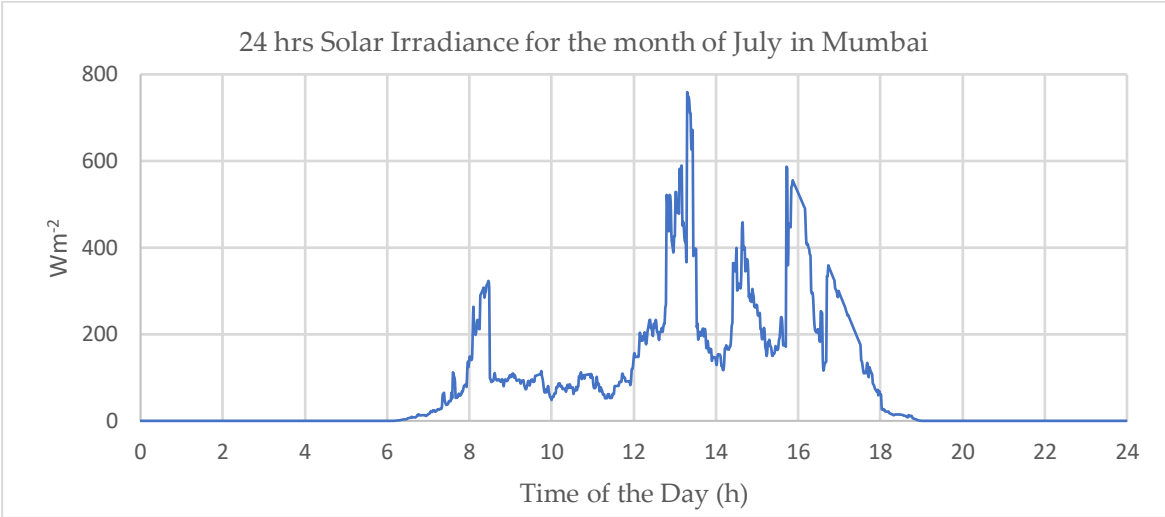

Figure 4-20 Solar irradiance in Mumbai of a typical cloudy weekday for the month of June

There are significant fluctuations in the solar irradiance during entire day and very less power is expected to be produced by PV system except between 12am to 2pm when PV panels receive maximum solar radiations. From 12 midnight to 12 noon there is very less solar irradiance with few spikes appear after 2pm which also do not last for longer time. With the presented load model and solar irradiance data it is expected that any of the energy sources, whether DGen, PV system, FESS or a combination of all three will be hardly resting over 24hrs of their operation.

Load Model of Kolkata for the month of June on Weekend (KT-June-WND)

The load model *KT-June-WND* presented in Figure 4.21 is different from the load model ND-July-WD and MB-June-WD. There are two significant peaks during the morning and evening respectively. The load demand profile (Figure 4.20) represents the energy consumption trend on a weekend. The peak demand in the morning appears between 8am to 10am (average 60kW) is less than the peak demand in the evening (average 80kW) due to less activity during the morning compared to the evening due to the fact majority of the people not going out for the work in the morning. The second peak appears in the evening between 6pm to 10pm, because people are expected to retire to sleep later at night on weekends. Between 12am to 4pm there is a dip in energy consumption with some spikes in the demand. Depending on the PV system output, energy can be stored and then used to flatten the next peak in the evening which could represent the significance of energy storage device in proposed PVHMS.

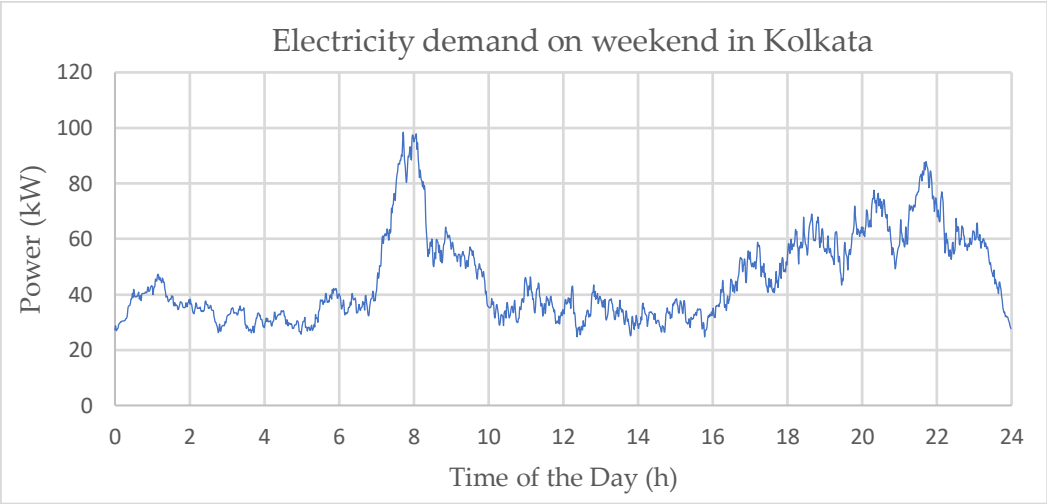

Figure 4-21 Load demand profile n weekend in Kolkata for the month of June

The solar irradiance for the corresponding load model KT-June-WND is presented in Figure 4.22. The solar irradiance curve represents a typical cloudy day. It can be seen that the irradiance model is challenging for the PV system to meet the load demand alone during entire day except between 11am to 12am in the afternoon when there could be the maximum power produced by the PV system. There are many highs and

lows in the irradiances due to cloud passing. After 12 am there is significant dip in the solar irradiance making difficult for the PV system to meet the demand alone. Depending on the state of charge of the FESS, the FESS can be used to share the demand with PV system avoiding the need of DGen. Comparing the peaks of load demand and solar irradiance (Figure 4.21 and 4.22) it can be seen that when the demand is high, the PV output power is expected to produce less than what is required therefore it is interesting to test the operation and dynamic performance PVHMS in supplying energy to the load.

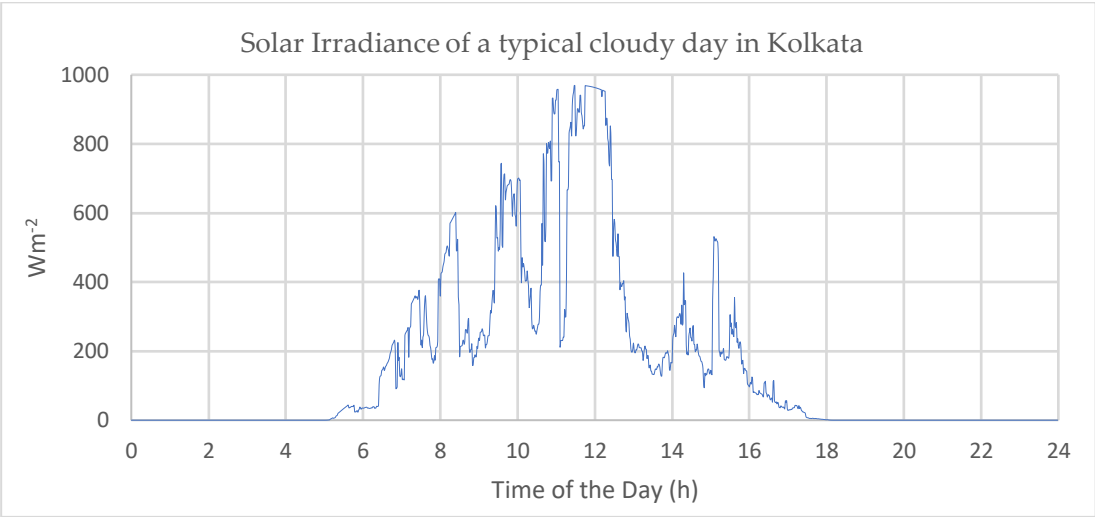

Figure 4-22 Solar irradiance in Kolkata of a typical cloudy day for the month of June on weekend

4.8 Validation of Solar PV and Diesel Generator Model

In this section, a description of how the Simulink model of the PV system and DGen were integrated and tested is given. The solar irradiance was changed in steps to test the responsiveness of the PV system to a sudden change in solar irradiance. A variable load demand was selected which changes irrespective of power output of the PV system. The DGen is used as a back-up power source, it is called when PV power is not sufficient to meet the load demand. Figure 4.23 shows the power curves of PV system along with DGen and load demand. The load demand profile has many peaks and spikes, the highest peak demand is close to 100kW and the maximum power generated by the PV system is approximately 80kW. Therefore, the need of operating the DGen for many periods is obvious. At t =3 min the power produced by the PV

declines to zero due to cloud passing. The DGen is called to provide power support to the system and entire peak load demand is supplied by the DGen. Between 4 and 6 mins the DGen is called to shave off the peak that is greater than PV output power.

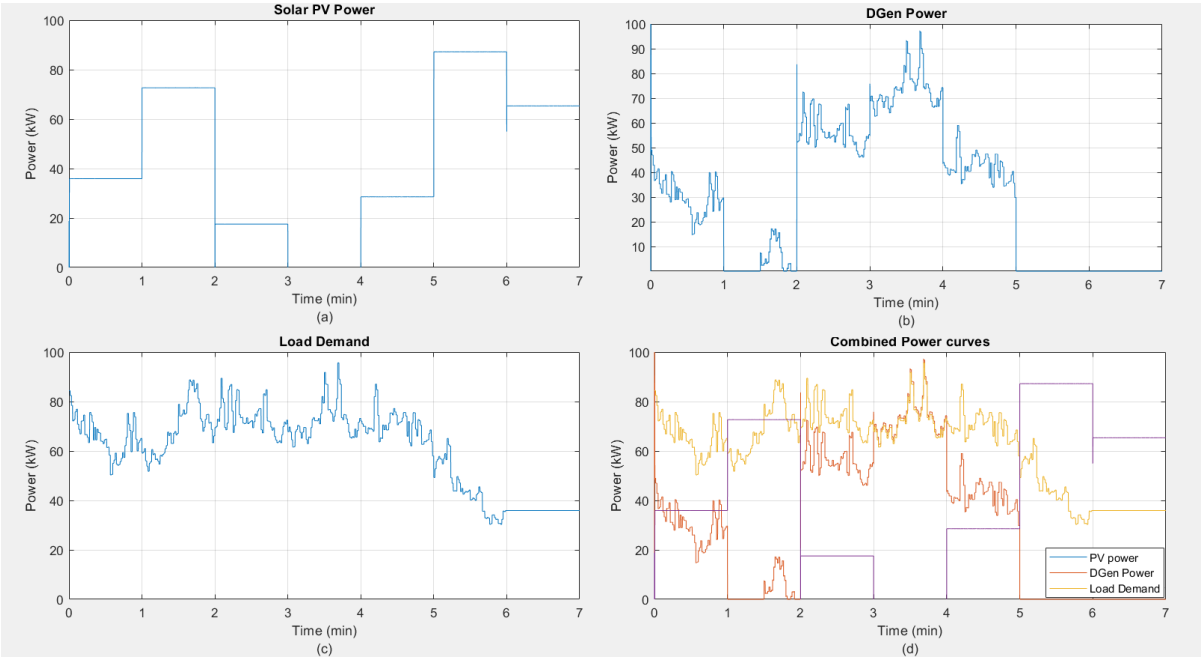

Figure 4-23 a) PV power; b) DGen power; c)Load demand; d) Combined power curves of load, DGen and PV system

The DGen is turned off between *t*=5 and *t*=6 mins when solar PV produces power more than the load demand and the DGen remains off for the rest of the operation. The events of solar irradiance are user defined, they are combination of different magnitudes, they have been defined regardless of DGen output and load demand. Figure 4.24 shows the DC link and PV system output voltage. The DC link voltage remains stable with some spikes which are due to switching of energy sources (DGen and PV). Figure 4.25 shows the currents of DGen conforming with its power variations. The validation results show the conformity with power fluctuations and input commands. The PV output voltage shows little spikes which appear due to switching effects of power sources. The coordination between power sources is based on logical control system based on the power outputs of each sources. The control system compares the power levels of load demand with output power of PV system which decides the on/off state of the DGen.

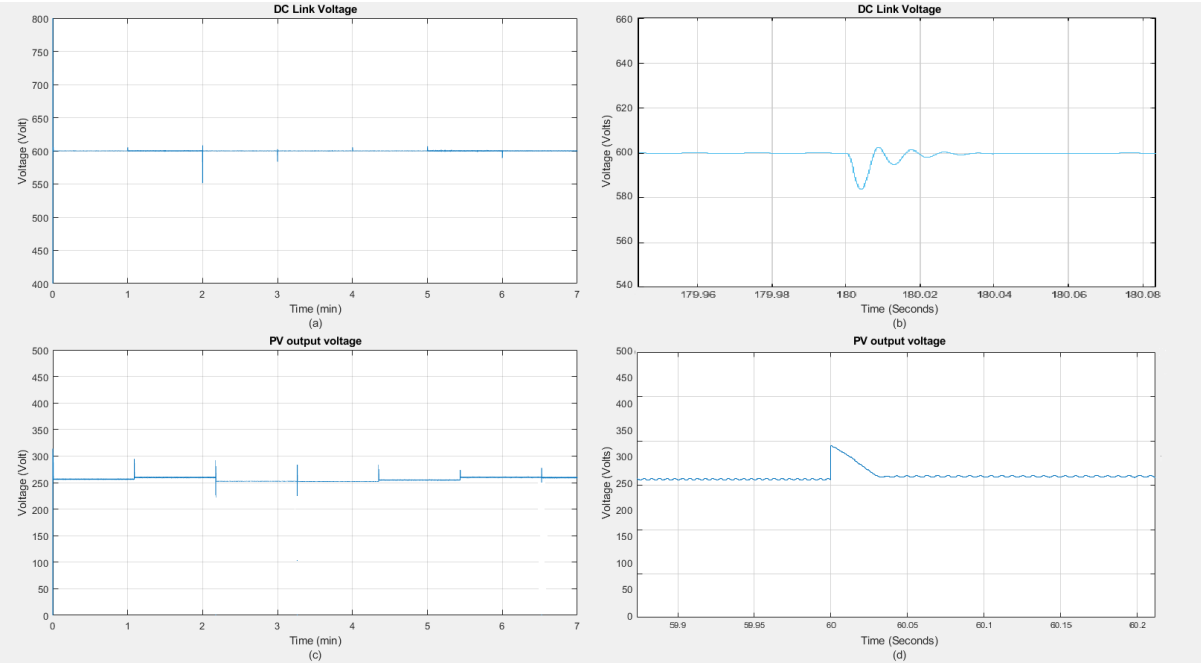

Figure 4-24 a) DC link voltage; b) Magnified view of DC link voltage; c) PV output voltage; d) Magnified view of PV voltage

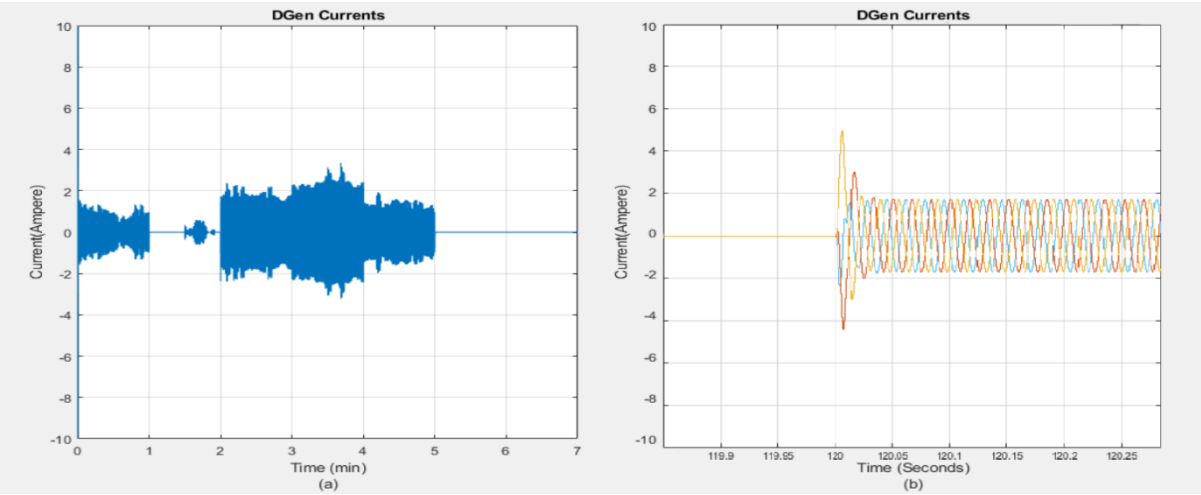

Figure 4-25 a) DGen stator currents; b) Magnified view of DGen three phase currents

Chapter 5

Results and Analysis

In this chapter results from the analysis of the hybrid model in this research are presented. Results of analysis of the hybrid system demonstrate that flywheel energy storage technology of appropriate size offers a viable solution to support the operation of the standalone PV system. The reduction in CO_2 emissions and fuel consumption has been quantified as compared with the case without flywheel energy storage under which the diesel generator but always be operating. Testing of this hypothesis is presented in terms of energy saving, performance of the flywheel compared to battery system and the control strategy. Also, it will be demonstrated with supporting results that FESS could be a feasible technology for providing back-up power which leads to reduced operation of a Diesel Generator (DGen) resulting in reduced fuel burn and lower emissions. The storage capacity of the flywheel technology is independent of temperature fluctuations, therefore, contrary to batteries, it would be a suitable alternative for the isolated grid system in countries with high temperatures [318].

By considering the generated load models presented in chapter 4, where the flywheel is connected to the DC bus between the DGen and PV system, the dynamic performance of the flywheel has been analysed for providing the energy support to the system by two different operational scenarios, described in next sections.

In this chapter, sections 5.1 and 5.2 present the description and methodology of operation scenarios and 5.3 and 5.4 present the results and their analysis of the standalone hybrid PV system. DGen fuel cost and consumption analysis is presented in 5.5. The chapter then concludes with a summary at the end.

5.1 Operation Scenario 1

In this scenario the load demand is shared between the PV system and DGen with no storage system connected to the system. In order to make realistic analysis, for the PV system it is assumed that the days are not clear and sunny, outside disturbances such as temperature changes, cloud passing, and system failure (zero PV power) are also considered so the output of the PV system will not be constant. The DGen must operate continually as a backup, given that it must be on standby to guarantee meeting the load since the PV system cannot be entirely relied upon on cloudy days and residents may experience power outages. The DGen is designed to provide a maximum power of 100kW in order to meet maximum load demand in all load models and PV system is designed supply the average load at a rating of its maximum power. Any sharp peaks in load demand above the power produced by PV system will be covered by the backup DGen. During some instances during the day, the PV system generates more power than the demand which leads to imbalance between demand and supply. Here, excess power must be dissipated in dump load resistors in order to keep the system stable. However, it is not an efficient solution since energy is wasted.

A diesel engine operates efficiently near full load whereas at partial load, the efficiency of the engine is poor and it leads to increased fuel cost as well as the environmental issues due to greater CO_2 emissions. There is also greater wear and tear on the engine.

5.2 Operation Scenario 2

In this operational scenario, the FESS is integrated into the hybrid PV microgrid as a storage system and its impact on the DGen and PV system is investigated. The introduction of FESS will fill the gaps between supply and demand and maintain system stability. It will increase the reliability of the system by allowing the DGen to be turned off without causing power outages. In this case the system supplies power to the load through PV system and FESS and the DGen will be turned on only when FESS and PV are not able to supply the load demand. When the FESS is almost

discharged and the PV system is not able to meet the demand alone then the three-phase circuit breaker will a receive signal from the controller which will restart and connect DGen with the system. Considering operation scenario 2, the storage device will frequently come off and on multiple times during the day, which is not a problem for FESS given its very high cycle life.

The proposed PVHMS is a standalone model consists of a DGen, PV system and FESS. The PV system is interfaced to DC-link through DC-DC boost converter it extracts the maximum power from PV modules under all load conditions. The DGen and the residential load are connected to an AC bus. The power flow from AC bus to DC-link takes place through AC-DC bi-directional converter.

The output power of the PV system is proportional to input solar irradiance (W/m2). When PV output reduces, the machine side converter (MSC) allows the FESS to provide the power back to DC bus. The output of the PV system is zero because of the zero-input solar irradiance during night time and during early hours of the day as shown in all three irradiance curves presented in chapter 4. During the night-time there is much less total electricity demand due to reduced activities in the dwellings. Therefore, at night-time, the DGen can be used to meet the load demand and, at the same time, charge the flywheel. The DGen can operate until the flywheel is fully charged and then leaving the flywheel to meet the load demand. During the day when there is maximum solar irradiance and the PV produces more power than the required power, the excess power can be used to charge the flywheel in order to store the kinetic energy. The stored energy can be converted into the electrical energy which can be used to feed the residential load when the power generated by PV system is not sufficient.

The proposed flywheel system is a C20 rating type with 100kW squirrel cage induction machine (SCIM) capable of storing 5kWh at speed range of 10 – 20 krpm. The power ratings of SCIM-FESS are suitable for total load demand of remotely located village and the C rating was chosen to making the flywheels too large. Stable operation of the

PVHMS is achieved by reliable coordination of the DGen, the FESS and the PV system. The flywheel is assumed to be charged 50% initially. The control scheme compares the %SoC of the flywheel with the difference of load demand and the PV output power. When the PV output is not enough to meet load demand and the FESS is charged enough then power is provided by discharging the FESS. Just before the FESS discharges to 0% and PV output is still not able to meet the load demand then the DGen is turned on to ensure continuity of power flow in the system in order to keep the system stable and running. The torque for charge-discharge cycles of the flywheel is generated based on the power demand expressed by Equation 5.1

$$Torque = \begin{cases} \text{Charge cycle} = \frac{(\text{DGen/PV} - \text{Load demand})\text{kW}}{(\text{FlywheelSpeed})\text{rpm}}\ \text{N.m}, & \text{DGen/PV power} > \text{Load demand} \\ \text{Discharge cycle} = \frac{(\text{PV} - \text{Load demand})\text{kW}}{(\text{FlywheelSpeed})\text{rpm}}\ \text{N.m}, & \text{PV power} < \text{Load demand} \end{cases} \tag{5.1}$$

If the load demand is greater than the PV output power, the FESS (if charged) will share the power with PV system and start discharging. In case when there is enough supply of power from PV then the flywheel goes into standby mode. The DGen will go on standby mode as soon as power is available from FESS or PV system

Figure 5.1 represents logic control scheme of power flow in PVHMS. The coordination of DGen, FESS and the PV system takes place according to logic-based decisions based on availability of electric power from PV system and DGen and state of charge of the flywheel.

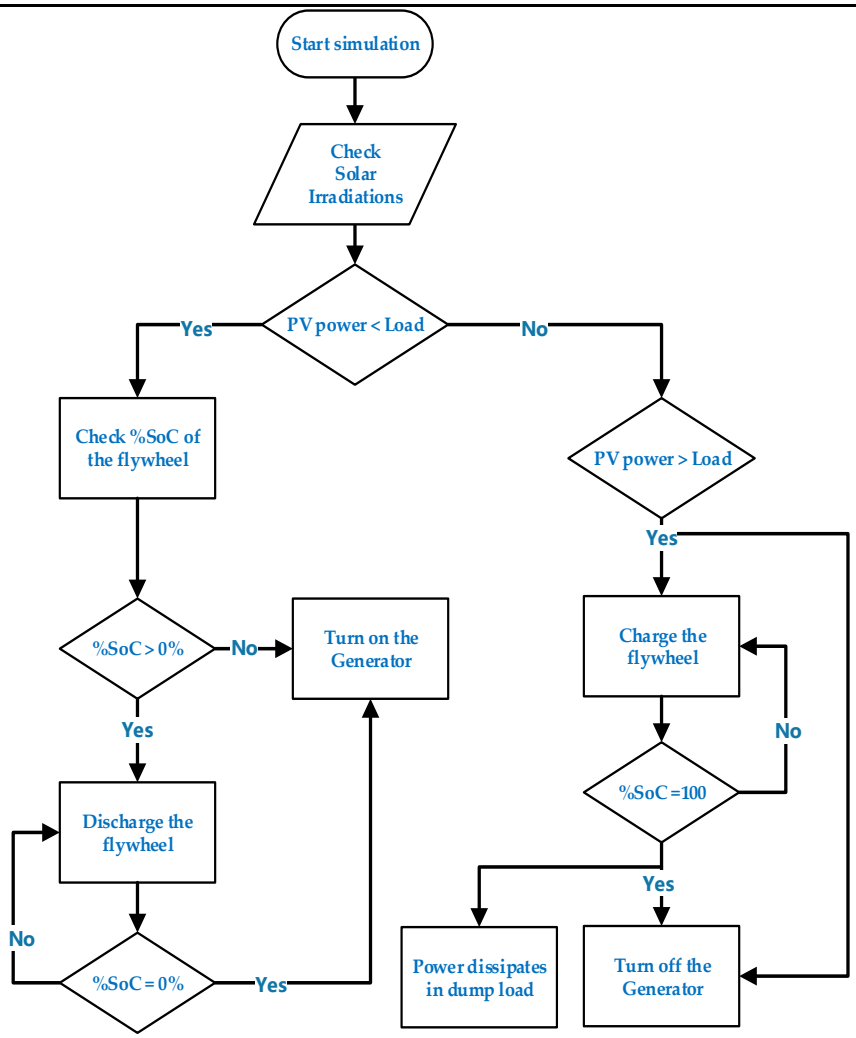

Figure 5-1 Logical power flow chart of PVHMS

5.3 Results and Analysis

In this section the simulated results of PVHM model integrated with residential load are presented and analysed. The dynamic behaviour of the system and power exchange between different power sources (FESS, DGen and PV) is studied. The performance of the system for load profiles of different patterns is tested by analysing power outputs of the DGen, the FESS and solar PV system. In order to analyse the role of the FESS in the model, first, the operation of DGen and solar PV is analysed without the FESS while supplying the load. This is helpful in allowing calculation of fuel consumption and amount of CO_2 emissions produced due to running of DGen. In order to ensure stability of the system, the DGen must be operated all the time when

there is no storage since the PV power can fall away at any time with cloud passing. If the DGen was switched off, it would take several seconds to start up and come back on line.

5.3.1 Operation Scenario 1

In this operation scenario, the electrical demand of the residential load is supplied by the DGen and solar PV system only. The maximum output power of the PV system is approximately 100kW, the electrical demand greater than maximum PV output power is supplied by the DGen. The DGen is designed for a maximum power of 100kW in order to meet the peak demand. In case of excess power in the system, when load demand is less than PV output, excess power generated by the PV system is dissipated in the dump resistor load to keep the system voltage and frequency stable. The results of the simulation are described in the following section.

Operation scenario 1 – Load demand ND-July-WD

Figure 5.2 presents the power curves of PV system, Load demand, DGen and dump load. There are several occasions then PV output is higher than the load demand, the excess power is dissipated into the dump resistor. From t = 0 to t = 8hrs, the load demand is supplied by the DGen only due to zero irradiance. Solar PV power starts to appear at t = 8hrs which is also not sufficient to meet the demand and the morning peak demand is almost entirely supplied by the DGen. Between t = 10hrs to t = 16hrs there is significant power produced by the PV and on some occasions the DGen reduces to zero so is operating at idle. Here, the PV system alone can meet the load demand because the load demand is lower but excessive power produced by the PV system is not utilised but rather must be wasted in dump resistor. After t = 16hrs the PV power starts to decrease and the electricity demand starts to increase. In order to keep system stable and running, the load demand is shared with the DGen and after t = 18hrs the entire load is shifted to the DGen for rest of the duration.

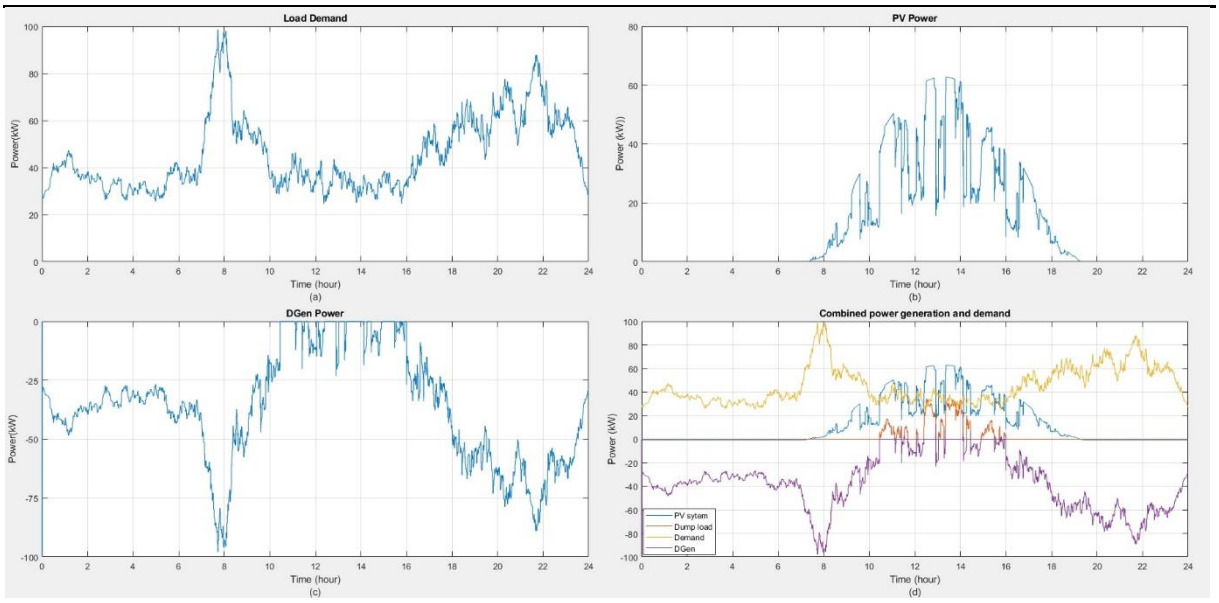

Figure 5-2 Power curves a) Load demand model ; b) PV output power; c) DGen power; d) Combined power curves

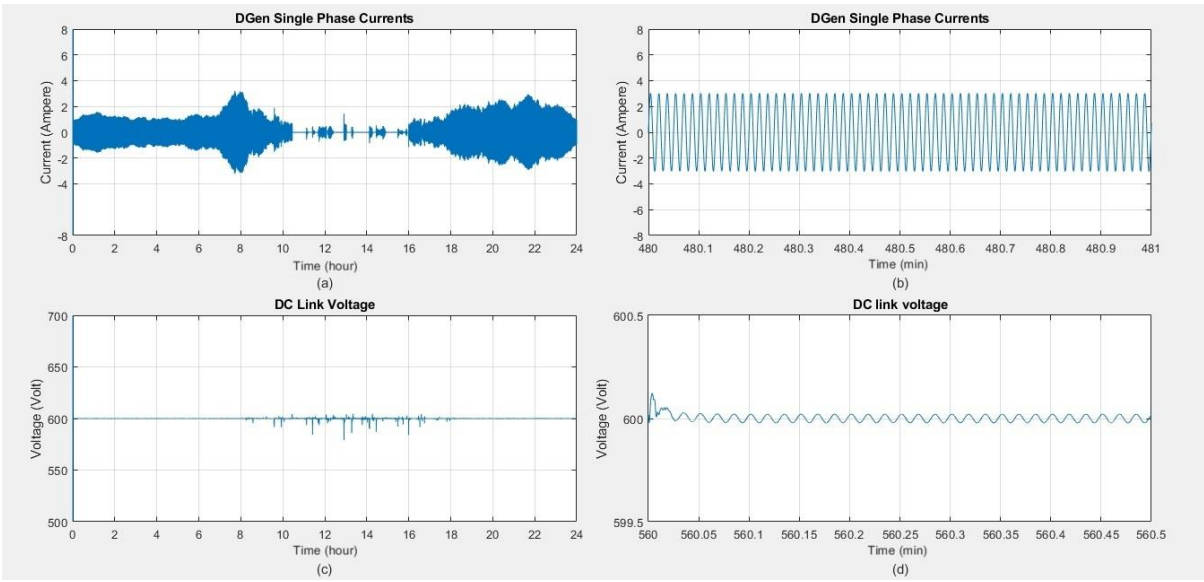

Figure 5-3 a) Phase current of DGen; b) Zoomed in view of current; c) DC link voltage; d) Zoomed in view of voltage

Figure 5.3 presents the DC link voltage and phase current of DGen, it can be seen that the current waveforms of the DGen comply with the variations in the power curve. In order to ensure stability of the system during power exchange between different sources (DGen, PV and FESS) the stability of the DC link voltage in the microgrid is very important. Also, the regulation of DC link voltage for successful interface of power sources with power electronics converters. The DC link voltage shown in

Figure 5.3 presents some spikes this is mainly during the time when PV system as well DGen are involved in supplying the power to the load (between 8hrs to 18hrs), the DC link voltage stays stable at the magnitude of 600V during entire operation of 24hrs. However, the voltage spikes and fluctuations are within acceptable limit of 5%. The analysis of dc link voltage switching ripple in three phase PWM inverters is been presented in [319] Authors in reference, have presented a control scheme to improve fluctuations in DC link voltage which occur during sudden load changes in AC microgrid. In ref. [320] and [321] The authors have presented a detailed analysis on DC link voltage fluctuations where voltage fluctuations under 5% threshold have been categorised as an acceptable limit. The value of DC link capacitance was determined by using equation $C_{DC} = I_0/2\omega v_{DC,pp}$, considering the ripple as 5% . Where I_0 is capacitor current, ω is angular frequency and $v_{DC,pp}$is ripple in capacitor voltage. The value of the capacitance was calculated to be 24000μF.

Operation scenario 1 - Load Model MB-July-WD

Figure 5.4 shows the power curves of PV, DGen for Load Model MB-July-WD. The power produced by the PV system is not sufficient enough to meet the load demand during entire day except for very few occasions for very less time span at t = 14hrs and t = 16 hrs where few spikes in PV power are seen.

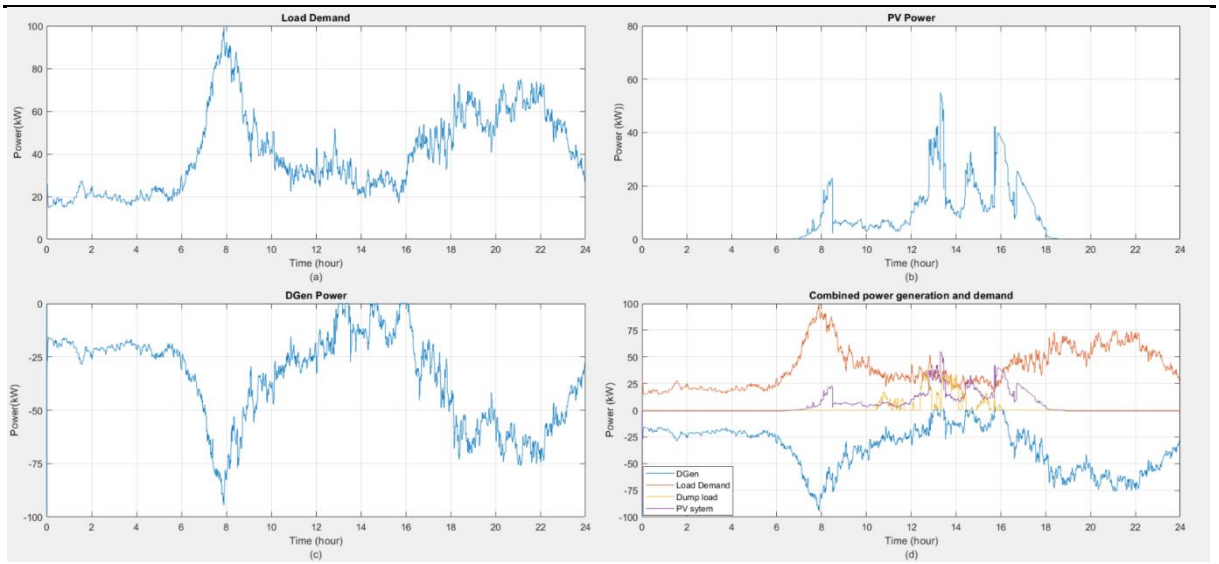

Figure 5-4 Power curves a) DGen power; b) PV output power; c) Load demand model 1; d) Combined power curves

The power curve of DGen is almost the mirror image of electricity demand and for most of the time the DGen is partially loaded except while supplying the morning peak at *t*=8hrs. The solar PV system is not receiving enough solar irradiance on the day due to cloud passing which makes operation of PV system very challenging to supply power to the residents alone. Integration of fast acting energy storage system in stand alone will not only reduce the dependency on DGen but also reduce cost and CO_2 emissions.

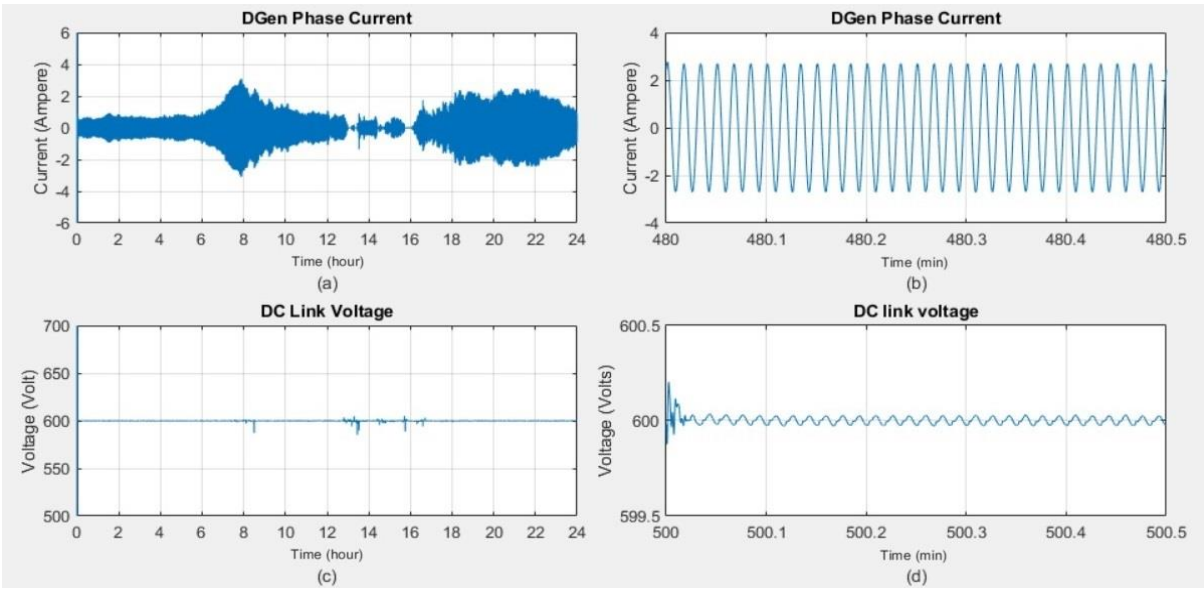

Figure 5-5 a) DGen phase current; b) zoomed in view of currents; c) DC link voltage; d) zoomed in view of DC link voltage

Figure 5.5 represents the DC voltage and phase currents of DGen. It can be seen that the DC link voltage remains stable during entire operation except some spikes due to transfer of power from one source to another which is not seen in case of load model MB-July-WD. The currents of the DGen can be seen to comply with power variations which justifies the stability of and smooth running of the model.

Operation scenario 1 - Load Model KT-Jun-WND

Power curves of all sources for Load Model KT-June-WND are presented in Figure 5.6, the morning peak of electricity demand is significantly shared with DGen by PV system. However, before t = 6hrs and after t = 18hrs, the DGen alone is supplying load demand due to zero power produced by PV system. There is only one occasion when PV power is slightly greater than demand and dump resistor receives very little power (Figure 5.6). The maximum power demand is 100kW which appears between t = 18 – 20 hrs which is supplied by the DGen. In this scenario, the DGen is generating power for almost all its entire operation, so no idling.

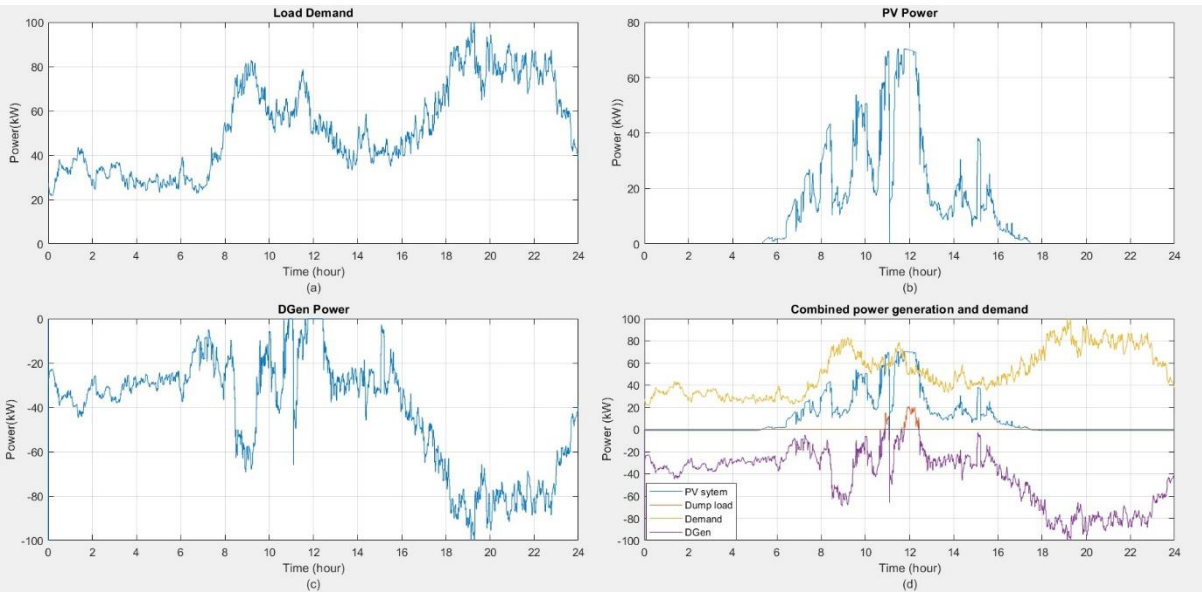

Figure 5-6 Power curves a) DGen power; b) PV output power; c) Load demand model 1; d) Combined power curves

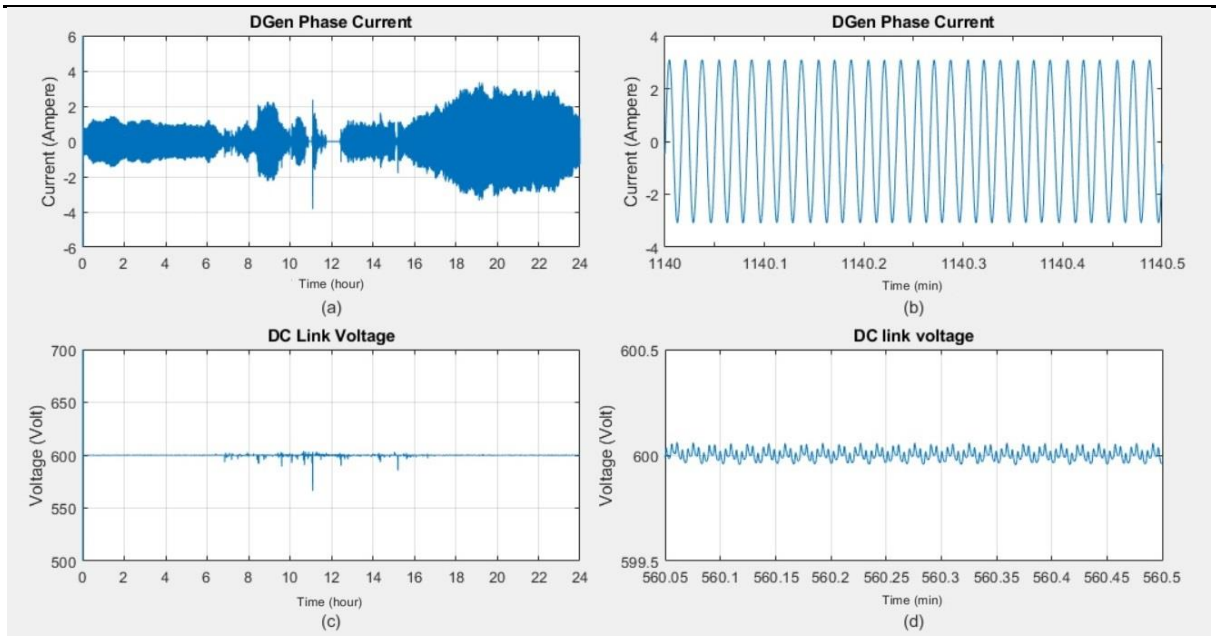

Figure 5-7 a) Phase currents of DGen; b) zoomed in view of currents; c) DC link voltage; d) Zoom in view of DC link voltage.

Figure 5.7 shows the DC link and phase currents of DGen showing compliance with power fluctuations and stability of the system. Some spikes in DC link voltage can be seen which was due to switching of three phase circuit breaker and power transfer from one source to another. Also, it can be seen that the DC link voltage does not have any spikes when only one source is operating, DGen, the spikes start appearing when the PV system and DGen start to share the load demand.

5.3.2 Operation Scenario 2

In this operation scenario the FESS is integrated into the microgrid as an energy storage device. The performance of DGen, PV system and the FESS is analysed. The object of the FESS in this scenario is to reduce the number of operating hours of DGen and provide backup energy support when PV system cannot meet the energy demand due to low irradiance or cloud passing. The operation of the PVHMS in this scenario will be based on the strategy that, DGen will operate when there is insufficient power available from FESS and PV system. The DGen will not only operate to provide energy support for PV system but also its net power will be utilised to charge the flywheel, this will keep DGen at its maximum loading capacity. Also, when there is excess power produced by PV system, the DGen will be turned off and this excess power will

be used to charge the FESS to store the kinetic energy. The results and analysis of all three load models for operation scenario 2 are presented in following sections.

Operation scenario 2- Load model ND-July-WD

PV output power, FESS power and DGen power are shown in Figure 5.8 for Load Model ND-July-WD. The PV output power in this case is not very close to ideal output, it can be seen that there is no PV output before t = 8hrs and after t = 20hrs due to no solar irradiance during these timings. It is unfortunate but unavoidable that there is no PV power generated when there is high demand after 20hrs. However, this compares to the demand before 8hrs in the morning when there are reduced activities with residents sleeping and there is only lightning loads on the system. The average load demand during night is 25kW which relies on DGen power, the DGen operates at its maximum capacity (100kW), the rest of the 75% of its power is utilised for charging the flywheel system. Therefore, between midnight and 6hrs in the morning, the flywheel performs many charge and discharge cycles since it charges quickly by getting more power from DGen. On the other hand, the load demand after 20hrs in the evening is high and the second peak demand of 100kW within the 24hrs cycle appears in the evening just minutes before 22hrs. The average demand after 20hrs is 60kW therefore the flywheel gets less power share for charging purposes and it can perform less charge-discharge cycles between 20hrs to 24hrs compared to the cycles between midnight and 8hrs.

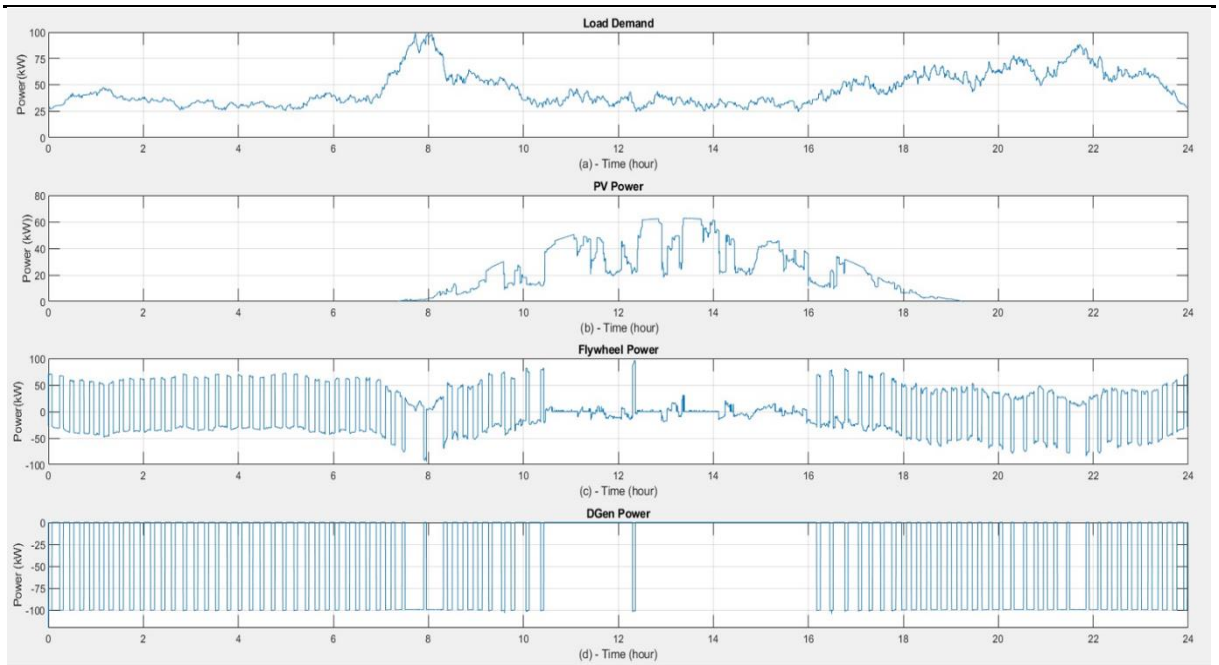

Figure 5-8 a) Load Demand; b) PV output power; c) Flywheel Power; d) DGen Power

The solar irradiance starts to appear just before t = 8hrs, and the PV system shares some load demand with DGen. Since the solar irradiance is fluctuating between 8hrs and 10hrs, the PV system is struggling produce enough power and catch up with load demand at stand-alone conditions. Therefore, between 8hrs to 10hrs DGen has to be involved and share the load demand with the PV system, however, the flywheel plays its part to meet the load demand by discharging its energy into the system by its fast response and numerous charge-discharge cycles. After t = 10hrs it can be seen that the PV system generates reasonably enough power to meet the load demand and during this period the demand is low due to reduced activities at home since residents leave their homes for work by 9 - 10hrs. The demand remains low from 10hrs to 15hrs and during this low demand period, ample PV power is produced hence the flywheel and the PV system only are engaged to supply power to the load. Figure 5.9 shows the charge-discharge cycles of the flywheel system.

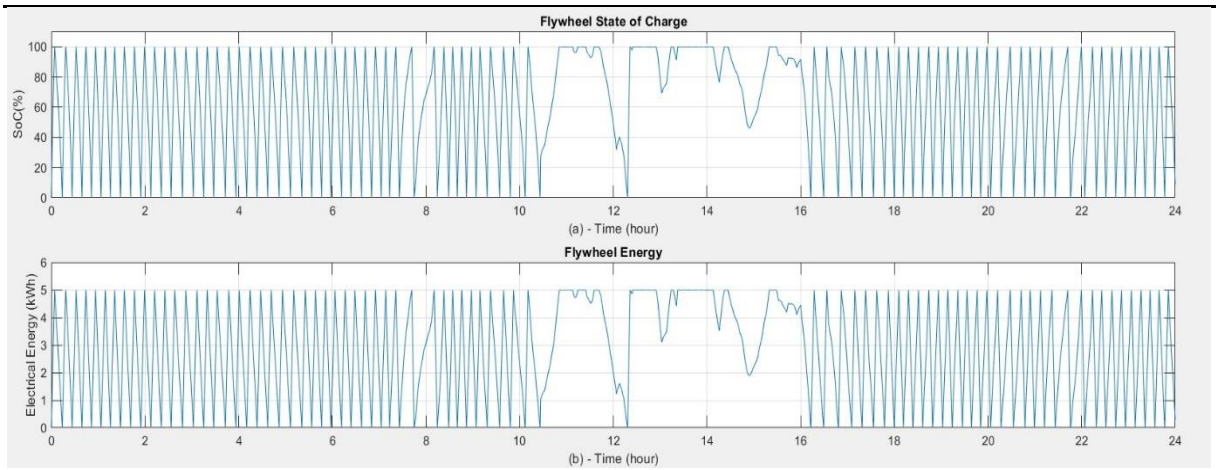

Figure 5-9 a) %SoC of flywheel; b)Flywheel energy

It can be seen from Figures 5.8 and 5.9 that the flywheel performs fewer charge-discharge cycles between 10hrs and 16hrs and it can be seen that the flywheel has gone into standby mode on several occasions, during these events the PV system is able to provide power to the load on its own. However, the flywheel has shared the load with the PV system by discharging its stored energy on some occasions between 10hrs to 16hrs. The maximum power produced by the PV system is 60kW between 12 to 14hrs it is when the demand is lowest and he flywheel is fully charged, still there is an excess power in the system which is dissipated in the dump resistor. The excess power can also be used to charge any other storage device such as BESS although this would add cost to the system. The magnified view of %SoC and energy cycles along with power curves between 10hrs to 16hrs are presented in Figure 5.10 and Figure 5.11 respectively. In order to aid examination of system operation during low/zero PV output in the morning period, the magnified view of power curves and the %SoC are presented in Figure 5.12 and 5.13 respectively. From Figure 5.12 it can be seen that there is no PV power output and the flywheel gets charged from DGen power. It can also be observed that the flywheel takes more time to discharge compared to its charging cycle, it is because while discharging the demand is very low whereas during the charging cycle the flywheel gets ample power to charge from the DGen since the demand is still low. Here, the controller generates more torque during charging cycle which leads to higher acceleration of flywheel rotor.

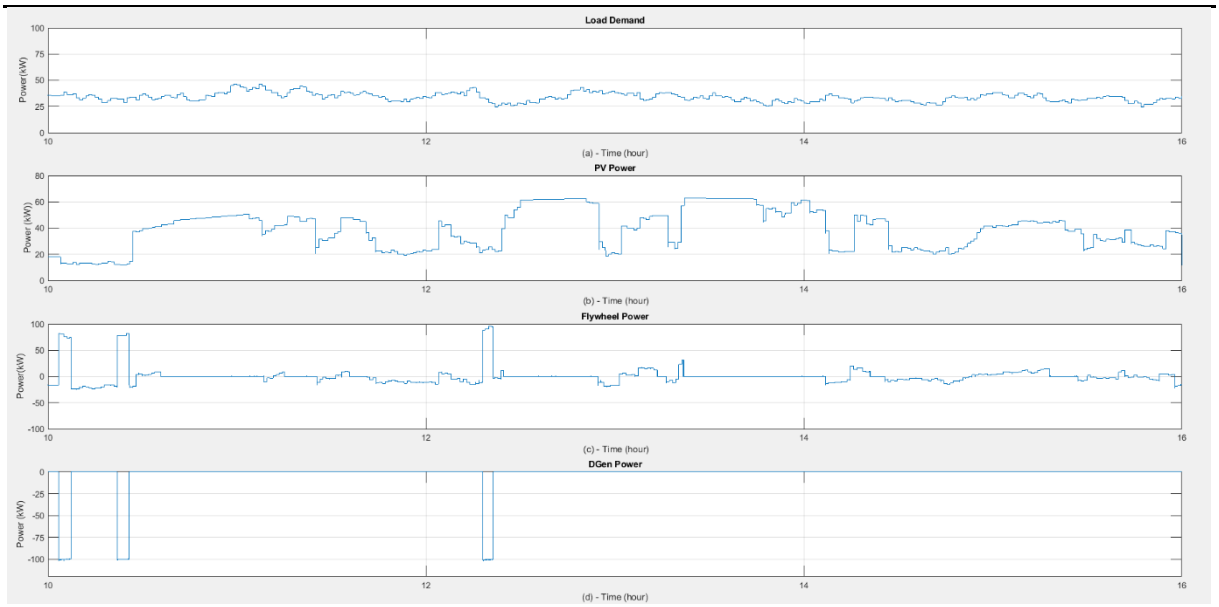

Figure 5-10. Magnified view of power curves between 10am to 4pm. a) Load Demand; b) PV output power; c) Flywheel Power; d) DGen Power

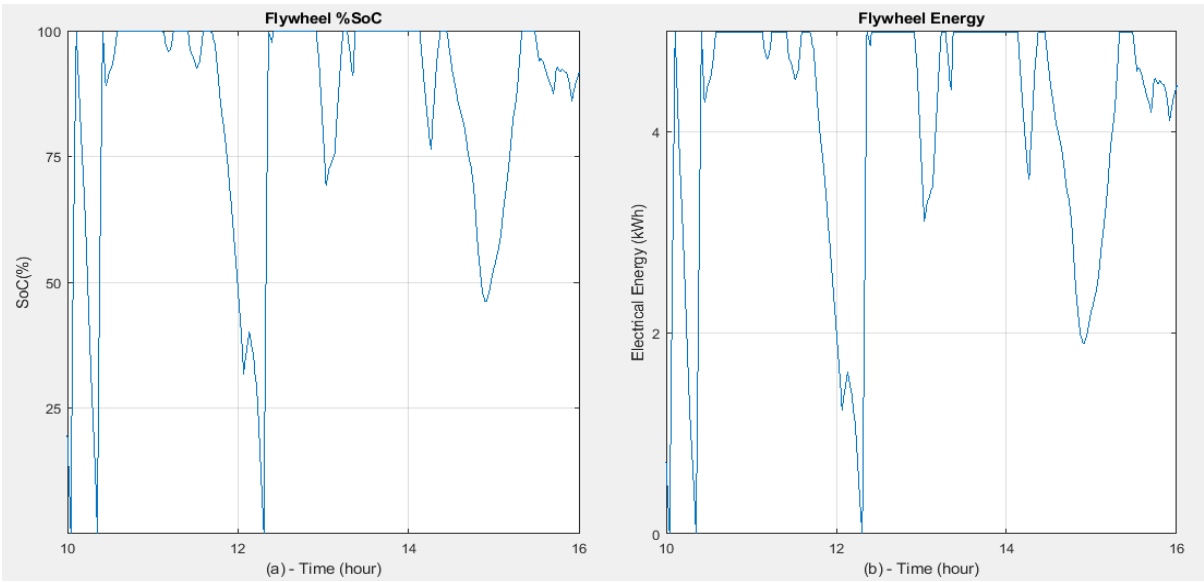

Figure 5-11 Magnified view of charge-discharge cycles between 10am to 4pm

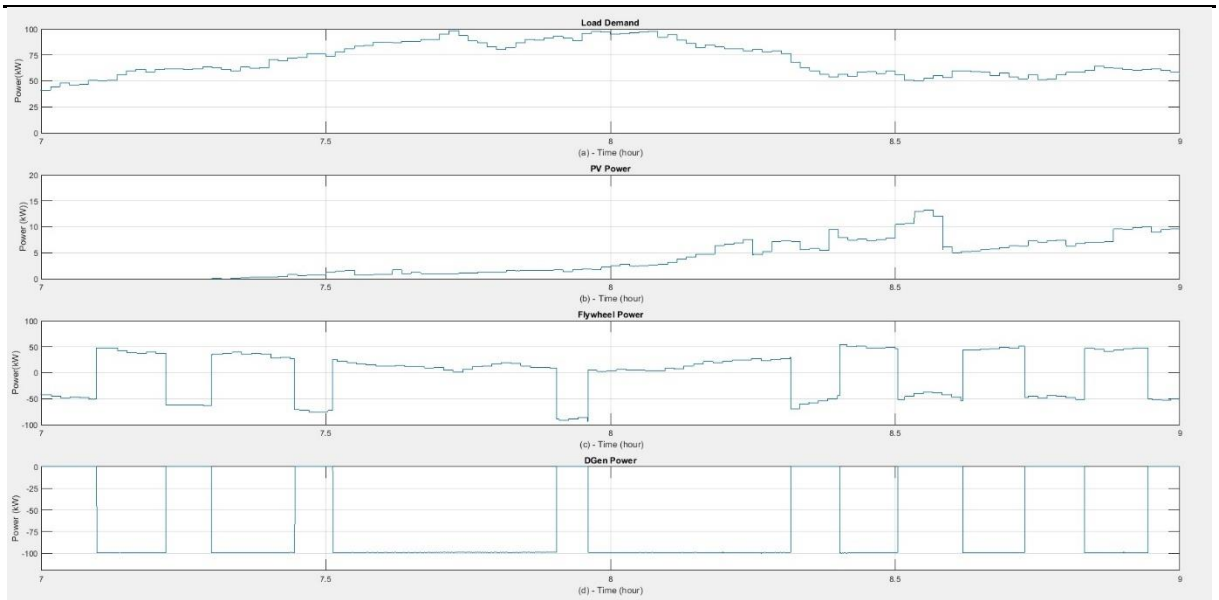

Figure 5-12 Magnified view of power curves between 7am to 9am. a) Load Demand; b) PV output power; c) Flywheel Power; d) DGen Power

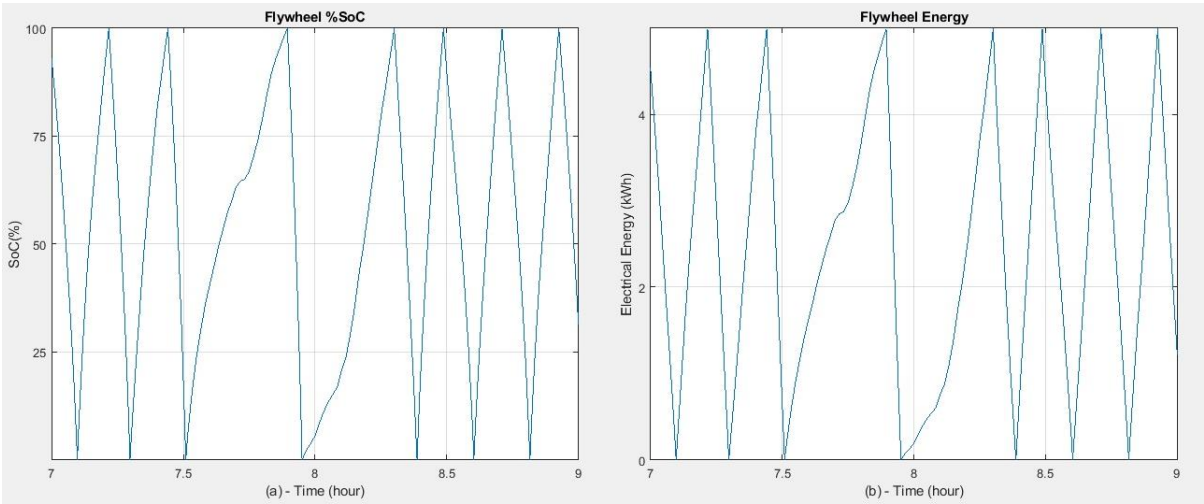

Figure 5-13. Magnified view of %SoC of the flywheel and energy between 6hrs to 8hrs

The DC-link voltage and phase currents of the DGen and are shown in Figure 5.14 and 5.15 respectively. It can be seen that the there are many spikes which are related to the switching of power sources and frequent charge discharge cycles of the flywheel. However, the DC link stays stable during 24hrs operation. The DGen currents in Figure 5.15 show conformity with power curves of the DGen as well. The magnified view of the DGen currents is also shown in Figure 5.15b, it can be seen the currents waveform stays stable despite frequent switching of the load from DGen.

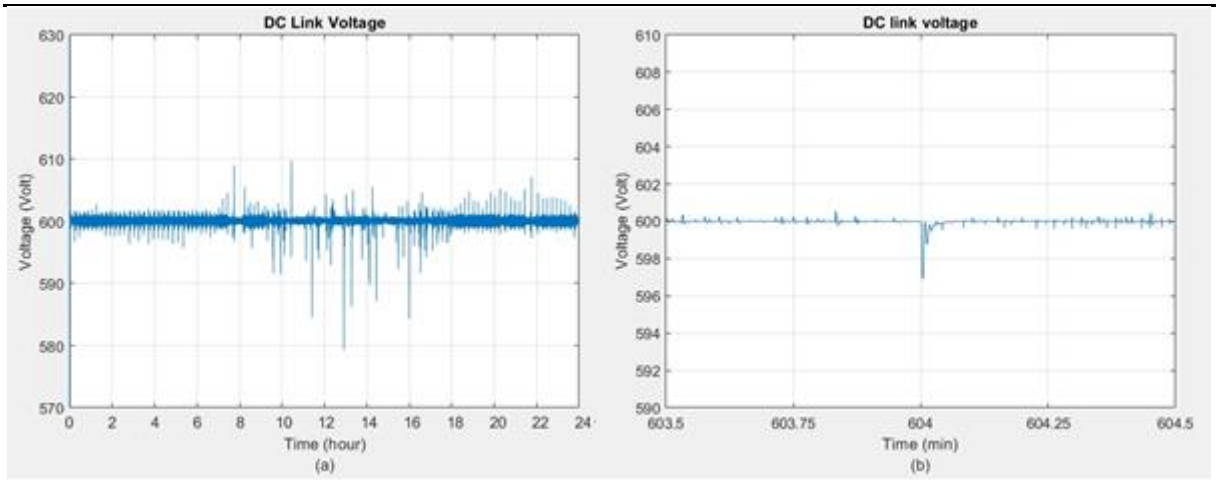

Figure 5-14 a) DC link voltage; b) zoomed in view of DC link voltage

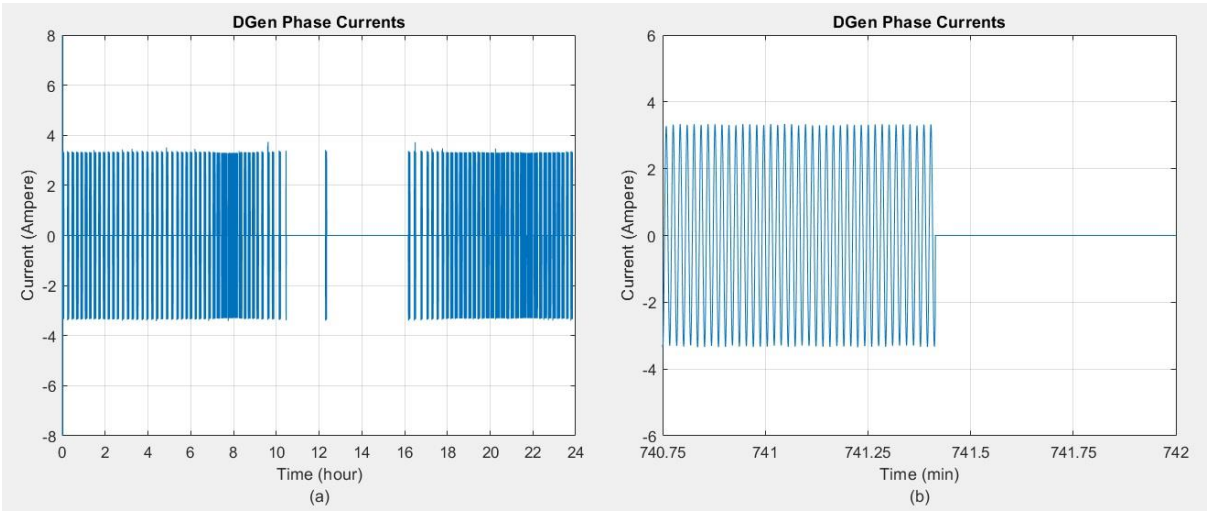

Figure 5-15 a) DGen phase current; b) Zoomed in view of currents

In the results discussed above, the DGen was operated at 100% loading conditions which made DGen perform many on/off cycles after every 5-7 minutes this switching may not be good for the engine. The alternative is for the DGen has to be turned on for 24hrs and remain on standby mode when not supplying load to the system. In order to improve running time of the DGen and reduce switching events, the DGen was made to run at base load of 75kW, however, when the demand is above 75kW and the flywheel is also not charged enough to brush off the demand above 75kW the DGen is then switched to 100% loading capacity. The power curves of the flywheel, DGen, PV system and the load demand are presented in Figure 5.15 representing the impact when DGen is made to operate at 75% of its loading capacity. Comparing to the results presented in Figure 5.8, it can be seen that the DGen performs fewer

standby cycles and after 16hrs the switching cycles of DGen are reduced and operating time of DGen is increased. The DGen has remained at load for longer period of time compared to when operating at 100% of loading capacity. This leads to the better fuel efficiency and health of the engine. In this case the DGen has ramped up its %Loading capacity at few occasions the demand is higher than 75kW. The flywheel can be seen performing its charging-discharging cycles, at *t*= 8hrs during the morning the peak has been shared by the flywheel power for few minutes.

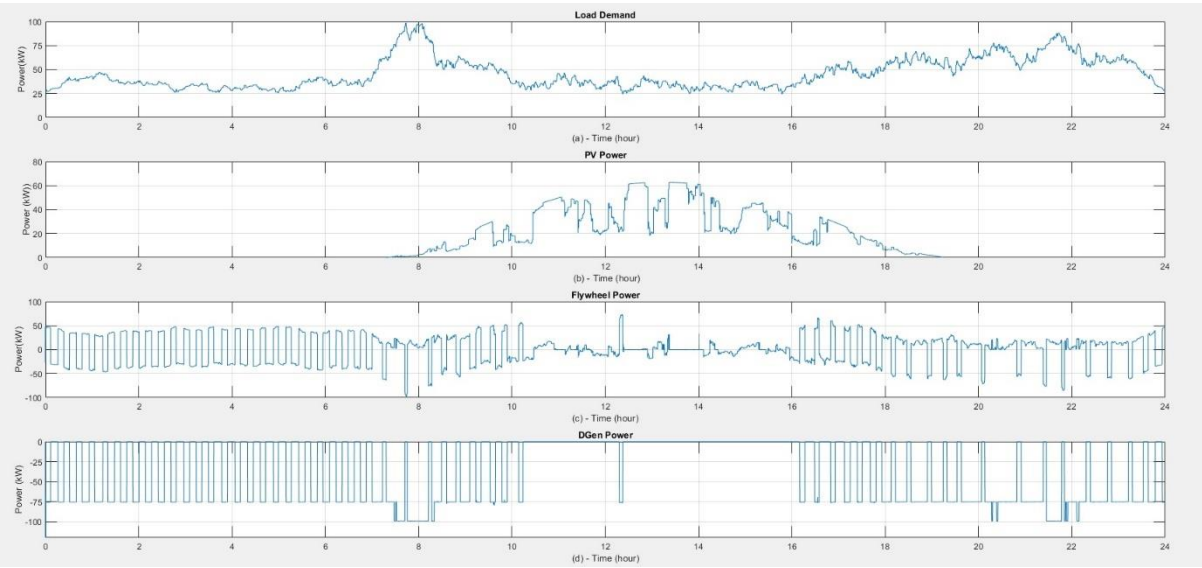

Figure 5-16 Power curves at 75% of DGen operation: a) Load Demand; b) PV output power; c) Flywheel Power; d) DGen Power

Figure 5.17 shows the comparison of flywheel power curves at 75% and 100% capacity operation of DGen. In this case the flywheel takes more time to charge since its power share from DGen is cut by 25% therefore after supplying the load demand the net power available for charging cycle is less compared to when DGen was operating at 100% loading capacity.

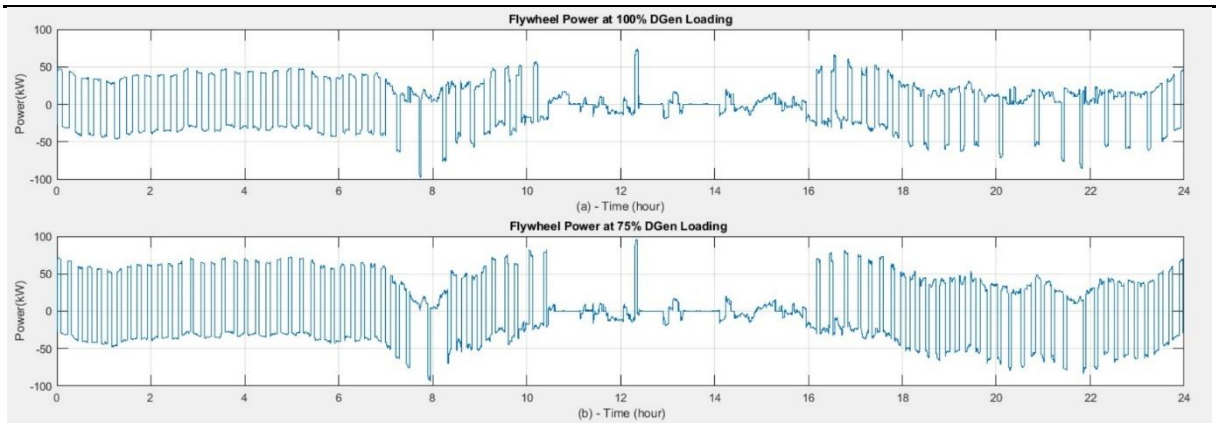

Figure 5-17 a) Flywheel power curves at 100% loading; b) Flywheel operation at 75% DGen loading

Operation Scenario 2 – Load model MB-July-WD

The power curves of flywheel, DGen, PV for operation of load model MB-July-WD are presented in Figure 5.18 and corresponding %SoC and energy curves are presented in Figure 5.19. The operation of all three sources is different in this case compared to load model ND-July-WD. The power curve of the PV system is very challenging in this case as there are many drastic variations in solar irradiance. In addition, the PV power output is low for the entire 24hrs except for a peak of 55kW between 12hr and 14hrs. Here, the demand is very low and the DGen is engaged more in this case as compared to load model ND-July-WD as represented by many switching cycles in Figure 5.18. The power curves and charge-discharge cycles remain almost same compared to the operation in case of ND-July-WD, since the load demand is low and an average load demand in this case too is 25kW.

The electricity demand starts to ramp up from t = 6hrs and reaches to 100kW around 8hrs. At the time of peak demand, the flywheel is fully charged and it is discharged to meet the load demand for few minutes, at this time there is some power available from the PV system as well and the load is taken off from the DGen. The power curves of the flywheel follow the variations in the power demand, when there is high demand the discharge power of the flywheel increases. The PV system power remains low until 12hrs and it starts to ramp up after 12hrs. Between 12hrs and 16hrs, good PV power is generated but with some fluctuations. However, it appears when there is very low

demand similar to the demand curve before t = 6hrs, for the span of 4hrs (between 12 to 16hrs) so the flywheel and PV system are much involved to meet the load demand and supply power to the load.

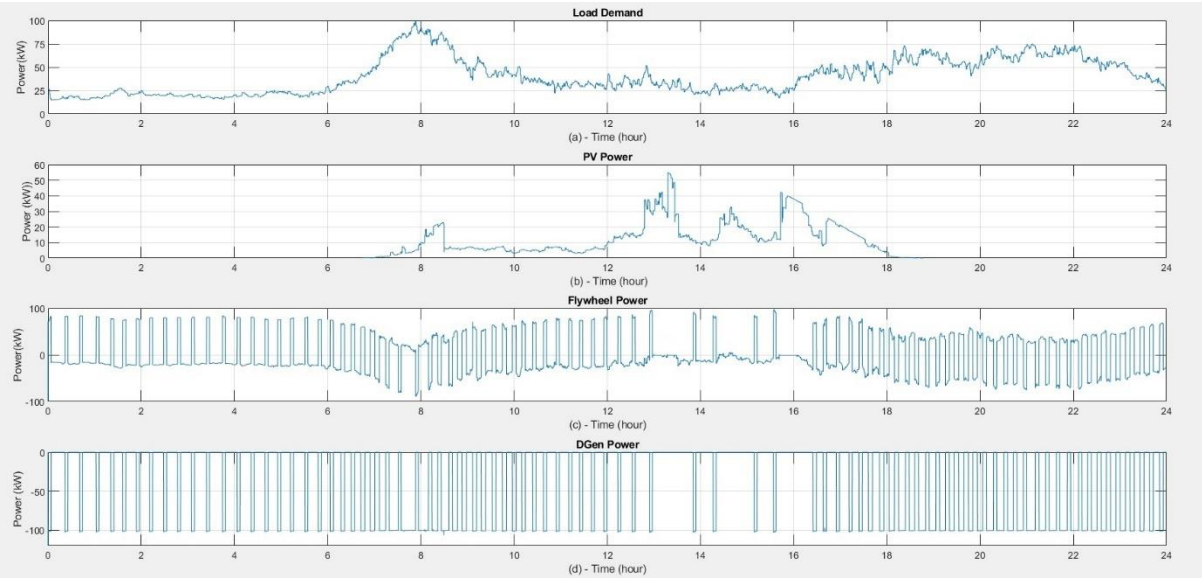

Figure 5-18 a) Load Demand; b) PV output power; c) Flywheel Power; d) DGen Power

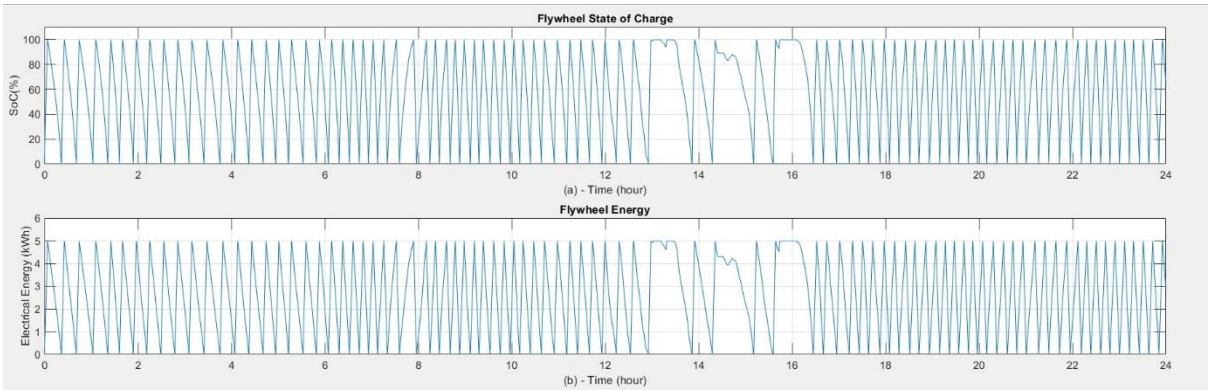

Figure 5-19 a)%SoC of flywheel; b)Flywheel energy

The DGen is also turned on for few times when power from the flywheel and the PV is not enough to meet the load demand. The magnified view of power curves between t= 10hrs to t = 14hrs is presented in Figure 5.20 and its corresponding charge-discharge cycles representing %SoC and energy are presented in Figure 5.21. The load demand in the evening time (after 18hrs) start to increase and remains high until t = 22hrs and the PV power is zero due to no solar irradiance. During the period between 18hrs to

24hrs, the flywheel and DGen together meet the load demand. The load is taken on and off several times during this period (Figure 5.20d).

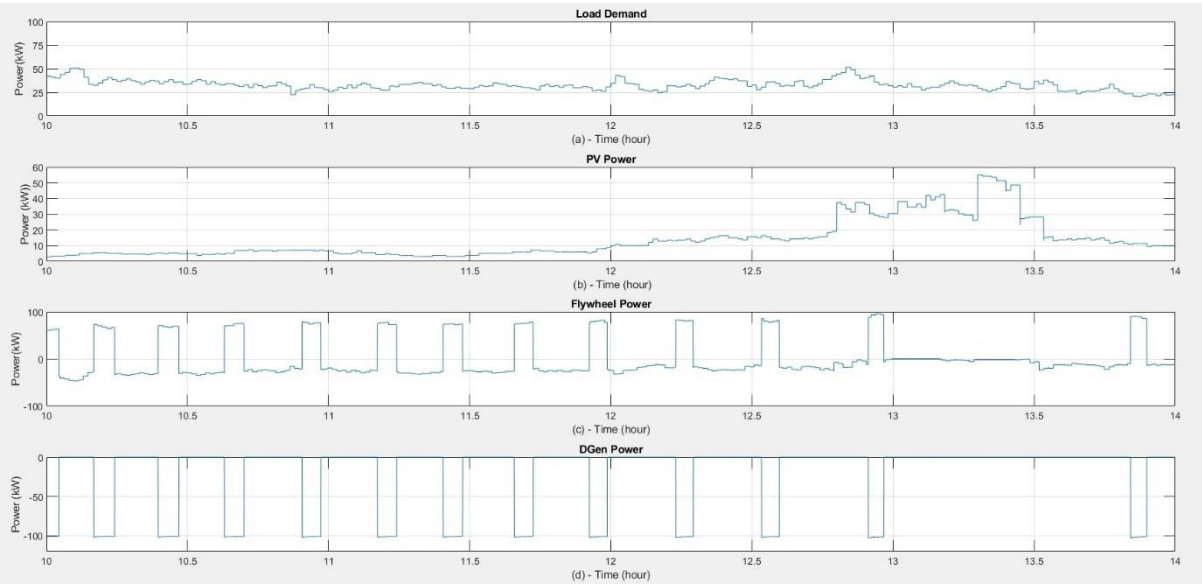

Figure 5-20 Magnified view of power curves between 10am to 2pm. a) Load Demand; b) PV output power; c) Flywheel Power; d) DGen Power

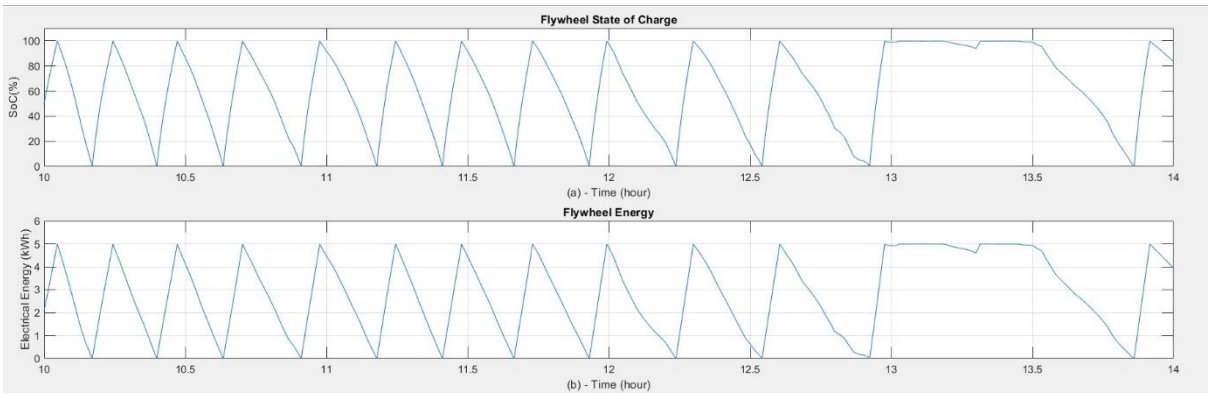

Figure 5-21 Magnified view of power curves between 10am to 2pm. a) Flywheel state of charge; b) Flywheel electrical energy

Because the flywheel discharges very quickly by operation in times of high demand, the torque generated by the controller is high which causes the flywheel energy to be depleted more quickly. The flywheel and DGen are taking turns after minutes of time to supply the load demand between t = 18hrs and t = 24hrs. It can be seen that during operation over 24hrs, the flywheel barely is resting and it continuously supplies the

load demand by its fast response. For greater clarity, separate views of power curves for flywheel under charging and discharging states are presented in Figure 5.22.

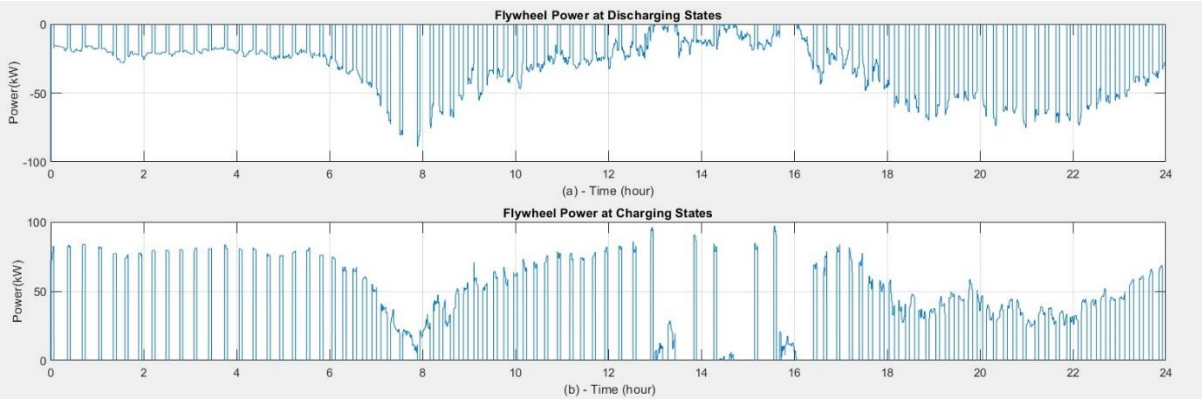

Figure 5-22 Power curves of the flywheel system during charging and discharging states

Figure 5.23 and Figure 5.24 show the phase currents of the DGen and DC-link voltage respectively. The involvement of the DGen can be visualised from the current waveforms shown in Figure 5.23, the DGen is more involved in the power supply in periods 6hrs to 8hrs and between 18hr to 22hrs. During these periods as mentioned earlier, the load demand is high and all peak demands appeared during these time periods. The DC-link voltage remains stable with multiple small spikes, it can be seen that there are more and higher spikes between 12hrs to 14hrs. During this time period, all three power sources (flywheel, DGen and PV) are contributing to the supply which leads to switching effects and spikes in the voltage. However, the spikes are within the acceptable limit and do not cause instability in the voltage magnitude.

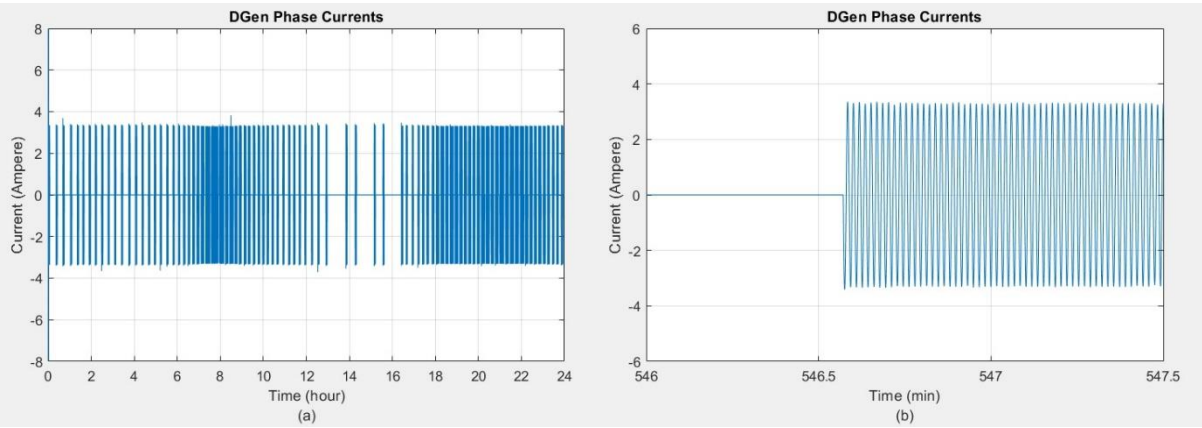

Figure 5-23 a) DGen phase current; b) Zoomed in view of currents

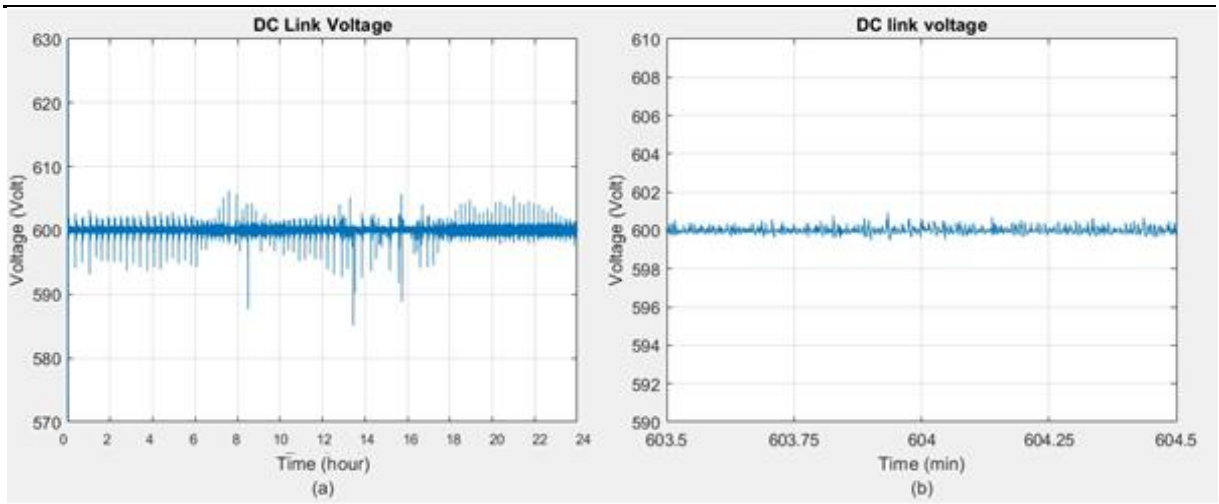

Figure 5-24 a) DC link voltage; b) zoomed in view of DC link voltage

The case of operation of the DGen at 75% loading capacity was also analysed for load model MB-July-WD, an interesting case since the corresponding irradiance profile for load demand MB-July-WD is very challenging due to frequent variations in solar irradiance. Here, the PV could not produce enough power for most of the time over the course of 24hrs therefore the DGen has to come on and off more frequently to provide backup power to the load and charge the flywheel. When the DGen was run at 75% of it loading capacity in this case, the switching events were significantly reduced and the operating timings DGen were increased. The DGen was continuously running at 75kW, however, during the peak demand hours the DGen was switched to its 100% loading capacity as shown in Figure 5.25.

The peak demand of 100kW morning peak demand is shared by the flywheel and the DGen with some slight power contributed by the PV system. The DGen steps up its loading capacity only during morning time when the demand is more than 75kW. After 16hrs it can be seen that the standby time of the DGen has greatly reduced and the power to the flywheel for charging purpose is diverted very less. The comparison of charge-discharge cycles of the flywheel operating at loading capacities of DGen is shown in Figure 5.26. It can be seen that utilisation of PV power in the system is more when DGen operates at 75% loading capacity since the flywheel goes into standby mode for less time as compared to the case with the DGen operating at 100% of loading

capacity. The comparison of DGen operation at 100% and 75% capacity is presented in Figure 5.27.

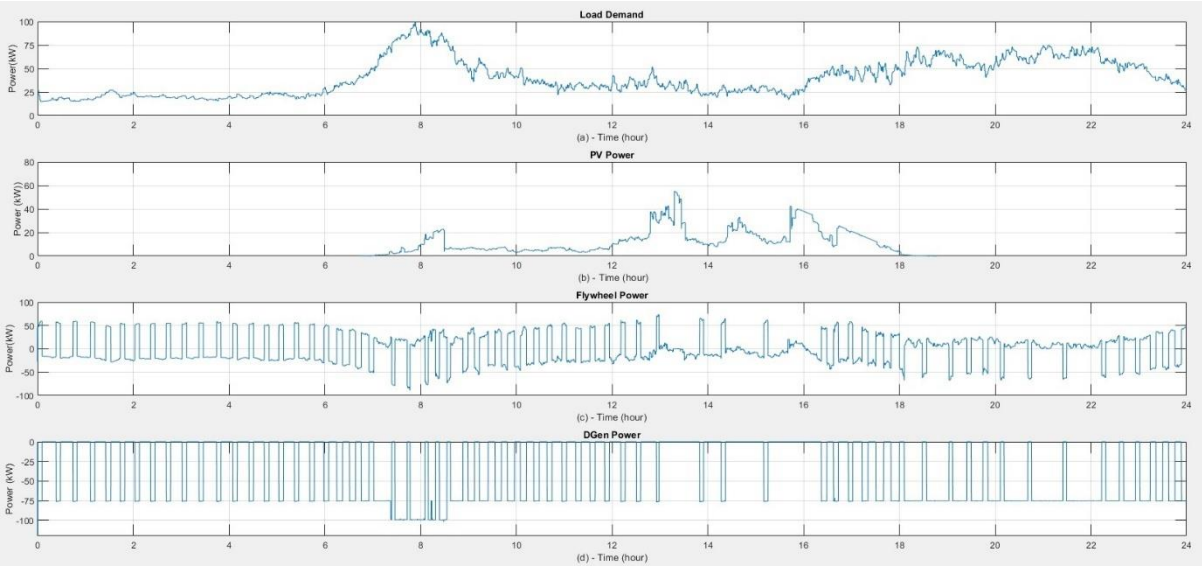

Figure 5-25 Power curves at 75% of DGen operation: a) Load Demand; b) PV output power; c) Flywheel Power; d) DGen Power

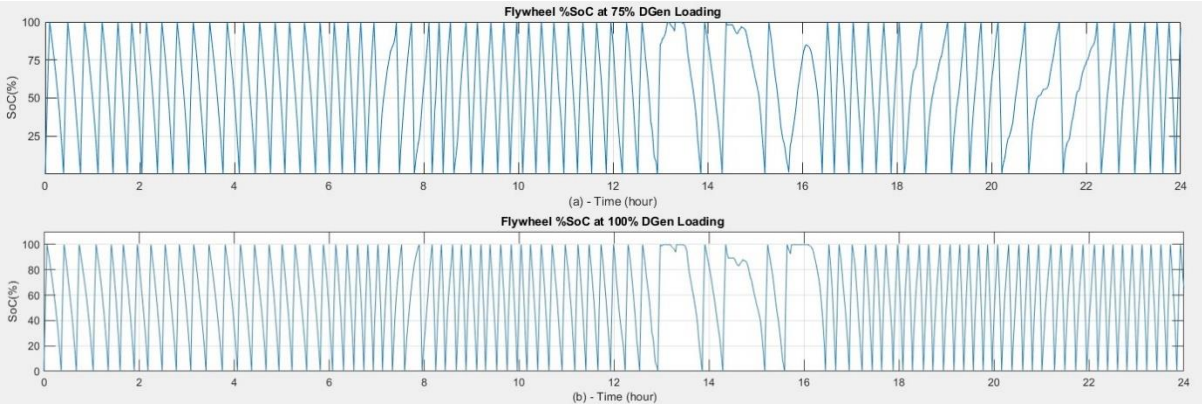

Figure 5-26 %SoC of the flywheel at 75% and 100% loading capacity of DGen

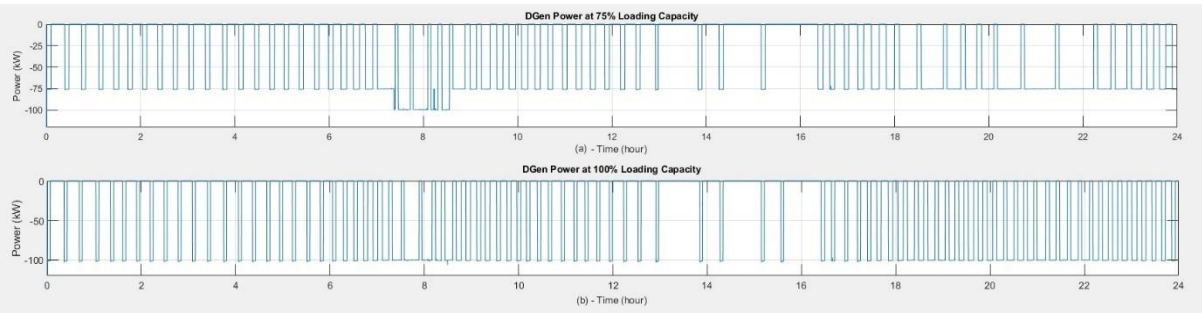

Figure 5-27 DGen operation at 100% and 75% Loading capacity

Operation Scenario 2 – Load model KT-June-WND

The load model KT-June-WND is different than the load model MB-July-WD and ND-July-WD discussed in the earlier sections. In this case the electricity consumption trend represents the load demand on the weekend. In the case of the load demands model MB-July-WD and ND-July-WD, the power consumption started to ramp up in early morning from *t*=6hrs and the peak demand occurred around 8hrs in the morning, since those trends represented the electricity consumption on a normal working day (weekday). For weekend, load model KT-June-WND, the demand remains low from midnight to *t*=8hrs in the morning and it starts to ramp up after *t*=8hrs in the morning. The first peak occurs between 8hrs and 10hrs which is also not a maximum demand during 24hrs, on the other hand the PV power output starts to appear around 6hrs in the morning which cause less switching of DGen as shown in Figure 5.28.

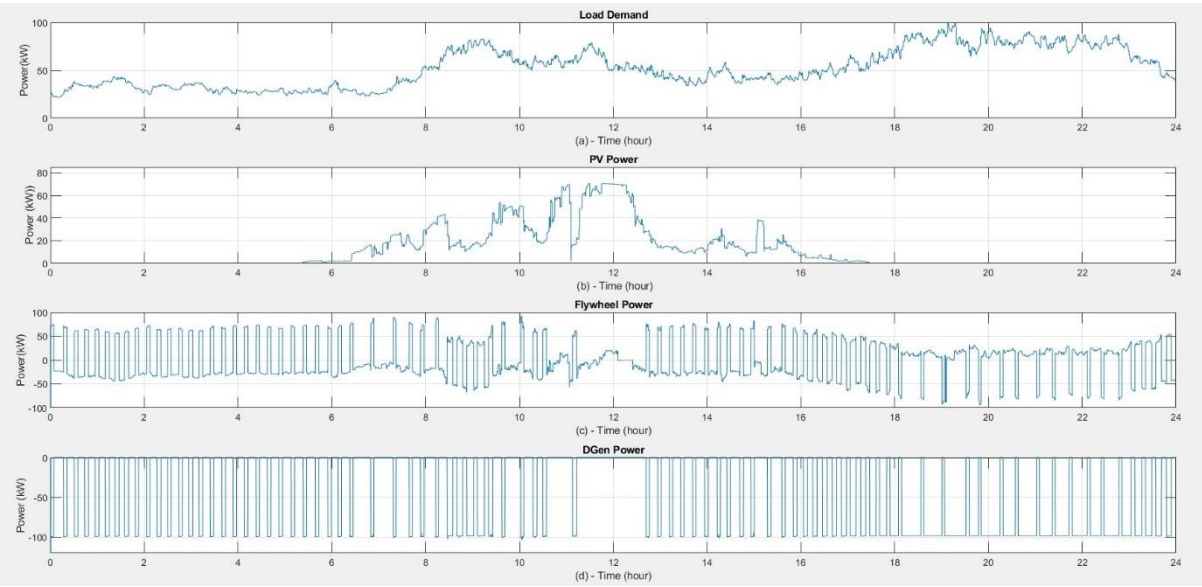

Figure 5-28 a) Load Demand; b) PV output power; c) Flywheel Power; d) DGen Power

The demand from midnight to 2am is slightly higher since residents sleep later due to weekend. The flywheel and DGen share the load demand from midnight to 6am, the PV system starts to share the load demand from *t*=6hrs, the PV output power increases and there is a significant power produced by the PV system until 9am. Before reaching

a power of 65kW, the power production of the PV system decreases to 20kW, it happens when the load demand touches the morning peak of 80kW, during which time the flywheel provides backup power support by performing fast charge-discharge cycles and the DGen providing power for charging cycles and supplying the load demand. Figure 5.29 shows the charge-discharge cycles of the flywheel representing %SoC and flywheel energy.

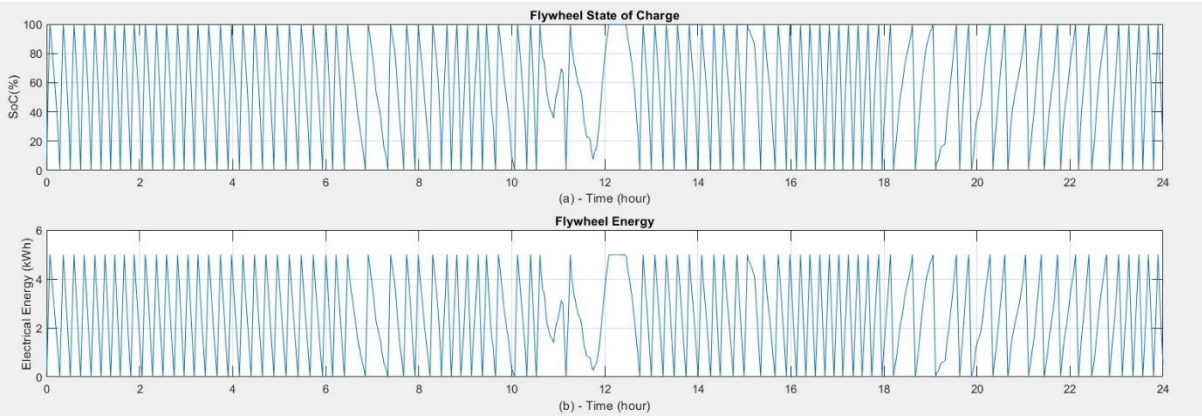

Figure 5-29 a)%SoC of flywheel; b)Flywheel energy

At *t*=11am, there is a sudden dip in PV power which discharges the flywheel very quickly and the load is shifted to the DGen which then also charges the flywheel. Followed by the sudden dip, the PV system reaches to its maximum power production during the entire 24hrs which is 70kW, at this stage the PV system can supply power to the load at standalone condition, the flywheel gets fully charged from PV power and goes into the standby more for few minutes (Figure 5.28). The power production from PV system remains steady around 12 noon and starts to decline at *t*=12hrs. The load demand during this time takes on a belly type shape and starts to increase after *t*=16hrs. Magnified views of the power curves between 11hrs to 13hrs when PV generates its maximum power is shown in Figure 5.30 and the corresponding charge discharge cycles representing the flywheel energy and %SoC are shown in Figure 5.31.

The flywheel plays its part to supply power to the load during load demand period between 12hrs and 14hrs when PV power is very low. After *t*=16hrs, the operating time of DGen increases and it performs power on cycles for greater time as compared

to the cycles before 6am since the load demand remains continuously above 80kW due to increased activities of the residents on weekend night. Also, the flywheel performs its discharges cycles to cover some portions of maximum demand in the evening by its fast response. Since the load demand is higher, the discharge cycles do not last as long and the flywheel gets much less power for its charging cycles. Therefore, the flywheel takes more time to fully charge whereas it takes less time to discharge due to high demand.

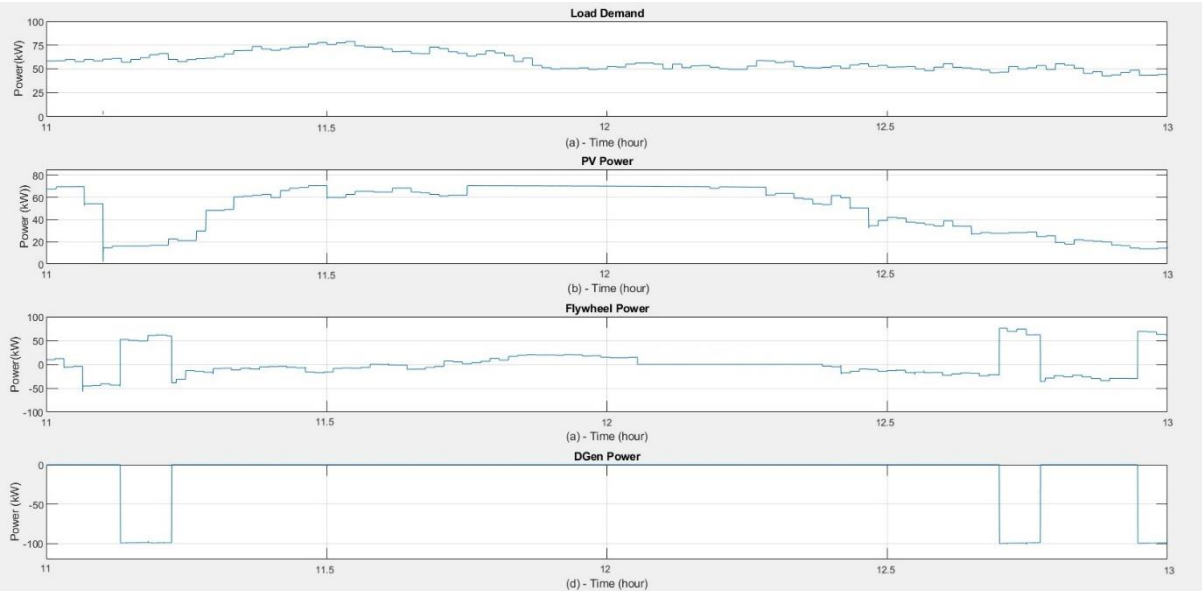

Figure 5-30 Magnified view of power curves between 11am to 13pm. a) Load Demand; b) PV output power; c) Flywheel Power; d) DGen Power

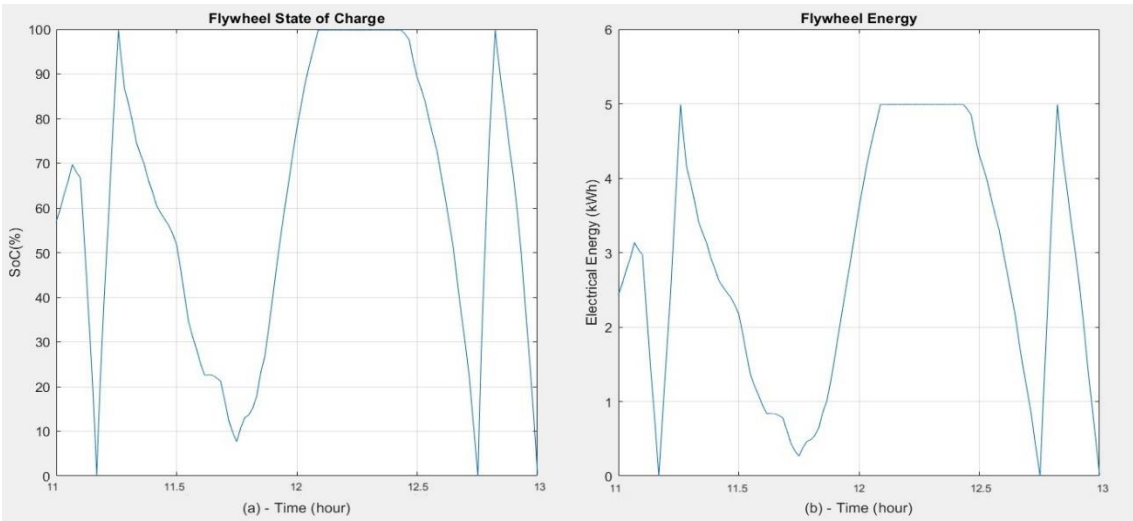

Figure 5-31 Magnified view of %SoC of the flywheel and energy between 11am to 1pm

The DGen currents and DC-link voltage are shown in Figure 5.32 and Figure 5.33 respectively. A magnified view of the DGen currents is shown in Figure 32b which shows the stability of the current waveforms. The DC-link voltage remains stable despite sudden and frequent switching events during the operation, however, the spikes are not significantly large.

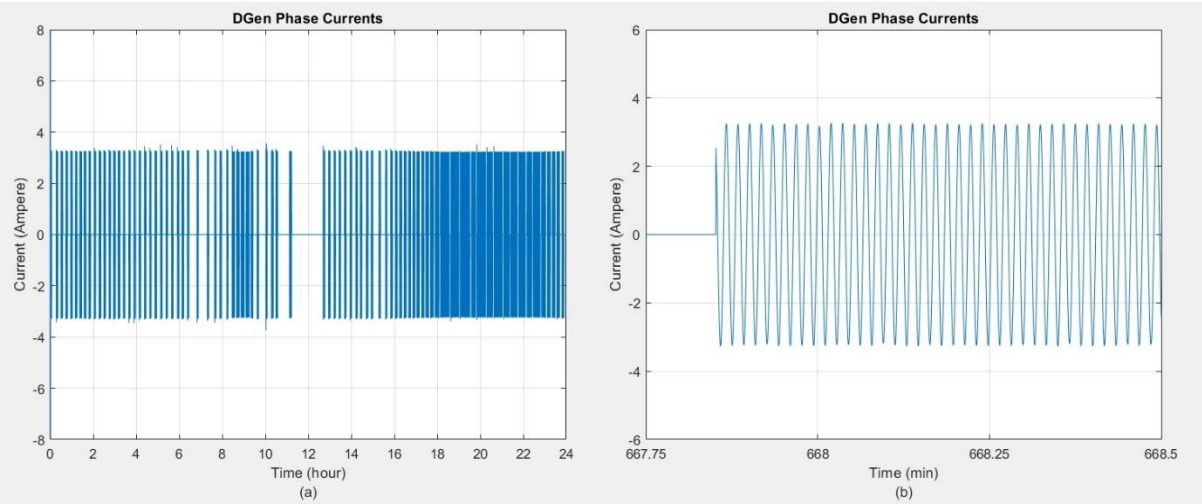

Figure 5-32 a) DGen phase current; b) Zoomed in view of currents

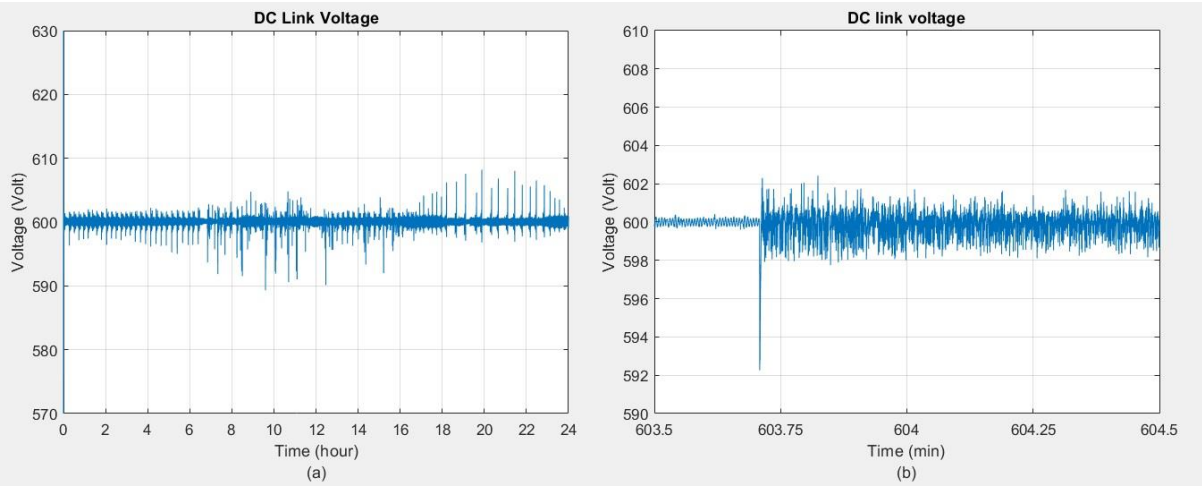

Figure 5-33 a) DC link voltage; b) zoomed in view of DC link voltage

Figure 5.34 represents the % SoC and energy cycles of the flywheel at 75% of DGen operation. The power diagram of the flywheel , PV system and the load demand are presented in Figure 5.35. In this case the DGen has operated at 75% before evening (before 18hrs), the load demand after 18hrs remains above 75kW except at very few occasions it falls below 75kW for few minutes which causes DGen to switch its %

loading capacity from 75% to 100% several times. However, the DGen has operated at 100% of its capacity for most of the time period after 18hrs till 23hrs. The loading capacity of DGen is decided by the controller based on the load demand and power generated by PV system. In this case the flywheel and PV system are involved to supply the load demand when there is maximum power generated by the PV system and for few minutes PV system alone has met the load demand while leaving the flywheel in standby model.

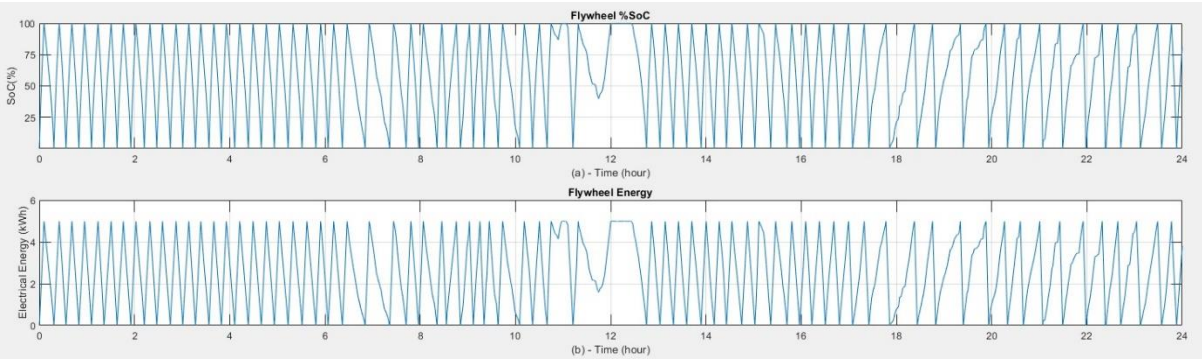

Figure 5-34 a)%SoC of flywheel; b)Flywheel energy

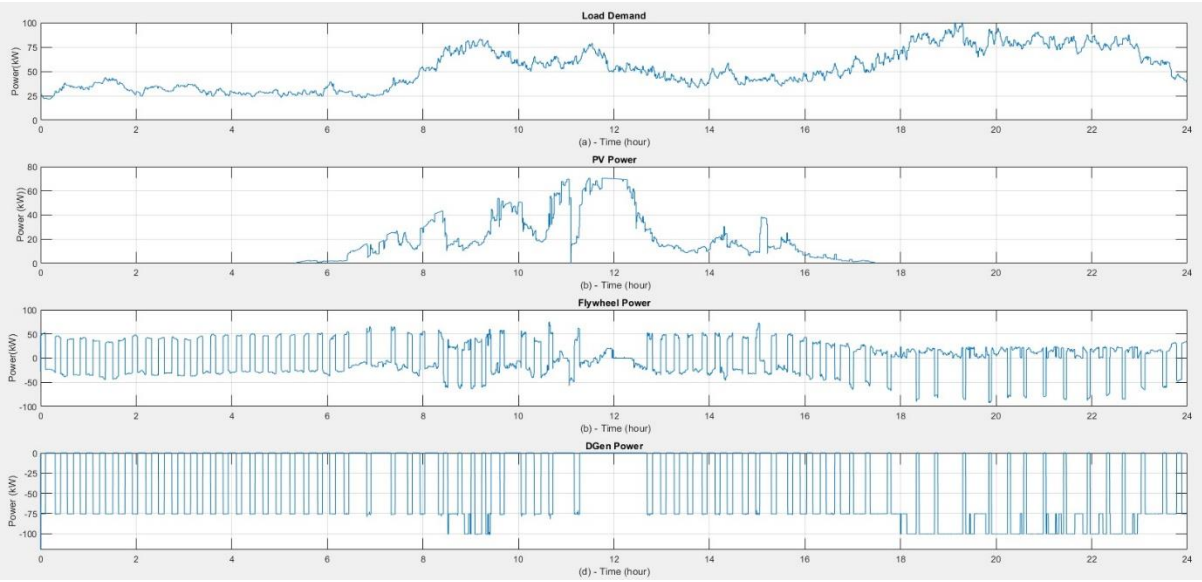

Figure 5-35 a) Load Demand; b) PV output power; c) Flywheel Power; d) DGen Power

5.4 Analysis of generator fuel consumption

Operation of the DGen in each load model scenario presented above has been dependent on %SoC of the flywheel and contribution of PV system. On some occasions it was seen that the demand was fully supplied by combined operation of PV system and the flywheel while DGen remained off. On the other hand, the DGen was involved in supplying demand for most of the time during entire course of operation (all load models in operation scenario 1). The consumption diesel fuel and the fuel cost savings were calculated for all 3 load profiles including operations with and without the FESS and results are presented and discussed in this section. The manufacturer's data sheet of the DGen is presented in Appendix B, where full specifications are provided. The DGen fuel consumption (F_c) is calculated using Equation 5.2

$$F_c = C_1 P_{Gn} + C_2 P_{Gout} \tag{5.2}$$

where:

C_1 : Fuel curve coefficient (L/hr/kW) at rated power

C_2 : Generator fuel curve slop (L/hr/kW) at output power

P_{Gn} : Rated power of DGen (kW)

P_{Gout} : Output power of DGen (kW)

The fuel coefficients are calculated from manufacturer's data specification, therefore for the DGen considered in this thesis, the values of C_1 and C_2 are estimated as 0.232 and 0.014 respectively. Further details on calculation of fuel consumption and fuel coefficient is provided in [322, 323, 324].

Figure 5.36 shows the fuel consumption of the DGen considered in this study. The red dotted line represents the fuel consumption at no load conditions calculated as based on extrapolation of Equation 5.2. Unfortunately, the idle fuel consumption was not available so extrapolation had to be used as the next best alternative.

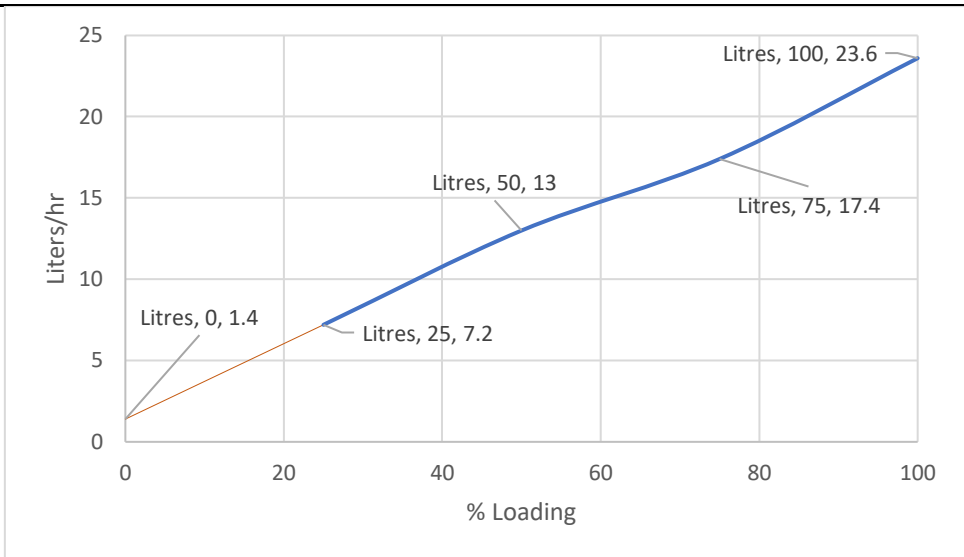

Figure 5-36 Fuel Consumption Curve for the Diesel Generator

The DGen cannot go on standby mode during 24hrs of operation when it is operating without a flywheel when there is not enough power production by the PV system. When operating without flywheel the output of DGen follows the load curves and specifically during night time and in the morning when PV output is zero. The DGen remains partially loaded since the load demand as well PV output are not constant. The fuel consumption of DGen when operating with the flywheel is found by taking % loading during its on states. Table 5.1 shows the % involvement of DGen in the cases of flywheel and without flywheel integrated in the system.

Table 5-1 DGen fuel consumption calculations for all three presented load models

Scenario	Load Model	Ratio Consumption at % Load					Total Fuel Consumption (litres)				
		0%	**25%**	**50%**	**75%**	**100%**	**0%**	**25%**	**50%**	**75%**	**100%**
1	*ND-July-WD*	4.1	29.1	41.6	16.6	8.3	1.4	50.4	130	69.6	47.2
	MB-July-WD	2.08	35.4	25	12.5	25	0	61.2	78	52.2	141.6
	KT-June-WND	2.08	38.9	22.1	11	19.4	0.7	67.32	95.03	46.28	109.9
2	*100% of DGen loading*										
	ND-July-WD	67.7	0	0	0	32.3	22.7	0	0	0	179.4
	MB-July-WD	63.4	0	0	0	36.6	21.3	0	0	0	207.3
	KT-June-WND	59.6	0	0	0	40.3	17.1	0	0	0	228.2
	75% of DGen loading										
	ND-July-WD	64.5	0	0	29.4	6.2	21.7	0	0	122.9	35.4
	MB-July-WD	32.2	0	0	63.5	4.1	10.8	0	0	265.35	23.6
	KT-June-WND	39.7	0	0	47.7	12.5	13.3	0	0	199.23	70.8

The fuel consumption of DGen when operating without flywheel is calculated based on its average % loading condition during in each hour. The DGen operates at constant output conditions when it is operating along with flywheel, since the flywheel acts as a load on terminals of DGen when it is in charging state. During discharging state of the flywheel, the DGen goes into standby mode. The involvement of the DGen for supplying power to meet the load is more when operating without the flywheel since the flywheel is available at all times so can avoid any imbalance between supply and demand. In case of load model ND-July-WD, the DGen is operating more at 50% loading condition, the % loading on the DGen increases during morning and evening times. Similar results are obtained in case load model MB-July-WD since both load profiles represent consumption trend of typical work day (weekday). On the other hand, load mode KT-June-WND represents the consumption trend on a weekend which is different. In this case the DGen, when operating without the flywheel, operates more at 25% of load conditions compared to when it operates at other loading conditions which is due to the peak demand on weekend occurred later in the day and which were being supplied more by the PV system. The DGen, when operating with the flywheel, operates only at no load or 100% loading conditions. Since the flywheel system proposed in this study is for energy management applications in a microgrid, the DGen is used to charge the flywheel, the flywheel discharges its energy back into the system by allowing DGen to be unloaded for more time. Since the rating of the proposed flywheel system is 100kW (C20 type), it takes less time to charge and spends more time in discharging state during the low demand period which reduces the fuel consumption of the DGen. The DGen still consumes fuel at no load condition to overcome friction losses and supply power to its other auxiliary mechanical parts. The comparison of fuel consumption of the DGen at different load conditions and when operating with and without flywheel is presented in Figure 5.37.

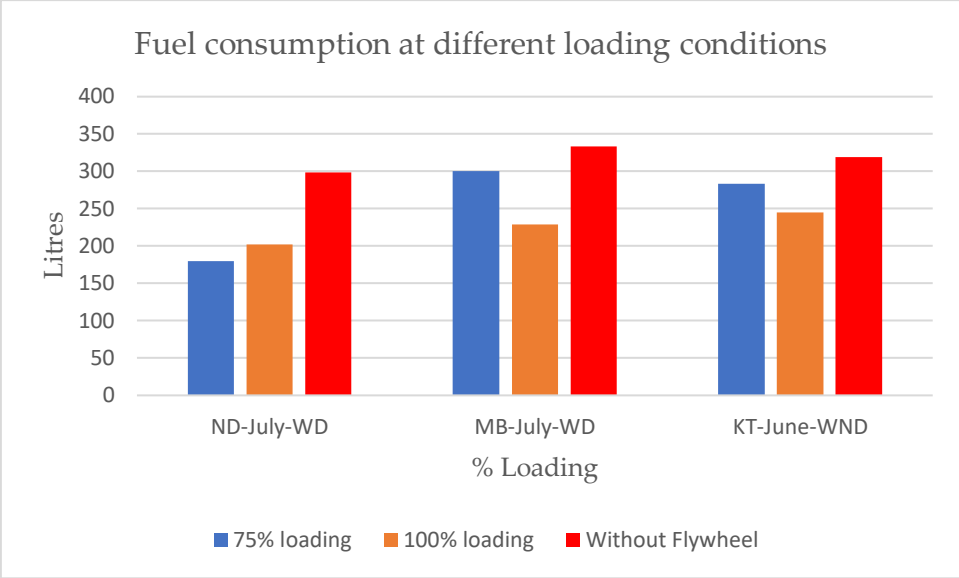

Figure 5-37 Diesel Fuel Consumption Comparison with and without Flywheel Operation

The diesel fuel consumption of DGen at 75% loading capacity is less in case of load model ND-July-WD when operating with flywheel, the PV power curve for ND-July-WD represented less fluctuations which caused to operate less at loading compared to no loading conditions, the PV system was more involved to supply the load demand which caused flywheel to go on standby mode as well. In case of MB-July-WD the fuel consumption at 75% is more compared to the fuel consumption at 100%, the PV power curve in this case was not consistent and represented very low power except at few occasions, since the DGen was operating at 75%, less power was sent to the flywheel for charging purpose, which took more time to complete its charging cycle of the flywheel compared to when the DGen was operating at 100%. Without integration of the flywheel, the DGen remains partially loaded during its entire operation for all three load profiles which leads to the poor performance of the DGen, increased fuel cost and CO_2 emissions. Therefore, adding energy storage along with RES in islanded system is the best solution to save cost and the environment, provided that the ESS is itself environmentally friendly such as the flywheel. The percentage loading of the DGen is categorized in different load levels in order to calculate the consumption according the manufacturer specifications.

The involvement of the flywheel in the microgrid operating together with DGen and PV has greatly reduced diesel consumption. Table 5.2 shows the fuel cost analysis with and without the flywheel operation. The current unit price[1] of diesel fuel in India is considered for cost calculation.

Table 5-2 Fuel cost comparison of DGen with and without flywheel

Operation Scenario		DGen Fuel Cost (£) over 24hrs		
		Model ND-July-WD	Model MB-July-WD	Model KT-June-WND
1		271.72	303.03	290.50
2	*At 100%*	183.91	208.02	223.22
	At 75%	163.82	254.83	257.83
Fuel saving (%)		32.6	31.2	24.1
Daily saving (£)		80	86	61.22
Annual saving (£)		24090	26008	18434

[1]Diesel fuel price in GBP = 0.91

The cost analysis presented above is based on the operation of DGen as per the load demand and solar irradiance curves presented. The daily savings on diesel fuel is for the day when the flywheel and DGen were operating by responding variations in the solar PV output. However, over the course of 365 days, solar irradiance would not be of the same pattern, therefore, the error of 25% is introduced in the annual savings in order to incorporate changes in solar irradiance over 365 day. The impact of the flywheel in scenario 2 has been important as can be seen from analysis presented in Table 5.2. In operation scenario 1 the DGen is 50% loaded most of the time during operation which leads to less efficient operation of the DGen and extra fuel cost. In operation scenario 2 it can be seen that the flywheel has hugely reduced the involvement of the DGen in the system has led DGen to be nearly 100% loaded in all three load models. Table 5.2 summarises the impact of the flywheel in reducing cost and fuel consumption.

It can be seen from the analysis presented in Table 5.2, in the case of load model ND-July-WD, the impact of the flywheel is significant compared to the other 2 load models. It is due to the availability of PV power and pattern of solar irradiance and

the consumption pattern. The irradiance model associated with load model ND-July-WD represents a less cloudy day therefore the PV output power is sufficient to meet the load demand alone at most of the time in case of operation scenario 1. Whereas in case of load model MB-July-WD and KT-June-WND the solar irradiance represents high fluctuations as mentioned before, which affects the PV output power therefore the contribution of DGen in case of load model MB-July-WD and KT-June-WND was more compared to load model ND-July-WD and the DGen was frequently used due to nature of the demand.

Table 5.3 represents the analysis of CO_2 emitted by DGen with and without the flywheel energy storage. The calculation of CO_2 emission depends on the type of the fuel and amount of its consumption by DGen. The diesel fuel emits 2.7 kg of CO_2 per litre. Different type of the fuels has different carbon contents however, an average carbon content in diesel fuel can be considered in order to estimate the CO_2 [325].

Table 5-3 CO_2 emission of DGen with and without FESS

Operation Scenario	DGen Carbon Emission Analysis		
	Model ND-July-WD	Model MB-July-WD	Model KT-June-WND
With flywheel (kg)	545.67	617.22	661.5
Without flywheel (kg)	806.22	900.99	861.3
Reduction (%)	33	32	24.7

The results of analysis show that the flywheel has a huge impact on amount carbon emission of DGen. The carbon emissions depend upon the operating hours of the DGen, interestingly the flywheel can reduce approximately 94,900 kg/year of carbon emissions in the case of load model ND-July-WD, which is a significant reduction. It can be seen that the operation of FESS and DGen is linked with the power output available from the PV system. Therefore, the FESS can prove to be a viable solution developing countries where there is great potential of renewable sources (PV and Wind) such as Pakistan, India, Nigeria etc.

The introduction of FESS as a backup storage system not only provides carbon and fuel savings but also increases the efficiency and lifetime of the diesel engine. It adds

stability to the system and it can withstand with sudden and unpredictable changes in load demand by its fast response. Moreover, by reducing the operating time of the DGen, greenhouse gases are reduced due to reduced CO_2 emissions. The life expectancy of the diesel generator depends on the number of hours it runs every year. However, the life of a diesel generator also depends on many other factors such as its sizing and maintenance practices [326]. For a typical generator set running under normal conditions the life expectancy is 20 years with operating time of 50 – 100 hours per year [327]. The research has been carried out to improve diesel engine performance and its combustion characteristics by using biodiesel with carbon nanomaterials. Gad et al. in [328], have proposed a biodiesel blend fuel for diesel engine which is mixture of diesel oil and waste cooking oil, the fuel can reduce carbon emission by 27% along with improvements in engine performance. However, the process of making biodiesel increases the cost of the fuel and carbon emissions are not reduced as much as compared to adding FESS. In [329], a multi-walled carbon nanotube has been proposed to further reduce carbon emissions due to biodiesel, the results presented in the researchers claim to achieve significant reduction in carbon emissions, however, introduction of nanotubes further increases the complexity of the system and added cost. Despite all this, the DGen is not termed as a clean source of energy. Further techniques for reduction of carbon emissions of diesel fuel are also discussed in [330] [331].

5.5 Chapter Summary

Frequent variations in solar irradiance due to cloud passing make it difficult for PV systems to meet the load demand alone in islanded mode operation, therefore a DGen must be used as a back-up power source to share the load demand with the PV system. Also, during the night time, power is still required and the PV system cannot meet this. More importantly, if reliable power is to be provided, even if the PV system can provide all the power demanded by the load, the DGen must always be available on standby should a cloud pass and unexpectedly reduce the PV output. During some instances during the day the PV system generates more power than the demand which leads to imbalance between demand and supply, dissipating the excess power in dump load can keep the system stable but is not an efficient solution. Therefore, storing the excess power in a storage device is a is a more sustainable option.

This chapter explained the model of a PV hybrid microgrid system involving the addition of a flywheel storage system as well as the diesel generator to reliably meet the residential load demand of 100 dwellings assumed to be situated in a remote area which is not connected to the grid. The load model and DGen were connected to an AC bus and PV system and the flywheel connected to an DC bus. The dynamic residential load model was developed from high (minute-minute) resolution CREST demand model. The CREST model generated an electricity demand model for residential consumers of UK and India. Different load profiles were generated for large cities of India, Kolkata, Delhi and Mumbai. The load models were analysed and simulated under 2 strategies namely operation scenario 1 and operation scenario 2. In operation scenario 1, the load demand was supplied by PV system and the DGen whereas operation scenario 2 involved combination of all three sources. The individual models of the flywheel, PV system and the DGen modelled in MATLAB/Simulink environment was briefly discussed a and their combination as PVHMS was presented.

The dynamic performance and coordination between system components was analysed when supplying power to the load and results were presented. The compliance of the system with variations in load and fluctuations in solar irradiance was verified with help of output plots including power, currents, voltage, of DGen and the PV system, stator currents of SCIM-FESS, state of charge and power of curves of the flywheel and the DC-link voltage during transient and steady state conditions. The stable performance of proposed PVHMS generally depends on the contribution of PV system and consumption electricity duty cycle (load model). It has been shown that at some instances, the PV system alone or FESS alone with a PV system can fully provide the power to the load, allowing the DGen to be turned off. However, for the case of not having the FESS in the system, the DGen must be left on idle just in case the PV output reduces due to a cloud pass. This is due to the start-up time of several seconds needed for a turned off DGen to become active. In some periods, the DGen and FESS were seen fully engaged most of the time to supply power to the load due to highly fluctuating model of solar irradiance. The impact of the flywheel energy storage has been remarkable, it has been shown in all three load models the flywheel was engaged in supply backup power to the system without going into standby mode and making continuous charge-discharge cycles. The flywheel has significantly reduced the operating timings of DGen at load and has reduced loading of the DGen by 55% in case of load model ND-July-WD and 34% and 48% in case of load model MB-July-WD and KT-June-WND respectively.

Considering both case studies (with and without FESS) of which results and analysis was presented the maximum savings as a result of reduction in diesel fuel was calculated to be £24090 for load model ND-July-WD, £26008 per annum for load model MB-July-WD and £18434 per annum for load model KT-June-WND. Flywheel energy storage in the stand-alone islanded system provides back-up storage, fuel savings and reduced greenhouse gasses. The performance of DGen is less efficient at partial loads which happens when PV system and DGen share the load demand. FESS

avoids the frequent variations in diesel generator output which leads to maximum loading of diesel generator.

For PV residential applications, electrochemical batteries are an obvious choice for energy storage system, however, flywheel technology has not been widely tested and considered for this application. When it comes to numerous charge-discharge per day and lifetime, flywheels can be the viable option for energy storage despite batteries being mass-produced and cost effective compared to flywheels. The performance of batteries is temperature sensitive and can occupy more space for similar ratings compared to flywheels. Additionally, there is growing concern regarding disposing of used chemical batteries especially in less developed countries where there are very less battery recycling plants. During the course of 24 hours, it was seen that the flywheel was performing an average of 70 cycles. If same ratio of cycles is assumed for each day of the year, the flywheel would reach approximately make 70 x 365 = 25,550 cycles per year. The flywheel will come on and off multiple times which ideally suits the nature of operation of flywheels without affecting their lifetime. If operational duty is applied to batteries, this would reduce the amount of cycling . However, this will reduce their lifetime and degrade their performance while also considering high temperatures and maintenance. Hence, flywheels can be an alternative to batteries for applications requiring high charge-discharge cycles and longer life span regardless of weather conditions. Considering annual savings calculated in this chapter and impact of flywheels in providing backup storage, reducing carbon emissions and operating hours of DGen in standalone PV system the payback time can be quicker than expected apart from introduction of green technology with life span of 20 years.

Chapter 6

Conclusions

In this thesis, flywheel energy storage device with an induction type electrical machine was presented as a potential alternative to battery energy storage technology for microgrid application. A detailed literature review was conducted on different energy storage technologies giving comparisons from different technical aspects relevant to the application. In addition, a brief review on microgrids and their analysis was presented. In the main, it was found that the majority of research in the public domain had focussed on applications of battery energy storage technologies in microgrid applications. A detailed review of flywheel energy storage system was presented along with its components and applications. The structure of a flywheel energy storage system (FESS) was defined with explanation of its main components given. These included the flywheel rotor, power electronics, electric machines, types of electric machines and bearing systems. Applications of flywheel energy storage were described for power quality enhancement, transportation, renewable energy systems, uninterruptible power supply and energy storage systems. Also, a description of some commercially available flywheels along with their characteristics was presented. The demand for FESS is increasing noticeably given its unique attributes of very high cycles, instant response, ease of recycling and high calendar life. Though the cost of Li-ion batteries is reducing continuously, flywheel technology still remains competitive to battery technology for certain microgrid applications.

In this research work, a small-scale flywheel energy storage system was presented for use in an isolated and weak microgrid. This was accomplished by modelling a microgrid system comprising of a solar photovoltaic (PV system), a backup diesel generator (DGen) and a FESS supplying the varying residential load of small town, assumed to be located remotely where extension of existing grid infrastructure was not a feasible option. The electricity demand of the residential load was met without

interruption by the combination of the DGen, PV system and FESS for different operational scenarios and control system strategies. The purpose of FESS was to keep operating time of DGen to the minimum possible, in particular to avoid idling and part load operation. The benefit of this is to reduce DGen fuel consumption, carbon emissions and increase the reliability of the system in comparison to a system operating without the FESS. Considering the large number of charge-discharge cycles needed, the application of battery energy storage in the system would lead to high cycle degradation unless it had a much larger capacity so could be operated in a different way. In addition, many microgrids are in countries with high temperature and this can cause additional degradation. It is therefore believed that the flywheel can off an alternative to battery technology as the energy storage device in microgrids.

6.1 Summary of the thesis

Increases in global temperatures due to greenhouse gas emissions from energy generation and other activities have led scientists and researchers around the world to find sustainable solutions which could help the world become less dependent on depleting fossil fuel resources. Global warming has left many destructive signs such as fire storms in Turkey, massive floods in Germany, China and India in June-2021 plus record temperatures in California, Pakistan and across the Europe. Unpredictable and heavy rainy spells across the world indicate a worsening scenario for the future. The increase in the population is also the major contributor to increased energy demand in transport and the power sector. Much of this increased electricity demand must be met by renewables and the demand for renewables in microgrids together with distributed generation has resulted in their massive penetration into the microgrids. However, intermittent power generation by renewable energy sources creates uncontrollable imbalance between load demand and electricity production which can cause deviations in frequency within a microgrid. This poses a challenge to stability of the power system; therefore, it has been vital to have energy storage technologies installed in a microgrid in order for it to operate stably and avoid

overload scenarios. The duty of the energy storage system depends on its type and duration of storage. For residential load applications at the distribution level, the energy storage device typically provides energy for longer duration than is required in keeping with the trend of using battery technology for these applications. This has generally hindered the advancement of other energy storage technology such as flywheels which operate in a very different way due to their characteristics. Major findings as to whether flywheel can be used as an alternative to electrochemical batteries for residential load applications were presented as follows:

Chapter 1: This chapter provided an overview of energy demand and consumption trend across the world together with the global efforts to tackle global warming. The need of energy systems was broadly explained by addressing their benefits such as their impact on stability and power quality improvements, providing support to renewable sources and distributed generation, balance of supply and demand. Additionally, a comparison was made between the characteristics of Li-ion and flywheel technology for microgrid applications. Also, a brief discussion was presented to stress on importance of microgrids and distributed generation in today's power systems.

Chapter 2 provided an overview on characteristics of flywheel energy storage system, a detailed literature review covering the status of global energy storage capacity and importance of energy storage systems given increasing penetration of renewable sources in microgrids. Integration of energy storage system in microgrids is a promising approach to increase penetration of renewable energy sources at distribution level, it was found that the development of microgrid was quicker than expansion of conventional electric network. However, microgrids require a robust control system for energy management system when operating in grid connected or islanded mode. From literature review of energy storage technologies, it was found that supercapacitors and superconducting magnetic energy storage have high capital cost ($/kWh) but they have highest maximum efficiency. Pumped hydro being mature

technology is widely implemented in the world, however, its construction is subjected to suitable geographical sites, similarly compressed air storage system provides high MWhs of energy at low cost but it is suitable to accessible sites requiring long transmission lines distance. The battery energy storage system was found to be the strong competitor of flywheel energy storage system in power applications. Amongst all types of batteries, Li-ion battery technology has high efficiency and the highest energy density. However, the lifetime of the Li-Ion batteries is temperature dependent and they degrade faster at higher temperatures. The flywheel provides fast response, calendar life of more than 20 years, high charge and discharge cycles and high round trip efficiency. However, the drawback of flywheels is their high self-discharge rate and safety issues when containment cannot withstand rotor failures. A detailed literature review on application of flywheels in different areas, according to the literature survey the flywheel is mainly used for UPS and power quality applications where high power for short duration of time is required. Also, flywheels are used in space satellites for altitude control, in military vehicles for providing high pulsed power and in transport vehicles for energy recovery systems. List of leading flywheel manufacturers and their flywheel products along with their characteristics was also given.

In Chapter 3, a detailed mathematical model of the induction machine-based flywheel energy storage system was described with help of its circuit diagrams and equations. The converter used in flywheel model was a back to back AC-DC-AC bidirectional converter that allowed power flow from microgrid to flywheel and vice versa with the help of its associated control system. The control systems for machine side converter and grid side converter used in flywheel model were discussed and analysed with help of diagrams and their related mathematical expressions together with voltage and torque controllers. Based on mathematical expressions, the flywheel model was implemented in MATLAB/Simulink and presented in the chapter with diagrams. The model of flywheel was validated and tested for charge-discharge cycles in

MATLAB/Simulink environment. The results showed that the flywheel model was responded as expected to different torque commands and providing quick response in milli seconds. At the end of the chapter, the modelling of electrical and mechanical losses of flywheel energy storage system was presented with the help of mathematical expressions and graphs. The analysis of loss model showed that for the maximum rated speed of 20 krpm, the bearing friction loss is approximated as 110 W and the windage loss at the atmosphere pressure level is about 90 W, giving a total of 200 W for combined windage and bearing losses. However, the system losses need to be kept at a minimum and particularly the standby losses, which is directly affected by the aerodynamic and bearing losses. For the core loss of induction machine, it was seen that the stator core losses increased exponentially with increase in speed and magnetic flux density. The stator specific core losses were not significant for values of magnetic flux density up to 1 Tesla and 3krpm speed. However, the specific core losses in stator of the IM increase significantly above 3krpm and even at 0.648 Tesla, the power losses due to hysteresis and eddy currents in stator core of IM operating at 20krpm is 16.48 W/kg. Rotor specific core losses of IM also increased exponentially with increase in maximum magnetic flux density. However, even at a high speed of 20krpm, the rotor specific core losses were 2W/kg which is not significant.

Chapter 4 provided an overview of modelling of microgrids and the related research work on different energy storage systems considered for microgrid applications. This included an overview of modelling of microgrids and related research work on different energy storage system considered for microgrid applications. MATLAB/Simulink modelling of PV hybrid microgrid system for residential applications was discussed. The mathematical modelling of microgrid components used in proposed hybrid system was also presented along with their circuit diagrams and equations. The scholastic modelling for residential load models was discussed by using CREST model developed by University of Loughborough. The modelling of residential loads was based on occupancy and activities of the residents over the

weekends and weekdays with minute resolution. The electricity consumption trend of occupants was selected over 24 hours of time. The residential load models were selected for different cities of India, the load was assumed to be of a small remotely located village. In order to validate the model, Simulink models of flywheel, diesel generator and PV system were separately run in Simulink and their results were presented and discussed. The model of diesel generator and the PV system was tested under different load and solar irradiance conditions respectively. The results showed that the hybrid PV model was compliant with different switching events of energy sources in the microgrid.

Results and analysis of developed PV hybrid microgrid system were presented in Chapter 5. The operation of the hybrid system was analysed for on two different operation scenarios to nearly match with real life conditions such as PV hybrid system with and without the flywheel energy storage system. The dynamic behaviour of the model and its response to load demand and communication between energy sources were analysed with the help of technical characteristics of the system such as power curves of PV system, the flywheel and diesel generator, their voltage and current waveforms and DC link voltage. The simulation of FESS based hybrid system was performed using 24 hours of data which is rarely found in the literature. The results were presented for the different operation scenarios showed that the flywheel greatly reduced fuel consumption of diesel generator thus carbon emissions. The maximum savings on fuel achieved was £24090 per annum along with 38% reduction in CO_2 emissions. However, if the number of flywheels were increased in the system, then more cost savings would likely be achieved over the same time span. Moreover, the performance of DGen is less efficient at partial loads which happens when a PV system and DGen share the load demand. The flywheel avoids the frequent variations in diesel generator output which allows maximum loading of diesel generator. Apart from cost savings, the use of flywheel in the hybrid system increases efficiency of diesel engine. The operation of the hybrid system was analysed at different loading

conditions of the DGen, it was seen that by operating DGen at 75% of loading capacity its switching time was greatly reduced. The integration of flywheel improved stability of the system, it was seen in the results that with its fast response the flywheel provided energy support to PV system with response to sudden power changes of PV system.

6.1 Contributions of the research

The use of flywheels in a standalone system integrated with renewable sources is limited and it has not been widely addressed in previous research. When it comes to numerous charge-discharge per day and lifetime, flywheels can be the viable option for energy storage despite batteries being mass-produced and cost effective compared to flywheels. This research work presented has contributed by demonstrating the effective use of FESS for stand-alone PV residential applications. The main contributions of the research work are presented as follows:

- Development of the flywheel energy storage system and its associated control system incorporating an induction machine and power electronics interface.
- Modelling of a high inertia flywheel storage system providing energy for longer duration of time to residential loads.
- Development of a model of a PV hybrid microgrid system with backup diesel generator and flywheel as an energy storage device providing power to residential loads for 24 hours.
- Performance of analytical calculations on fuel cost savings and carbon emissions due to integration of flywheel energy storage and its impact on efficiency of diesel generator.
- Performance of simulations of the flywheel based microgrid for 24 hours of operation under various load demand conditions and, in particular, effects of cloud passing which affects PV output.
- Analysis of mechanical and electrical losses for the flywheel energy storage system.

6.2 Future Research

Currently, flywheel products marketed by manufacturers are targeted for power quality applications, however, flywheels being environmentally friendly and having high cycle life alternative to battery can be used in other areas such grid stability, hybrid distributed energy generators and peak shaving. Higher energy density and lower cost are the desired factors for success of flywheels which can be achieved by development of low-cost designs. Higher capital cost and safety issues have been major challenges for emergence of the flywheel energy storage applications in microgrids so chemical batteries with low cost due to mass manufacture have been an obvious choice for such applications. The cost of the flywheel depends mainly on flywheel rotor since this part is not only quite expensive, it dominates the cost of the containment means. In addition, bearings, electric machines along with associated power electronics converters can also be expensive. The use of carbon composite rotors has made cost of the flywheel five times more than the steel rotor flywheels. However, the use of laminated steel rotor flywheel can further reduce the cost and safety matters. Additionally, based on strength per unit cost ratio (MPa/$), steel rotors have 1400 MPa/$ whereas for carbon composite it is 200 MPa/$ which is a significant cost advantage when steel rotors are used [332]. Steel materials are easily recyclable compared to batteries and the recycling will not be needed for longer period of time as calendar life of the flywheel is more than 20 years.

Standby losses are often considered as a major challenge for flywheel technology losses in bearings and electric machines. However, better quality of mechanical or fluid bearings are suitable for FESS of 20 – 40 krpm, at higher speeds the mechanical and fluid bearings are less suitable and superconducting and electromagnetic bearings can be used.

This research addressed the application of flywheel in stand-alone PV system for residential applications, the results and analysis on impact of flywheel energy storage on improving system stability, reducing generator fuel consumption and carbon

emission was presented. The savings on fuel cost of the diesel generator due to flywheel energy storage presents the one aspect of an impact of flywheel on cost savings, however, the levelised cost of the flywheel is needed in order to calculate payback period of capital cost of the flywheel system.

Further to the work presented in this thesis individual assessment of flywheel and battery storage for isolated grids using PV and diesel generator is recommended. Application of batteries for isolated grid applications have been widely reviewed in the literature, however, for the same application a like-for-like comparison for of storage systems can be an area of attention. Considering the multiple charge-discharge cycles in a day the analysis of battery technology for the same application will provide significantly clear picture about degradation of battery's performances over the period of time when compared to flywheels.

In this work the analysis of the flywheel performance was done by considering the peak demand and load fluctuations. The load demand challenged the operation of the flywheel for number of cycles and depth of discharge as flywheel was undergoing complete charge-discharge cycles which could not be feasible if battery was used on place of the flywheel. However, the battery storage could have been the feasible option compared to the flywheel if it was used for the loads which were reasonably fluctuating during off-peak demand. Additionally, research on combined operation of battery and flywheel in standalone PV system is recommended as this can improve efficiency of not only PV system but also the battery storage, the research can also help to reduce the environmental impact and cost reduction.

The control system for DGen can be modified to operate it between 50% and 100% of its loading or energy ratings of the flywheel can be increased to get better assessment of fuel savings. The FESS model presented in this research can be improved by modelling its cooling systems, mechanical system (bearings) and life cycle can be assessed for better comparison to batteries.

The research could have been more improved and more results could have been produced, however, there were many challenges which affected the progress of the research such as compatibility of the software package to process large data. Initially, low resolution model was built which produced results in minutes resolution this was due to memory issues with MATLAB and the time taken by MATLAB to process 24hrs data. For each case of load demand MATLAB/Simulink took 3 days to finish the simulation and produce one output parameter (i.e. power curve of the flywheel). In order to overcome this issue, each load profile was analysed for 30 minutes, after the deep dive review, the 30 minutes results were not enough to get better assessment of flywheel performance and fuel consumption of DGen. The author of this thesis discovered a way to run the simulation for 24hrs, this happened at the time when deadline was very near, however, this was a major accomplishment and a breakthrough in the research, the author calls it a novel work due to the fact that literature review couldn't show any research on flywheel based on its 24hrs operation in microgrid. If issue with compatibility of the software packages are resolved, the performance of the flywheel can be analysed for several years which can give a better assessment of life cycle, losses, cost and fuel cost savings. Also, the development and testing of a physical system were initially a part of research objectives, efforts were also made to purchase a flywheel from dynamic boosting systems (DBS), unfortunately the flywheel rotor could not be delivered by the company due to COVID situation and testing couldn't be possible due to lab closures at university. Therefore, building and testing a physical system of FESS is recommended for future research work.

Appendix A

Reference Frame Transformation

Conversion of *abc* variables of three phase AC quantities into *dq*-axes constant quantities is referred as transformation. The *dq* variables are orthogonal to each other, the direction of *d*-axis (direct axis) component is chosen as direction of magnetic flux in an AC machine and the flux vector is normally aligned with *d*-axis. The q-axis variable is always at 90° ahead of *d*-axis and the torque producing vector component is aligned with *q*-axis. There are two types of reference frames depending on state of *dq*-axes whether they are stationary or rotating. In stationary reference frame the *dq*-axes components do not rotate and in rotating reference frame the *dq*-axes components rotate at an angular speed of ω. The Clark's transformation and Park's transformation are the mathematical tools used for transformation of three phase *abc* quantities to stationary and rotating reference frame respectively. The Clark's and Park's transformation are described in below sections.

A.1 Clark's Transformation

The Clark's transformation calculates three phase quantities *abc* into two phases orthogonal $\alpha\beta$ quantities, the $\alpha\beta$ quantities are transformed in stationary coordinate system. For three phase currents of an AC machine the Clark's transformation is performed by following equations

$$i_\alpha = \frac{2}{3} \cdot i_a - \frac{1}{3}(i_b - i_c) \tag{A.1}$$

$$i_\beta = \frac{2}{\sqrt{3}}(i_b - i_c) \tag{A.2}$$

$$i_0 = \frac{2}{3}(i_a + i_b + i_c) \tag{A.3}$$

Where, i_α and i_β are orthogonal components in stationary reference frame and i_0 is homopolar component and it is zero for balanced three phase system. In order to transform orthogonal $\alpha\beta$ quantities back to three phase *abc* variables then inverse

Clark's transformation is applied, mathematical expressions for inverse transformation are given by following equations.

$$i_a = i_\alpha \tag{A.4}$$

$$i_b = -\frac{1}{2} \cdot i_\alpha + \frac{\sqrt{3}}{2} \cdot i_\beta \tag{A.5}$$

$$i_c = -\frac{1}{2} \cdot i_\alpha - \frac{\sqrt{3}}{2} \cdot i_\beta \tag{A.6}$$

A.2 Park's Transformation

The park's transformation is used to transform two axis $\alpha\beta$ quantities from stationary reference frame to dq rotating reference frame. The mathematical expressions are given as follows:

$$\begin{bmatrix} i_d \\ i_q \end{bmatrix} = \begin{bmatrix} cos\,\theta & sin\,\theta \\ -sin\,\theta & cos\,\theta \end{bmatrix} \begin{bmatrix} i_\alpha \\ i_\beta \end{bmatrix} \tag{A.7}$$

The inverse Park transformation is given by Equation A.8

$$\begin{bmatrix} i_\alpha \\ i_\beta \end{bmatrix} = \begin{bmatrix} cos\,\theta & -sin\,\theta \\ sin\,\theta & cos\,\theta \end{bmatrix} \begin{bmatrix} i_d \\ i_q \end{bmatrix} \tag{A.8}$$

Where $\theta = \omega t$ is an electrical angle.

The three phase variable quantities can also be directly transformed to dq rotating reference frame by the following equations.

$$\begin{bmatrix} i_d \\ i_q \\ i_0 \end{bmatrix} = \frac{2}{3} \begin{bmatrix} \cos(\theta) & \cos(\theta - 120°) & \cos(\theta + 120°) \\ \sin(\theta) & \sin(\theta - 120°) & \sin(\theta + 120°) \\ 1/2 & 1/2 & 1/2 \end{bmatrix} \begin{bmatrix} i_a \\ i_b \\ i_c \end{bmatrix} \tag{A.9}$$

$$\begin{bmatrix} i_a \\ i_b \\ i_c \end{bmatrix} = \frac{2}{3} \begin{bmatrix} cos(\theta) & sin\,\theta & 1 \\ cos(\theta - 120°) & sin(\theta - 120°) & 1 \\ cos(\theta + 120°) & sin(\theta + 120°) & 1 \end{bmatrix} \begin{bmatrix} i_d \\ i_q \\ i_0 \end{bmatrix} \tag{A.10}$$

Appendix B

Manufacturer specifications of Generac diesel genset

SD100 | 6.7L | 100 kW

INDUSTRIAL DIESEL GENERATOR SET

EPA Certified Stationary Emergency

GENERAC | INDUSTRIAL POWER

STANDARD FEATURES

ENGINE SYSTEM

General

- Oil Drain Extension
- Air Cleaner
- Fan Guard
- Stainless Steel flexible exhaust connection
- Critical Exhaust Silencer (enclosed only)
- Factory Filled Oil
- Radiator Duct Adapter (open set only)

Fuel System

- Fuel lockoff solenoid
- Primary fuel filter

Cooling System

- Closed Coolant Recovery System
- UV/Ozone resistant hoses
- Factory-Installed Radiator
- Radiator Drain Extension
- 50/50 Ethylene glycol antifreeze
- 120 VAC Coolant Heater

Engine Electrical System

- Battery charging alternator
- Battery cables
- Battery tray
- Solenoid activated starter motor
- Rubber-booted engine electrical connections

ALTERNATOR SYSTEM

- UL2200 GENprotect™
- 12 leads (3-phase, non 600 V)
- Class H inculation material
- Vented rotor
- 2/3 pitch
- Skewed stator
- Auxiliary voltage regulator power winding
- Amortisseur winding
- Brushless Excitation
- Sealed Bearings
- Automated manufacturing (winding, insertion, lacing, varnishing)
- Rotor dynamically spin balanced
- Full load capacity alternator
- Protective thermal switch

GENERATOR SET

- Internal Genset Vibration Isolation
- Separation of circuits - high/low voltage
- Separation of circuits - multiple breakers
- Silencer Heat Shield
- Wrapped Exhaust Piping
- Silencer housed in discharge hood (enclosed only)
- Standard Factory Testing
- 2 Year Limited Warranty (Standby rated Units)
- 1 Year Limited Warranty (Prime rated Units)
- Silencer mounted in the discharge hood (enclosed only)

ENCLOSURE (IF SELECTED)

- Rust-proof fasteners with nylon washers to protect finish
- High performance sound-absorbing material
- Gasketed doors
- Stamped air-intake louvers
- Air discharge hoods for radiator-upward pointing
- Stainless steel lift off door hinges
- Stainless steel lockable handles
- Rhino Coat™- Textured polyester powder coat

TANKS (IF SELECTED)

- UL 142
- Double wall
- Vents
- Sloped top
- Sloped bottom
- Factory pressure tested (2 psi)
- Rupture basin alarm
- Fuel level
- Check valve in supply and return lines
- Rhino Coat™- Textured polyester powder coat
- Stainless hardware

CONTROL SYSTEM

Control Panel

- Digital H Control Panel - Dual 4x20 Display
- Programmable Crank Limiter
- 7-Day Programmable Exerciser
- Special Applications Programmable PLC
- RS-232/485
- All-Phase Sensing DVR
- Full System Status
- Utility Monitoring
- Low Fuel Pressure Indication
- 2-Wire Start Compatible
- Power Output (kW)
- Power Factor
- kW Hours, Total & Last Run
- Real/Reactive/Apparent Power
- All Phase AC Voltage
- All Phase Currents
- Oil Pressure
- Coolant Temperature
- Coolant Level
- Engine Speed
- Battery Voltage
- Frequency
- Date/Time Fault History (Event Log)
- Isochronous Governor Control
- Waterproof/sealed Connectors
- Audible Alarms and Shutdowns
- Not in Auto (Flashing Light)
- Auto/Off/Manual Switch
- E-Stop (Red Mushroom-Type)
- NFPA110 Level I and II (Programmable)
- Customizable Alarms, Warnings, and Events
- Modbus protocol
- Predictive Maintenance algorithm
- Sealed Boards
- Password parameter adjustment protection
- Single point ground
- 15 channel data logging
- 0.2 msec high speed data logging
- Alarm information automatically comes up on the display

Alarms

- Oil Pressure (Pre-programmable Low Pressure Shutdown)
- Coolant Temperature (Pre-programmed High Temp Shutdown)
- Coolant Level (Pre-programmed Low Level Shutdown)
- Low Fuel Pressure Alarm
- Engine Speed (Pre-programmed Over speed Shutdown)
- Battery Voltage Warning
- Alarms & warnings time and date stamped
- Alarms & warnings for trancient and steady state conditions
- Snap shots of key operation parameters during alarms & warnings
- Alarms and warnings spelled out (no alarm codes)

STARTING CAPABILITIES (sKVA)

sKVA vs. Voltage Dip

		480 VAC						208/240 VAC					
Alternator	kW	10%	15%	20%	25%	30%	35%	10%	15%	20%	25%	30%	35%
Standard	100	79	118	157	197	236	200	59	89	118	148	177	206
Upsize 1	130	116	174	323	290	348	406	87	131	174	218	261	305
Upsize 2	150	133	199	265	332	398	464	100	149	199	249	299	348
Upsize 3	200	187	280	373	467	560	653	140	210	280	350	420	490

FUEL CONSUMPTION RATES*

Fuel Pump Lift - ft (m)
3 (1)

Total Fuel Pump Flow (Combustion + Return)
29.1 gal/hr

Diesel - gal/hr (l/hr)

Percent Load	Standby
25%	2.2 (8.3)
50%	4.2 (15.9)
75%	5.9 (22.3)
100%	7.3 (27.6)

* Fuel supply installation must accommodate fuel consumption rates at 100% load.

COOLING

		Standby
Coolant Flow per Minute	gal/min (l/min)	44.6 (168.8)
Coolant System Capacity	gal (L)	5.65 (21.4)
Heat Rejection to Coolant	BTU/hr	269,130
Inlet Air	cfm (m^3/hr)	6360 (180)
Max. Operating Radiator Air Temp	F° (C°)	122 (50)
Max. Ambient Temperature (before derate)	F° (C°)	110 (43.3)
Maximum Radiator Backpressure	in H_2O	0.5

COMBUSTION AIR REQUIREMENTS

		Standby
Flow at Rated Power	cfm (m^3/min)	325 (9.2)

ENGINE

		Standby
Rated Engine Speed	rpm	1800
Horsepower at Rated kW**	hp	152
Piston Speed	ft/min (m/min)	1559 (475)
BMEP	psi	165

**Refer to "Emissions Data Sheet" for maximum bHP for EPA and SCAQMD permitting purposes.

EXHAUST

		Standby
Exhaust Flow (Rated Output)	cfm (m^3/min)	1022 (28.94)
Max. Backpressure (Post Silencer)	inHg (Kpa)	1.5 (5.1)
Exhaust Temp (Rated Output)	°F (°C)	885 (474)
Exhaust Outlet Size (Open Set)	mm (in)	101.6 (4)

Deration – Operational characteristics consider maximum ambient conditions. Derate factors may apply under atypical site conditions. Please consult a Generac Power Systems Industrial Dealer for additional details. All performance ratings in accordance with ISO3046, BS5514, ISO8528 and DIN6271 standards.

SD100 | 6.7L | 100 kW

INDUSTRIAL DIESEL GENERATOR SET

EPA Certified Stationary Emergency

GENERAC | INDUSTRIAL POWER

DIMENSIONS AND WEIGHTS*

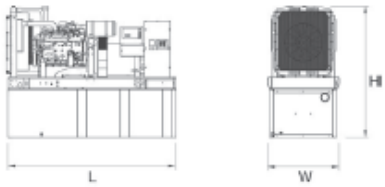

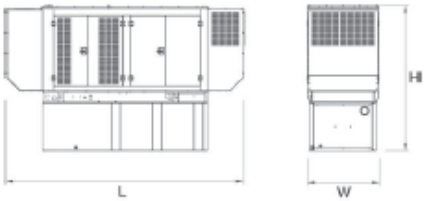

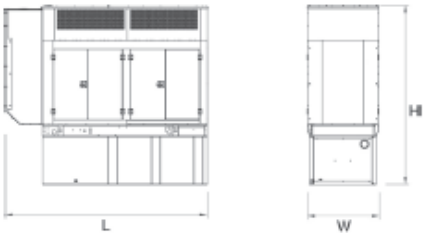

YOUR FACTORY RECOGNIZED GENERAC INDUSTRIAL DEALER

OPEN SET

RUN TIME HOURS	USABLE CAPACITY GAL (L)	L x W x H in (mm)	WT lbs (kg) - Tank & Open Set
NO TANK	-	110 (2794) x 40 (1016) x 65 (1651)	3104 (1408)
12	90 (340.7)	110 (2794) x 40 (1016) x 77 (1955.8)	3813 (1730)
30	220 (832.8)	110 (2794) x 40 (1016) x 89 (2260.6)	4146 (1881)
48	350 (1324.9)	110 (2794) x 40 (1016) x 101 (2565.4)	4488 (2036)
70	510 (1930.6)	110 (2794) x 40 (1016) x 105 (2667)	4469 (2029)
81	589 (2229.6)	128 (3251.2) x 49 (1244.6) x 107 (2717.8)	4948 (2244)
95	693 (2623.3)	136 (3454.4) x 53 (1346.2) x 107 (2717.8)	4667 (2117)

STANDARD ENCLOSURE

RUN TIME HOURS	USABLE CAPACITY GAL (L)	L x W x H in (mm)	WT lbs (kg) - Enclosure Only	
			Steel	Aluminum
NO TANK	-	133 (3378) x 40 (1016) x 64 (1625.6)	500 (227)	165 (75)
12	90 (340.7)	133 (3378) x 40 (1016) x 77 (1956)		
30	220 (832.8)	133 (3378) x 40 (1016) x 89 (2261)		
48	350 (1324.9)	133 (3378) x 40 (1016) x 101 (2565)		
70	510 (1930.6)	133 (3378) x 47 (1194) x 105 (2667)		
81	589 (2229.6)	133 (3378) x 49 (1125) x 107 (2718)		
95	693 (2623.3)	133 (3378) x 53 (1346) x 107 (2718)		

LEVEL 1 ACOUSTIC ENCLOSURE

RUN TIME HOURS	USABLE CAPACITY GAL (L)	L x W x H in (mm)	WT lbs (kg) - Enclosure Only	
			Steel	Aluminum
NO TANK	-	154 (3912) x 40 (1016) x 64 (1626)	750 (340)	250 (112)
12	90 (340.7)	154 (3912) x 40 (1016) x 77 (1956)		
30	220 (832.8)	154 (3912) x 40 (1016) x 89 (2261)		
48	350 (1324.9)	154 (3912) x 40 (1016) x 101 (2565)		
70	510 (1930.6)	154 (3912) x 47 (1194) x 105 (2667)		
81	589 (2229.6)	154 (3912) x 49 (1245) x 107 (2718)		
95	693 (2623.3)	154 (3912) x 53 (1346) x 107 (2718)		

LEVEL 2 ACOUSTIC ENCLOSURE

RUN TIME HOURS	USABLE CAPACITY GAL (L)	L x W x H in (mm)	WT lbs (kg) - Enclosure Only	
			Steel	Aluminum
NO TANK	-	145 (3683) x 40 (1016) x 81 (2057)	1000 (454)	330 (150)
12	90 (340.7)	145 (3683) x 40 (1016) x 84 (2134)		
30	220 (832.8)	145 (3683) x 40 (1016) x 106 (2692)		
48	350 (1324.9)	145 (3683) x 40 (1016) x 118 (2997)		
70	510 (1930.6)	145 (3683) x 47 (1194) x 122 (3099)		
81	589 (2229.6)	145 (3683) x 49 (1245) x 124 (3150)		
95	693 (2623.3)	145 (3683) x 53 (1346) x 124 (3150)		

*All measurements are approximate and for estimation purposes only. Sound dBA can be found on the sound data sheet. Enclosure Only weight is added to Tank & Open Set weight to determine total weight.

Specification characteristics may change without notice. Dimensions and weights are for preliminary purposes only. Please consult a Generac Power Systems Industrial Dealer for detailed installation drawings.

CODES AND STANDARDS

Generac products are designed to the following standards:

UL2200, UL508, UL142, UL498

NFPA70, 99, 110, 37

NEC700, 701, 702, 708

ISO9001, 8528, 3046, 7637, Pluses #2b, 4

NEMA ICS10, MG1, 250, ICS6, AB1

ANSI C62.41

POWERING AHEAD

For over 50 years, Generac has led the industry with innovative design and superior manufacturing.

Generac ensures superior quality by designing and manufacturing most of its generator components, including alternators, enclosures and base tanks, control systems and communications software.

Generac's gensets utilize a wide variety of options, configurations and arrangements, allowing us to meet the standby power needs of practically every application.

Generac searched globally to ensure the most reliable engines power our generators. We choose only engines that have already been proven in heavy-duty industrial application under adverse conditions.

Generac is committed to ensuring our customers' service support continues after their generator purchase.

Appendix C

Load profiles for Delhi city over the period of 12 months

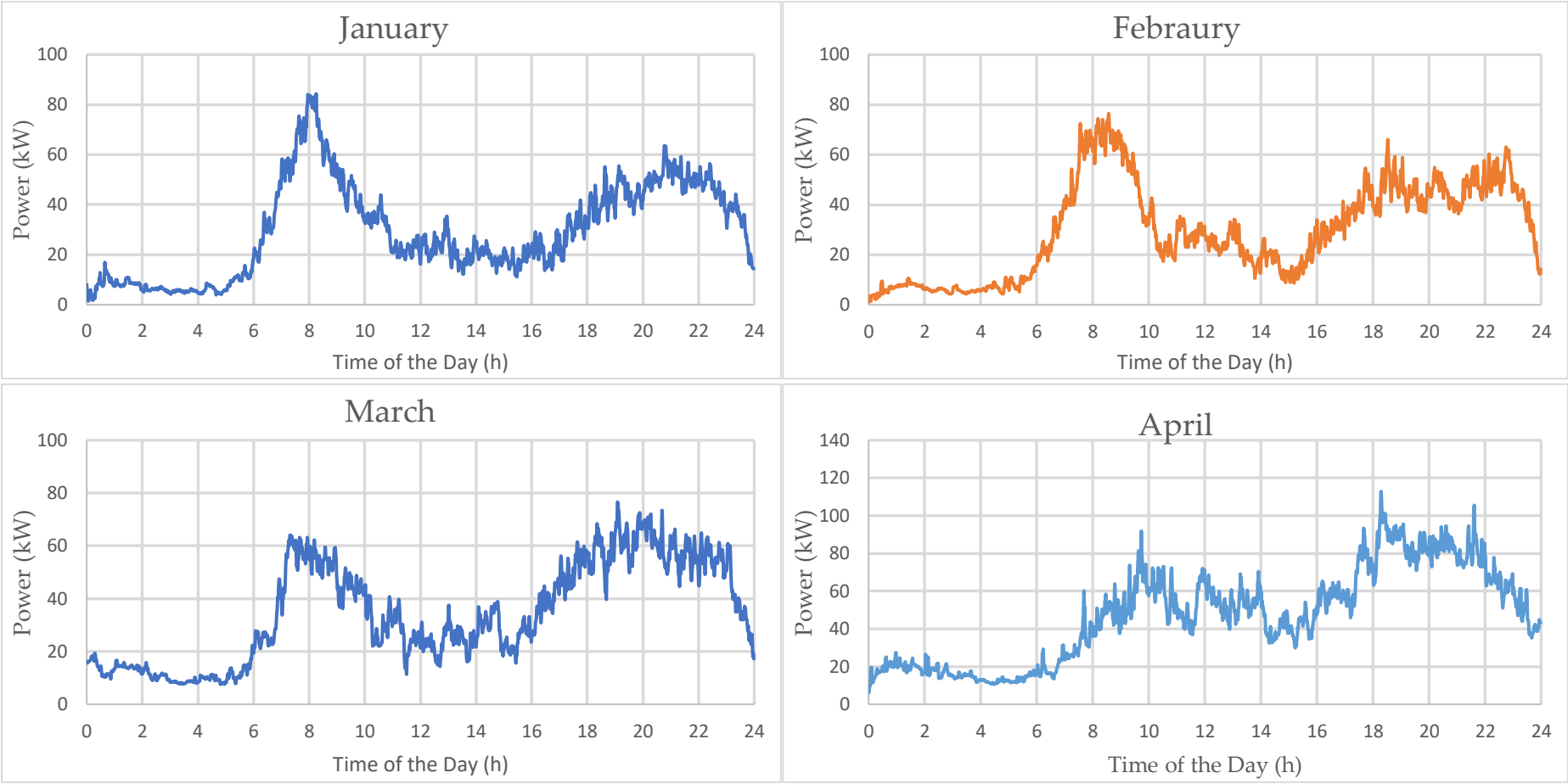

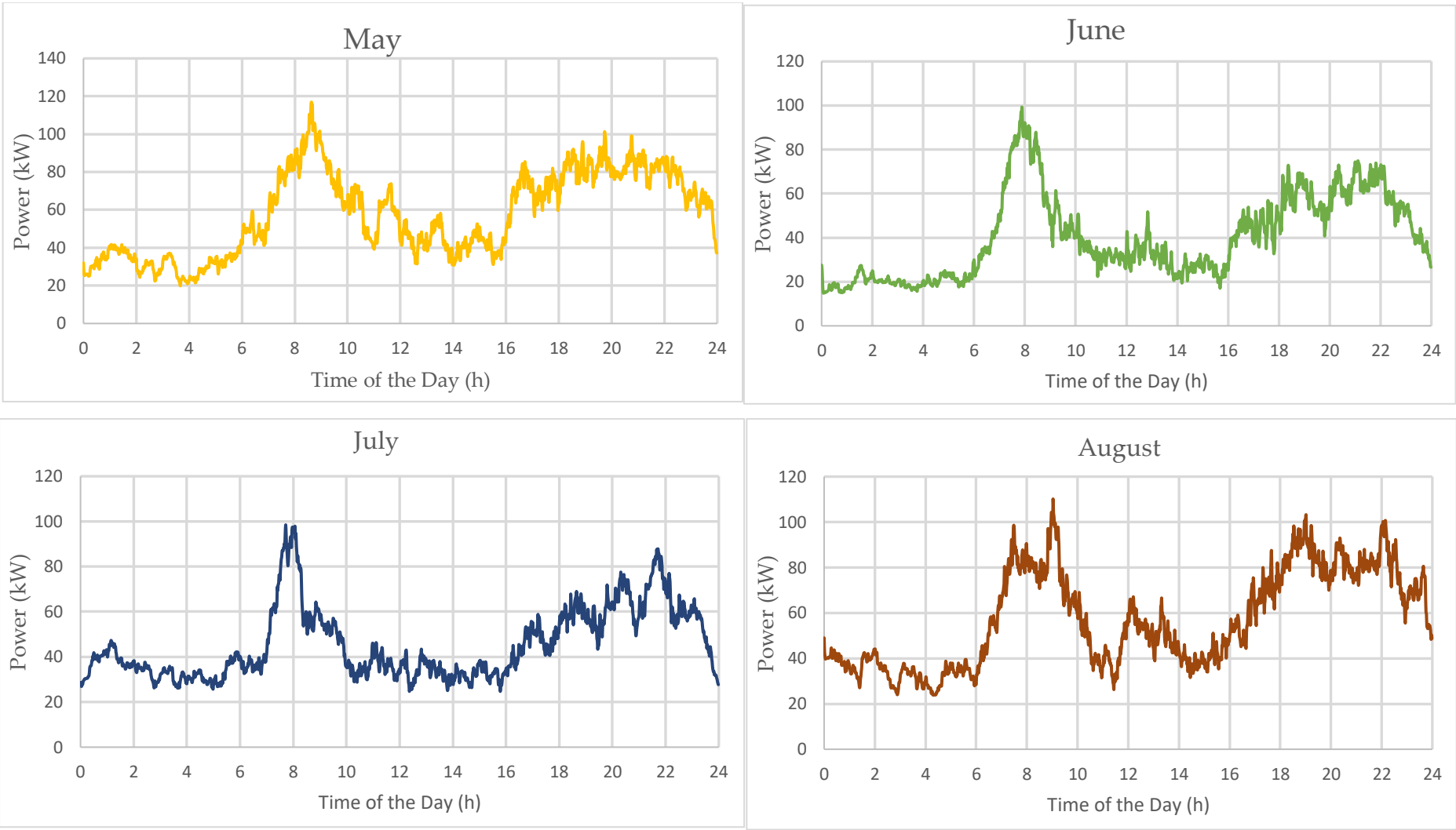
May
Power (kW)
Time of the Day (h)
June
Power (kW)
Time of the Day (h)
July
Power (kW)
Time of the Day (h)
August
Power (kW)
Time of the Day (h)

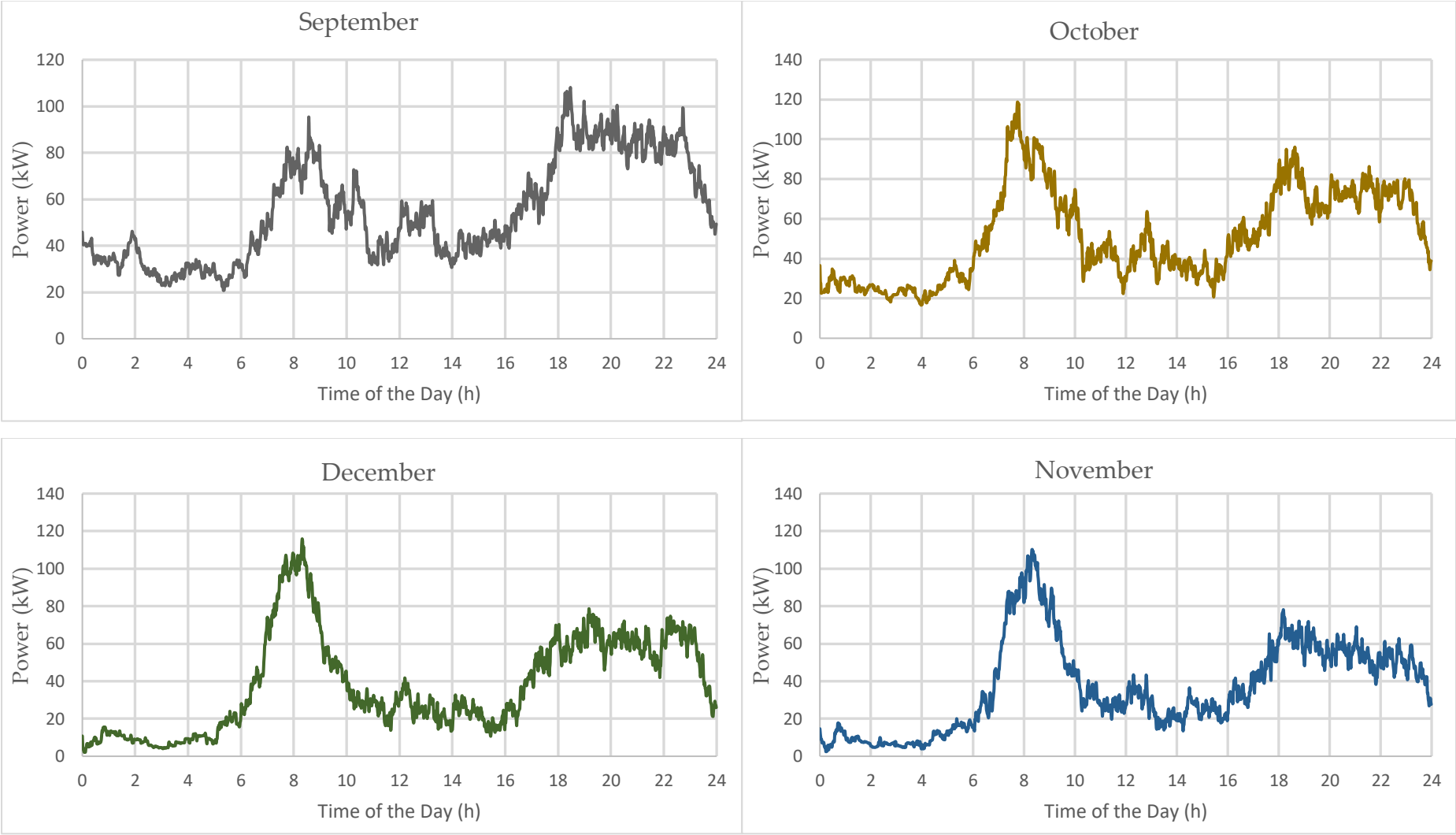
September
October
December
November
Power (kW)
Time of the Day (h)
0
2
4
6
8
10
12
14
16
18
20
22
24
20
40
60
80
100
120
140

Appendix D

Space Vector Pulse Width Modulation - SVPWM

SVPWM is a technique used to in a final step of FOC to generate signals for inverter switches. SVPWM is driven from the concept of rotating magnetic field of IM. In SVPWM three phase voltage (V_{abc}) are represented as a space vector in space vector diagram, the voltage reference vector is modulated output voltage vectors of three phase inverter. For a two-level voltage source inverter (VSI), eight possible switching states represented by active and zero voltage vectors. The active vectors are the six modes of two-level inverter. The zero voltage vectors are obtained when all upper or all lower switches are closed on positive and negative DC rail respectively. A schematic diagram of SVPWM vectors is shown in Figure D.1.

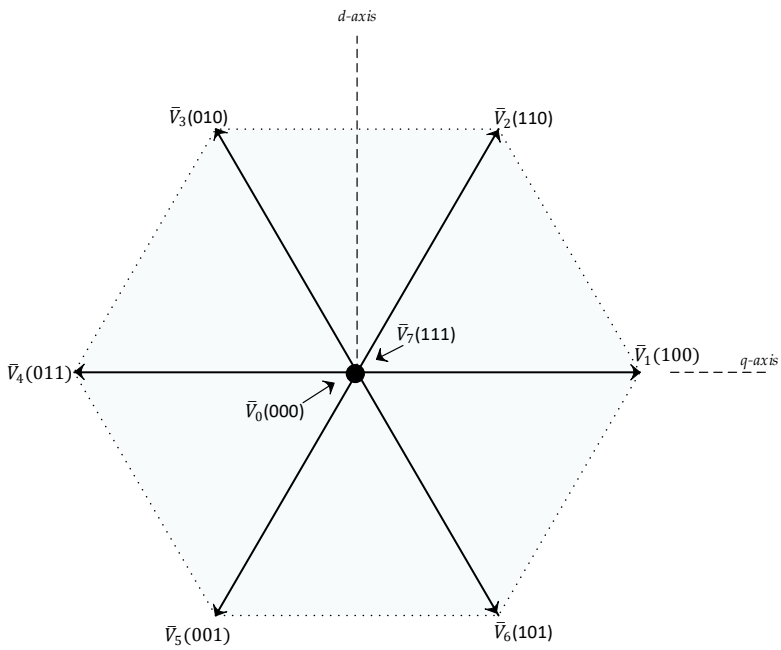

Figure D.1 Eight space voltage vectors in space vector diagram.

The six active voltage vectors V1(100), V2(110), V3(010), V4(011), V5(001), and V6(101) vectors make hexagonal star diagram with 60 degrees phase difference between adjacent vectors with magnitude of 2Vdc/3. The vectors V0(000) and V7(111) are called null vectors, they are plotted at the origin of the hexagonal structure and are either

positive or negative. The aim of SVPM is to generate a switching sequences corresponding to voltage vector during PWM to achieve rotating space vector. The output of SVPWM is mean vector which is equal to voltage vector (V_{out}) of any magnitude and at any position within the hexagon structure. The generation of voltage vector with any magnitude and direction is achieved by controlling the switching sequence and ON time duration of pulses between two nearest active and zero vectors. . The nearest active and zero vectors are stationary whereas the reference voltage vector (V_{ref}) is continuously rotating in within the hexagon at an angle (θ) and frequency (ω) . The ω is the desired output frequency of three phase two-level inverter and the amplitude of V_{ref} is fundamental component of V_{out}. The eight switching states SVPWM for two-level inverter are shown in Table D.1

Table D.1. Eight switching states of SVPWM

State	Turn-on	V_a	V_b	V_c	Vector
0	$S_4S_5S_6$	0	0	0	$\bar{V}_0(000)$
1	$S_1S_5S_6$	$2V_{dc}/3$	$-V_{dc}/3$	$-V_{dc}/3$	$\bar{V}_1(100)$
2	$S_1S_2S_6$	$V_{dc}/3$	$V_{dc}/3$	$-2V_{dc}/3$	$\bar{V}_2(110)$
3	$S_4S_2S_6$	$-V_{dc}/3$	$2V_{dc}/3$	$-V_{dc}/3$	$\bar{V}_3(010)$
4	$S_4S_2S_3$	$-2V_{dc}/3$	$V_{dc}/3$	$V_{dc}/3$	$\bar{V}_4(011)$
5	$S_4S_5S_3$	$-V_{dc}/3$	$-V_{dc}/3$	$2V_{dc}/3$	$\bar{V}_5(001)$
6	$S_1S_5S_3$	$V_{dc}/3$	$-2V_{dc}/3$	$V_{dc}/3$	$\bar{V}_6(101)$
7	$S_1S_2S_3$	0	0	0	$\bar{V}_7(111)$

The formation of V_{ref} vector is assumed to be in the space vector diagram (hexagon), the hexagon is formed by six output voltage vectors of two-level three phase inverter. The alternative of the voltage vectors adjacent to reference vector, six active voltage vectors and a zero vector are used to generate the output voltage [279]. Figure D.2 shows an example of V_{ref} calculation, The output voltage is resolved into two components Va and Vb in direction of $\bar{V}_1(100)$ and $\bar{V}_2(110)$ respectively.

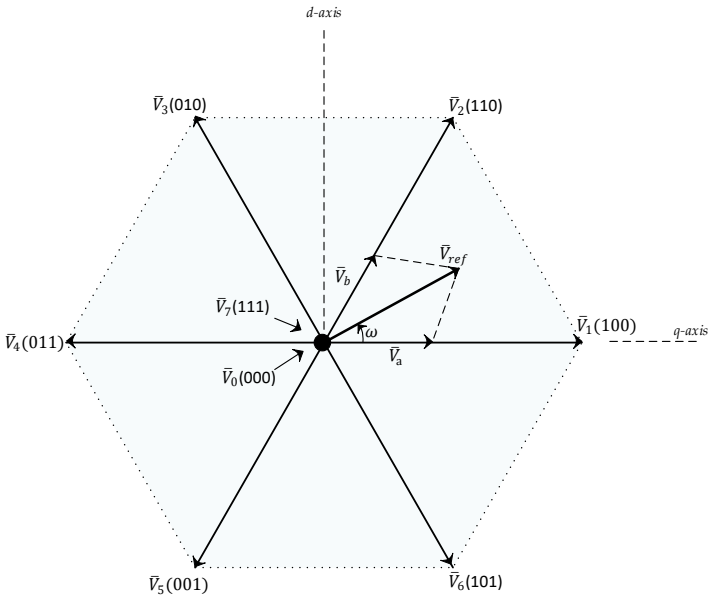

Figure D.2 Formation of reference voltage in SVPWM

Equations D.1 and D.2 represents the magnitude and time duration of V_a and V_b

$$\begin{cases} V_a = V_{ref} cos\omega - \frac{1}{2} V_b \\ V_b = V_{ref} \frac{2}{\sqrt{3}} V_{ref} sin\omega \end{cases} \tag{D.1}$$

$$\begin{cases} T_a = \frac{V_a}{(2V_{dc}/3)} \cdot T \\ T_b = \frac{V_b}{(2V_{dc}/3)} \cdot T \end{cases} \tag{D.2}$$

Further, the switching time calculations of each sector are shown graphically in Figure D.3 [333].

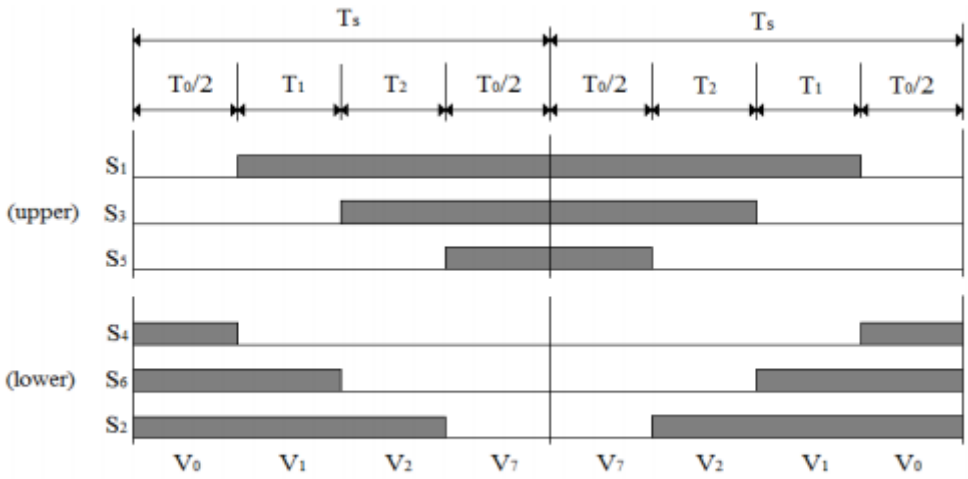

(a) Sector 1

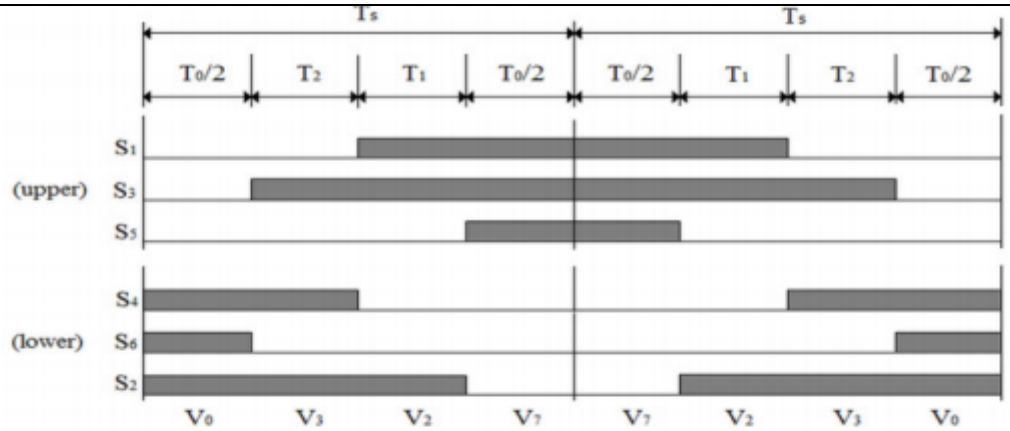

(b) Sector 2

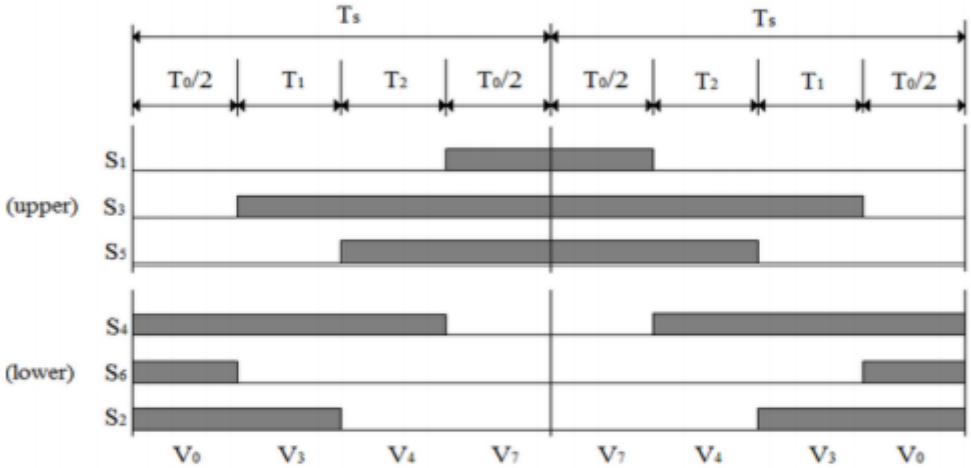

(c) Sector 3

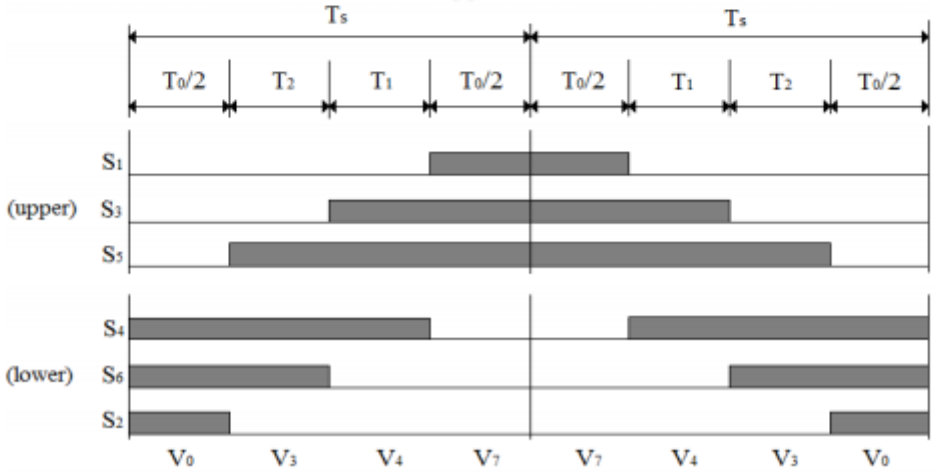

(d) Sector 4

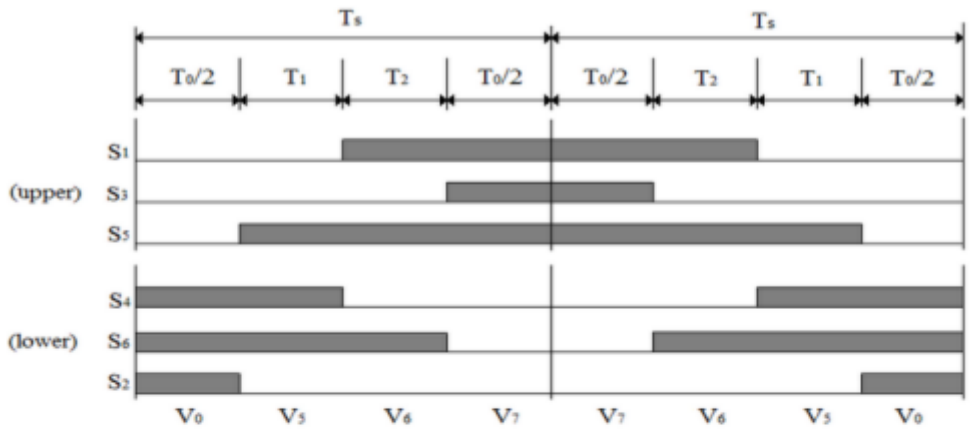

(e) Sector 5

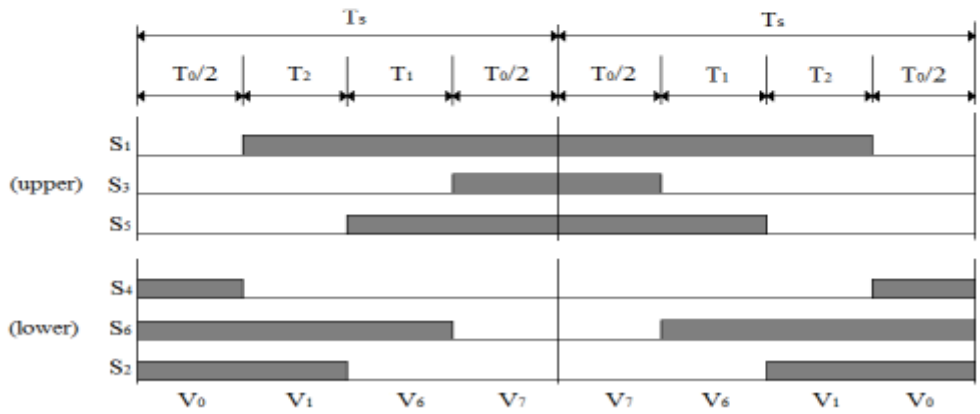

(f) Sector 6

Figure D.3 Timing diagram of six sectors of SVPWM.

Appendix E

Magnified Results

E.1 Load Model ND-July-WD

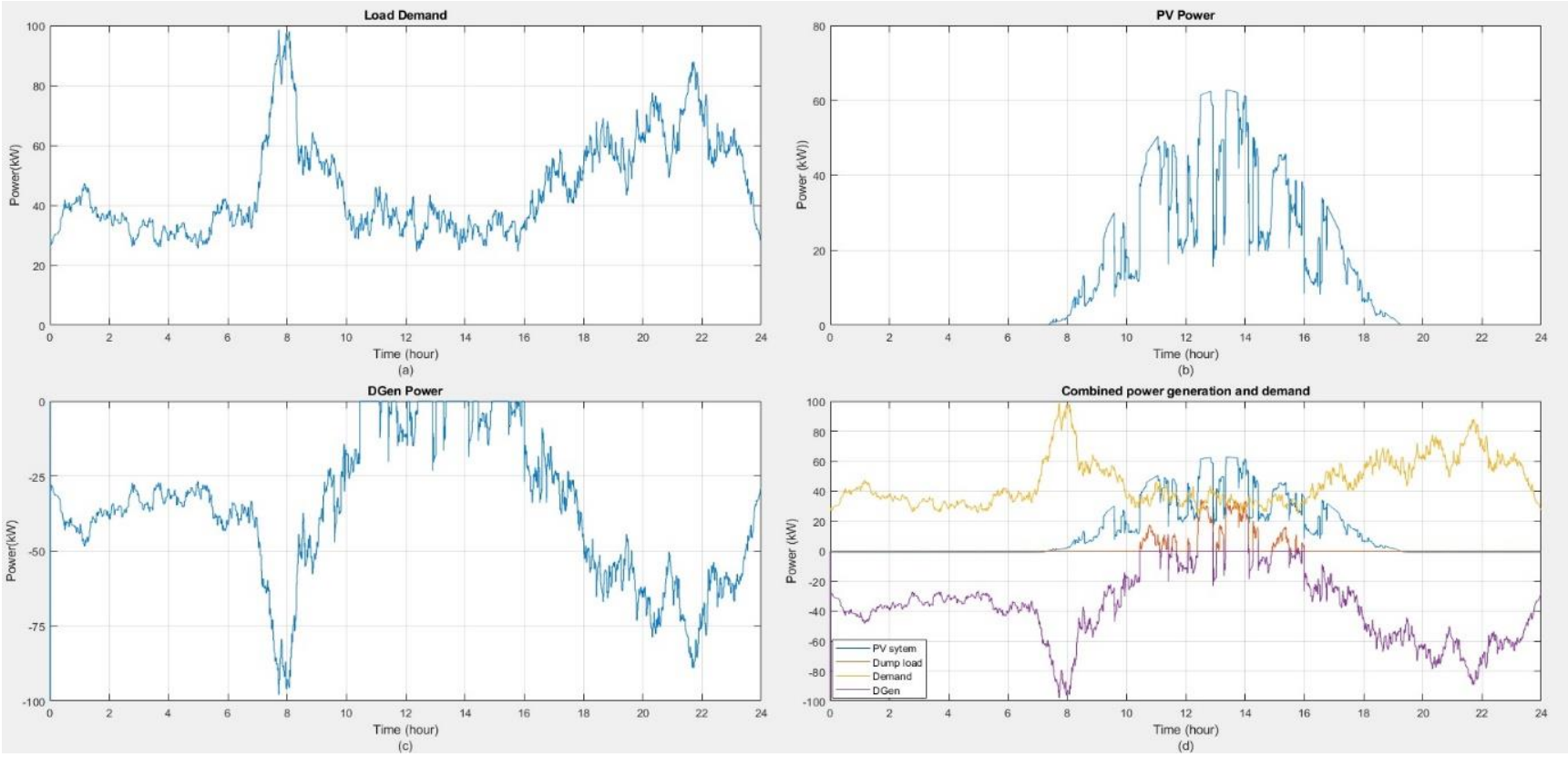

Operation of microgrid without Flywheel

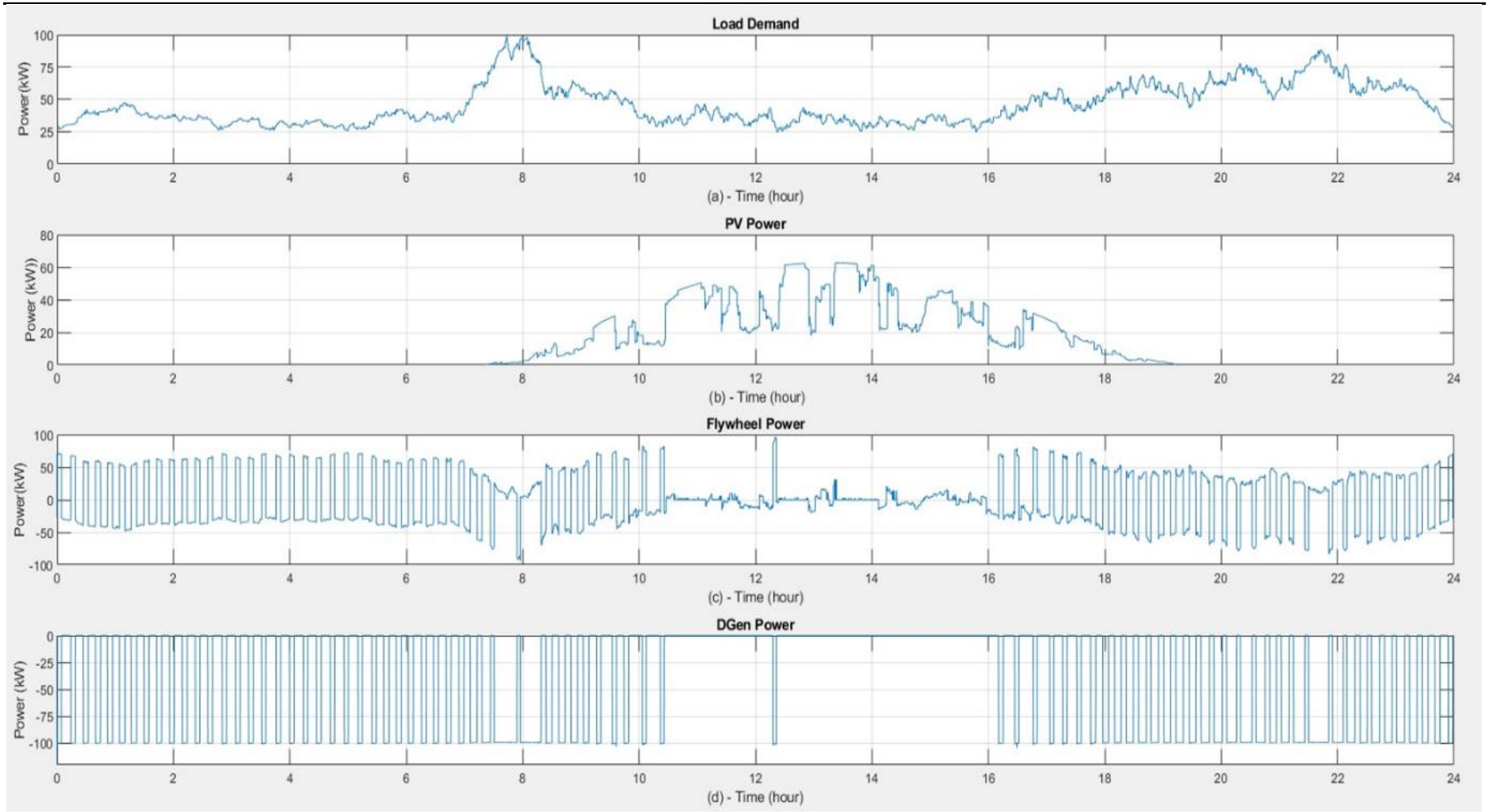

Operation of Flywheel at 100% DGen capacity

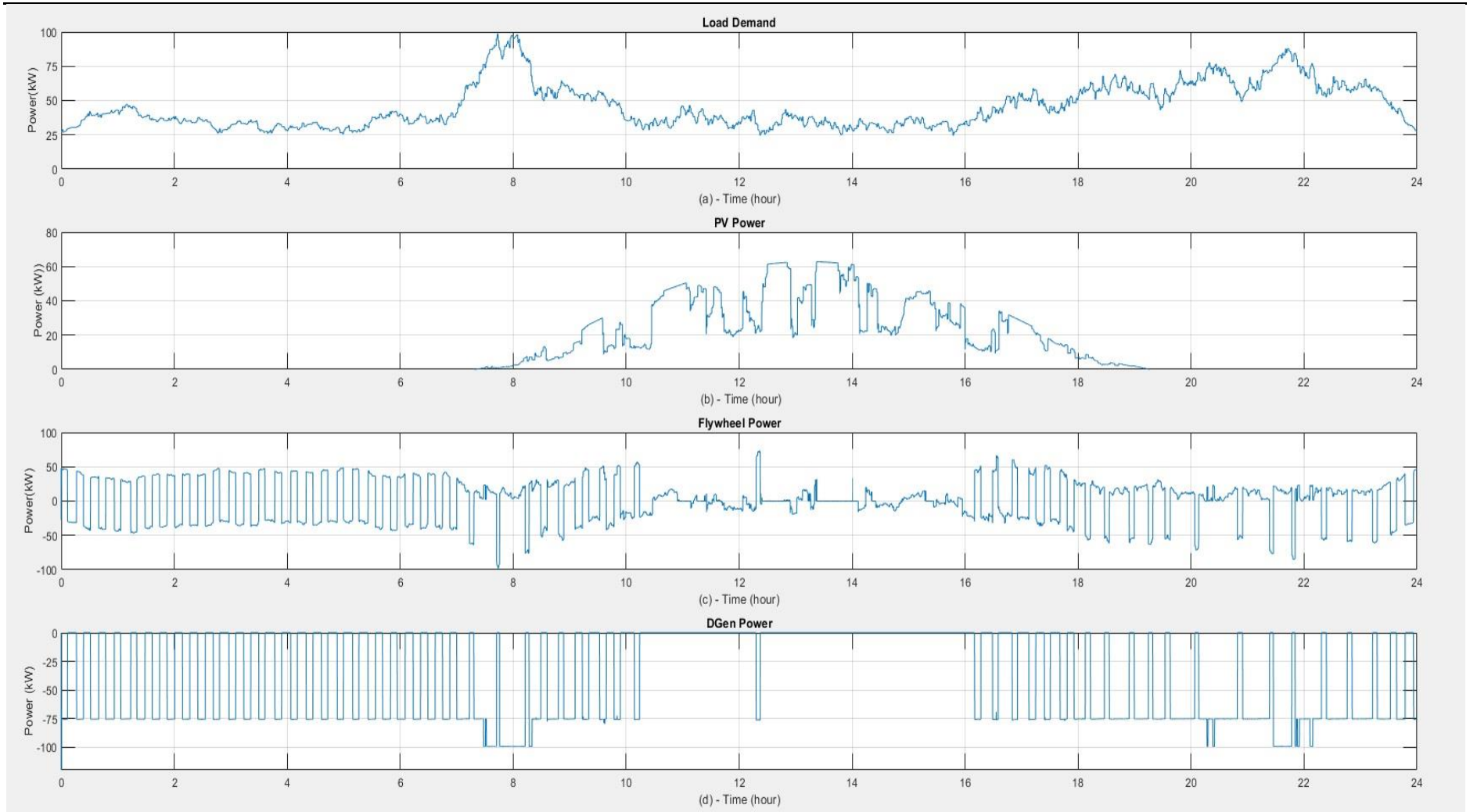

Operation of Flywheel at 75% DGen capacity

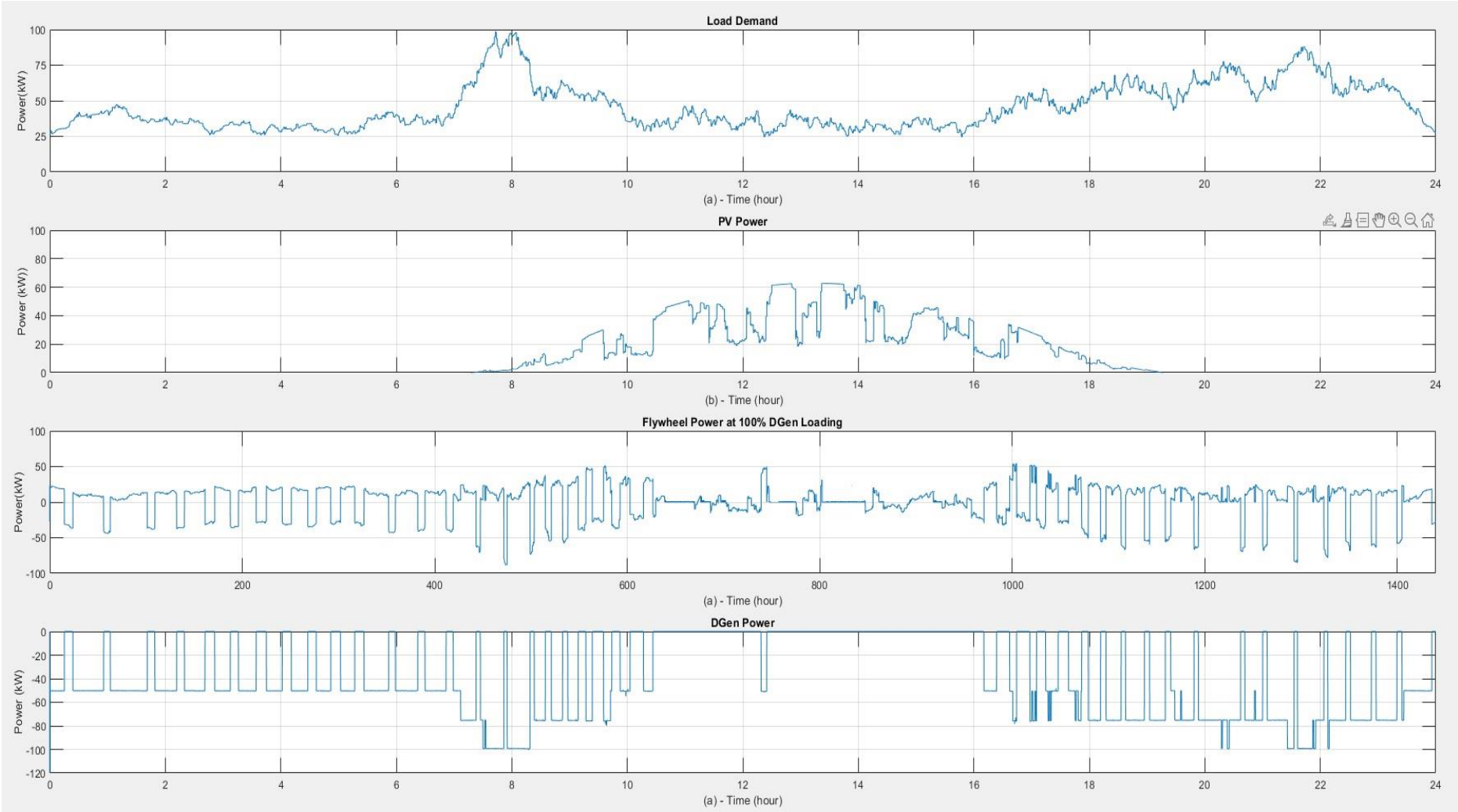

Operation of Flywheel at 50% DGen capacity

Load Model MB-June-WD

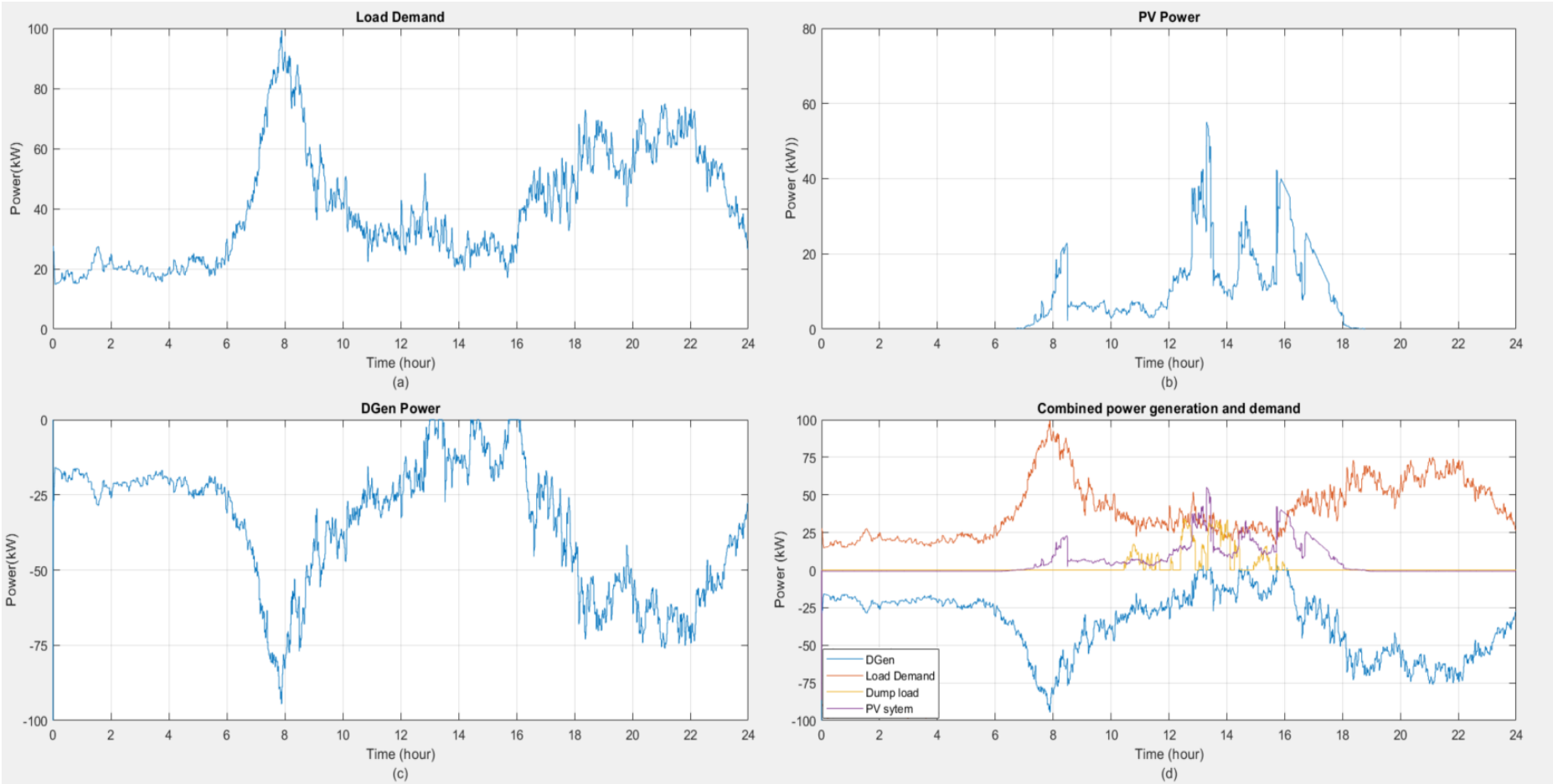

Operation of microgrid without Flywheel

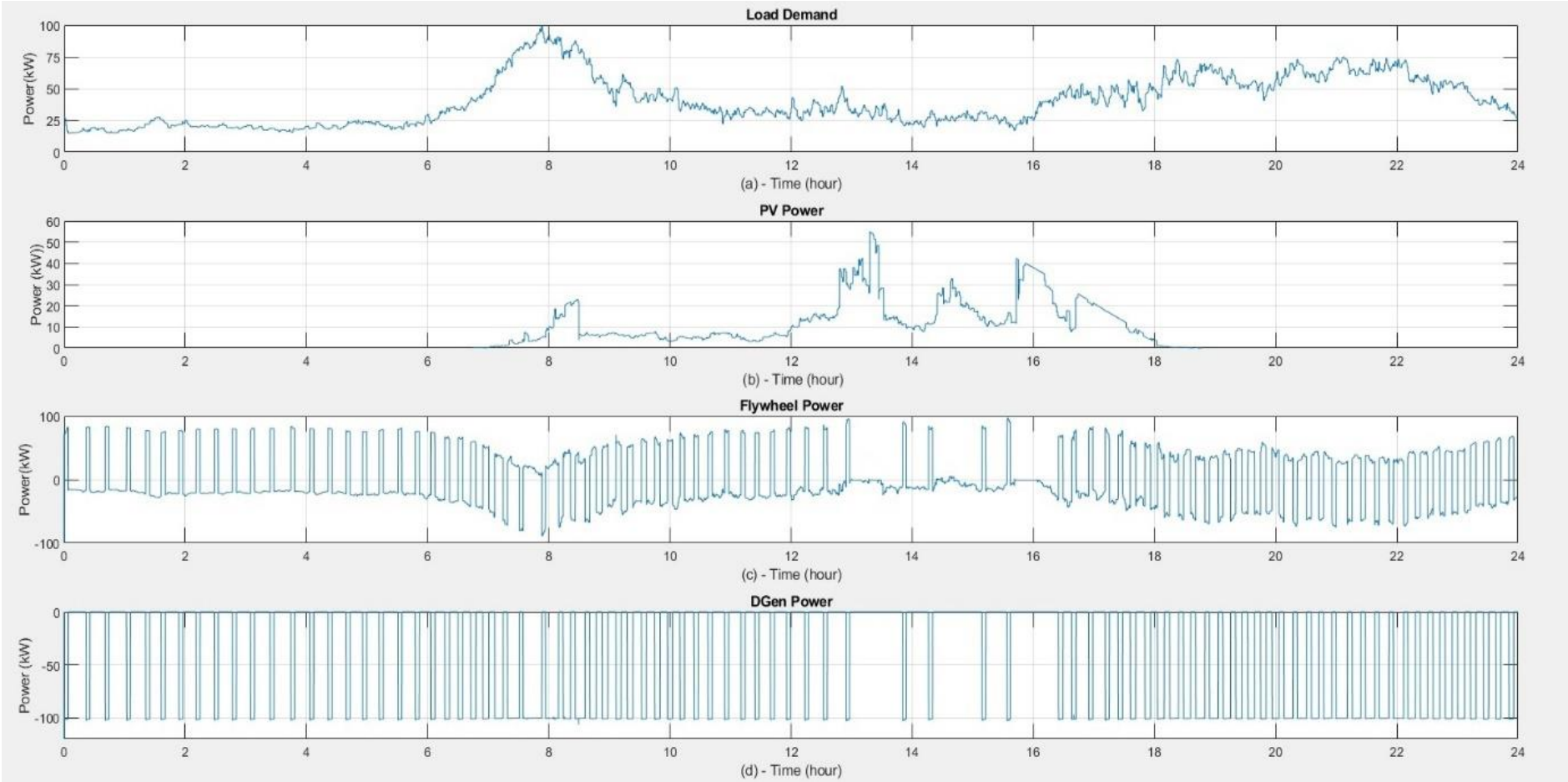

Operation of Flywheel at 100% DGen capacity

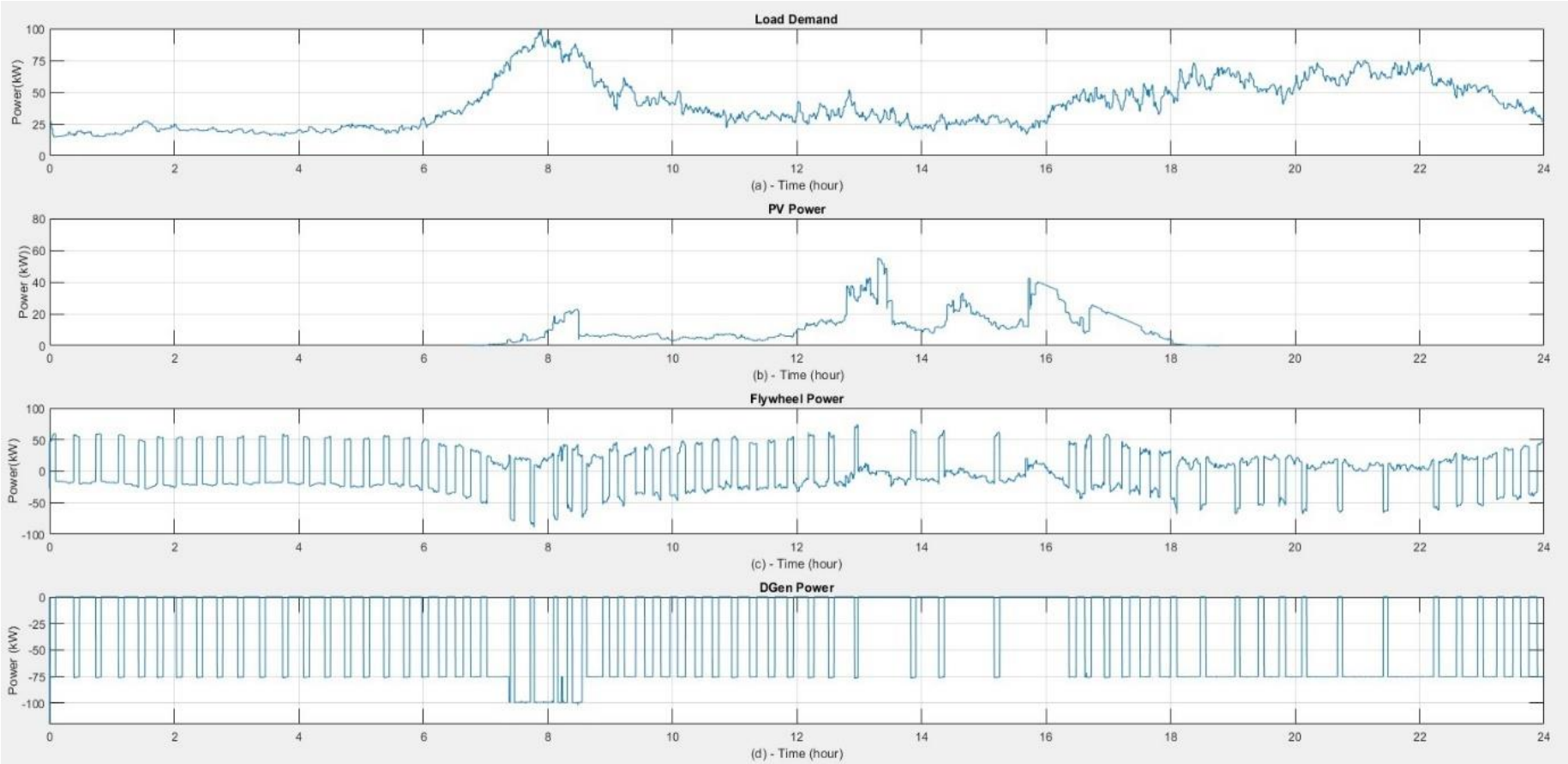

Operation of Flywheel at 75% DGen capacity

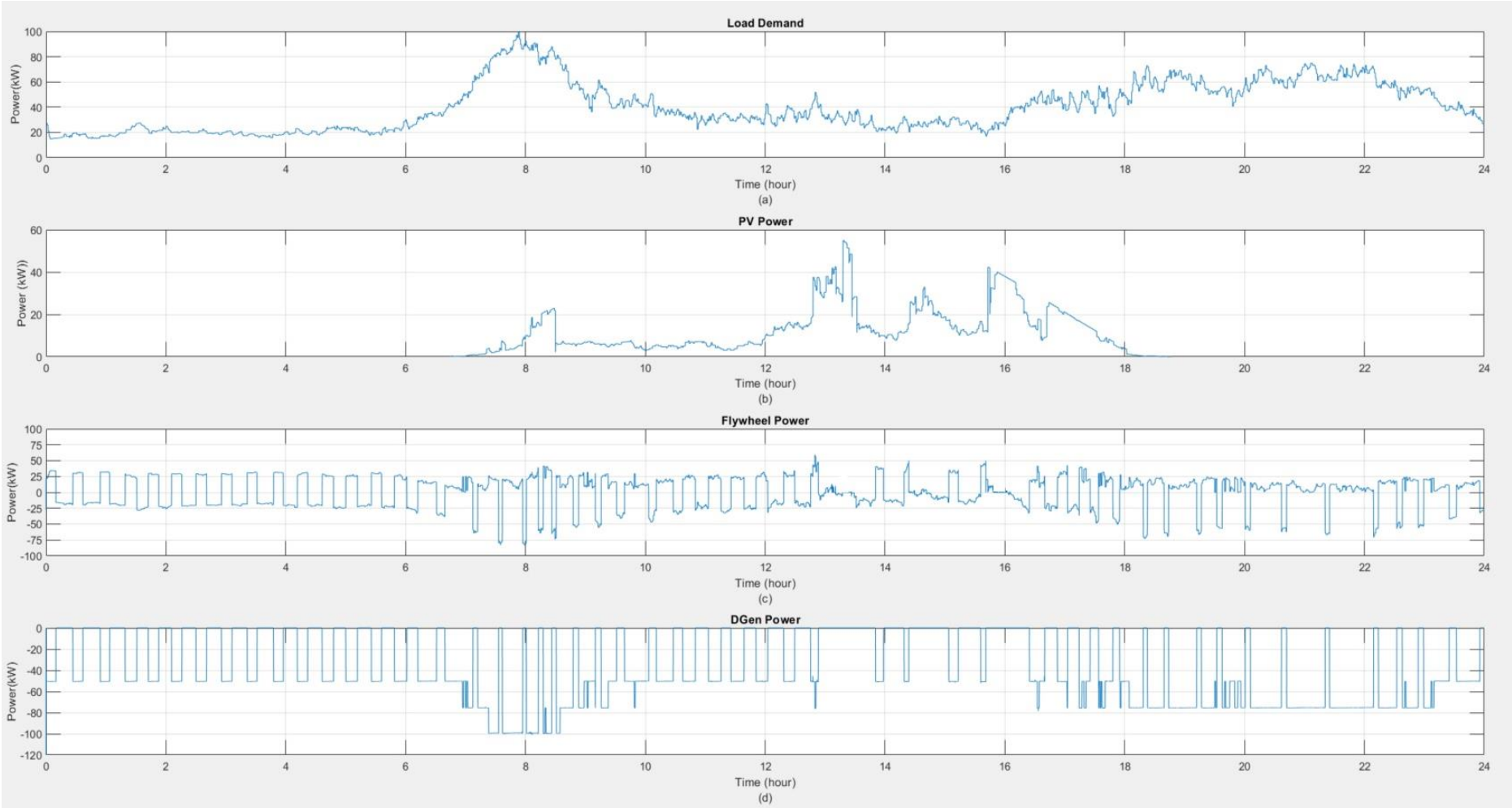

Operation of Flywheel at 50% DGen capacity

Load Model KT-July-WND

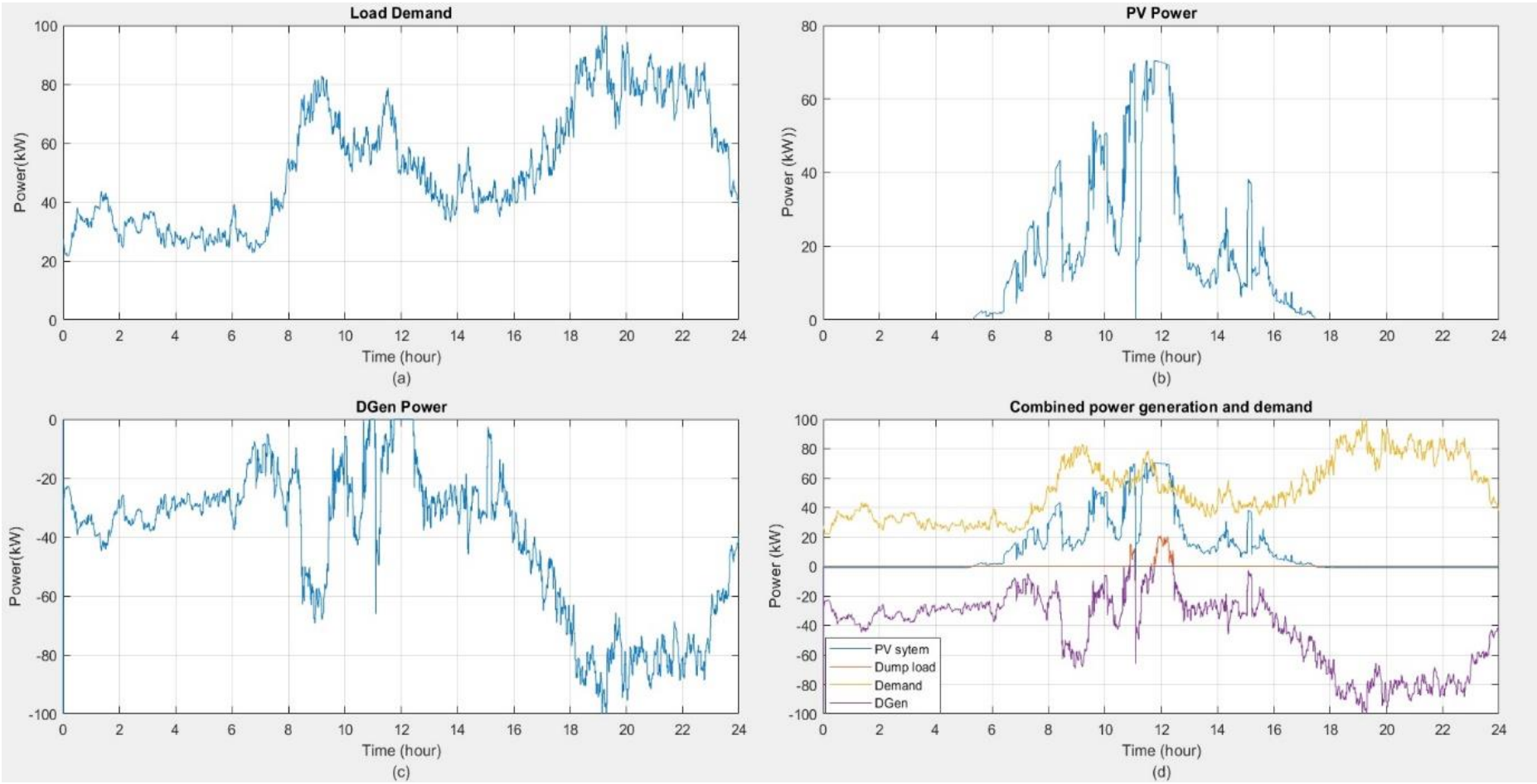

Operation of microgrid without Flywheel

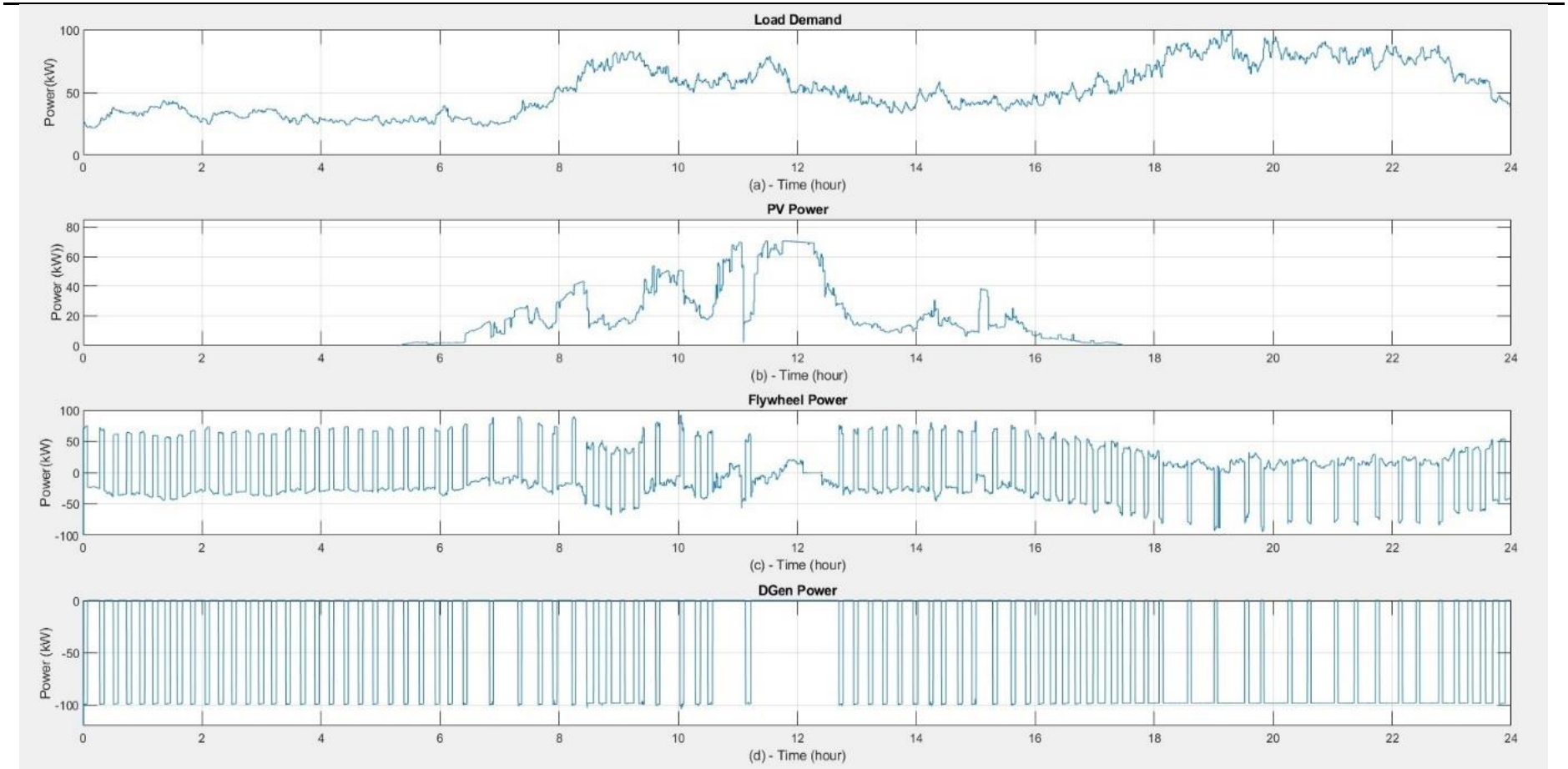

Operation of Flywheel at 100% DGen capacity

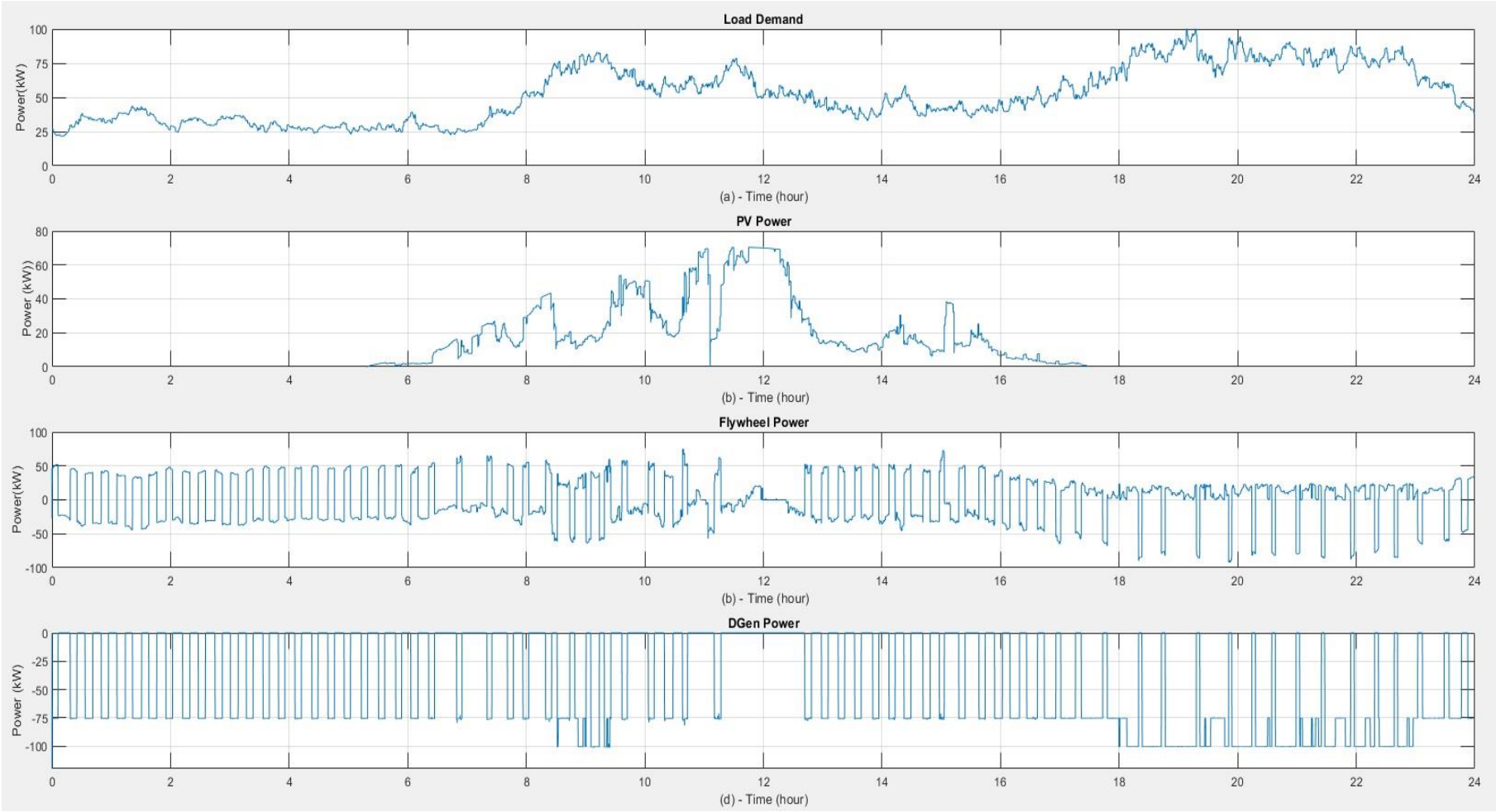

Operation of Flywheel at 75% DGen capacity

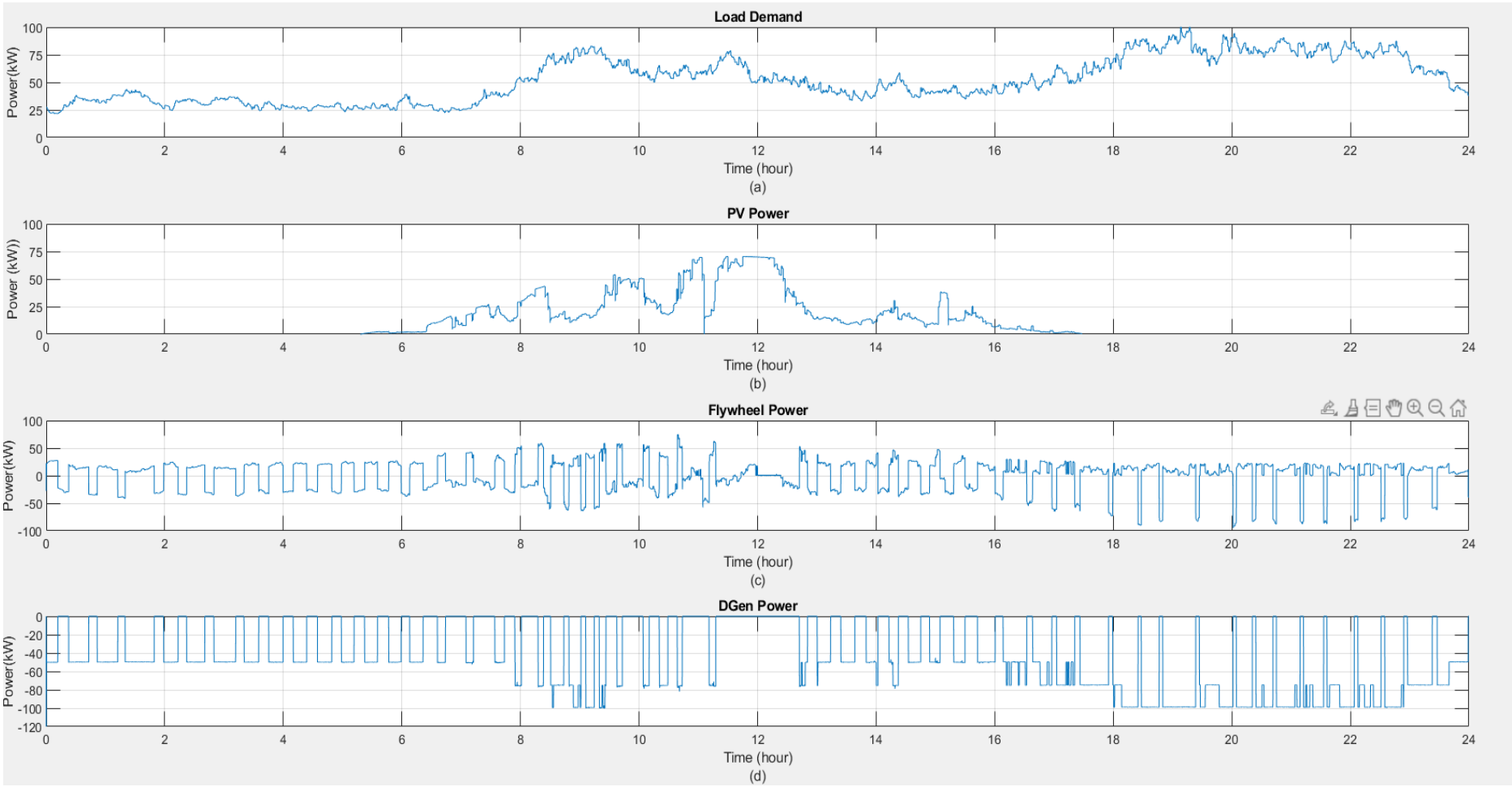

Operation of Flywheel at 50% DGen capacity

Appendix F

Electrical Properties of Rotor Material

Typical data for SURA® M470-50A

T	W/kg at 50 Hz	VA/kg at 50 Hz	A/m at 50 Hz	W/kg at 100 Hz	W/kg at 200 Hz	W/kg at 400 Hz
0,1	0,03	0,10	52	0,13	0,19	0,52
0,2	0,12	0,28	68	0,42	0,76	1,98
0,3	0,25	0,49	77	0,78	1,58	4,16
0,4	0,42	0,72	84	1,21	2,62	6,90
0,5	0,61	0,98	91	1,71	3,86	10,3
0,6	0,82	1,27	98	2,26	5,29	14,3
0,7	1,05	1,59	106	2,86	6,94	19,2
0,8	1,30	1,94	114	3,59	8,86	25,2
0,9	1,57	2,34	124	4,30	11,2	32,3
1,0	1,87	2,79	136	5,22	13,7	40,6
1,1	2,21	3,34	152	6,04	16,6	50,4
1,2	2,59	4,02	178	7,29	19,9	61,7
1,3	3,01	4,97	224	8,32	23,7	74,6
1,4	3,53	6,65	326	9,72	28,1	89,9
1,5	4,13	11,2	630	11,4	32,7	105
1,6	4,78	27,6	1612			
1,7	5,39	74,2	3963			
1,8	5,82	163	7773			

Loss at 1.5 T, 50 Hz, W/kg	4,13
Loss at 1.0 T, 50 Hz, W/kg	1,87
Anisotropy of loss, %	6
Magnetic polarization at 50 Hz	
H = 2500 A/m, T	1,63
H = 5000 A/m, T	1,71
H = 10000 A/m, T	1,83
Coercivity (DC), A/m	85
Relative permeability at 1.5 T	1600
Resistivity, μΩcm	33
Yield strength, N/mm²	250
Tensile strength, N/mm²	390
Young's modulus, RD, N/mm²	210000
Young's modulus, TD, N/mm²	220000
Hardness HV5 (VPN)	120

RD represents the rolling direction
TD represents the transverse direction
Values for yield strength (0.2 % proof strength) and tensile strength are given for the rolling direction
Values for the transverse direction are approximately 5% higher

cogent
Surahammars Bruks AB

October 2008

Works Cited

[1] K. Holmberg and A. Erdemir, “The impact of tribology on energy use and CO2emission globally and incombustion engine and electric cars,” *Tribology International,* no. 135, pp. 389-396, 2019.

[2] S. S. Akadiri, A. A. Alola, G. O. Williams and M. U. Etokakpan, “The role of electricity consumption, globalization and economic growth in carbon dioxide emissions and its implications for environmental sustainability targets,” *Science of the Total Environment,* no. 780, p. 10, 2020.

[3] T. Ahmad and D. Zhang, “A critical review of comparative global historical energy consumption and future demand: The story told so far,” *Energy Reports,* vol. 6, pp. 1973-1991, 2020.

[4] International Energy Agency, “Global Energy Review 2021,” International Energy Agency -IEA, 2021.

[5] Climate Action Tracker, “Addressing global warming,” Climate Action Tracker, 01 07 2021. [Online]. Available: https://climateactiontracker.org/global/temperatures/. [Accessed 25 7 2021].

[6] “Today In Energy,” US Energy Information Administration, 24 09 2019. [Online]. Available: https://www.eia.gov/todayinenergy/detail.php?id=41433. [Accessed 21 05 2021].

[7] I. Tiseco, “Global CO2 emissions 2018-2050,” Statista, 2020.

[8] “Reducing UK emissions : 2019 Progress Report to Parliament,” Committee on Climate Change, 2019.

[9] P. Shrestha, “Global energy use projected to nearly double by 2050,” Energy Live News, 8 1 2020. [Online]. Available: https://www.energylivenews.com/2020/01/08/global-energy-use-projected-to-nearly-double-by-2050/#:~:text=Energy%20use%20in%20the%20global,British%20thermal%20units%20(Btu).. [Accessed 21 5 2021].

[10] U.S. Energy Information Administration (EIA), “International Energy Outlook 2019,” U.S. Energy Information Administration, 2019.

[11] J. Ren and X. Ren, “Sustainability ranking of energy storage techologies under uncertainties,” *Journal of Cleaner Production,* no. 170, pp. 1387-1398, 2017.

[12] H. Ritchie and M. Roser, “Energy,” Our world in data, 2014. [Online]. Available: https://ourworldindata.org/energy. [Accessed August 2020].

[13] F. Diaz-Gonzalez, A. Sumper, O. Gomis-Bellmunt and R. Villafafila-Robles, “A review of energy storage technologies for wind power applications,” *Renewable and Sustainable Energy Reviews,* no. 16, pp. 22154-2171, 2012.

[14] M. Beaudin, H. Zareipour, A. Schellenberglabe and R. William , “Energy storage for mitigating the variability of renewable electricity sources: An updated review,” *Energy for Sustainable Development,* vol. 4, pp. 302-314, 2010.

[15] “Data and statistics,” IEA, 2021. [Online]. Available: https://www.iea.org/data-and-statistics/data-tables/?country=WORLD&energy=Electricity&year=2018. [Accessed 21 05 2021].

[16] J. Lee and F. Zhao, “GWEC | Global Wind Report 2021,” Global Wind Energy Council, Brussels, 2021.

[17] Y. Abdelilah, H. Bahar, T. Cridwell, P. Bojek, F. Briens and P. Le Feuvre, “Renewables 2020 : Analysis and Forcast to 20245,” International Energy Agency, 2020.

[18] H. E. Murdock, D. Gibb and T. Andre, “Renewables 2020 global status report,” Renewable Energy Now REN21, Paris, 2020.

[19] International Energy Agency-IEA, “Renewables bucked the trend in 2020,” International Energy Agency-IEA, 2021.

[20] IRENA, “Renewable Energy Integration in Power Grids,” International Renewable Energy Agency -IRENA, 2015.

[21] Business Wire, “Global Distributed Generation (DG) Market Report 2021: Market is Projected to Reach $183.2 Billion by 2025, Driven by the Growing Focus Shed on Decarbonizing Power Generation and Transmission - ResearchAndMarkets.com,” Business Wire, 21 04 2021. [Online]. Available: https://www.businesswire.com/news/home/20210421005614/en/Global-Distributed-Generation-DG-Market-Report-2021-Market-is-Projected-to-Reach-183.2-Billion-by-2025-Driven-by-the-Growing-Focus-Shed-on-Decarbonizing-Power-Generation-and-Transmission---ResearchA. [Accessed 25 07 2021].

[22] United States Environmental Protection Agency, “Distributed Generation of Electricity and its Environmental Impacts,” United States Environmental Protection Agency, [Online]. Available: https://www.epa.gov/energy/distributed-generation-electricity-and-its-environmental-impacts. [Accessed 25 07 2021].

[23] D. Akinyele and R. Rayudu, “Review of energy storage technologies for sustainable power networks,” *Sustainable Energy Technology and Assessments,* no. 8, pp. 74-91, 2014.

[24] C. R. Matos, J. F. Carneiro and P. P. Silva, “Overview of Large-Scale Underground Energy Storage Technologies for Integration of Renewable Energies and Criteria for Reservoir Identification,” *Jounal of Energy Storage,* no. 21, pp. 241-258, 2019.

[25] M. S. Guney and Y. Tepe, “Classification and assessment of energy storage systems,” *Renewable and Sustainable Energy Reviews,* vol. 75, pp. 1187-1197, 2017.

[26] M. E. Amiryar, D. Nankoo and K. R. Pullen, “Development of a High-Fidelity Model for an Electrically Driven Energy Storage Flywheel Suitable for Small Scale Residential Applications,” *Applied Sciences,* vol. 8, p. 29, 2018.

[27] D. Manz, R. Piwko and N. Miller, “Look Before You Leap: The Role of Energy Storage in the Grid,” *IEEE Power and Energy Magazine,* vol. 10, no. 4, pp. 75-84, 2012.

[28] S. Sabihuddin, A. E. Kiprakis and M. Markus, “A Numerical and Graphical Review of Energy Storage Technologies,” *Energies,* vol. 8, pp. 172-216, 2015.

[29] F. Mohamad, J. Teh, C.-M. Lai and L.-R. Chen, “Development of Energy Storage Systems for Power Network Reliability: A Review,” *Energies,* vol. 11, no. 2278, p. 19, 2018.

[30] S. Rehimi, R. Mirzaei and H. Bevrani, “Interconnected microgrids frequency response model@ An inertial-based approach,” *Energy Repots,* vol. 6, pp. 179-186, 2019.

[31] P. Saxena, N. Singh and A. K. Pandey, “Enhancing the dynamic performance of microgrid using derivativecontrolled solar and energy storage based virtual inertia system,” *Journal of Energy Storage,* vol. 31, p. 11, 2020.

[32] H. Chen, T. N. Cong, W. Yang, C. Tan, Y. Li and Y. Ding, “Progress in electrical energy storage system: A critical review,” *Progress in Natural Science,* no. 19, pp. 291-312, 2009.

[33] P. Breeze, “An Introduction to Energy Storage Technologies,” in *Power System Energy Storage Technologies*, Elsevier Limited, 2018, pp. 1-11.

[34] E. Hittingera, J. Whitacre and J. Apta, “What properties of grid energy storage are most valuable?,” *Journal of Power Sources,* vol. 206, pp. 436-449, 2012.

[35] A. Smallbone, V. Julch, R. Wardle and A. P. Roskilly, “Levelised Cost of Storage for Pumped Heat Energy Storage in comparison with other energy storage technologies,” *Energy Conversion and Management,* vol. 152, pp. 221-228, 2017.

[36] S. Koohi-Fayegh and M. A. Rosen, “A review of energy storage types, applications and recent developments,” *Journal of Energy Storage,* vol. 27, 2020.

[37] P. J. Hall and E. J. Bain, “Energy-storage technologies and electricity generation,” *Energy Policy,* vol. 36, pp. 4352-4355, 2008.

[38] Asian Development Bank, “HHandbook on Battery Energy Storage System,” Asian Development Bank, 2018.

[39] K. R. Pullen, “United Nations UNEP-European Energy Centre EEC,” [Online]. Available: https://energy-learning.com/index.php/opinion/78-what-s-new/162-flywheel-energy-storage. [Accessed 19 07 2020].

[40] M. E. Amiryar, *An Assessment of Flywheel Storage for Efficient Provision of Reliable Power for Residential Premises in Islanded Operation,* London: City University of London, 2019.

[41] R. Harbner, J. Beno and A. Walls, *Flywheel Batteries come around again,* IEEE Spectrum, 2002.

[42] S. Wicki and E. G. Hansen, “Clean energy storage technology in the making: An innovation systems perspective on flywheel energy storage,” *Journal of Cleaner Production,* vol. 162, pp. 1118-1134, 2017.

[43] H. Ibrahim, A. Ilinca and J. Perron, “Energy storage systems—Characteristics and comparisons,” *Renewable and Sustainable Energy Reviews,* vol. 12, pp. 1221-1250, 2008.

[44] R. Arghandeh, M. Pipattanasomporn and S. Rahman, “Flywheel Energy Storage Systems for Ride-through Applications in a Facility Microgrid,” *IEEE Transactions on Smart Grid,* vol. 3, no. 4, pp. 1955-1962, 2012.

[45] K. R. Pullen, “The Status and Future of Flywheel Energy Storage,” *Joule,* vol. 3, pp. 1394-1403, 2019.

[46] D. Bender, “Flywheels,” in *Electrical Energy Storage Techniques*, System Surety Engineering, Sandia National Laboratories, California, United States of America, 2016, pp. 183-201.

[47] H. Ibrahim, M. Rezkallah, A. Ilinca and M. Ghandour, “Hybrid energy storage systems,” in *Hybrid Renewable Energy Systems and Microgrids*, Academic press, 2021, pp. 351-375.

[48] Loughborough University, “Centre for Renewable Energy Systems Technology,” Loughborough University, 2021. [Online]. Available: https://www.lboro.ac.uk/research/crest/. [Accessed 10 09 2021].

[49] P. Atanasoae, R. D. Pentiuc, D. L. Milici, E. D. Olariu and M. Poienar, “The cost-benefit analysis of the electricity production from small scale rrenwable energy sources in the conditions of Romania,” in *The 12th international conference interdisciplinarity in engineering*, 2019.

[50] International Energy Agnecy, “The resilience of renewables is driven by the electricity sector,” IEA, 2021.

[51] E. Muljadi, C. O. Butterfield, B. Parsons and A. Ellis, “Effect of Variable Speed Wind Turbine Generator on Stability of a Weak Grid,” *IEEE Transactions on Energy Conversion,* vol. 22, no. 1, pp. 29-36, 2007.

[52] C. L. Anderson and J. B. Cardell, “Reducing the Variability of Wind Power Generation for Participation in Day Ahead Electricity Markets,” in *Proceedings of the 41st Annual Hawaii International Conference on System Sciences (HICSS 2008)*, Waikoloa, HI, USA, 2008.

[53] E. D. Casronuovo and J. A. Lopes, “On the optimization of the daily operation of a wind-hydro power plant,” *IEEE Transactions on Power SystemS,* vol. 19, no. 3, 2004.

[54] H. Ding, Z. Hu and Y. Song, “Stochastic optimization of the daily operation of wind farm andpumped-hydro-storage plant,” *Renewable Energy,* vol. 48, pp. 571-578, 2012.

[55] M. T. Weis and A. Ilinca, “The utility of energy storage to improve the economics of wind–diesel power plants in Canada,” *Renewable Energy,* vol. 33, pp. 1544-1557, 2008.

[56] X. Luo, J. Wang, M. Dooner and J. Clarke, “cOverview of current development in electrical energy storage technologies and the application potential in power system operation,” *Applied Energy,* vol. 137, pp. 511-536, 2015.

[57] A. Evans, V. Strezov and T. J. Evans, “Assessment of utility energy storage options for increased renewable energy penetration,” *Renewable and Sustainable Energy Reviews,* vol. 16, pp. 4141-4147, 2012.

[58] M. Beaudin, Hamidreza Zareipour, A. Schellenberg and W. Rosehar, “Chapter one: Energy Storage for Mitigatingthe Variability of Renewable Electricity Sources,” in *Eergy storage for smart grids*, Elsevier Inc., 2015.

[59] L. Wagner, “Overview of energy storage methods,” MORA Associates, 2007.

[60] T. Kousksou, P. Bruel, A. Jamil, T. El Rhafiki and Y. Zeraouli, “Energy storage: Applications and challenges,” *Solar Energy Materials & Solar Cells,* vol. 120, pp. 59-80, 2014.

[61] V. A. Boicea, “Energy Storage Technologies: The Past and the Present,” *Proceedings of IEEE,* vol. 102, no. 11, pp. 1777-1794, 2014.

[62] H. Gualous, D. Bouquain, A. Berthon and J. M. Kauffmann, “Experimental study of supercapacitor serial resistance and capacitance variations with temperature,” *Journal of Power Sources,* vol. 15, no. 1, pp. 86-93, 2003.

[63] A. Kusko and J. DeDad, “Short-term, long-term, energy storage methods for standby electric power systems,” in *Fourtieth IAS Annual Meeting. Conference Record of the 2005 Industry Applications Conference, 2005.*, Hong Kong China, 2005.

[64] M. S. Guney and Y. Tepe, “Classification and assessment of energy storage systems,” *Renewable and Sustainable Energy Reviews,* vol. 75, pp. 1187-1197, 2017.

[65] M. S. Guney and Y. Tepe, “Classification and assessment of energy storage systems,” *Renewable and Sustainable Energy Reviews,* no. 75, pp. 1187-1197, 2017.

[66] B. Zakeri and S. Syri, “Electrical energy storage systems:Acomparative life cycle cost analysis,” *RenewableandSustainableEnergyReviews,* vol. 42, pp. 569-596, 2015.

[67] D. L. Chandler, “New type of electrolyte could enhance supercapacitor performance,” Massachisetts Institute of Technology, 12 08 2019. [Online]. Available: https://news.mit.edu/2019/new-electrolyte-supercapacitor-0812#:~:text=enhance%20supercapacitor%20performance-,New%20type%20of%20electrolyte%20could%20enhance%20supercapacitor%20performance,less%20risk%20of%20catching%20fire.. [Accessed 04 07 2021].

[68] P. J. Hall and E. J. Bain, “Energy-storage technologies and electricity generation,” *Energy Policy,* vol. 36, no. 12, pp. 4352-4355, 2008.

[69] X. Tan, Q. Li and H. Wang, “Advances and trends of energy storage technology in Microgrid,” *International Journal of Electrical Power & Energy Systems,* vol. 44, no. 1, pp. 179-191, 2013.

[70] C. Gandolfi, R. Chuimeo, D. Raggini, r. fARANDA, A. Morandi, C. Ferdehghini, M. Tropeano and S. Turu, “Study of a Universal Power SMES Compensator for LV Distribution Grid,” in *2018 AEIT International Annual Conference*, Bari, 2018.

[71] C. Shaw, “Superconducting Magnetic Energy Storage System – Commercialisation and Marketing Challenges,” ESA- Energy Storage Association, 2016.

[72] X. Granados, “EERA Joint Program SP5 – Superconducting Magnetic Energy Storage,” European Energy Research Allince, Brussels, 2019.

[73] H. Ibrahim, A. Ilinca and J. Perron, “Energy storage systems—Characteristics and comparisons,” *Renewable and Sustainable Energy Reviews,* vol. 12, pp. 1221-1250, 2008.

[74] Highview Power, “Plants,” Highview Power, 2021. [Online]. Available: https://highviewpower.com/plants/. [Accessed 21 08 2021].

[75] P. Denholm, E. Ela, B. Kirby and M. Milligan, “The Role of Energy Storage with Renewable Electricity Generation,” National Renewable Energy Laboratory, Colorado, 2010.

[76] S. Kapila, A. O. Oni and A. Kumar , “The development of techno-economic models for large-scale energy storage systems,” *Energy,* vol. 140, pp. 656-672, 2017.

[77] L. Mears, H. Gotschall and H. Kamath, “EPRI-DOE Handbook of Energy Storage for Transmission and Distribution Applications,” Electric Power Research Insttute, Inc. and the U.S Department of Energy, Palo Alto, CA and Washington, 2003.

[78] Energy Research Partnership Technology, “The future role for energy storage in the UK,” Energy Research Patnership - ERP, London, 2011.

[79] S. Sabihuddin, A. E. Kiprakis and M. Mueller, “A Numerical and Graphical Review of Energy Storage Technologies Storage Technologies,” *Energies,* vol. 8, pp. 172-216, 2015.

[80] Arizona Public Service Company, “Study of Compressed Air Energy storage with grid and photovoltaic energy generation,” ARIZONA Research institute for solar energy, Arizona, 2010.

[81] I. Hadjipaschalis, A. Poullikkas and V. Efthimiou, “Overview of current and future energy storage technologies for electric power applications,” *Renewable and Sustainable Energy Reviews,* vol. 13, pp. 1513-1522, 2009.

[82] Internatinal Renewable Energy Agency-IRENA, “Innovative Operation of Pumped Hydropower Storage,” Internatinal Renewable Energy Agency, Abu Dhab, 2020.

[83] A. Abele, E. Elkind, J. Intrator and B. Washom, “2020 Strategic analysis of energy storage in california,” University of California, California, 2011.

[84] C. Bueno and J. A. cATRA, “Wind powered pumped hydro storage systems, a means of increasing the penetration of renewable energy in the Canary Islands,” *Renewable and Sustainable Energy Reviews,* vol. 10, no. 4, pp. 312-340, 2006.

[85] J. P. Deane, B. P. Gallachoir and E. j. McKeogh, “Techno-economic review of existing and new pumped hydro energy storage plant,” *Renwable and Sustainable Energy Reviews,* vol. 14, no. 4, pp. 1293-1302, 2010.

[86] Electric Mountain, “Dinorwig Power Station,” Electric Mountain, [Online]. Available: https://www.electricmountain.co.uk/Dinorwig-Power-Station. [Accessed 28 08 2021].

[87] E. Pürer, “A second option - Kops II pumped storage plant,” International Water Power and Dam Construction, 25 02 2005. [Online]. Available: https://www.waterpowermagazine.com/features/featurea-second-option-kops-ii-pumped-storage-plant/. [Accessed 28 08 2021].

[88] R. Uría-Martínez, M. M. Johnson and R. Shan, “U.S. Hydropower Market Report,” US Department of Energy, Oak Ridge, 2021.

[89] A. Poullikkas, “A comparative overview of large-scale battery systems for electricity storage,” *Renewable and Sustainable Energy Reviews,* no. 27, pp. 778-788, 2013.

[90] O. Palizban and K. Kauhaniemi, “Distributed cooperative control of battery energy storage system in ACmicrogrid applications,” *Journal of Energy Storage,* no. 3, pp. 43-51, 2015.

[91] K. C. Divya and J. Ostergaard, “Battery energy storage technology for power systems—An overview,” *Electric Power Systems Research,* no. 79, pp. 511-520, 2008.

[92] N.-K. C. Nair and N. Garimella, “Battery energy storage systems: Assessment for small-scale renewable energy integration,” *Energy and Buildings,* no. 42, pp. 2124-2130, 2010.

[93] A. Poullikkas, “A comparative overview of large-scale battery systems for electricity storage,” *Renewable and Susainable Energy Reviews,* vol. 27, pp. 778-788, 2013.

[94] PowerThru, “Lead Acid Battery Working - Lifetime Study,” PowerThru.

[95] J. Wen, D. Zhao and C. Zhang, “An overview of electricity powered vehicles: Lithium-ion battery energy storage density and energy conversion efficiency,” *Renewable Energy,* vol. 162, pp. 1629-1648, 2020.

[96] A. Zablocki, “Fact Sheet | Energy Storage (2019),” Environmental and Energy Study Institute -EESI, 22 02 2019. [Online]. Available: https://www.eesi.org/papers/view/energy-storage-2019#1. [Accessed 16 07 2021].

[97] Z. Hameed, S. Hashemi, H. H. Ipsen and C. Traesholt, “A business-oriented approach for battery energy storage placement in power systems,” *Applied Energy,* vol. 298, p. 117186, 2021.

[98] P. Kurzweil, “Chapter 16Lithium Battery Energy Storage:State of the Art Including LithiumeAirand LithiumeSulfur Systems,” in *Electrochemical Energy Storage for Renewable Sources and Grid Balancing*, Amberg, Germany, Elsevier, 2015, pp. 269-307.

[99] G. Zubi, R. S. Adhikari, N. E. Sanchez and W. Acuna-Bravo, “Lithium-ion battery pack for solar home systems: Layout, cost analysis and implementationperspecgive,” *Journal of Enregy Storage,* vol. 32, 2020.

[100] S. Huan, X. Zhu, S. Sarkar and Y. Zhao, “Challenges and opportunities for supercapacitors,” *APL Materials,* vol. 7, no. 10, 2019.

[101] R. Ostergard, “Master thesis: Flywheel Energy Storage a conceptual study,” Uppsala Universitet, 2011.

[102] T. T. A. M. H.S.C.Matseelar, T. Mahlia, T. Saktisahdan, A. Jannifar, M. Hasan and H. Matseelar, “A review of available methods and development on energy storage; technology update,” *Renewable and Sustainable Energy Reviews,* vol. 33, pp. 532-545, 2014.

[103] J. Wen, D. Zhao and C. Zhang, “An overview of electricity powered vehicles: Lithium-ion battery energy storage density and energy conversion efficiency,” *Renewable Energy,* vol. 162, pp. 1629-1648, 2020.

[104] R. D. Brown and W. D. Chvala, “Flywheel Energy Storage: An Alternative to Batteries For UPS Systems,” *Energy Engineering,* vol. 102, no. 5, pp. 7-26, 2005.

[105] D. Bender, “Flywheelrs,” Sandia National Laboratories, 2015.

[106] T. Porsinger, P. Janik, Z. Leonowicz and R. Gono, “Modelling and Optimization in Microgrids,” *energies,* vol. 523, no. 10, p. 22, 2017.

[107] A. Mohd, E. Ortjohann, A. Schmelter, N. Hamsic and D. Morton, “Challenges in Integrating Distributed Energy Storage Systems into Future Smart Grid,” in *2008 IEEE International Symposium on Industrial Electronics*, Cambridge, UK, 2008.

[108] G. Shahgholian, “A brief review on microgrids: Operation, Application, modelling and control,” *Jhon Wiley and Sons,* vol. 31, p. 28, 2021.

[109] L. Mariam, M. Basu and M. F. Conlon, “Microgrid: Architecture, policy and future trends,” *Renewable and Sustainable Energy Reviews,* no. 64, pp. 477-489, 2016.

[110] United Nations, “The Paris Agreement,” United Nations Climate Change, Paris, 2015.

[111] HivePower, “The Rise of Microgrids in Developing Countries,” Hive Power, 18 01 2021. [Online]. Available: https://hivepower.tech/the-rise-of-microgrids-in-developing-countries/. [Accessed 24 07 2021].

[112] R. J. Shah and N. Chandrasekaran, “Why microgrids are key to solving energy poverty worldwide,” Fortune, 21 01 2020. [Online]. Available: https://fortune.com/2020/01/21/microgrids-energy-poverty-africa-asia/. [Accessed 24 07 2021].

[113] (C2ES) Center for Climate and Energy Solutions (C2ES), “Microgrids,” (C2ES) Center for Climate and Energy Solutions (C2ES), [Online]. Available: https://www.c2es.org/content/microgrids/. [Accessed 24 07 2021].

[114] F. Lambert, “Tesla has over 120 operational microgrids around the world,” electrik, 19 10 2020. [Online]. Available: https://electrek.co/2020/10/19/tesla-120-operational-microgrids-world/. [Accessed 24 07 2021].

[115] G. Kariniotakis, “More Microgrids Project,” Centre for Energy and Processes, MINES-Paris Tech, Paris, 2010.

[116] M. A. Jirdehi, V. S. Tbar, S. Ghassemzadeh and S. Tohidi, “Different aspects of microgrid management: A comprehensive review,” *Journal of Energy Storage,* no. 30, p. 101457, 2020.

[117] K. S. Rajesh, S. S. Dash, R. Rajagopal and R. Sridhar, “A review on control of ac microgrid,” *Renewable and Sustainable Energy Reviews,* no. 71, pp. 814-819, 2017.

[118] T. S. Ustun, C. Ozansoy and A. Zayegh, “Recent development in microgrids and exampl cases around the world - A review,” *Renewable and sustainable energy reviews,* vol. 15, pp. 4030-4041, 2011.

[119] E. Hossain, E. Kabalci, R. Bayindir and R. Perez, “Mocrogrid testbeds around the world: State of art,” *Energy conversion and management,* vol. 86, pp. 132-153, 2014.

[120] M. Soshinskaya, W. H. Crijns-Graus, J. M. Guerrero and J. C. Vasquez, “Microgrids: Experiences, barriers and success factors,” *Renewable and sustainable energy reviews,* vol. 40, pp. 659-672, 2014.

[121] O. Palizban and K. Kauhaniemi, “Hierarchical control structure in microgrids with distributed generation: Island and grid-connected mode,” *Renewable and Sustainable Energy Reviews,* no. 44, pp. 797-813, 2015.

[122] S. Marzal, R. Salas, R. Gonzalez-Medina, G. Garcera and E. Figueres, “Current challenges and future trends in the field of communication architectures for microgrids,” *Renewable and Sustainable Energy Reviews,* no. 82, pp. 3610-3622, 2018.

[123] L. Mariam, M. Basu and M. F. Conlon, “Microgrid: Architecture, policy and future trends,” *Renewable and Sustainable Energy,* no. 64, pp. 477-489, 2016.

[124] “Mix-mode energy management strategy and battery sizing for economic operation of grid-tied microgrid,” *Energy,* no. 118, pp. 1322-1333, 2017.

[125] L. Lu, W. Yuan, C. Su, P. Wang, C. Cheng, D. Yan and Z. Wu, “Optimization model for the short-term joint operation of a grid-connected wind-photovoltaic-hydro hybrid energy system with cascade hydropower plants,” *Energy Conversion and Management,* no. 236, p. 114055, 2021.

[126] A. Alzahrani, M. Ferdowsi, P. Shamsi and C. H. Dagli, “Modeling and Simulation of Microgrid,” in *omplex Adaptive Systems Conference with Theme: Engineering Cyber Physical Systems, CAS*, Chicago, 2017.

[127] T. L. Vnadoorn, J. D. De Koonin, B. Meersman and L. Vandevelde, “Review of primary control strategies for islanded microgrids with power-electronic interfaces,” *Renewable and Sustainable Energy Reviews,* no. 19, pp. 613-628, 2013.

[128] H. M. Andishgar, E. Gholipour and R.-A. Hooshmand, “An overview of control approaches of inverter-based microgrids in islanding mode of operation,” *Renewable and Sustainable Energy Reviews,* no. 80, pp. 1043-1060, 2017.

[129] N. Hatziargyriou, Microgrids: Architectures and Control, Wiley-IEEE Press, 2014.

[130] M. S. Mahmoud, Advanced Control Methods and Renewable Energy System Integration, Elsevier Ltd., 2017.

[131] I. Patrao, E. Figueres, G. Garcera and R. Gonzalez-Medina, “Microgrid architectures for low voltage distributed generation,” *Renewable and Sustainable Energy Reviews,* no. 43, pp. 415-424, 2015.

[132] M. S. Mahmoud, “Chapter 1: Microgrid Control Problems and Related Issues,” in *Microgrids:Advanced Control Methods and Renewable Energy System Integration*, Elsevier Ltd, 2017, pp. 1-42.

[133] M. E. Amiryar and K. E. Pullen, “Assessment of the Carbon and Cost Savings of a Combined Diesel Generator, Solar Photovoltaic, and Flywheel Energy Storage Islanded Grid System,” *Energies,* no. 12, p. 25, 2019.

[134] A. K. Arani, H. Karami, G. Gharehpetian and M. Hejazi, “Review of Flywheel Energy Storage Systems structures and applications in power systems and microgrids,” *Renewable and Sustainable Energy Reviews,* vol. 69, pp. 9-18, 2017.

[135] A. Soomro, K. R. Pullen and M. E. Amiryar, “Hybrid PV System with High Speed Flywheel Energy Storage for Remote Residential Loads,” *Clean Technologies,* vol. 3, no. 2, pp. 351-376, 2021.

[136] G. Boukettaya and L. Krichen, “A dynamic power management strategy of a grid connected hybrid generation system using wind, photovoltaic and Flywheel Energy Storage System in residential applications,” *Energy,* vol. 71, pp. 148-159, 2014.

[137] F. Diaz-Gonzalez, A. Sumper, O. Gomis-Bellmunt and F. D. Bianchi, “Energy management of flywheel-based energy storage device for wind power smoothing,” *Applied Energy,* no. 110, pp. 207-219, 2013.

[138] P. Poggi, M. Perrin, P. Serre-Combe and M. Muselli, “Using a flywheel associated to PV power plant in order to increase the integration of PV into island electrical grid,” in *International Conference on Renewable Energies and Power Quality (ICREPQ’13)*, Bilbao Spaind, 2013.

[139] R. Sebastian and R. P. Alzola, “Flywheel energy storage systems: Review and simulation for an isolated wind power system,” *Renwable and Sustainable Energy Reviews,* no. 16, pp. 6803-6813, 2012.

[140] M. Moncecchi, C. Brivio, S. Maandelli and M. Merlo, “Battery Energy Storage Systems in Microgrids: Modeling and Design Criteria,” *energies,* no. 13, p. 2006, 2020.

[141] A. C. Luna, N. L. Diaz, M. Graells, J. C. Vasquez and J. M. Guererro, “Mixed-Integer-Linear-Programming-Based Energy Management System for Hybrid PV-Wind-Battery Microgrids: Modeling, Design, and Experimental Verification,” *IEEE Transactions on Power Electronics,* vol. 32, no. 4, pp. 2769-2783, 2017.

[142] U. Akram, M. Khalid and S. Shafiq, “An Innovative Hybrid Wind-Solar and Battery-Supercapacitor Microgrid System—Development and Optimization,” *IEEE Access,* vol. 5, pp. 25897-25912, 2017.

[143] P. K. Dash, P. Nayak, P. Satapathy and L. Tripathy, “Optimal control of PV–WS battery-based microgrid using an adaptive water cycle technique,” *Springer,* vol. 102, pp. 2193-2210, 2020.

[144] K. Gholami and S. Jazebi, “Energy demand and quality management of standalone diesel/PV/battery microgrid using reconfiguration,” *International Transactions on Energy Systems,* no. 30, p. 12550, 2020.

[145] S. Vasantharaj, V. Indraandhi, V. Subramaniyaswamu, Y. Teekaraman, R. Kuppusamy and S. Nikolovski, “Efficient Control of DC Microgrid with Hybrid PV—Fuel Cell and Energy Storage Systems,” *Energies,* vol. 11, no. 14, p. 3234, 2021.

[146] W. Bai, M. R. Abedi and K. Y. Lee, “Distributed generation system control strategies with PV and fuel cell in microgrid operation,” *Control Engineering Practice,* vol. 53, pp. 184-193, 2016.

[147] Z. Behrooz, “Equivalent model parameter estimation of grid-connected fuel cell-based microgrid,” *International transactions on electrical energy systems,* vol. 28, no. 6, pp. 2050-7038, 2018.

[148] Z. Liang, Y. Qin, F. Wu, Y. Llu, K. Ll and S. Berti , “Standalone condition diagnosing of fuel cell in microgrid composed of wind turbine/fuel cell/combined heat & power using Variational Mode

Decomposition analysis model," *International Journal of Hydrogen Energy,* vol. 43, no. 39, pp. 18452-18462, 2018.

[149] F. Cinhoz, A. Elrayyah and Y. Sozer, "Optimized Resource Management for PV–Fuel-Cell-Based Microgrids Using Load Characterizations," *IEEE Transactions on Industry Applications,* vol. 52, no. 2, pp. 1723-1735, 2015.

[150] K. Honghai and W. Zhengqiu, "Research of Super Capacitor Energy Storage System Based on DG Connected to Power Grid," in *2009 International Conference on Sustainable Power Generation and Supply*, Nanjing, China, 2009.

[151] N. Lidula and A. D. Rajapakse, "Mrogrids research: A review of experimental microgrids and test systems," *Renewable and Sustainable Energy Reviews,* no. 15, pp. 186-202, 2011.

[152] S. H. Chae, G. H. Kim, Y.-J. Choi and E.-H. Kim, "Design of Isolated Microgrid System Considering Controllable EV Charging Demand," *Sustainability,* no. 12, p. 9746, 2020.

[153] F. Wu, Y. Zhou, D. Feng, Y. Shi, T. Lei and C. Fang, "Day-Ahead Scheduling of a Microgrid-Like Fast Charging Stations," in *2019 IEEE 3rd International Electrical and Energy Conference (CIEEC)*, Beijing, 2019.

[154] M. F. Shaaban, S. Mohamed, M. Ismail, K. A. Qaraqe and E. Serpedin, "Joint Planning of Smart EV Charging Stations and DGs in Eco-Friendly Remote Hybrid Microgrids," *IEEE Trans. Smart Grid,* no. 10, pp. 5819-5830, 2019.

[155] Y. Li, P. Han, J. Wang and X. Song, "Modeling and optimization oriented to the micro-grid-EV joint system," in *12th International Conference on Natural Computation, Fuzzy Systems and*, Changsha, 2016.

[156] R. D. Mistry, F. T. Eluyemi and T. M. Masau, "Impact of aggregated EVs charging station on the optimal scheduling of battery storage system in islanded microgrid," in *In Proceedings of the 2017 North American Power Symposium (NAPS)*, Morgantown, 2017.

[157] N. Agarwal, A. Kumar and Varun, "Optimization of grid independent hybrid PV–diesel–battery system forpowergeneration in remote villages of Uttar Pradesh, India," *Energy for Sustainable Development,* vol. 17, pp. 210-219, 2013.

[158] A. Chauhan and R. P. Saini, "Techno-economic optimization based approach for energymanagement of a stand-alone integrated renewable energy system forremote areas of India," *Energy,* vol. 94, pp. 138-156, 2016.

[159] K. Kusakana and H. J. Vermaak, "Hybrid diesel generator/renewable energy system performance," *Renewable Energy,* vol. 67, pp. 97-102, 2014.

[160] K. V. Vidyanandan, "Frequency regulation in a wind–diesel powered microgrid using flywheels and fuel cells," *IET Generation, Transmission & Distribution,* vol. 10, no. 3, pp. 780-788, 2015.

[161] M. B. Khan, R. Jidin, J. Pasupuleti and S. A. Shaaya, "Optimal combination of solar, wind, micro-hydro and diesel systemsbased on actual seasonal load profiles for a resort island in the SouthChina Sea," *Energy,* vol. 82, pp. 80-97, 2015.

[162] T. Khatib, A. Mohamed, K. Sopian and M. Mahmoud, “Optimal sizing of building integrated hybrid PV/diesel generator system for zero load rejection for Malaysia,” *Energy and Buildings,* vol. 43, no. 12, pp. 3430-3435, 2011.

[163] M. M. Rahman, M. M.-U.-H. Khan, M. A. Ullah, Z. Zhang and a. Kumar, “A hybrid renewable energy system for a North American off-grid community,” *Energy,* vol. 97, pp. 151-160, 2016.

[164] L. M. Halabi, S. Mekhile, L. Olatomiwa and J. Hazelton, “Performance analysis of hybrid PV/diesel/battery system using HOMER: A case study Sabah, Malaysia,” *Energy Conversion and Managment,* vol. 144, no. 15, pp. 322-399, 2017.

[165] M. S. Adaramola, M. Angelin-Chaab and S. S. Paul, “Analysis of hybrid energy systems for application in southern Ghana,” *Energy Conversion and Management,* vol. 88, pp. 284-298, 2014.

[166] J. Schmedt, R. Cancella and A. O. Jr. Pereira, “An optimal mix of solar PV, wind and hydro power for a low-carbon electricity supply in Brazil,” *Renewable Energy,* vol. 85, pp. 137-147, 2016.

[167] B. Yildirim, “Gain and phase margins based stability region analysis of time-delayed shipboard microgrid with sea wave energy,” *IET Electric ower Applications,* vol. 14, no. 8, pp. 1347-1359, 2020.

[168] R. Shelke and D. Dighole, “A Review paper on Dual Mass Flywheel system,” *International Journal of Science, Engineering and Technology Research,* vol. 5, no. 1, 2016.

[169] G. Genta, Kinetic Energy Storage: Theory and Practice of Advanced Flywheel System, London, UK, 1985.

[170] M. Aneke and M. Wang, “Energy storage technologies and real life applications – A state of the art review,” *Applied Energy,* no. 179, pp. 350-377, 2016.

[171] B. Bolund, H. Bernhoff and M. Leijon, “Flywheel energy and power storage systems,” *Renewable and Sustainable Energy Reviews,* no. 11, pp. 235-258, 2007.

[172] H. Liu and J. Jiang, “Flywheel energy storage—An upswing technology for Energy Sustainability,” *Energy and Buildings,* vol. 39, pp. 599-604, 2006.

[173] M. E. Amiryar, *PhD thesis: An Assessment of Flywheel Storage for Efficient Provision of Reliable Power for Residential Premises in Islanded Operation,* London: City University of London, 2019.

[174] M. E. Amiryar and K. R. Pullen, “A review of flywheel energy storage system technolpgoes and their applications,” *Applied Science,* vol. 7, no. 286, 2017.

[175] M. E. Amiryar and K. R. Pullen, “High Speed Flywheels,” London, 2021.

[176] S. Mousavi G, F. Faraji, A. Majazi and K. Al-Haddad, “A comprehensive review of Flywheel Energy Storage System technology,” *Renewable and Sustainable Energy Reviews,* vol. 67, pp. 477-490, 2017.

[177] H. Hofmann, “PhD Thesis: High-speed synchronous reluctance machine for flywheel applications,” UNIVERSITY of CALIFORNIA, BERKELEY, 1998.

[178] B. Schweighofer, M. Recheis, P. Fulmek and H. Wegleiter, “Rotor Losses in a Switched Reluctance Motor - Analysis and Reduction Methods,” *EPJ Web of Conferences,* pp. 1-4, 2013.

[179] “A Flexible Mathematical Model for Dissimilar Operating Modes of a Switched Reluctance Machine,” *IEEE Access,* vol. 6, pp. 9643-9649, 2018.

[180] D. A. Torrey, “Switched Reluctance Generators and Their Control,” *IEEE TRANSACTIONS ON INDUSTRIAL ELECTRONICS,* vol. 49, no. 1, pp. 3-14, 2002.

[181] M. Hedlund, T. Kamf, J. de Santiago, J. Abrahamsson and H. Bernhoff, “Reluctance Machine for a Hollow Cylinder Flywheel,” *Energies,* vol. 10, no. 316, 2016.

[182] T. Siostrzonek and S. Pirog, “The Flywheel Energy Storage with Brushless DC Motor - the Practical Results,” in *12th International Power Electronics and Motion Control Conference*, 20016.

[183] H. Hofmann, W. Wang and C. E. Bakis, “Ultrahigh Speed Permanent Magnet Motor/Generator for Aerospace Flywheel Energy Storage Applications,” in *IEEE International Conference on Electric Machines and Drives*, 2005.

[184] A. Nagorny, N. Dravid, R. Jansen and B. Kenny, “Design Aspects of High Speed Permanent Magnet Synchronous Motor/Generator for Flywheel Applications,” in *IEEE International Conference on Electric Machines and Drives*, 2005.

[185] D. Gerada, A. Mebarki, N. L. Brown, C. Gerada, A. Cavagnino and A. Bolglietti, “High-Speed Electrical Machines: Technologies,,” *IEEE TRANSACTIONS ON INDUSTRIAL ELECTRONICS Trends, and Developments,* vol. 61, no. 6, pp. 2946-2957, 2014.

[186] S. Derammelare, M. Haemers, J. D. Viane, F. Verbelen and K. Stockman, “A quantitative comparison between BLDC, PMSM, Brushed DC and stepping motor technology,” *CORE.*

[187] R. Pena-Alzola, R. Sebastian, J. Quesada and A. Colmenar, “Review of Flywheel based Energy Storage Systems,” in *2011 International Conference on Power Engineering, Energy and Electrical Drives*, Malaga, 2011.

[188] L. Huang, J. Feng, S. Guo, J. Shi and Z. Q. Zhu, “Analysis of power factor in variable flux reluctance machine with MMF-permeane model,” *IET Electric Power Applications,* vol. 10, no. 1049, 2018.

[189] S. J. Amodeo, A. E. León, H. G. Chiacchiarini, J. A. Solsona and C. A. Busada, “Non linear Control Strategies of a Flywheel driven by a Synchronous Homopolar Machine,” Universidad Nacional del Sur and CONICET.

[190] P. Tsao, M. Senesky and S. Sanders, “A synchronous homopolar machine for high-speed applications,” in *2002 IEEE Industry Applications Conference. 37th IAS Annual Meeting (Cat. No.02CH37344)*, Pittsburgh, PA, USA, 2002.

[191] A. A. K. Arani, B. Zaker and G. B. Gharehpetian, “Induction machine-based flywheel energy storage system modeling and control for frequency regulation after micro-grid islanding,” *Int Trans Electr Energ Syst.,* pp. 1-12, 2017.

[192] E. Severson, R. Nilssen and T. Undeland, “Magnetic Equivalent Circuit Modeling of the AC Homopolar Machine for Flywheel Energy Storage,” *IEEE TRANSACTIONS ON ENERGY CONVERSION,* vol. 30, no. 4, 2015.

[193] C. Ye, J. Yang, F. Xiong and Q. Z. Zhu, “Relationship Between Homopolar Inductor Machine and Wound-Field Synchronous Machine,” *IEEE TRANSACTIONS ON INDUSTRIAL ELECTRONICS,* vol. 67, no. 2, p. 12, 2020.

[194] A. Soomro, M. Amiryar E, K. R. Pullen and D. Nankoo, “Comparison of performance and controlling schemes of synchronous and induction machines used in flywheel enregy storage systems,” *Energy Procedia,* vol. 151, pp. 100-110, 2018.

[195] Z. Q. Zhu and D. Howe, “Electrical Machines and Drives for Electric, Hybrid, and Fuel Cell Vehicles,” *Proceedings of IEEE,* vol. 95, no. 4, pp. 746-765, 2007.

[196] M. Amiryar E and K. R. Pullen, “A Review of Flywheel Energy Storage System Technologies and Their Applications,” *Applied Sciences,* no. 7, p. 286, 2017.

[197] R. Nilsen, T. Undeland and N. Mohan, “Suspension Force Model for Bearingless AC Homopolar Machines Designed For Flywheel Energy Storage,” in *2013 IEEE GCC Conference and exhibition*, Doha, 2013.

[198] M. N. Recheis, B. Schweighofer, P. Fulmek and H. Wegleiter, “Selection of Magnetic Materials for Bearingless High-Speed Mobile Flywheel Energy Storage Systems,” *IEEE Transactions on Magnetics,* vol. 50, no. 4, 2014.

[199] W. Li, K. T. Chau, T. W. Ching, Y. Wang and M. Chen, “Design of a High-Speed Superconducting Bearingless Machine for Flywheel Energy Storage Systems,” *IEEE Transactions on Applied Superconductivity,* vol. 25, no. 3, 2015.

[200] M. A. Awadullah and B. Venkatesh, “Energy Storage in Flywheels: An Overview,” *Canadian Journal of Electrical and Computer Engineering,* vol. 38, no. 2, pp. 183-193, 2015.

[201] Y. Yuan, Y. Sun, Q. Xiang, Y. Ren and Q. Liu, “The study of switched reluctance motor for 4-DOF bearingless motor,” *Journal of Electrical Engineering & Technology,* vol. 14, pp. 179-189, 2019.

[202] E. Severson, NilssenRober, T. Undeland and N. Mohan, “Suspension Force Model for Bearingless AC Homopolar Machines Designed For Flywheel Energy Storage,” in *2013 IEEE GCC Conference and exhibition, November 17-20*, Doha, Qatar, 2013.

[203] G. G. Sotelo, R. d. Andrade and A. C. Ferreira, “Magnetic Bearing Sets for a Flywheel System,” *IEEE TRANSACTIONS ON APPLIED SUPERCONDUCTIVITY,* vol. 17, no. 2, pp. 2150-2153, 2007.

[204] H. Liu and J. Jiang, “Flywheel energy storage—An upswing technology,” *Energy and Buildings,* vol. 39, pp. 599-604, 2007.

[205] M. Ren, Y. Shen, Z. Li and K. Nonami, “Modeling and Control of a Flywheel Energy Storage System Using Active Magnetic Bearing for Vehicle,” in *2009 International Conference on Information Engineering and Computer Science*, Wuhan, China, 2009.

[206] S. S. Shah, “PhD Thesis: The Design and Development of a High Speed Composite Flywheel for Hybrid Vehicles,” Imperial College London, London, 2006.

[207] F. Thoolen, *Development of an advanced high speed flywheel energy storage system Eindhoven,* Technische Universiteit Eindhoven, 1993.

[208] Adams and L. J. Maurice, Bearings - Basic Concepts and Design Applications, CRC Press, 2018.

[209] A. Olabi, T. Wilberforce, M. A. Abdelkareem and M. Ramadan, “Critical Review of Flywheel Energy Storage System,” *Energies,* vol. 14, p. 2159, 2021.

[210] A. Ruddell, “Investigation on Storage Technologies for Intermittent Renewable Energies: Evaluation and recommended R&D strategy,” CCLRC-Rutherford Appleton Laboratory Chilton, Didcot, 2003.

[211] G. G. Sotelo, E. Rodriguez, F. S. Costa, J. G. Oliveira, J. d. Santiago and R. M. Stephan, “Tests with a hybrid bearing for a flywheel energy storage system,” *Superconductor Science and Technology,* vol. 29, no. 9, 2016.

[212] K. Nagashina, H. Seino, N. Sakai and M. Murakami, “Superconducting magnetic bearing for a flywheel energy storage system using superconducting coils and bulk superconductors,” *Physica C,* vol. 469, pp. 1244-1249, 2009.

[213] C. Zhang and K. Jet Tseng, “A Novel Flywheel Energy Storage System With Partially-Self-Bearing Flywheel-Rotor,” *IEEE Transactions on Energy Conversions,* vol. 22, no. 2, pp. 477-487, 2007.

[214] Y. Qiu and H. Ding, “Flywheel Energy Storage System with PermanentMagnetic Bearing and Spiral Groove Bearing,” in *8th International Conference on Mechanical and Intelligent Manufacturing Technologies*, Cape Town, South Africa, 2017.

[215] S. Jian and Y. Qiu, “Reducing friction power losses of flywheel energy storage systems using PTFE composites: A technical note,” *J Engineering Tribology,* vol. 233, no. 10, p. 6, 2019.

[216] G. O. Cimuca, C. Saudemont, B. Robyns and M. R. Radulescu, “Control and Performance Evaluation of a Flywheel Energy-Storage System Associated to a Variable-Speed Wind Generator,” *IEEE Transactions on Inductrial Electronics,* vol. 53, no. 4, 2006.

[217] T. Friedli, J. W. Kolar, J. Rodriguez and P. W. Wheeler, “Comparative Evaluation of Three-Phase AC–AC Matrix Converter and Voltage DC-Link Back-to-Back Converter Systems,” *IEEE Transactions on Inductrial Electronics,* vol. 59, no. 12, 2012.

[218] B. Wang and G. Venkataramanan, “Dynamic Voltage Restorer Utilizing a Matrix Converter and Flywheel Energy Storage,” *IEEE Transactions on Industry Applications,* vol. 45, no. 1, 2009.

[219] A. A. K. Arani, H. Karami, G. B. Gharehpetian and M. Hejazi, “Review of Flywheel Energy Storage Systems structures and applications in power systems and microgrids,” *Renewable and Sustainable Energy Reviews,* no. 69, pp. 9-18, 2017.

[220] A. Alias, A. R. Nasrudin and M. A. Hussain, “Bidirectional Three Phase Power Converter,” in *2011 IEEE First Conference on Clean Energy and Technology CET*, 2011.

[221] J. Oliveria, H. Schettino, V. Gamma, R. Carvalho and H. Bernhoff, “Implementation and Control of an AC/DC/AC Converter for Double Wound Flywheel Application,” *Advances in Power Electronics,* p. 8, 2012.

[222] A. Elserougi, A. M. Massoud and S. Ahmed, “Flywheel energy storage system based on boost DC-AC converter,” in *IET Conference on Renewable Power Generation (RPG 2011)*, 2011.

[223] S. R. Gurumurthy, V. Agarwal and A. Sharma, “High-Efficiency Bidirectional Converter for Flywheel Energy Storage Application,” *IEEE Transactions on Industrial Electronics,* vol. 63, no. 9, 2016.

[224] M. I. Nassedf, A. H. Ashour and H. Desouki, “Battery-less hybrid micro-grid power management using bi-directional three phase power converter,” in *2015 IEEE First International Conference on DC Microgrids (ICDCM)*, Atlanta, GA, 2015.

[225] X. Zheng, F. Goa, H. Ali and H. Liu, “A droop control based three phase bidirectional AC-DC converter for more electric aircraft applications,” *Energies,* vol. 10, no. 3, 2017.

[226] V. Babuska, S. M. Beatty, B. J. deBlonk and J. L. Fausz, “A Review of Technology Developments in Flywheel Attitude Control and Energy Transmission Systems12,” *2004 IEEE Aerospace Conference Proceedings,* 2004.

[227] C. S. Hearn, “PhD Thesis: Design Methodologies for Advanced Flywheel Energy Storage,” The University of Texas at Austin, Texas, 2013.

[228] P. Fairley, “Flywheels keep the grid in tune,” *IEEE Spectrum,* vol. 48, no. 7, pp. 16-18, 2011.

[229] M. Kheawcun and S. Sangwongwanish, “A Case Study on Flywheel Energy Storage System Application for Frequency Regulation of Islanded Amphoe Mueang Mae Hong Son Microgrid,” in *17th International Conference on Electrical Engineering/Electronics, Computer, Telecommunications and Information Technolog*, 2020.

[230] A. Colthrope, “Flywheel-lithium battery hybrid energy storage system joining Dutch grid services markets,” Energy Storage NEWS, 2 September 2020. [Online]. Available: https://www.energy-storage.news/news/flywheel-lithium-battery-hybrid-energy-storage-system-joining-dutch-grid-se. [Accessed 21 Feb 2021].

[231] M. Hedlund, J. Lundin, J. d. Santiago, J. Abrahamsson and H. Bernhoff, “Flywheel Energy Storage for Automotive Applications,” *energies,* vol. 8, p. 28, 2015.

[232] J. Kho, “Pentadyne Spins $22M for Flywheels,” greentechmedia, 23 09 2008. [Online]. Available: https://www.greentechmedia.com/articles/read/pentadyne-spins-22m-for-flywheels-1458. [Accessed 23 04 2021].

[233] “Kinetic Traction Systems,” Kinetic Traction, [Online]. Available: https://kinetictraction.com/flywheel-energy-storage-applications/. [Accessed 23 04 2021].

[234] D. Townley, “Introducing Pentadyne Power Flywheel Energy Storage System,” Sandia Laboratories.

[235] ABB, “Renewable microgrid stabilization,” ABB, Madrid, 2017.

[236] GE, “Flywheel UPS Systems 50-1000kVA using TLE or SG series UPS,” General Electric, Plano, 2016.

[237] M. Lafoz, J. Santiago and I. Etxaniz, “KINETIC ENERGY STORAGE BASED ON FLYWHEELS: BASIC CONCEPTS, STATE OF THE ART AND ANALYSIS OF APPLICATION,” EUROPEAN ENERGY RESEARCH ALLIANCE, 2013.

[238] Beacon Power, “Stephentown, New York,” Beacon Power, 2018. [Online]. Available: https://beaconpower.com/stephentown-new-york/. [Accessed 21 08 2021].

[239] H. S. LLC, “20 MW Flywheel Frequency Regulation Plant,” Hazle Spindle, LLC, Pennsylvania, 2016.

[240] C. K. Das, O. Bass, G. Kothapalli, T. s. Mahmoud and D. Habibi, “Overview of energy storage systems in distribution networks: Placement,sizing, operation and power quality,” *Renewable and Sustainable Energy,* no. 91, pp. 1205-1230, 2018.

[241] G. O. Suvire, M. G. Molina and E. P. Mercado, “Improving the Integration of Wind Power Generation Into AC Microgrids Using Flywheel Energy Storage,” *IEEE Transactions on Smart Grids,* vol. 3, no. 4, p. 10, 2012.

[242] R. Sebastian and R. P. Alzola, “Flywheel energy storage systems Review and simulation for an isolated wind power system,” *Renewable and Sustainable Energy Reviews,* no. 16, pp. 6803-6813, 2012.

[243] *Coral Bay wind/diesel/PowerStore Western Australia,* 2012.

[244] T. Richard, R. Belhomme, N. Buchheit and F. Gorgette, “Power quality improvement-Case study of the connection of four 1.6MVA flywheel dynamic UPS system to a medium voltage distribution network,” in *2001 IEEE/PES Transmission and Distribution Conference and Exposition*, Atlanta, GA, USA, 2001.

[245] K. Shuhei, C. Miao-miao, S. Hideo and S. Ryuichi, “Semiconductor Power Converterless Voltage Sag Compensator and UPS Using a Flywheel Induction Motor and an Engine Generator,” in *Power Conversion Conference*, Nagoya, Japan, 2007.

[246] N. Kimura, M. Sonoda, T. Morizane, K. Taniguchi and F. Kurokawa, “Emergency Power Supply using Flywheel and Doubly Fed Induction Generator,” in *INTELEC 2009 - 31st International Telecommunications Energy Conference*, Icheaon, South Korea, 2009.

[247] Offioes, “5 MW Flywheel energy storage,” [Online]. Available: [1] Offioes, "5 MW Flywheel Energy Storage," 26 02 2021. [Online]. Available: https://www.stantec.com/en/projects/canada-projects/g/guelph-hydro-arlen-transformer-station-5mw-flywheel-energy-storage.. [Accessed 26 02 2021].

[248] “Backup Power/UPS,” VYCON, [Online]. Available: https://vyconenergy.com/products/ups/.. [Accessed 26 02 2021].

[249] “Energy Storage Flywheels and Battery Systems,” PILLER, [Online]. Available: https://www.piller.com/en-GB/183/energy-storage. [Accessed 26 02 2021].

[250] “Active Power's Storage Flywheel Technology,” Active Power, [Online]. Available: https://www.activepower.com/en-GB/2813/flywheel-technology. [Accessed 26 02 2021].

[251] S. Samineni, B. K. Johnson, H. L. Hess and J. D. Law, “Modeling and Analysis of a Flywheel Energy Storage Systems for Voltage Sag Correction,” *IEEE Transactions,* vol. 42, no. 1, p. 11, 2006.

[252] J. Zhang, Z. Chen and Y. Zhai, “Flywheel Energy Storage System Design for Distribution Network,” in *2000 IEEE Power Engineering Society Winter Meeting*, Singapore, 2000.

[253] L. Zhou and Z. Qi, “Modeling and simulation of flywheel energy storage system with IPMSM for voltage sags in distributed power network,” in *2009 International Conference on Mechatronics and Automation*, Changchun, China, 2009.

[254] R. Hebner, J. Beno and A. Walls, “Flywheel Batteries Come Around Again,” *IEEE Spectrum,* vol. 39, no. 4, 2003.

[255] R. J. Hayes, J. P. Kajs, R. C. Thompson and J. H. Beno, “Design and Testing of a Flywheel Battery for a Transit Bus,” *Society of Automotive Engineers, Inc,* p. 10, 1999.

[256] J. Hilton, “Mechanical Hybrid Systems,” in *Engine Expo 2008*, Stuttgart Messe, Stuttgart Germany, 2008.

[257] J. Rendell, “Jaguar's advanced XF 'flybrid,” AutoCar, 17 09 2010. [Online]. Available: https://www.autocar.co.uk/car-news/concept-cars/jaguars-advanced-xf-flybrid. [Accessed 27 02 2021].

[258] G. Richards, “Audi is first manufacturer to take Le Mans 24 Hours race with hybrid,” The Guardian, 17 june 2012. [Online]. Available: https://www.theguardian.com/sport/2012/jun/17/audi-le-mans-24-hours-race. [Accessed 27 02 2021].

[259] B. Howard, “Volvo hybrid drive: 60,000 rpm flywheel, 25% boost to mpg,” Extreme Tech, 29 04 2013. [Online]. Available: https://www.extremetech.com/extreme/154405-volvo-hybrid-drive-60000-rpm-flywheel-25-boost-to-mpg. [Accessed 27 02 2021].

[260] “911 GT3 R Hybrid Celebrates World Debut in Geneva,” Porsche, 02 11 2010. [Online]. Available: https://www.porsche.com/usa/aboutporsche/pressreleases/pag/?id=2010-02-11&pool=international-de. [Accessed 27 02 2021].

[261] M. B. Richardson, “Flywheel energy storage system for traction applications,” in *2002 International Conference on Power Electronics, Machines and Drives*, Sante Fe, NM, USA, 2002.

[262] “Vycon Allows the LA Metro to Achieve Nearly 20 Percent in Rail Energy Savings,” Mass Transit, 31 10 2014. [Online]. Available: https://www.masstransitmag.com/rail/press-release/12015255/vycon-vycon-technology-allows-the-la-metro-to-be-the-first-transit-agency-in-us-using-flywheels-to-achieve-nearly-20-percent-in-rail-energy-savings. [Accessed 27 02 2021].

[263] A. M. Gee and R. W. Dunn, “Analysis of Trackside Flywheel Energy Storage in Light Rail Systems,” *IEEE Transactions on Vehicular Technologyu,* vol. 64, no. 9, pp. 3858-3870, 2015.

[264] L. V. Truong, F. J. Wolff and N. V. Dravid, “Simulation of a flywheel electrical system for aerosapce applications,” Glen Research Center, Ohio, 2000.

[265] J. Edwards, D. A. Christopher, J. W. Aldrich, R. F. Beach and J. R. Barton, “Flight Test Demonstration of a Flywheel Energy Storage System on the International Space Station,” in *Proceedings of the IEEE 1997 National Aerospace and Electronics Conference. NAECON 1997*, Dayton, OH, USA, 1997.

[266] B. H. Kenny, P. E. Kascak, R. Jansen, T. Dever and W. Santiago, “Control of a High-Speed Flywheel System for Energy Storage applications,” *IEEE Transactions on Industry Applications,* vol. 41, no. 4, 2015.

[267] K. Aydin and M. T. Aydemir, “A control algorithm for a simple flywheel enrgy storage system to be used in space applications,” *Turkish Journal of Electrical Engineering & Computer Sciences,* vol. 21, pp. 1328-1339, 2013.

[268] K. Aydin and M. T. Aydemir, “Sizing design and implementation of a flywheel energy stoage system for space applications,” *Turkish Journal of Electrical Engineering & Computer Sciences,* vol. 24, pp. 793-806, 2016.

[269] K. H. Barbara, P. E. Kascak, H. Heath, M. Mackin, S. Walter and R. Jansen, “Advanced Motor Control Test Facility for NASA GRC Flywheel Energy Storage System Technology Development Unit,” in *36th Intersociety Energy Conversion Engineering Conference*, Savannah, GA, 2013.

[270] E. Lee, “A micro HTS renewable energy/attitude control system for micro/nano satellites,” *IEEE Transactions on Applied Superconductivity,* vol. 13, no. 2, pp. 2263-2266, 2003.

[271] D. Lamsal, V. Sreeram, Y. Mishra and D. Kuamr, “Output power smoothing control approaches for wind and photovoltaic generation systems: A review,” *Renewable and Sustainable Energy Reviews,* no. 113, p. 22, 2019.

[272] I. J. Iglesias, L. Garcia-Tabares, A. Agudo, L. Cruz and L. Arribas, “Design and simulation of a stand-alone wind-diesel generator with a flywheel energy storage system to supply the required active and reactive power,” in *2000 IEEE 31st Annual Power Electronics Specialists Conference. Conference Proceedings*, Galway, Ireland, 2000.

[273] N. Hamsic, A. Schmelter, A. Mohd, E. Ortjohann, E. Schultze, E. Tuckey and J. Zimmermann, “Increasing Renewable Energy Penetration in Isolated Grids Using a Flywheel Energy Storage System,” in *International Conference on Power Engineering, Energy and Electrical Drives (POWERENG)*, Portugal, 2007.

[274] R. Sebastian, M. Castro, J. Peire and F. Yeves, “Control of the Diesel-Flywheel-Synchronous Set(s) in the Hybrid Wind-Diesel System of Jandia Plant in Fuerteventura (Spain),” in *ISES 2001 Solar World Congress*, 2000.

[275] S. Faias, P. Santos, J. Sousa and R. Castro, “An Overview on Short and Long-Term Response Energy Storage Devices for Power System Applications,” in *International Conference on Renewable Energy and Power Quality*, Santander, Spain, 2008.

[276] Staff Writer, “olar + Flywheel Microgrid Saves 400,000 Litres of Diesel Annually,” Solar Quotes, 10 09 2015. [Online]. Available: https://www.solarquotes.com.au/blog/solar-flywheel-microgrid-saves-400000-litres-of-diesel-annually/. [Accessed 07 03 2021].

[277] “US Department of Energy Global Energy Storage Database,” Office of Electricity Delivery and Energy Reliability, 17 11 2020. [Online]. Available: https://www.sandia.gov/ess-ssl/global-energy-storage-database-home/. [Accessed 07 03 2021].

[278] “Microgrid stabilisation system to boost renewable energy use in Kenya,” Sustainability Matters, 07 09 2015. [Online]. Available: https://www.sustainabilitymatters.net.au/content/energy/case-study/microgrid-stabilisation-system-to-boost-renewable-energy-use-in-kenya-581638850. [Accessed 07 03 2021].

[279] A. J. Ruddell, “Flywheel energy storage technologies for wind energy systems,” Rutherford Appleton Laboratory, UK, Woodhead Publishing Limited, 2010, 2010, pp. 366-391.

[280] “Flywheel energy storage system for Rubber Tired Gantry Cranes,” Green Car Congress, 28 04 2009. [Online]. Available: https://www.greencarcongress.com/2009/04/flywheel-energy-storage-system-for-rubber-tired-gantry-cranes.html. [Accessed 19 03 2021].

[281] D. W. Swett and G. J. Blanche, “Flywheel Charging Module for Energy Storage Used in Electromagnetic Aircraft Laucnh System,” *IEEE Transaction on Magnetics,* vol. 41, no. 1, 2005.

[282] S. Hatakeyma, F. Yoshino, H. Tsutsui and S. Tsuji-lio, “Flywheel induction motor-generator for magnet power supply in small fusion device,” *Review of Scientific Instruments,* vol. 87, 2016.

[283] F. Diaz-Gonzalez, A. Sumper and O. Gomis-Bellmunt, Energy Storage in Power Systems, John Wiley and Sons Ltd, 2016.

[284] R. Östergård, Writer, *Flywheel energy storage a conceptual study.* [Performance]. Uppsala Universitet, 2011.

[285] S.-H. Kim, Electric Motor Control, Elsevier Science, 2017.

[286] Hughes, Austin, Drury and Bill, Chapter 6: Electric Motors and Drives - Fundamentals, Types and Applications (5th Edition), Elsevier, 2019.

[287] F. Giri, AC Electric Morotrs Control - Advanced Design Techniques and Applications, Chichester, West Sussex: John Wiley & Sons Ltd., 2013.

[288] M. Popescu, “Induction Machine Modelling for Vector Control Purpose,” Helsinki University of Technology - Laboratory of Electromechanics, 2000.

[289] H. Sun, Y. Ren, H. Li, Z. An, J. Liu, H. Hu and H. Liu, “DFIG Wind Power Generation Based on Back-to-back PWM Converter,” in *IEEE International Conference on Mechatronics and Automation*, 2009.

[290] L. Amezquita-Brooks, J. Liceaga-Castro and E. Liceaga-Castro, “Speed and Position Controllers Using Indirect Field-Oriented Control: A classical Control Approach,” *IEEE Transactions on Industrial Electronics,* vol. 61, no. 4, pp. 1928-1943, 2014.

[291] L. Wang, S. Chai, D. Yoo, L. Gan and K. Ng, PID and Predictive Control of Electrical Drives and Power Power Converters Using MATLAB/Simulink, Singapore: John Wiley & Sons, 2015.

[292] N. Mohan, Electric Mahines and Drives, John Wiley & Sons, 2012.

[293] X. Sheng, *Under Graduate Honors Thesis: Design and Prototyping of a Low-Speed Flywheel System for Automotive Brake Energy Recovery,* Ohio: The Ohio State University , 2012.

[294] D. M. Ionel, M. Popescu, M. I. McGlip, T. Miller, S. J. dELLINGER and R. J. Heideman, "Computation of Core Losses in Electrical Machines Using Improved Models for Laminated Steel," *IEEE Transactions on Industry Applications,* vol. 49, no. 6, pp. 1554-1564, 2007.

[295] R. Roy, K. K. Prabhakar and P. Kumar, "Core-loss calculation in different parts of Induction Machine," *IET Electric Power Applications,* vol. 11, no. 9, p. 11, 2017.

[296] P. Cogent, "Typical data for SURA® M470-50HP," Cogent Power, [Online]. Available: chrome-extension://oemmndcbldboiebfnladdacbdfmadadm/https://cogent-power.com/cms-data/downloads/m470-50hp.pdf. [Accessed 30 07 2019].

[297] S. J. Chapman, Elecrical Machinery Fundamentals, McGraw-Hill Inc., 1991.

[298] J. Pyrhonen, T. Jokinen and V. Hrabovcova, Design of Rotating Electrical Machines, Lappeenranta University of Technology, 2008.

[299] N. S. Harris, Modern vacuum practice, McGraw-Hill, 1989.

[300] S. Shah, *PhD Thesis: The design and development of a high speed composite flywheel for hybrid vehicles,* London: Imperial College London, 2006.

[301] R. A. Millikan, "Coefficients of Slip in Gases and the Law of Reflection of Molecules from the Surfaces of Solids and Liquids," *Physucal review,* vol. 217, no. 21, 1923.

[302] T. A. Harris, Rolling bearing analysis, 2007.

[303] M. Tu, *Master of Sceience Thesis: Validation and modeling of power losses of NJ 406 cylindrical roller bearings,* Stockholm: KTH Industrial Engineering and Management, 2016.

[304] SKF, "Bearing friction, power loss and starting torque," SKF, [Online]. Available: https://www.skf.com/uk/products/bearings-units-housings/principles/bearing-selection-process/operating-temperature-and-speed/friction-powerloss-startingtorque/index.html. [Accessed 02 April 2019].

[305] D. R.W, "Notes on Induction Motor Losses," *American Institute of Electrical Engineers,* vol. 32, no. 2, p. 2, 1913.

[306] J. Tamura, "Calculation Methods of Losses and Efficiency of Wind Generators," in *Wind Energy Conversion systems*, Springer, 2012, pp. 25-51.

[307] H. Karimi, H. Nikkhajoei and R. Iravani, "A Linear Quadratic Gaussian Controller for a Stand-alone Distributed Resource Unit-Simulation Case Studies," in *2007 IEEE Power Engineering Society General Meeting*, Tampa, USA, 2007.

[308] O. F. A. Sanchez, G. Reina and M. Mauledoux, “Modeling a Microgrid that Integrates Renewable Energies in IEC 61850-7-420 and IEC 61400-25-3,” *Journal of Engineering Science and Technology Review 1,* vol. 4, no. 1, pp. 174-179, 2018.

[309] “Energy management of smart micro-grid with response loads and distributed generation considering demand response,” *Journal of Cleaner Production,* vol. 197, no. 1, pp. 1069-1083, 2018.

[310] W. Hu, Z. Wu and V. Dinavahi, “Dynamic Analysis and Model Order Reduction of Virtual Synchronous Machine Based Microgrid,” *IEE Access,* vol. 1109, no. 10, pp. 106585-106600, 2020.

[311] M.-F. Bravo-Lopez, A. Garces and J.-J. Mora-Florez, “Simplified dynamic models for three-phase microgrids,” *John Wiley & Sons Ltd,* vol. 1002, no. 10, pp. 1-19, 2020.

[312] S. Sen and V. Kumar, “Microgrid modelling: A comprehensive survey,” *Annual Reviews in Control,* no. 46, pp. 216-250, 2018.

[313] W. Xiao, W. G. Dunford and A. Capel, “A novel modeling method for photovoltaic cell,” in *IEEE 35th Annual Power Electronics Specialists Conference, PESC04, Aachen, 20 June 2004 - 25 June 2004, 63911*, Vancouver, Canada, 2004.

[314] J. A. Gow and C. D. Manning, “Development of a photovoltaic array model for use in power-electronics simulation studies,” *IEE Proceesdings of Electric Power Applications,* vol. 146, no. 2, pp. 193-200, 1999.

[315] A. R. Jordehi, “Parameter estimation of solar photovoltaic (PV) cells: A review,” *Renewable and Sustainable Energy Reviews,* vol. 61, pp. 354-371, 2016.

[316] S. Benhamed, H. Ibrahim, K. Belmokhtar, H. Hosni, A. Ilinca, D. Rousse, A. Chandra and D. Ramdenee, “Dynamic Modeling of Diesel Generator Based on Electrical and Mechanical Aspects,” in *2016 IEEE Electrical Power and Energy Conference (EPEC)*, 2016.

[317] J. Keirstead and A. Sivankumar, “Using Activity-Based Modeling to SimulateUrban Resource Demands at High Spatialand Temporal Resolutions,” *Journal of Industrial Ecology,* vol. 16, no. 6, p. 12, 2012.

[318] E. J. Palacios-Garcia, A. Moreno-Munoz, I. Santiago, I. M. Moreno-Garcia and M. I. Milanes-Montero, “PV hosting capacity analysis and enhancement using high resolution stochastic modeling,” *Energies,* no. 10, p. 1488, 2017.

[319] E. McKenna and M. Thomson, “High-resolution stochastic integrated thermal–electrical domestic demand model,” *Applied Energy,* no. 165, pp. 445-461, 2016.

[320] R. Baetens, R. De Coninck, J. V. Roy, B. Verbruggen, J. Driesen, L. Helsen and D. Saelens, “Assessing electrical bottlenecks at feeder level for residential net zero-energybuildings by integrated system simulation,” *Applied Energy,* vol. 96, pp. 74-83, 2012.

[321] The MathWorks, Inc., “MATLAB/Simulink PV Array,” The MathWorks, Inc., 2021 2021a. [Online]. Available: https://uk.mathworks.com/help/physmod/sps/powersys/ref/pvarray.html?searchHighlight=PV%20ARRAY&s_tid=srchtitle. [Accessed 10 09 2021].

[322] H. Bourdoucen and A. Gastli, “Analytical Modelling and Simulation of Photovoltaic Panelsand Arrays,” *The Journal of Engineering Research ,* vol. 4, no. 1, pp. 75-81, 2007.

[323] S. Silvestre, A. Boronat and A. Chouder, “Study of bypass diodes configuration on PV modules,” *Applied Energy,* vol. 86, no. 9, pp. 1632-1640, 2009.

[324] B. K. Dey, I. Khan, N. Mnadal and A. Bhattacharjee, “Mathematical Modelling and Characteristic analysis of Solar PV Cell,” in *2016 IEEE 7th Annual Information Technology, Electronics and Mobile Communication Conference (IEMCON)*, Vancouver, Canada, 2016.

[325] S. Bailey and R. Raffaelle, “Chapter 9: Space Solar Cells and Arrays,” in *Handbook of Photovoltaic Science and Engineering, Second Edition*, John Wiley & Sons, Ltd, 2010, pp. 365-401.

[326] Y. Shimoda, Asahi Takahiro, A. Taniguchi and M. Mizuno, “Energy 32 (2007) 1617–1633Evaluation of city-scale impact of residential energy conservationmeasures using the detailed end-use simulation model,” *Energy,* vol. 32, pp. 1617-1633, 2007.

[327] J. Widen and E. Wackelgard, “A high-resolution stochastic model of domestic activity patterns and electricity demand,” *Applied Eenergy,* vol. 87, no. 6, pp. 1880-1892, 2010.

[328] I. Richardson, M. Thomson, D. Infield and C. Clifford, “Domestic electricity use: A high-resolution energy demand model,” *Energu and Buildings,* vol. 10, p. 42, 2010.

[329] A. E. Mustafa and P. R. Keith, “Assessment of the Carbon and Cost Savings of a Combined Diesel Generator, Solar Photovoltaic, and Flywheel Energy Storage Islanded Grid System,” *Energies,* no. 12, p. 25, 2019.

[330] A. Q. Jakhrani, K. A. Othman, R. H. A. Rigit, S. R. Samo and S. A. Kamboh, “Estimation of Carbon Footprints from Diesel Generator Emissions,” in *2012 International Conference in Green and Ubiquitous Technology*, 2012.

[331] N. K. Vinayagam, A. T. Hoang, J. M. Solomon, M. Subramaniam, B. Balasubramanian, A. I. El-Seesy and X. P. Nguyen, “Journal of Cleaner Production 306 (2021) 127310Available online 29 April 20210959-6526/© 2021 Elsevier Ltd. All rights reserved.Smart control strategy for effective hydrocarbon and carbon monoxide emission reduction on a conventional diesel engine using t,” *Journal of Cleaner Production,* vol. 306, p. 127310, 2021.